Controlled Delivery of Antimicrobial and Anti-inflammatory Agents from Un-cemented Prosthesis

A thesis submitted in accordance with the conditions governing candidates for the degree of

Philosophiae Doctor in Cardiff University

by

Hadil Faris Al-otaibi

April 2019

Cardiff School of Pharmacy and Pharmaceutical Sciences

Cardiff University

Summary

The prevalence of joint replacement procedure increased by more than 119% in the last decade as a result to that the demand for a prosthesis is very likely to increase. Uncemented prosthesis is the first-choice treatment option for patient age less than 68 years, due to its long-term and more stable fixation. The two major limitations that lead to the failure of joint replacement surgery are a prosthetic joint infection and aseptic loosening.

To encounter these limitations this study aimed to develop a coating that can control the release of the antimicrobial agent (chlorhexidine) and the anti-inflammatory agent (dexamethasone) to provide prophylaxis from postsurgical inflammation and infection. The antibacterial and anti-inflammatory coating was built initially on titanium nanoparticles followed by the validation on the medical grade Ti alloys surfaces. The multilayer coating was achieved employing a Layer by Layer (LbL) technology incorporating a drug of interest between polyelectrolyte layers of alginate and poly-beta amino esters. Physico-chemical characterisations of the obtained nanoparticles were conducted, and amount of chlorhexidine and dexamethasone released from the multi-layered system was quantified. Cytotoxicity and anti-inflammatory activity were assessed in *in-vitro* human macrophage cellular model, also cytocompatibility towards human osteoblasts cells were examined.

The results showed that chlorhexidine was released in a controlled manner for 60 days from the nanoparticular system providing inhibition of growth for a number of clinically relevant gram- positive and gram-negative bacterial strains. Dexamethasone released for up to 30 days was able to suppress TNF-α and IL-6 production. Study on Ti alloys surfaces confirmed the efficacy of the multi-layered systems. Moreover, no cytotoxic effects were observed towards osteoblasts surrounding prosthetic device confirming not just efficacy but also a safety of the proposed system.

Declaration of Authorship

This work has not been submitted in substance for any other degree or award at this or any other university or place of learning, nor is being submitted concurrently in candidature for any degree or other award.

Signed …… (Hadeel Faris Al-otaibi) Date ……

STATEMENT 1

This thesis is being submitted in partial fulfilment of the requirements for the degree of PhD.

Signed …… (Hadeel Faris Al-otaibi) Date ……

STATEMENT 2

This thesis is the result of my own independent work/investigation, except where otherwise stated, and the thesis has not been edited by a third party beyond what is permitted by Cardiff University's Policy on the Use of Third Party Editors by Research Degree Students. Other sources are acknowledged by explicit references. The views expressed are my own.

Signed …… (Hadeel Faris Al-otaibi) Date ……

STATEMENT 3

I hereby give consent for my thesis, if accepted, to be available online in the University's Open Access repository and for inter-library loans after expiry of a bar on access previously approved by the Academic Standards and Quality Committee.

Signed …… (Hadeel Faris Al-otaibi) Date ……

Acknowledgements

I would like to thank my supervisors, Dr Polina Prokopovich and Dr Stefano Perni for their patience, understanding, invaluable expertise and guidelines and advice that they provided me during a course of my PhD study.

I also express my gratitude to the colleagues and other PhD fellows in the School of Pharmacy and Pharmaceutical Sciences.

I thank my sponsor Princess Nourah bint Abdulrahman University for supporting my PhD research in Cardiff.

Finally, I thank my family, my father, my mother, my four sisters, my brother and my daughter Lina, and my friends for supporting and encouraging me through the course of my PhD study.

Research outputs

1.Alotaibi, Hadil Faris, Al Thaher, Yazan, Perni, Stefano and Prokopovich, Polina 2018. Role of processing parameters on surface and wetting properties controlling the behaviour of layer-by-layer coated nanoparticles. *Current Opinion in Colloid and Interface Science*, 36, pp. 130-142.

2. Alotaibi, Hadil Faris, Perni, Stefano and Prokopovich, Polina 2019. Prolonged release of anti-inflammatory drugs from LbL coating for un-cemented joint replacement devices.

Nanomedicine: Nanotechnology, Biology and Medicine, under review.

Peer reviewed conference contributions

1. Hadil Faris Alotaibi, Perni, Stefano and Prokopovich, Polina. Controlled Delivery of Antimicrobial Agent from Uncemented Prosthesis. Proceedings of the 29th Annual Conference of the European Society for Biomaterials (ESB), 9-13 September 2018, Masstricht, Netherlands.

2. Hadil Faris Alotaibi, Perni, Stefano and Prokopovich, Polina. Controlled Delivery of Anti-inflammatory and Antimicrobial Agent from Uncemented Prosthesis. Proceedings of the Postgraduate Research Day of School of Pharmacy, Cardiff University, 28th March 2018, Cardiff, UK.

Content

List of Figures

List of Tables

List of Abbreviations

APTS	3-Aminopropyltriethoxysilane
ANOVA	One-way analysis of variance
BHI	Brain heart infusion
CFU	Colony forming unit
CHX	Chlorhexidine
DLS	Dynamic light scattering
DEX	Dexamethason-phosphate
FBS	Fetal bovine serum
HPLC	High Performance Liquid Chromatography
LbL	Layer-by-layer
MIC	Minimum inhibitory concentration
MTT	Methylthiazolyl tetrazolium
NP	Nanoparticles
PBAE	Poly-beta-amino-ester
PBS	Phosphate buffer saline
PJI	Prosthetic joint infections
Q	Quadruple layer
RPM	Revolutions per minute
RPMI 1640	Roswell Park Memorial Institute medium
SD	Standard deviation
TiO_2	Titanium nanoparticles
TEM	Transmission electron microscopy
TGA	Thermogravimetric analysis
THR	Total hip replacement

TJR	Total joint replacement
TKR	Total knee replacement

Chapter 1: Introduction

1.1 Arthroplasty

Joint arthroplasty is the surgical procedure of replacing a damaged joint with an implant, commonly known as prosthesis. Prostheses are designed to restore the function of worn joints due to conditions that causes joint deformation such as osteoarthritis, hip fracture, septic arthritis, and bone dysplasia (Johnson 2014). The implants are usually made of metal, ceramic, or high-density polyethylene (López-López et al. 2017).

The National Joint Registry UK reported that the numbers of hip-, knee-, shoulder-ankle, and elbow-replacement procedure conducted in the calendar year 2017 were 91,698, 102,177, 6,526, 734 and 612, respectively (National Joint Registry 2018). More than 90% of these cases were caused by osteoarthritis and most of the patients were 61-76 years old (National Joint Registry 2018; Prieto-Alhambra et al. 2014). This is not surprising since the global prevalence of osteoarthritis among the elderly (>65 years old) was more than 30% in 2007 (Kim et al. 2010). In the period between 1991 and 2006, the rates of total knee replacement (TKR) performed in UK have more than tripled in women (from 42.5 to 138.7 per 100,000 person-years) and men (from 28.7 to 99.4 per 100,000 person-years) (Culliford et al. 2010). The relative population of elderly people is continuously rising globally as the obesity epidemic; because both of these are risk factors for OA, the demand for prosthesis is very likely to increase (Zhang and Jordan 2010).

1.2 Characteristics of prosthesis for cemented or uncemented fixation

In general, damaged joint can be replaced with a prosthesis fixed using two distinctive methods; in cemented prosthesis PMMA bone cement is employed as grout between device and bone while in uncemented prosthesis the device is initially forced into the bone (“press fit”) and long term fixation is achieved through bone growth embedding the device (Maggs and Wilson 2017).

The difference between the two type of fixation methods also requires different device design, cemented stems can either categorised as: taper-slip (“force-closed”) or composite beam (“shape-closed”) (Davies et al. 2012). Taper-slip stems, such as the Exeter stem, are collarless and have a polished surface, they accomplish final fixation through post-operative micromotion and subsidence of the stem inside the

cement mantle; the resulting radial stresses and compression at the bone-cement and prosthesis-cement interfaces provide the necessary interlock (Jayasuriya et al. 2013). Composite bar stems, such as the Charnley Stem, have rough surfaces and achieve stability through a strong bond between stem, cement and bone, without micromovement between device and cement mantle (Jayasuriya et al. 2013). The design characteristics of these two stem types are shown in Figure 1.

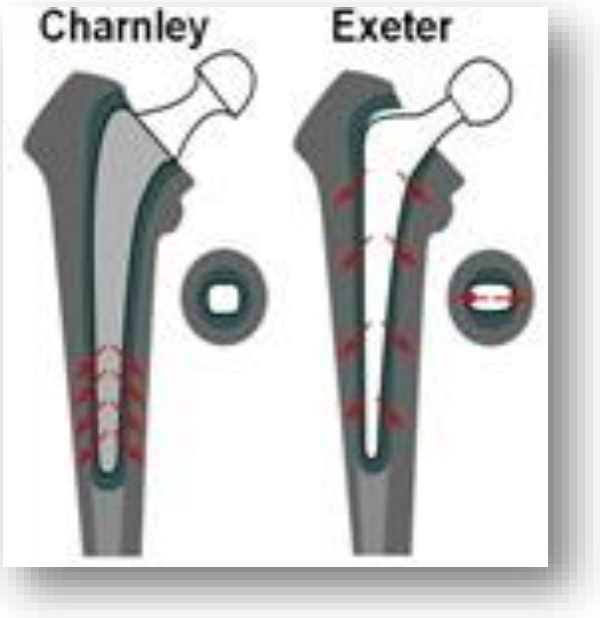

Figure 1. Drawing showing the principal design characteristics of the femoral prostheses (Jayasuriya et al. 2013).

Cemented sockets tend to be thick-walled polyethylene cups with grooves on the external surface and an implanted wire marker to permit the assessment of position on postoperative X-rays (Maggs and Wilson 2017). A schematic representation of an uncemented prosthesis is presented in Figure 2; in knee joint prosthesis is mainly composed of femoral component and tibial component. A spacer/liner is placed between these two parts. For hip prosthesis, it composes of acetabular component, femoral head, and femoral stem. A plastic liner is placed between the acetabular component and the femoral head.

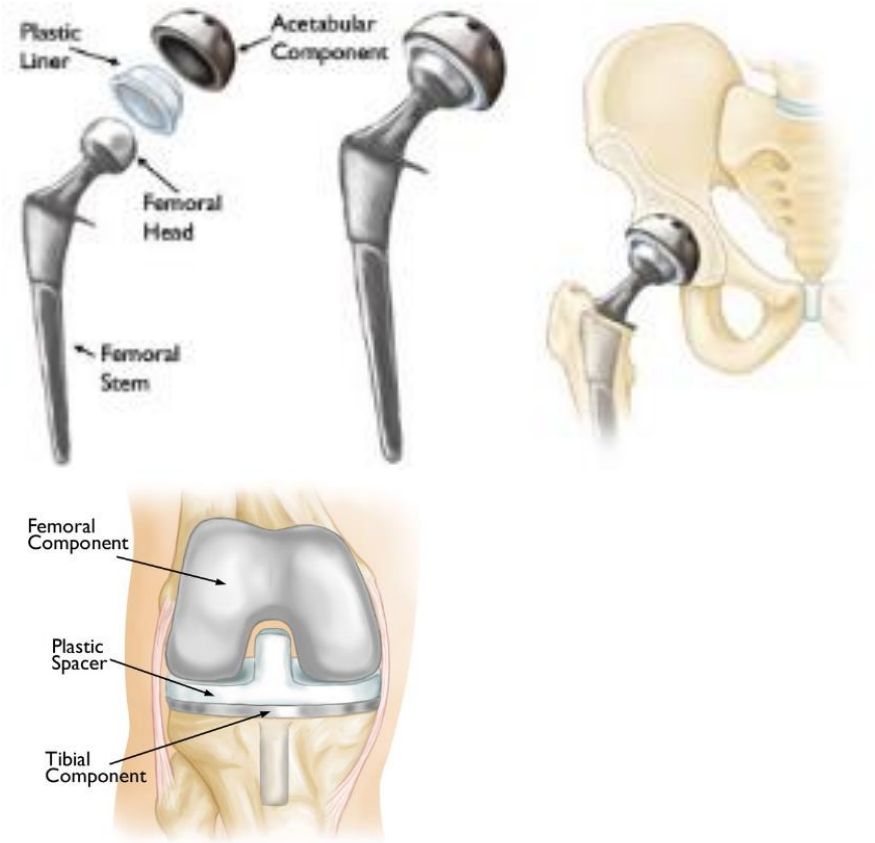

Figure 2. Uncemented prosthesis for hip (a) and knee (b) joint replacement. Figure adapted from http://orthoinfo.aaos.org/topic.cfm?topic=a00221

Uncemented stems have been developed in numerous designs (with wedged, tapered, cylindrical, modular and other anatomic shapes); recently, shorter stem plans have been brought to market with the point of making a more "physiological" loading of the proximal femur. However, all these designs have the same objective to maximise the initial stability and allow for surrounding bone growth in the months and years post operation (Maggs and Wilson 2017). Initial stability is vital because the degree of micromotion at this stage determines the type of tissue forming at the bone prosthesis interface. Micromotion of more than 150 μm leads to fibrous tissue, between 40 and 150 μm results in the formation of a mixture of bone and fibrous tissue while under 20 μm results predominantly bone tissue (Engh et al. 1992; Pilliar, Lee, and Maniatopoulos 1986; Jasty et al. 1997).

Uncemented prostheses are surface-engineered two ways to favour the interlock between device and bone. "On-growth" surfaces are manufactured by grit blasting or plasma spraying hydroxyapatite (HA) onto the device surface to make a create a textured surfaced onto which bone can grow (Khanuja et al. 2011). On the other hand,

“in-growth” surfaces are made utilizing sintered beads, fibres and permeable metals, these devices have microscopic pores into which bone can develop; the ideal pore size for in-growth is 50–400 μm and the optimum percentage of voids inside the coating, to maintain mechanical strength, is 30%–50% (Berry 2001).

Instead of providing a scaffold for osteoblasts growth, coating prostheses with bioactive materials such as HA and tricalcium phosphate can actively promote cells growth increasing and such stability. Coating can either be total or fractional; total coating presents an extended area for fixation, but can diminish loading of the proximal bone, driving to stress-shielding. While only proximal coating channels the strengths of weight bearing through the femoral metaphysis, but has a smaller area available for fixation (Maggs and Wilson 2017).

Uncemented sockets present porous coatings over the entire circumference, fixation is achieved using screws, pegs, or spikes to achieve initial stability. Most systems use a metal shell with a polyethylene liner fastened securely inside it. However, results are not unequivocal in demonstrating improved performance of these devices (Maggs and Wilson 2017).

1.2.1 Advantages and Limitations of cemented Prosthesis

Joint replacement using cemented fixation technique has many advantages that out preform other prosthesis type. Its allow long term Survivorship based in clinical studies in the UK and New Zealand. Also, cemented stem can be considered to be customized for the patient and can be used in almost all situations, including where there is femoral deformity. The cement mantle allows components to be positioned optimally with respect to the patient's anatomy and leg length. However, the common limitation associated with this kind of prosthesis are Bone-cement implantation syndrome and higher rate of Aseptic loosening of a cemented femoral component after TJA is a potential cause of pain and loss of function, resulting in the subsequent need for a revision. In rare cases, patients have an allergic reaction to the bone cement and must undergo a second surgery to remove the prostheses.

1.2.2 Advantages and Limitations of Uncemented Prosthesis

Joint replacement using uncemented fixation technique has been increasingly popular due to its ability to allow bone ingrowth, the ability of osteoblasts to grow into the pores

of implants and stabilize it (Aprato et al. 2016; Prudhon and Verdier 2017). Uncemented prosthesis offer better long-term survival, a more stable fixation and lower risk of bone loss /osteolysis over cemented implants (Giebaly et al. 2016). They also are superior to cemented prosthesis in terms of shorter operating room time, preservation of bone stock and ease of revision (Aprato et al. 2016); additionally un-cemented fixation is not affected by any of the possible complications associated with cemented fixation like third body wear, retained loose fragments and bone cement implantation syndrome (Aprato et al. 2016; Donaldson et al. 2009).

Despite the numerous aforementioned benefits of un-cemented joint replacements, their instability was a major drawback that prevented the diffusion of these devices (Maggs and Wilson 2017). Modern designs have solved this problem leading to an increasing number of cementless fixation procedures. For example, in the UK for hip arthroplasty the proportion of uncemented joint replacement device has increased steadily from 16.8% in 2003 to 42.5% in 2013 but fell slightly to 38% in 2017, as shown in Figure 3 (National Joint Registry 2018, 2017). Although uncemented fixation has become more popular in hip replacement, uncemented fixation technique require sufficient blood flow and healthy bone that is able to stabilize the prosthesis (Abdulkarim et al. 2013). Therefore, uncemented prosthesis is more suitable for younger patients (less than 65 years old) (Wyatt et al. 2014). Uncemented femoral prosthesis has better survival rates and lower risk of revision ($p < 0.002$) in patients aged less than 55; while elderly patients (more than 65 years old) with uncemented prosthesis are at increased risk of revision and periprosthetic fracture (12.4% vs 6.8%) (Moskal, Capps, and Scanelli 2016).

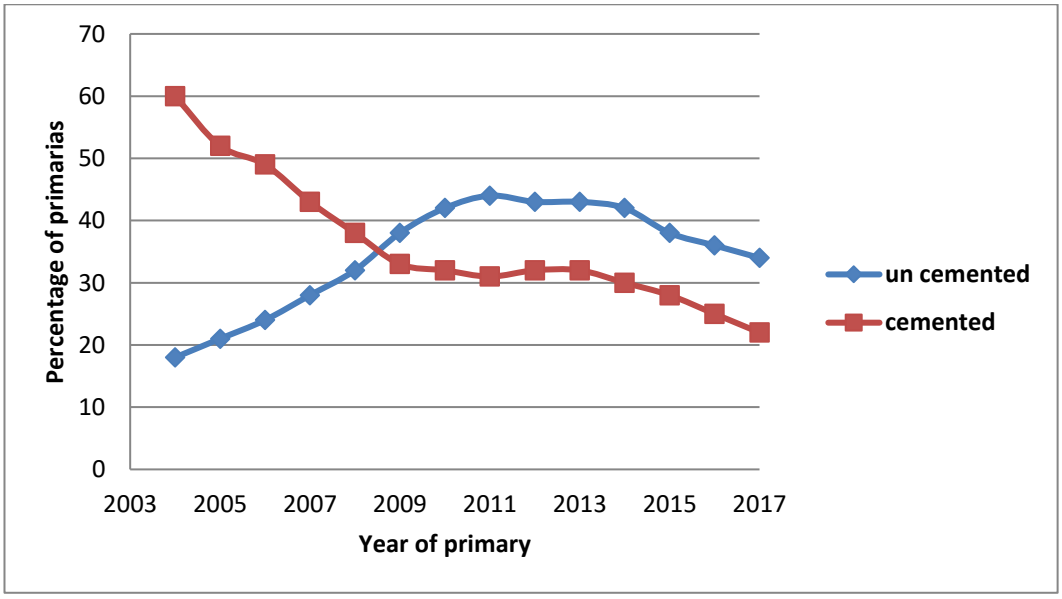

Figure 3. The percentage of cemented and uncemented hip replacements in the UK from 2003 to 2017. (National Joint Registry 2018)

An analysis of five national joint replacement registries (Norway, Sweden, England-Wales, Australia and New Zeeland) has revealed that cemented prostheses slightly outperform uncemented implants in terms of revision risk, particularly in younger patients; however, registries generally record only revision as end-point but not patient reported outcome such as pain, quality of life or mobility therefore a full comparison simply based on revision rate would not be provide a complete comparison (Zhang, Yan, and Zhang 2017).

1.2.3 Materials for Components of Uncemented Prosthesis

The materials employed to manufacture implant has to fulfil numerous requirements such as biocompatibility, strength and corrosion resistance (Matsuno et al. 2001). Uncemented prosthetic devices can be made using chrome alloy, and stainless steel (Ansari, Takahashi, and Pandit 2018); however the "gold standard" material used as prosthesis is titanium alloy, a metal with high resistance to corrosion (Gong et al. 2012; Moskal, Capps, and Scanelli 2016). The advances in material science has led to development of functionally graded material (FGM), a class of micro-structured materials for biomedical application. The most popular FGM, titanium and hydroxyapatite, have been used in combination as materials for joint prosthesis (Hedia 2007) and have demonstrated enhanced bone remodelling (Gong et al. 2012). Beside the material employed in the stem and socket, the contacting surfaces combination (ball and socket) in uncemented prosthesis can be metal-on-metal, metal-on-polyethylene, ceramic-on-polyethylene, ceramic-on-ceramic, and ceramic-on–metal (National Joint Registry 2018). The trends in the preferences for metal-on-metal, metal-on-polyethylene, ceramic-on-polyethylene, ceramic-on ceramic, and ceramic-on –metal hip joint prosthesis is illustrated in Figure 4.

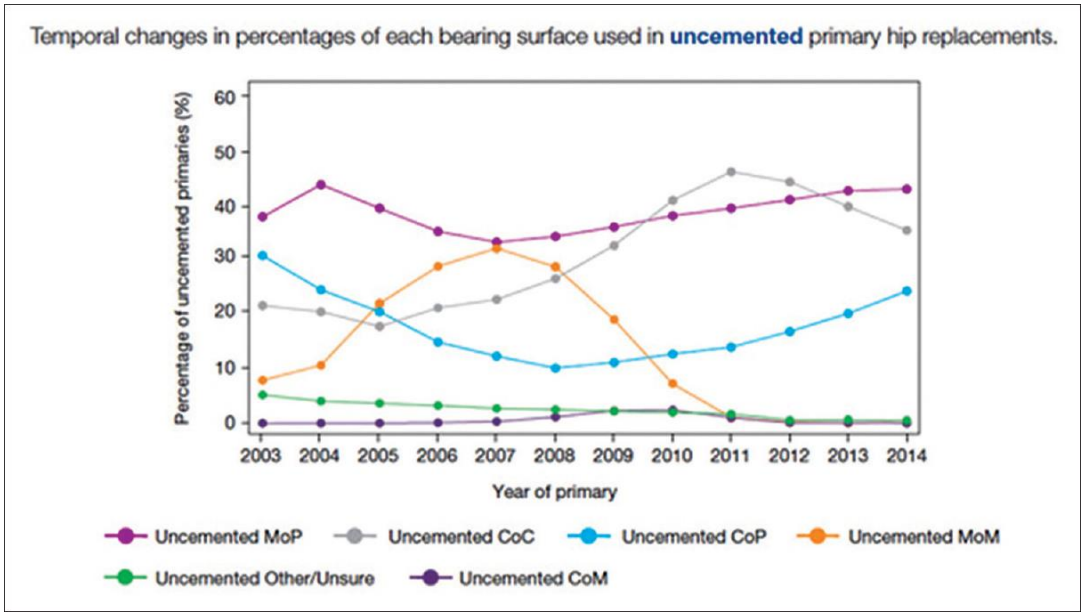

Figure 4. The preferences for surface materials for uncemented hip prosthesis. MoP: metal-on-polyethylene, CoP: ceramic-on-polyethylene, CoC: ceramic-on ceramic, CoM: ceramic-on–metal, MoM: metal-on-metal. Figure adapted from National Joint Registry (2018)

Metal-on-metal (MoM) prosthesis is of a huge concern due to reportedly high rate of revision (Matharu et al. 2018; Pijls et al. 2016) and metal toxicity (Martin et al. 2015; Harris et al. 2015). The number of MoM prosthesis used therefore has decreased drastically from 2007 to 2011 (Figure 4). Metal-on-highly cross-linked polyethylene (MoP) has been produced to reduce linear and volumetric wear than conventional polyethylene that cause osteolysis. However, the erosion of the polymeric constituents results in failure of these devices, for example at 10-year follow, osteolysis was observed in 26% of cases while aseptic loosening occurred in 3% (D'Antonio, Capello, and Naughton 2012). Hard bearing surfaces which produce even less volumetric wear, such as ceramic-on-ceramic (CoC) has also been developed to address the problem of osteolysis. In light of their remarkable wear performance, Coc are favoured in young patients; however, concerns regarding the best technique for implantation to avoid fracture and squeaking still remains (Hernigou et al. 2016; Wang et al. 2016).

Recently, there has been a growing attention on development of prosthesis with antimicrobial activity (Goodman et al. 2013; Raphel et al. 2016; Zhang, Zhang, and Li 2013). Currently available uncemented prosthesis in the United Kingdom are often coated with osseoconductive materials. For example, Pressfit® (Waldemar), CSF®

(Joint Replacement Instrumentation Ltd.), Trident® and ABG II® (Stryker) are a few of hip joint implants that are coated with hydroxyapatite. Metha® (B Braun), Cerafit® (Corin) prostheses are coated with pure calcium phosphate. Antibactericidal agent-coated prosthesis is not available in the market yet, but ongoing research showed promising results (Gallo, Holinka, and Moucha 2014; Getzlaf et al. 2016; Riool, Dirks, et al. 2017); however this technology have not been tested in clinical trials or have demonstrated antimicrobial activity only for a short period of time (days).

1.2.4 Fixation Procedure for Uncemented Prosthesis

The prosthesis can be attached to the surrounding bone using cement material such as poly(methyl methacrylate) (PMMA), (Vaishya, Chauhan, and Vaish 2013; J. and F. 2007) which is then termed cemented prosthesis, or without cement; the latter is commonly known as uncemented prosthesis (Aprato et al. 2016). Figure 5 illustrates the differences between cemented and uncemented prosthesis for hip joint replacement. In hip joint replacement, the head of the femur is removed and a medullary cavity is created. Hip prosthesis consists of acetabular cup, insert, femoral head, femoral stem, and the shaft (Figure 5a). The acetabular cup of prosthesis is then fitted to the socket while the stem of the prosthesis is inserted to the medullary cavity of the femur. In cemented prosthesis, both acetabular cup and femoral stem of the prosthesis is anchored with cement material to ensure great stability (Figure 5b). When uncemented prosthesis is used, the femoral stem is inserted into the medullary cavity securely without the use of cement material. This stem is designed to have porous surface to promote bony ingrowth (Figure 5c).

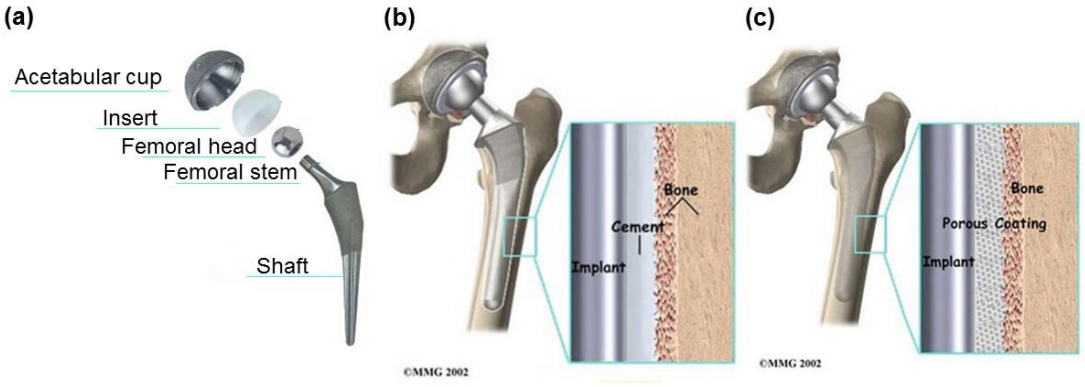

Figure 5. Schematic illustration of hip implant parts (a) and differences between cemented prosthesis (b) and uncemented prosthesis (c) for hip joint replacement. https://www.healthpages.org/surgical-care/hip-joint-replacement-surgery/ accessed on 5/02/2019

X-rays of patients undergoing hip replacement are shown in Figure 6 and Figure 7 for cemented and cementless procedures, respectively.

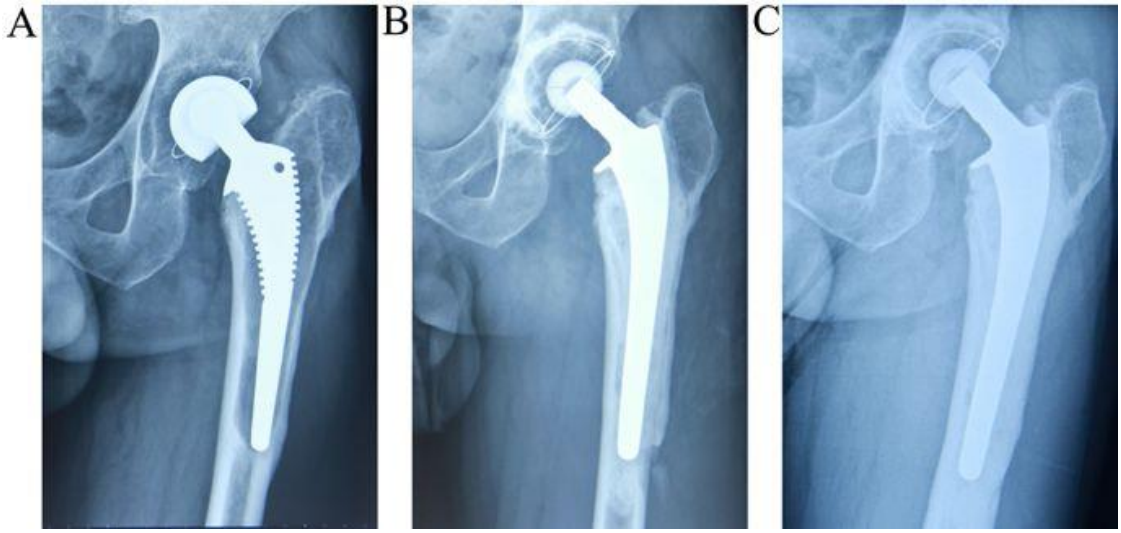

Figure 6. Serial radiographs of a 69-year-old man who experienced revision with the cemented stem. (a) Radiograph before revision, showing a loosened stem. (b) Radiograph instantly after revision with cemented femoral stem. (c) Radiograph 7 years after revision. (Wang et al. 2013)

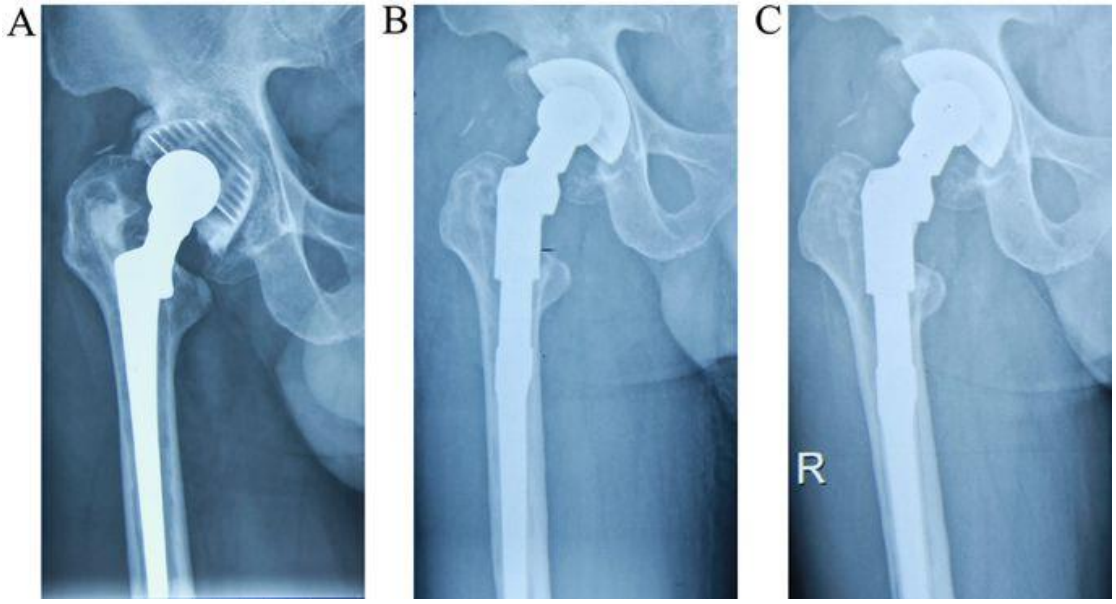

Figure 7. Serial radiographs of a 60-year-old man who experienced revision with the cementless modular femoral stem. (a) Radiograph before revision, showing a loosened stem. (b) Radiograph instantly after revision with the cementless modular femoral prosthesis. (c) Radiograph 4 years after the revision. The patient had a good clinical result, and the stem remains stable with no subsidence. (Wang et al. 2013)

1.3 Prosthetic-associated infections

Like any other surgical intervention, post-operative infections are a potential adverse event associated to joint replacement. Sterility during surgical procedure is of the utmost importance. However, prophylaxis treatment using antimicrobial agents is essential to further minimise bacterial attachment to prosthetic surface. The increased use of prosthesis in the last decades has been constantly followed by increased incidence of prosthesis-associated infection (Getzlaf et al. 2016).

Overall, the annual incidence of PJI in the United Kingdom is around 0.5 to 2% (Williams, Mihok, and Murray 2016). This relatively low figure, however, should be taken as a concern since the demand for joint arthroplasty is increasing steadily (Inacio, Graves, et al. 2017; Hooper 2013). Moreover, most of PJI cases are caused by multidrug-resistant *Staphylococcus,* which is difficult to eradicate (Getzlaf et al. 2016; Raphel et al. 2016). The most common PJI-causing bacteria are listed in Table 1.

Table 1. Most common Prosthetic-joint-infection-Causing Bacteria (Tande and Patel 2014)

Bacteria	Hip (%)	Knee (%)	Shoulder (%)	Elbow (%)
Staphylococcus aureus	13	23	18	42
Coagulase-negative *Staphylococcus*	30	23	41	41
Streptococcus spp.	6	6	4	4
Enterococcus spp.	2	2	3	3
Gram-negative bacilli	7	5	10	7
Propionibacterium acne	1	2	24	1
Polymicrobial	7	11	15	5

Treatment options for PJI include both non-operative measures with long term exposure to antibiotics and surgical such as debridement and implant retention (DAIR), one- or two-stage revision arthroplasty, arthrodesis and amputation (Qasim, Swann, and Ashford

2017). Implant retention without infection is ideal and DAIR has been reported to have variable success rates depending on patient factors, duration of infection, infecting micro-organisms, choice of procedure, single or multiple debridement procedures, arthroscopic or open, antibiotic choice and duration of antibiotic use (Qasim, Swann, and Ashford 2017). From the total of 27,605 hip joint revision procedures took place from 2017 in the United Kingdom, 3,872 cases (13.8%) were caused by prosthetic-joint infection (PJI) (National Joint Registry 2018). Therefore, prosthetic joint infection surgery is not a likely life-changing event potentially life-threating but also poses significant financial burden as it involves multiple procedures, prolonged antibiotics administration, lengthy hospital stays and more expensive implants for revision surgery (Merollini, Crawford, and Graves 2013).

1.3.1 Role of biofilms in prosthetic-associated infection

As in more than half of human infections (Williams and Costerton 2012), the main mechanism involved in PJI is biofilm formation (Getzlaf et al. 2016; Gbejuade, Lovering, and Webb 2015). The initial stage of biofilm formation is adhesion of bacteria to the surface of prosthesis and it a process mediated by various mechanisms (Costerton, Stewart, and Greenberg 1999; Arciola et al. 2012). Firstly, PJI-causing bacteria might form non-specific adhesion with an inert biomaterial surface due to roughness, hydrophobicity, or weak chemical interaction (Chen and Wen 2011). The latter is mediated either by Lewis acid-base reaction, van der Waals force, electrostatic force, or all of them (Hall-Stoodley and Stoodley 2005). Prosthetic surface possessing electron-accepting groups / acidic groups can provide adhesion site for bacteria via electron-donation (Getzlaf et al. 2016). Meanwhile, opposite electrostatic charge between prosthesis surface and bacterial cell wall might lead to electrostatic force-mediated adhesion (Hall-Stoodley and Stoodley 2005; Stoodley et al. 2012).

Pili, hair-like protein fibres found on the surface of bacterial cells, are able to overcome electrical repulsive force between bacterial cells and prosthetic surface, allowing strong adhesion (Costerton, Stewart, and Greenberg 1999; Hall-Stoodley and Stoodley 2005; Stoodley et al. 2012). More importantly, hydrophobic interaction between hydrophobic surface of prosthesis and bacterial cell wall becomes the most critical factor for non-specific bacterial adhesion (Getzlaf et al. 2016).

The initial phase of bacterial adhesion with aforementioned mechanisms (non-specific adhesion and adhesin-mediated attachment) is reversible but often proceed to irreversible phase due to further cellular interactions involving expression of biofilm-

generating genes (Gallo, Holinka, and Moucha 2014). Once the reversable phase is passed, generally in a matter of minutes from the initial adhesion, a biofilm is formed (Dunne 2002).

The stages in biofilm formation are shown in Figure 8; as bacterial adhesion onto prosthesis reach irreversible phase, a conditional film is formed. This film occurs as covering layer, preventing attachment of prosthesis to the host body (Gallo, Holinka, and Moucha 2014). Later, biofilm-forming bacteria will express biofilm-generating genes which are responsible for secreting highly resistant slime. Once the biofilm is formed, the probability of eradicating bacteria decreases because biofilms are more resistant to antimicrobial agents than the floating counterpart (Singh et al. 2017; Eze, Chenia, and El Zowalaty 2018). Biofilm matrix mainly consists of polysaccharides which has the ability to cover micro-colonies and inhibit penetration of antimicrobial agents (Gallo, Holinka, and Moucha 2014). Moreover, bacteria such as *Staphylococcus* can attach to the surface of other bacteria through microbial surface component recognizing adhesive matrix molecules; consequently, biofilm might contain various bacterial species, which leads to higher resistance to antimicrobial agent (Gallo, Holinka, and Moucha 2014).

Therefore, the only window of opportunity to inhibit biofilm formation lies in the reversible phase of bacterial adhesion (Gallo, Holinka, and Moucha 2014).

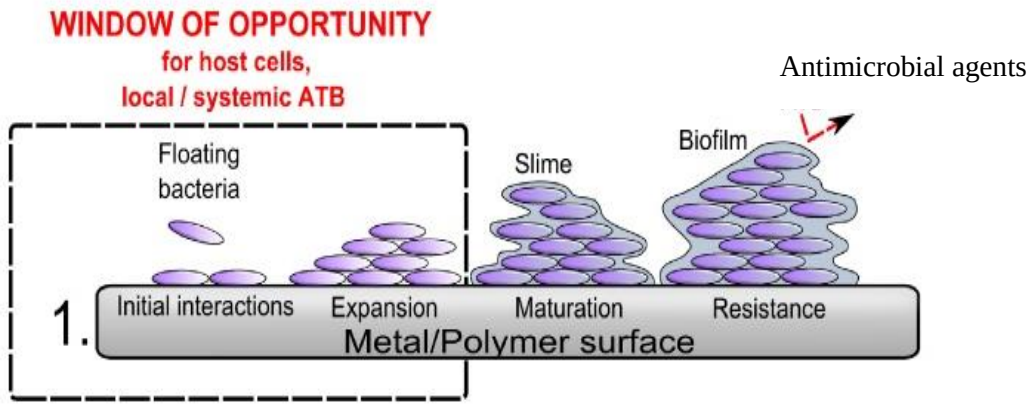

Figure 8. the prosthetic surface and the Four stages involved in biofilm formation: initial attachment of floating bacteria, expansion, biofilm maturation, and resistant biofilm establishment. Figure adapted from Gallo, Holinka, and Moucha (2014)

1.3.2 Prophylaxis for Prosthetic-associated infection

A successful preventive measure to encounter PJI requires multi-disciplinary considerations (Wang et al. 2017). Sterility during surgical procedure is of the utmost

importance (Kearns et al. 2011); however, prophylaxis treatment using antimicrobial agents is essential to further minimise bacterial proliferation and attachment to the prosthetic surface (Parvizi, Shohat, and Gehrke 2017). Prosthetic devices can be designed to have antimicrobial property. This can be achieved by modifying the surface of implants or incorporating antimicrobial compound(s) onto the implants (Williams, Mihok, and Murray 2016; Getzlaf et al. 2016).

1.3.2.1 Surface modification

The surface of prosthetic device can be modified, physically or chemically, to reduce the risk of bacterial attachment. Physical modification by roughness reduction have been reported in a large number of studies (Table 2). Smoother surfaces present a lower number of potential contact sites for bacterial attachment compared to highly porous and rough surfaces (Figure 9), thus reducing the ability of bacteria to colonise (Getzlaf et al. 2016).

Table 2. Strategies to prevent prosthetic joint infections by modification of surface properties of titanium-based orthopaedic implant materials. Adapted from Getzlaf et al. (2016)

Method	Organism(s)	Antibacterial	System	Observation(s)	Reference
Oxidative nanopatterning of Ti	MRSA, *Candida albicans*	Surface topography	in vitro	*S. aureus* adhesion reduced; *C. albicans* aggregations reduced	Variola et al. (2014)
UV irradiation	*S. aureus, S. epidermidis*	Spontaneous wettability	in vitro	Bacteria adhere but not firmly attached	Gallardo-Moreno et al. (2009)
UV C irradiation	*S. aureus, S. epidermidis*	Increased ROS	in vitro	Bacteria killed for 60 min after UV treatment	Gallardo-Moreno et al. (2010)
Zn TiO_2	*E. coli, S. aureus*	ZnO mediated ROS	in vitro	Inhibition attachment	Hu et al. (2012)

Method	Organism(s)	Antibacterial	System	Observation(s)	Reference
Zn-implanted Ti	*E. coli*, *S. aureus*	Zn ions	in vitro	Partial antibacterial effect; *E. coli* more inhibited than *S. aureus*	Jin et al. (2014)
Alkali treatment	*S. aureus*, *E. coli*	Nanoroughness, increase local pH	in vitro	Bacteriostatic effect, reduced proliferation	Li et al. (2014)
Superhydrophobic TiO_2 nanotube	*S. aureus*	Superhydrophobic surface	in vitro	Reduced adhesion	Tang et al. (2011)
Photocatalytic TiO_2 layer	*S. aureus*, *S. epidermidis*, *P. aeruginosa*	Increased ROS	in vitro	Antibacterial effect after 60 min UV treatment	Zaborowska et al. (2015)
Silk Sericin surface	*S. aureus*, *S. epidermidis*	Silk sericin	in vitro	Reduced adhesion	Zhang et al. (2008)
Ag-doped TiO_2 nanotube	*S. aureus*	Ag ions	in vitro	Planktonic clearing, reduced adhesion	Zhao et al. (2011)

Other approaches rely on the modification of the chemical properties of the materials therefore interacting with the electrochemical and van der Waals attraction between bacteria and material; the use of UV, oxidizing agents and alkali treatment fall in this type of treatments.

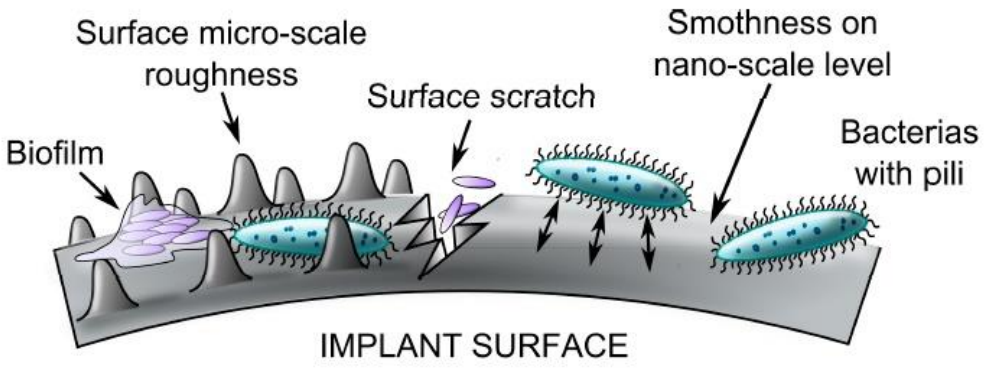

Figure 9. Relationship between surface roughness and bacterial adhesion. Figure adapted from Gallo, Holinka, and Moucha (2014)

1.3.2.2 Surface coatings

Chemical modification by using coating technique has been explored extensively (Table 3). There are various coating types that can be applied on implant surfaces in order to minimize the risk of PJI:

Anti-adhesive/anti-fouling surfaces are prepared by coating the implants with materials that has very low affinity to bacterial surface or bacterial adhesins such as polyelectrolytes, metals and hydrogels. Two major limitations of this approach exist: (1) the system can only inhibit bacterial adhesion instead of killing the pathogens (Raphel et al. 2016), (2) the attachment of osteogenic cells to the implant might be hindered (Getzlaf et al. 2016). Consequently, this approach is not suitable for cementless fixation, considering the need of bony ingrowth (Getzlaf et al. 2016).

Table 3. Strategies to prevent prosthetic joint infections by coating of titanium-based orthopaedic implant materials. Adapted from Getzlaf et al. (2016)

Method	Organism(s)	Antibacterial	System	Observation(s)	Reference
Antiseptic dye coating	*S. aureus*	Gendine (chlorhexidine)	in vitro	Total prevention of bacterial adherence	Bahna et al. (2007)
Antibiotic loaded hydrogel	*S. aureus, S. epidermidis*	Various antibiotics	in vitro	Inhibition of biofilm and planktonic	Drago et al. (2014)

Method	Organism(s)	Antibacterial	System	Observation(s)	Reference
coating				growth	
Ag coating	*Staphylococcus sp., Bacillus sp., Enterococcus sp., Corneybacterium*	Ag ions	in vivo	Reduced infection r	Masse et al. (2000)
Material painting of N,N-dodecyl, methyl-PEI coating	*S. aureus*	Immobilized hydrophobic polycationic chains	Both	Total absence of infection	Schaer et al. (2012)
Mesoporous TiO_2 coating	*E. coli*	Cephalothin controlled release	in vitro	All bacteria killed on contact	Xia et al. (2012)

1.3.2.3 Antimicrobial elution

Antimicrobial agents, including antibiotics, antimicrobial peptides, and immunomodulatory chemokines, can be fixed to prosthetic devices (Table 4). Unlike the previous approaches, the success of this technique depends on bacterial susceptibility to the compounds used as well as the rate of drug release (Al Thaher, Perni, and Prokopovich 2017). The principles in this approach is that antibiotic should be released in a way that the concentration is always above the minimum inhibitory concentration (MIC) throughout the duration of prophylactic therapy (Williams, Mihok, and Murray 2016).

Table 4. Strategies to prevent prosthetic joint infections by antimicrobial eluting titanium-based orthopaedic implant materials surfaces. Adapted from Getzlaf et al. (2016)

Method	Organism(s)	Antibacterial	System	Observation(s)	Reference

Method	Organism(s)	Antibacterial	System	Observation(s)	Reference
Antibiotic impregnated microspheres	*S. aureus*	Tobramycin	in vivo	Total absence of infection; no effect on bone ingrowth	Ambrose et al. (2014)
Covalently tethered vancomycin	*S. epidermidis*	Vancomycin	in vitro	Prevention of colonization and biofilm formation	Antoci et al. (2008)
HA-chitosan polyelectrolyte with arginine-glycine-aspartic acid (RGD) peptide	*S. aureus*	Chitosan	in vitro	Adhesion reduced by 80% for 21 days	Chua et al. (2008)
Silk Sericin surface	*S. aureus, S. epidermidis*	Silk sericin	in vitro	Reduced adhesion	Zhang et al. (2008)
Titanium with surface-grafted dextran	*Staphylococcus aureus and Staphylococcus epidermidis*	Dextran	in vitro	Reduced adhesion	Shi et al. (2009)
carboxymethyl chitosan (CMCS) or hyaluronic acid-catechol (HAC) conjugated with vascular endothelial growth factor	*Staphylococcus aureus*	carboxymethyl chitosan (CMCS) or hyaluronic acid-catechol (HAC)	in vitro	Reduced adhesion	Hu et al. (2010)

Method	Organism(s)	Antibacterial	System	Observation(s)	Reference
Gentamicin and bone morphogenic protein-2 (BMP-2)-delivering heparinized	*Staphylococcus aureus*	Gentamicin	In vitro	Reduced growth	Lee et al. (2012)

Prosthetic device can be coated with a tailored drug eluting system instead of simply impregnated with antibiotic solution to overcome short-lived elution (Williams, Mihok, and Murray 2016). Antibiotic eluting system can be divided into two categories: matrix system and reservoir system. A biodegradable matrix system is used to sustain antibiotic release from implant devices (Al Thaher, Perni, and Prokopovich 2017), while in matrix system, the drug is loaded onto swellable polymers. The polymers undergo swelling upon hydration and the drug is eluted from the matrix pores (Gao et al. 2016). If the matrix material is biodegradable, drug elution is mainly facilitated via matrix erosion hence biodegradable materials such as polyester, polyamino acid, polyalkyl α-cyanoacrylate has been widely used due to its ability to be degraded under physiologic environment either by hydrolytic mechanism or enzymatic degradation (Gao et al. 2016). The main advantage of this system is the simple loading process; however, the limitation of matrix system is the limited drug loading (Hsu, Park, et al. 2014).

The reservoir system differs from matrix system in the drug loading site. In reservoir system, the drug is deposited on a 'drug-loaded' core and the core is layered with coating materials to generate diffusion-mediated release. Therefore, permeability and the thickness of coating material controls the release rate of loaded drug (Kazemzadeh-Narbat et al. 2013; Al Thaher et al. 2018; Al Thaher, Perni, and Prokopovich 2017). The main advantage of coating system is that the coating layer creates a well-controlled environment that can enhance drug stability (Stevenson, Santini, and Langer 2012). However, a small rupture of the coating layers can lead to abrupt drug release (Coelho et al. 2010).

One of the most recent antibiotic eluting systems used in antimicrobial prosthetic devices is polyelectrolyte multilayers, generally known as layer-by-layer (LBL) deposition technique, a multiple coating layers that consist of multiply charged materials

(Chuang, Smith, and Hammond 2008; Hammond 2012; Hsu, Hagerman, et al. 2014; Hsu, Park, et al. 2014; Smith et al. 2009). Polyelectrolytes are deposited on the surface of implant. The layer is then deposited with oppositely charged materials, forming a bilayer. The drug is entrapped in between the layer and is expected to be released via film-erosion mechanism (Chuang, Smith, and Hammond 2008; Deng et al. 2013; Shah et al. 2013; Wong et al. 2010).

The main advantage of polyelectrolyte multilayer coating system is that the amount of drug loaded into the film can be adjusted based on the total number of layering films and thus this approach is versatile for many therapeutic compounds. The limitation of polyelectrolyte multilayer is that the number of layers required to sustain the release can reach few hundreds, which means labour/time intensive manufacturing process (Hammond 2012).

The majority of studies in the field of anti-infective prosthesis focused on controlling the release of gentamicin (Bertazzoni Minelli et al. 2015; Chang et al. 2013; Chuang, Smith, and Hammond 2008; Lee et al. 2012; Neut et al. 2011; Tamanna, Bulitta, and Yu 2015). Gentamicin belongs to aminoglycoside groups that is effective against gram-negative and gram-positive bacteria (Chang et al. 2013). Gentamicin is frequently used to treat osteomyelitis and septic arthritis caused by *P. aeruginosa, K. pneumonia, E. coli, S. aureus* or other *staphylococci* (Chuang, Smith, and Hammond 2008; Neut et al. 2011; Tamanna, Bulitta, and Yu 2015). Its rapid bactericidal effect and excellent stability in aqueous environment makes gentamicin a suitable agent for long-term PJI prevention (Tamanna, Bulitta, and Yu 2015)

Nevertheless, in many cases bacteria has become less susceptible to various antibiotics due to emerging resistance. Therefore, the use of alternative antimicrobial agents is encouraged (Williams, Mihok, and Murray 2016) and overuse of existing broad-spectrum antibiotic should be avoided (Munita and Arias 2016). The application of antimicrobial peptides such as recombinant human β-defensin-2 (rHUβD2) (Etienne et al. 2004), melamine (Chen et al. 2016), GL13K (Holmberg et al. 2013) or HHC36 (Kazemzadeh-Narbat et al. 2012) is increasingly popular in prosthetic devices. These are linked to the titanium surface similarly to antibiotic (Figure 10). However, the major limitation of antimicrobial peptides is their high susceptibility to proteolytic degradation and thermal degradation (Raphel et al. 2016). Secondly, the conformation of these peptide must be flexible enough if the peptide is to be immobilized onto the implant surface (Raphel et al. 2016).

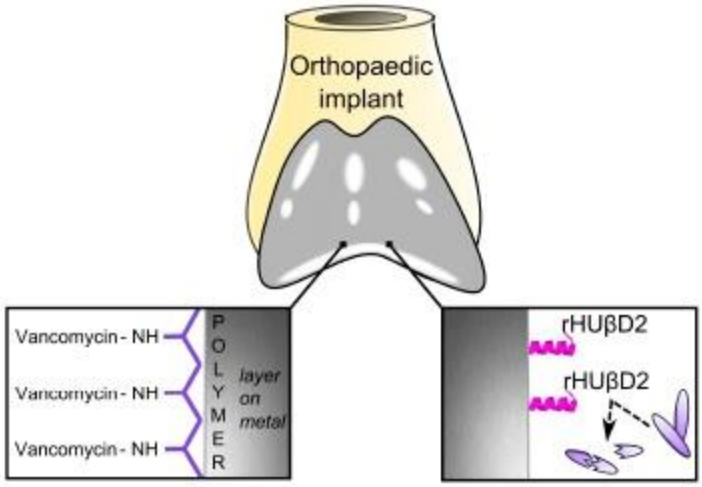

Figure 10. Implant surface with antimicrobial activity. Antibiotics (left) or antimicrobial peptides (right) can be covalently linked to prosthetic surface to eradicate biofilm-forming bacteria. RHUβD_2=Recombinant human β-defensin-2 (Gallo, Holinka, and Moucha 2014)

1.3.2.4 Multifunctional surfaces

Recently, an attempt on creating high-quality implants has been proposed by using two or more approaches. Multi-functional surfaces are designed to perform various tasks at once (Figure 11), for example inhibiting bacterial attachment using anti-adhesive compound and antimicrobial peptide while promoting osseointegration (Muszanska et al. 2012; Yamaguchi et al. 2017; Gallo, Holinka, and Moucha 2014). A number of approaches has been developed for multifunctional surface. Firstly, prosthetic device can be coated with an antimicrobial compound in combination with an osseoinductive agents to promote osseointegration. For example, polyethylene glycol (PEG) has been used as non-fouling/anti-adhesive coating material, which is grafted physically onto the surface of prosthetic device reducing 90% of bacterial adhesion (Etienne et al. 2004). The coating was then modified by incorporating arginine-glycine-aspartic acid (RGD) containing peptides that can enhance the integration of osteoblasts with the device (Rammelt et al. 2006).

In another study, antimicrobial peptide BMP-2 was covalently tethered onto dextran, the anti-adhesive coating (Shi et al. 2009). The goal of this approach was to retain the bactericidal activity for a longer period of time in comparison with antibiotic eluting systems. Coating of dextran-BMP-2 on Ti6Al4V has successfully decreased the

adhesion of *S. aureus* and *S. epidermidis* by 50% compared to uncoated device (Shi et al. 2009).

Alternatively, Titanium-based nanotube coating can be applied to enhance the interaction of implant with osteogenic cells (Popat et al. 2007). Silver nitrate was deposited on anodized titanium to the nanotube, the viability of *P. aeruginosa* was reduced 1000 times compared to uncoated nanotubes (Das et al. 2008).

Chitosan, a biopolymer that has antibacterial properties (Ordikhani et al. 2015; Mattioli-Belmonte et al. 2014). has been widely used as implant coating in combination with osteogenic agents (RGD-containing peptides) and antibiotic (vancomycin, ciprofloxacin) to create dual function for prosthetic devices (Ordikhani et al. 2015; Mattioli-Belmonte et al. 2014). Lastly, antibiotic can be covalently immobilized / tethered onto the surface of prosthesis in order to maintain bactericidal activity for a longer period in comparison with antibiotic eluting system (Raphel et al. 2016). Vancomycin tethered Ti6Al4V implant has shown prolonged antibacterial activity for nearly 1 year with lower osteolysis rate (Antoci et al. 2007; Hickok and Shapiro 2012).

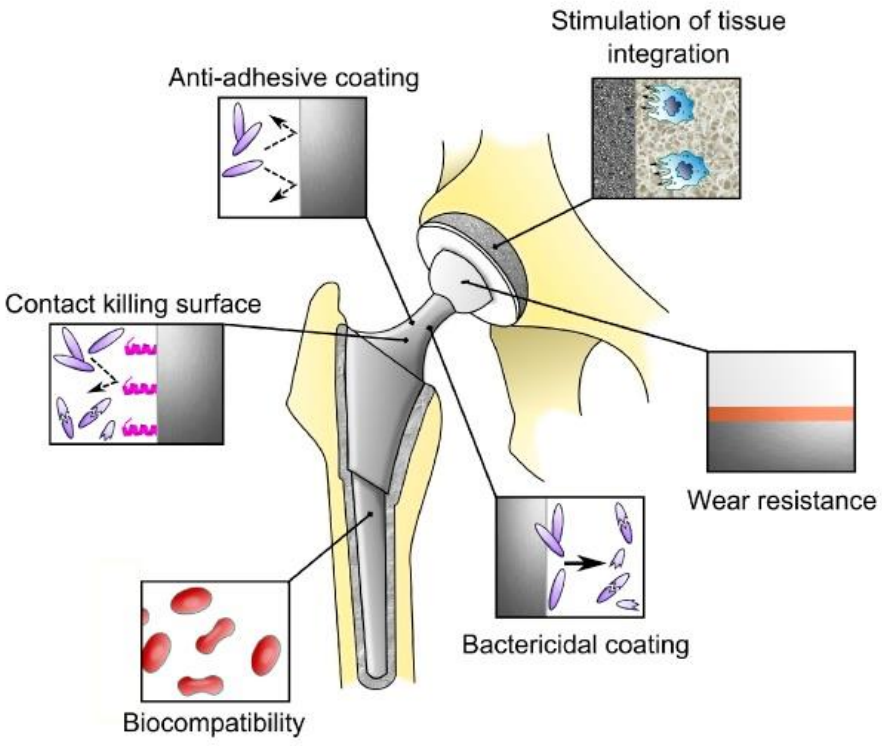

Figure 11. Various biological tasks performed by prosthesis with multi-functional surface intended for total hip arthroplasty. The device may have at least two of the following approaches: anti-adhesive coating, contact killing / antibiotic-tethered coating, bactericidal eluting coating, and osseoinductive coating (Gallo, Holinka, and Moucha 2014).

1.3.3 Rationale for antimicrobial uncemented prosthesis

The opportunity of adding antibiotics to PMMA bone cement has allowed the treatment and prevention of infections post joint replacement surgery through a local delivery instead of through systemic administration of antibiotics. This opportunity is not available in un-cemented prosthesis Despite the previously numerous benefits of un-cemented joint replacements, their instability was a major drawback that prevented the diffusion of these devices (Maggs and Wilson 2017). Modern designs have solved this problem hence the research focus has shifted towards providing antimicrobial activity. For example, vancomycin covalently bound to TiO rods strongly inhibited colonization and biofilm formation, the modified titanium surface exhibited potent antibacterial activity after pre-incubation for 45 days (Antoci et al. 2007). Similarly, gentamicin was deposited onto titanium devices but provided antimicrobial activity for a shorter period of time than antibiotic loaded bone cement 4 days and 7 days, respectively (Neut et al. 2011).

Implant coating with antimicrobial agents seems to be the most preferred option, there are two key considerations: the implant should demonstrate excellent antimicrobial activity and does not negatively affect tissue fixation / osseointegration process. Research has been focusing on RGD-containing peptide (Chua et al. 2008; Rammelt et al. 2006) and hydroxyapatite (HA) (Havelin, Espehaug, and B Engesaeter 2002; Oosterbos et al. 2002), which has shown to promote bony ingrowth (Alt et al., 2011). Meanwhile, studies on antimicrobial coating for prosthesis are in a great range, as summarized in Table 5. Aside from antimicrobial activity and degree of osseointegration, there are more criteria to be fulfilled, including excellent biocompatibility, mechanical resistance, and duration of antimicrobial activity (Alt 2017). The latter is generally controlled by constructing a system which can release antimicrobial agent in a suitable / controlled manner.

Table 5. Antimicrobial agents loaded in prosthesis coating. (Alt 2017)

Type	Compound
Inorganic	Silver nanoparticle
	Titanium dioxide
	Selenium

	Copper
	Zinc
Organic	Chitosan derivative
	Microbial peptides
	Cytokines
	Cationic biopolymers
Other	Lytic bacteriophage

1.3.3.1 Controlled release

Antimicrobial coating for prosthetic surface should be able to release the drug in a controlled manner to ensure optimum anti-infective activity in a determined period (Getzlaf et al. 2016). This is of the greatest importance since the failure to carry those tasks might potentially lead to development of antimicrobial resistance (Getzlaf et al. 2016). Although there is no 'gold standard' for local antibiotic release from antibiotic-coated prosthesis to date, antimicrobial activity should last for the lifetime of the device, roughly 20 years (Raphel et al. 2016) or at least over the critical period after implantation (e.g. 1 year) (National Joint Registry 2018). The risk of prosthesis revision due to infection is the highest during the first year following surgery but fall in subsequent years (National Joint Registry 2018). Controlled release of antibiotic can be assumed as two time-framed strategy (Raphel et al. 2016): (1) early manifestation, in the first 3 months, (2) late infection which commonly occurs more than 3 months or even several years post-implantation. A number of studies revealed that *S. aurerus* infections tend to occur in the first 3 months, while other, less virulent bacteria, such as coagulase-negative staphylococci and *P. acnes*, typically attack during the late period (Del Pozo and Patel 2009).

Local antibiotic delivery for preventing PJI should be able to be released in several weeks or months depending on the vehicle / carrier (Williams, Mihok, and Murray 2016). Yet no single anti-infective prosthesis that can achieve such goal is available in the market, for example a gentamicin-containing coating for uncemented implant showed relatively short release, about 99% in 24 hours (Alt et al. 2011). Another type of coating for uncemented prosthesis was shown to sustain antimicrobial activity of gentamicin up to 4 days (Neut et al. 2011). Therefore, it is clear that a more reliable system is required to allow prolonged release of antimicrobial agent.

Controlled release of small anti-infective agents can be achieved by using biodegradable polymers such as polyglycolic acid (PGA), polylactic acid (PLA), and chitosan (CS) for coating materials (Alt 2017), poly-beta-amino esters, a class of synthetic polyelectrolytes, have also been employed in LbL coating entrapping gentamicin and providing prolong antimicrobial activity (Chuang, Smith, and Hammond 2008; Wong et al. 2010).

1.3.3.2 Cytocompatibility

Negligible cytotoxicity towards osteoblast cells cannot be compromised for uncemented antimicrobial prosthesis. Earlier, silver (Ag) was used to be incorporated into prosthesis coating. However, cytotoxicity possessed by Ag limited its utility (Getzlaf et al. 2016). Alternative antimicrobial metals including copper, and zinc has been applied to overcome the poor biocompatibility possessed by silver (Raphel et al. 2016). These two agents were incorporated into Titanium nanotubes and showed good cytocompatibility and bactericidal properties, as indicated by osteogenic markers (osteocalcin, osteoprotegerin, collagen I) and the limited growth of *S. aureus* (Raphel et al. 2016). Zinc ion has gained more interest as the alternative for silver because zinc ion is bactericidal and is one of the minerals required for bone formation (Raphel et al. 2016).

1.3.3.3 Antimicrobial susceptibility

The most common PJI-causing bacteria is *Staphylococcus aureus* and *Staphylococcus epidermidis*, contributing for over 60% of PJI cases (Gallo, Holinka, and Moucha 2014). The National surveillance for England reported that 8% of PJI cases detected in 2010/11 were due to methicillin-resistant *Staphylococcus aureus* (MRSA), which has dropped from 25% in 2006 (Lamagni 2014). The remaining PJIs were caused by coagulase-negative staphylococci (31%), enterococci (12%) and *Escherichia coli* (7%), *Enterobacter* (7%), *Pseudomonas* (7%), and streptococci (7%); furthermore over a quarter were polymicrobial infection (Lamagni 2014).

While in the UK the rate of PJIs caused by MRSA has decreased in recent years, the global trend is instead increasing steadily, particularly in the United States (Gallo, Holinka, and Moucha 2014). Moreover, the growing incidence of antimicrobial resistance causes difficulty of designing treatment and antibiotic choice (Getzlaf et al. 2016). The problem is even more complicated in polymicrobial infection due to remarkably variable susceptibility (Getzlaf et al. 2016). Therefore, antimicrobial

susceptibility is critical to prevent PJI-related morbidity (Gallo, Holinka, and Moucha 2014). A susceptibility assay should be conducted for anti-infective orthopaedic prosthesis to ensure an effective prophylactic treatment (Molina-Manso et al. 2012).

The threat of multi-drug resistance has driven research to explore highly susceptible alternative anti-infective agents (Williams, Mihok, and Murray 2016). For instance, chitosan has gained profound interest due to its antiseptic property and ability to promote cell growth and chitosan has been used as implant coating material loaded with antibiotic such as gentamicin (Williams, Mihok, and Murray 2016), chlorhexidine ((Riool, Dirks, et al. 2017), and tetracycline (Cai et al. 2016). Alternatively, existing anti-infective agents can be used simultaneously to achieve synergistic effect; the combination of antibiotic and anti-inflammatory drug, gentamicin and bupivacaine, exhibited better antimicrobial activity towards *Staphylococcus aureus* (P. et al. 2014). Antimicrobial peptides derived from eukaryotic and prokaryotic organisms are currently being studied as anti-infective coating material in combination with hydroxyapatite (Riool, de Breij, et al. 2017; Taha et al. 2018).

1.4 Layer by Layer Technique for prosthetic coating

In many cases, burst release is not favourable due to the risk of toxicity and short duration of action (Smith et al. 2009). Most of the anti-infective coatings for implant surface has diffusion-controlled release with high release rate (Hsu, Park, et al. 2014); these systems are often sophisticated for high-scale manufacture (Hsu, Hagerman, et al. 2014; Wong et al. 2010). The LbL technique has been developed to overcome such problems. The use of LbL technique for prosthetic coating has been covered in various studies. Polyelectrolyte multilayers can be applied on various surface including metal and plastic (Etienne et al. 2004). Gentamicin was successfully deposited onto the surface of orthopaedic implant using LbL technique with ten bilayers consisting of N,N-dodecyl, methyl-poly(ethyleneimine) as polycation source and poly(acrylic acid) as polyanion; nearly 70% of gentamicin was released in the first 3 days but sustained for more than 4 weeks (Wong et al. 2010). 40 bilayers of poly(L-glutamic acid)-triethylene glycol-based LbL films have successfully controlled the release of diclofenac, a small molecule, up to 14 months (Hsu, Park, et al. 2014). Therefore, the challenge of developing antibiotic coatings with multi-months-sustained release could be met using LbL technique.

1.4.1 Underlying principles of layer-by-layer technique

Layer-by-layer (LbL) is a self-assembly technique employed to produce coatings and requires polyelectrolyte solutions of opposing charges (Figure 12). For instance, after each layer of a polyanion is deposited a polycation layer follows. The layers are bound to each other via electrostatic interactions and active compounds have been successfully entrapped between layers (Chuang, Smith, and Hammond 2008; Hammond 2012; Macdonald et al. 2011; Smith et al. 2009; Wong et al. 2010). Recently, the multilayer build-up can be performed by using an automatic slide stainer for laboratory scale. Such instrument is equipped with a number of liquid staining baths and can be programmed so that a substrate (i.e. a metal coupon) is submerged with alternate solutions of polyelectrolytes for a certain period (Chuang, Smith, and Hammond 2008). Before coating with subsequent a layer (oppositely charged solution), the slide is washed in a water rinsing bath.

The challenge of achieving high loading efficiency and controlled release from medical devices using LbL technique, however, remains an issue to be tackled. Direct incorporation of poorly charged molecules is difficult and thus further strategies are required (Hsu, Park, et al. 2014). Secondly, extensively prolonged release is most likely achievable when a high number of layers are used, which implies that an enormous amount of materials is needed (Hsu, Park, et al. 2014).

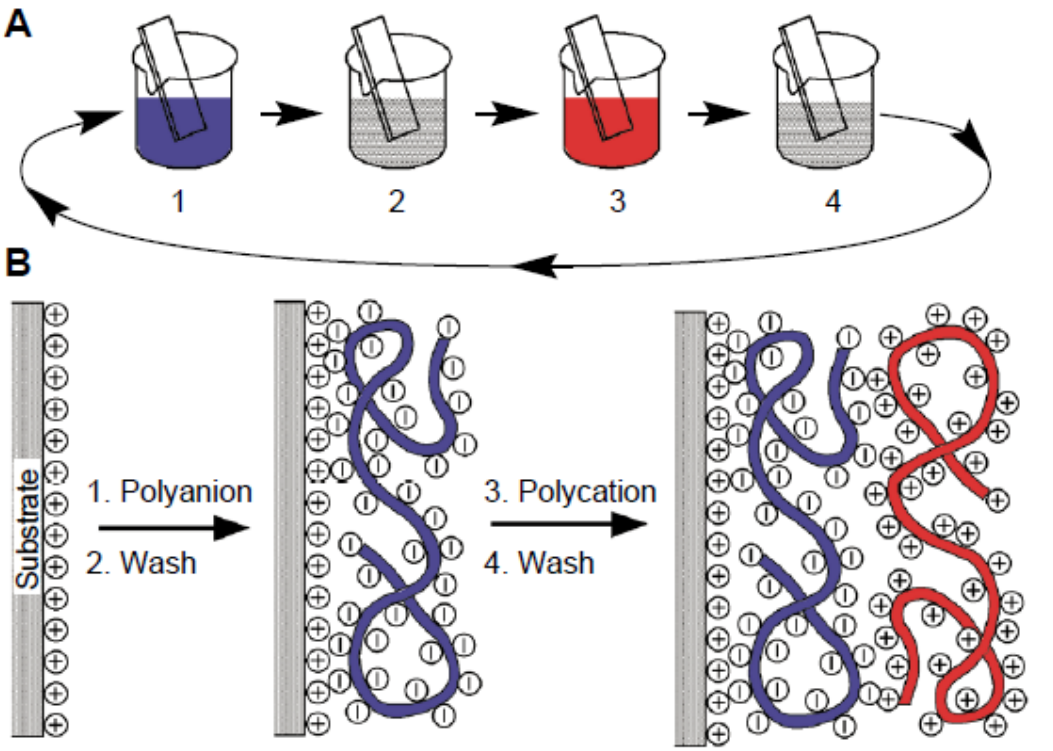

Figure 12. Formation of polyelectrolyte layers in LbL coating (A): polyanion coating, water rinsing, polyanion coating, subsequent water rinsing. The multilayer build-up is stabilized via electrostatic interaction (B). Figure adapted from Decher (1997).

1.4.2 Controlled release by layer-by-layer coating

Drug release profile from LbL coating was found to be controlled by layer erosion/degradation (Smith et al. 2009). Upon contact with body fluid, LbL films are eroded via hydrolytic mechanism under physiological condition and the entrapped drug is then eluted (Chuang, Smith, and Hammond 2008). The schematic illustration of drug release from LbL film is shown in Figure 13.

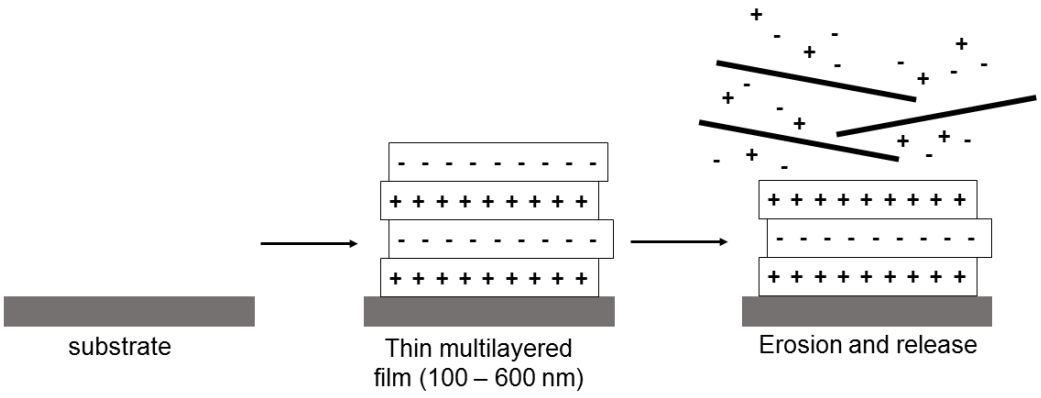

Figure 13. Erosion of the polyelectrolyte layers causes release of entrapped drug. Figure adapted from Cai et al. (2005).

Prolonged drug release from LbL coatings consisted of charged cyclodextrin as the anionic carrier and poly(β-amino esters) (PBAEs) as the polycation lasted up to 17 days; moreover, the release kinetic was not affected by the active compound loaded (Smith et al. 2009). In addition, the release kinetic can be tailored by selecting the most suitable polymers, optimising the number of polyelectrolyte layers and the concentration of polymers/polyelectrolytes, and modifying binding affinity of polyelectrolytes (Getzlaf et al. 2016; Etienne et al. 2004). Some of the polymers that have been used as the building block of polyelectrolyte layers are summarized in Table 6.

Table 6. Polycation and polyanion combinations in Layer-by-Layer antimicrobial coating for Joint Prosthesis.

Polycation	Polyanion	Antimicrobial agent	Number of layers	Release Time	Reference
Polyethyleneimine (PEI), poly(allylaminehydrochloride) (PAH), poly(L-lysine) (PLL)	poly(sodium 4-styrenesulfonate) (PSS), poly(L-glutamic acid) (PGA)	Defensin	10	Data Not Available	Etienne et al. (2004)
N,N-dodecyl,methyl-poly(ethyleneimine)	Poly(acrylic acid) (PAA)	Gentamicin	data not available	4 weeks	Wong et al. (2010)
LPEI, Poly(*β*-amino esters) (PBAE)	PSS, Hyaluronic acid (HA)	Gentamicin	100	10 hr	Chuang, Smith, and Hammond (2008)

In general, small molecule release from LbL films exhibits dual phase pattern (Chuang, Smith, and Hammond 2008; Wong et al. 2010; Hsu, Hagerman, et al. 2014); and follows pseudo first-order kinetic (Hsu, Hagerman, et al. 2014; Tamanna, Bulitta, and Yu 2015). Figure 14 represents the dual phase release pattern. During hydrolysis, polymer erosion is taking over and the chain length of the polymer decreases; consequently, the molecular weight changes over time and the mobility of the polymer increases (Siepmann et al. 2004; Klose et al. 2008). Drug molecules can diffuse more easily as the polymer chains are shortened and thus the diffusion constant increases as the molecular weight of the polymer changes (Siepmann et al. 2004; Klose et al. 2008).

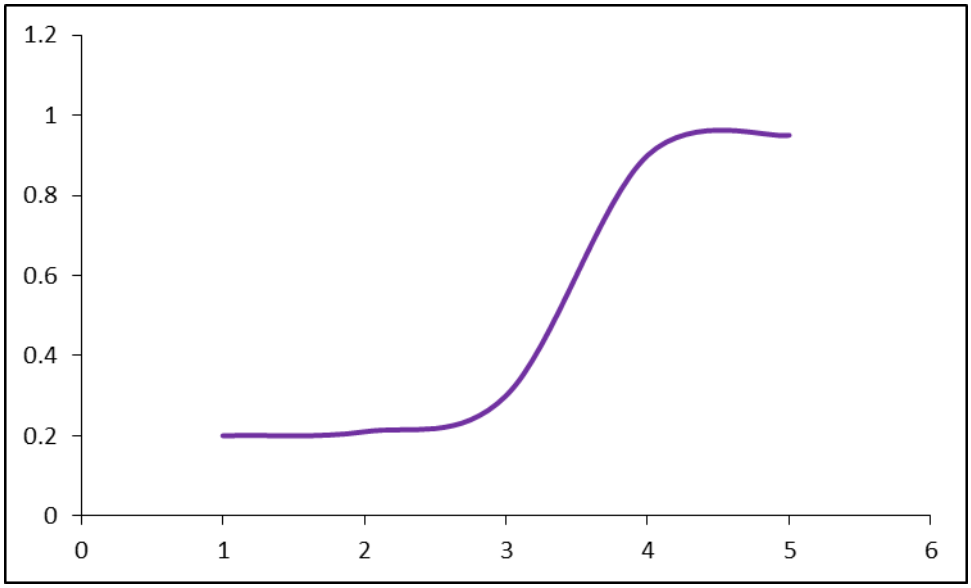

Figure 14. Example of dual phase release kinetic.

The relationship between drug diffusion and molecular weight change in pseudo first-order kinetic is described in Equation 1,

$$\boldsymbol{D(M_w) = D_0 + \frac{k}{M_w}} \qquad (1)$$

where D_0 is the initial diffusion coefficient of the drug at t = 0, k is a constant, and M_w is the molecular weight of polymer (Siepmann et al. 2004). The change in M_w during polymer erosion is described in Equation 2,

$$\boldsymbol{M_w(t) = M_{W0}.\exp(-k_{degr}.t)} \qquad (2)$$

where $M_{w(t)}$ is the molecular weight of polymer at time = t, M_{w0} is initial molecular weight, and k_{degr} is the degradation rate constant of the polymer (Siepmann et al. 2004; Klose et al. 2008).

In the first phase of antibiotic release from LbL multilayers, the drug diffuses out rapidly from the film; antibiotic release is also encouraged mainly by destabilization of LbL films. These events lead to initial burst release of antibiotic up to 80% in the first few period (can last for hours or days depending on the film ingredients) (Chuang, Smith, and Hammond 2008) and film hydrolysis does not contribute substantially to the release of drug in this stage. In the second stage, antibiotic diffuses out from uneroded film and is released on a relatively slower rate (Chuang, Smith, and Hammond 2008). This event is followed by erosion of LbL films due to hydrolytic degradation, during this stage the drug is released at a rate that diminishes over time (Chuang, Smith, and Hammond 2008).

Antibiotic release from LbL coatings can be prolonged for several days, weeks, or months depending on the number of layers, polymer type and concentration (Chuang, Smith, and Hammond 2008). Incorporation of gentamicin into LbL films with ten bilayers consisting of N,N-dodecyl,methyl-poly(ethyleneimine) as polycation source and poly(acrylic acid) as polyanion source exhibited 70% release in the first 3 days but sustained for more than 4 weeks (Wong et al. 2010). Forty bilayers of poly($_{L}$-glutamic acid)-triethylene glycol-based LBL films have successfully controlled the release of diclofenac for 14 months (Hsu, Park, et al. 2014).

The major problem of controlling release rate of antibiotic from LbL film is that antibiotic can rapidly diffuses towards the outermost layer of LbL during preparation, causing accumulation of antibiotic on the surface of LbL films, consequently, burst release is inevitable (Chuang, Smith, and Hammond 2008). This explains typical dual phase in release kinetic of antibiotic from LBL films (Hsu et al., 2014).

1.5 Aseptic Loosening

Aseptic loosening is a major cause of revision surgery after joint arthroplasty (National Joint Registry 2018). Because of the different definitions and methods of diagnosing loosening in the literature, the exact percentage of aseptic loosening is difficult to define. In general, aseptic loosening refers to the failure of the bond between an implant and bone which results in micro- or macro-motion of the implant relative to the adjacent bone (Abu-Amer, Darwech, and Clohisy 2007). Aseptic loosening is complicated to diagnose, especially if it is in sub-millimeter range (Claassen et al. 2014; Reish et al. 2006). To find out whether an implant is loose, various surrogate measures, such as increased uptake on bone scan or radiolucent lines adjacent to implants are normally

used (Nam, Barrack, and Potter 2014). However, these measures' interobserver agreement and their accuracy limits are unknown (Reish et al. 2006).

Failure of primary ingrowth of bone into the prosthesis, wear debris induced osteolysis or bad technique of cementing may cause loosening to occur (Abu-Amer, Darwech, and Clohisy 2007). On the other hand, mechanical overload, physiologic bone resorption, or a combination of both at the bone–implant interface can cause loosening of a previously solidly fixed implant to occur months or years after implantation. Hence, clinical presentation of loosening varies, ranging from no pain to persistent pain commencing instantaneously after joint arthroplasty, to late-onset pain starting several months or years (Sundfeldt, Carlsson, et al. 2006). Detection of a partially lose implant may complicate matters further. While joint arthrodesis often have bone-to-bone healing across only a portion of the joint surface, bone ingrowth may occur only over a segment of the bone–implant interface, as shown by recent computed tomography (CT) scan studies (Makino et al. 2018). Depending on the location and amount of ingrowth present, the bone may not fix to a sufficient portion of the implant, thus creating a cantilever effect, akin to a diving board, where one side of the implant is stable, but the other side experiences micromotion (Penner M.J., Almousa S.A., and Kolla L.). These complexities make understanding aseptic loosening very challenging (Thienpont 2016).

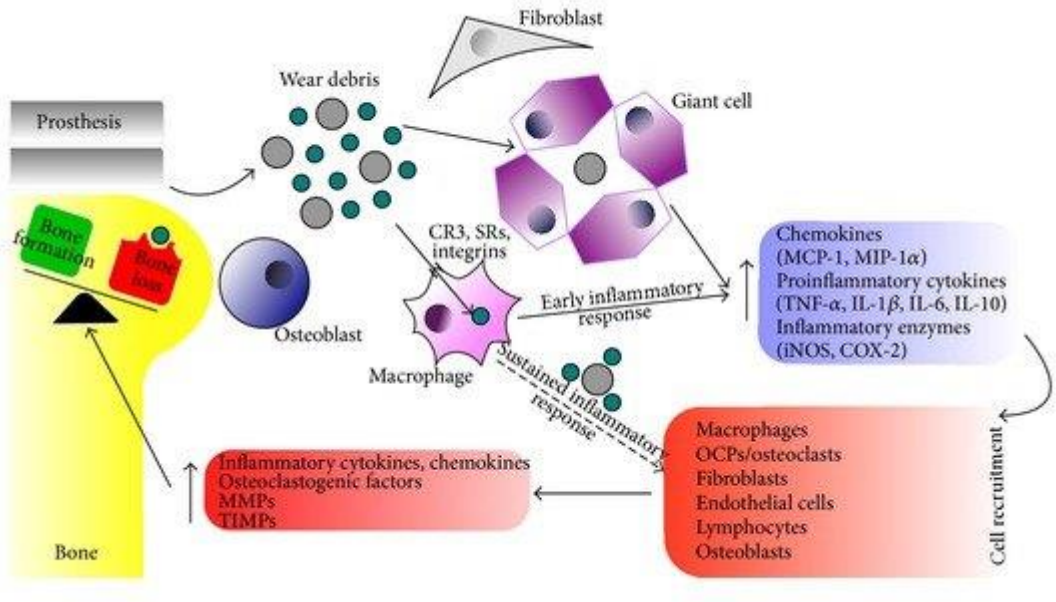

Figure 15. Schematic representation of periprosthetic loosening and osteolysis.

1.5.1 Biologic response to wear debris

The role of particulate debris in periprosthetic bone loss was first recognized by (Willert and Semlitsch) in 1977 and has been studied extensively ever since. Biologic response to wear particles is now the currently accepted leading cause of periprosthetic osteolysis and aseptic loosening of prosthetic hip and knee implants (Ren et al. 2013; Sundfeldt, Carlsson, et al. 2006; Abu-Amer, Darwech, and Clohisy 2007).

As shown in Figure 15, implant-derived wear debris induces an early fiery response from the inhabitant or invading macrophages within the periprosthetic tissue. Small particles are phagocytosed, though the bigger induce fusion of macrophages and gaint cell arrangement. Activated macrophages release proinflammatory cytokines, chemokines, and enzymes that recruit different cell types inside periprosthetic tissue, which are further activated by the particles resulting in sustained irritation, increased secretion of cytokines/chemokines/osteoclastogenic factors/MMPs/TIMPs, and osteolysis (Syggelos et al. 2013).

Polyethylene liners, metal components, and cement all are subjected to wear and produce wear particles (Kretzer et al. 2014). Of these, polyethylene particles are the most important in the pathogenesis of osteolysis (Catelas, Wimmer, and Utzschneider 2011). The host biologic response is affected by particle type, concentration and size; a "critical size" in the range 0.3 to 10.0 μm, causes particles to trigger a macrophage-based inflammatory response (Green et al. 1998). Critical-sized wear particles are phagocytized by macrophages, which in turn trigger a cascade of intracellular reactions leading to the production of inflammatory mediators, including tumor necrosis factor (TNF)-α, interleukin (IL)-1, IL-6, and macrophage colony-stimulating factor (M-CSF) (Green et al. 1998). Fibroblast proliferation, tissue fibrosis, and activation of osteoclasts are induced by IL-6 and TNF-α which leads to extensive periprosthetic bone resorption (Kobayashi et al. 2000; Lam et al. 2000; Cenni et al. 2002; Cochran and Finch-Arietta 1992; Udagawa et al. 1995; Yoshitake et al. 2008). The concept of effective joint space, that is the space surrounding the prosthetic joint encompassing all of the implant–bone surfaces through which synovial fluid can flow and disperse wear particles explains how wear particles reach areas distant from the articular surface (Schmalzried, Jasty, and Harris 1992).

In this regard, it should be noted that differentiation of bone marrow macrophages (osteoclast precursors) into mature osteoclasts requires recognition and binding of the osteoblast, fibroblast, and T cell secreted factor Receptor activator of nuclear factor-kappa B ligand (RANKL) by its cognate receptor, RANK, which is expressed on the

surface of osteoclast precursors (Dougall 2012). This process is regulated by another factor secreted by osteoblasts, namely OPG, which acts as a decoy receptor by binding to RANKL and reducing its bioavailability (Dougall 2012). On the other hand, binding of RANKL to RANK prompts induction of several intracellular pathways by this receptor, leading to activation of key transcription factors, most notably NF-κB (Wright et al. 2009) and TNFα (Luo et al. 2018).

The NF-κB family of transcription factors has been reported to be fundamental to pathologic responses and essential for osteoclast differentiation. It consists of several family members that primarily form heterodimers. These dimers are found bound to an inhibitory protein (inhibitor of NF-κB [IκB]) that, in the absence of stimulation, retains the complex in the cytoplasm. Stimulation by RANKL or other specific stimuli causes the upstream IκB kinases (IKKs) to be activated, which in turn causes the IκB to phosphorylate, leading to its dissociation from the NF-κB complex and eventually to its degradation by the proteosome system. IκB-liberated NF-κB then translocates to the nucleus, binds to specific DNA sites, and induces basal transcription (Oeckinghaus and Ghosh 2009; Dougall 2012; Kobayashi et al. 2000; Lam et al. 2000; Yoshitake et al. 2008).

1.5.2 Potential therapeutic intervention

The biologic mechanisms of debris-mediated osteolysis are complex and involve many cell types and inflammatory cytokines of the periprosthetic membrane (Cochran and Finch-Arietta 1992; Hartmann et al. 2017; Kobayashi et al. 2000; Lam et al. 2000). Therefore, in combination with improvements in implant integration, strategies to target the cellular components (osteoblasts and osteoclasts) that contribute to implant failure represent potentially effective therapeutic interventions (Apostu et al. 2018).

Several approaches that utilize knowledge of the inflammatory pathways leading to osteoclasteogenesis have been designed to perturb these pathways and hence alleviate the deleterious effects of inflammatory osteolysis (Abu-Amer, Darwech, and Clohisy 2007). Considerations have been given to a number of approaches to osteoclast-based therapy; the first involves targeting osteoclast precursor cells, which are recruited to inflammatory sites by circulating cytokines. The second entails targeting precursors that are stimulated by the particle-mediated cellular response to differentiate and form bone resorbing osteoclasts. The third approach involves targeting activation mechanisms of mature osteoclasts (Abu-Amer, Darwech, and Clohisy 2007).

There are various approaches to inhibit precursor cells from differentiating to osteoclasts. First and foremost, direct inhibition of osteoclast differentiation may be achieved by application of RANKL decoy molecules such as osteoprotegerin (OPG) (Luan et al. 2012; Kong et al. 1999) and the soluble fusion protein RANK-Fc.(Miller et al. 2007) Indeed, in vitro osteoclast cultures and studies in animal models and have identified significant inhibition of osteoclastogenesis and reduced hallmarks of osteolysis.(Simonet et al. 1997; Bucay et al. 1998) Other approaches include targeting key intracellular signal transduction pathways that are essential for osteoclast differentiation and inflammation. The core of this process is the transcription factor NF-κB which is essential for both inflammatory and osteolytic responses; for example transduction of a dominant-negative form of the NF-κB inhibitory protein, IκB, which retains NF-κB in the cytoplasm, was sufficient to block the formation and activity of osteoclast.(Abbas and Abu-Amer 2003) Another possible approach is to block the upstream IKK complex from activating, which is responsible for phosphorylation of IκB and subsequent activation of NF-κB.(Israël 2010) This was done by introducing a small peptide that perturbs assembly of the IKK complex and attenuates activation of NF-κB.(Dai et al. 2004) More importantly, administration of the dominant-negative IκB protein or the IKK inhibitory small peptide to arthritic mice was found to significantly block bone erosion associated with inflammatory arthritis and particle-induced osteolysis of calvaria in the mice.(Dai et al. 2004) Since NF-κB is central to most host immune and inflammatory responses and induces expression of a large number of genes encoding proteins that are associated with bone pathology, efforts have been directed toward identifying specific NF-κB-mediated genes and their products. Steps in this direction should lead to the design of a future generation of selective inhibitors that may be effective in alleviating inflammatory bone loss (Lin et al. 2017; Sundfeldt, V Carlsson, et al. 2006).

The use of anti-inflammatory approaches to neutralize mediators such as TNF, IL-1, IL-6, and others are required in inhibiting recruitment of osteoclast precursor and other cells to the inflammatory site. It has been proposed that pharmacologic interventions targeted at macrophages may provide the means to slow the response to wear debris.(Schwarz, Looney, and O'Keefe 2000; Ren et al. 2013) Indeed, inflammation in the periprosthetic tissue may be reduced by local cytokine inhibition, along with several biologic mediators identified as useful for clinical application. In particular, the IL-1 receptor antagonist protein has been reported to reduce inflammation,(Arend and Gabay 2000) and the anti-inflammatory cytokine IL-10 appears to able to reduce cell mediated

reactions in inflammation.(Naiyer et al. 2013) Considering the use of particle-stimulated murine air pouch and calvarial models for the evaluation of the potentials of gene therapy to treat orthopedic wear debris inflammation, recent studies have shown that retroviral vectors that encodes human IL-1 receptor antagonist, human TNF receptor, and viral IL-10 led to significant decreases in inflammation, decreased fluid accumulation in pouches, and reduction of macrophage influx.(Sud et al. 2001) In the murine air pouch study, histologic assessments revealed that a 40% reduction in inflammatory cell infiltration was exhibited in pouches transduced with viral IL-10 or IL-1 receptor antagonist when compared with nonviral controls or LacZ transduced membranes. These findings were reproduced in rabbit knees (Lechman et al. 1999; Keravala et al. 2006)

Useful molecular targets could be unveiled by clarifying the molecular mechanisms underlaying the anti-osteoclastogenic actions of these anti-inflammatory cytokines. Therefore, recent reports have demonstrated some advancements in showing the anti-osteoclastogenic action of IL-4 and IFN-γ.(Amarasekara et al. 2018) Specifically, IL-4 docks on membrane receptors that are expressed on the osteoclast precursor surfaces, then it activates key transcription factors, particularly the signal transducer and activator of transcription (STAT6).(Xiong et al. 2014) The mechanism of action behind this involves the activation by IL-4 of Janus kinases, which phosphorylate STAT6, thus, prompting its dimerization and translocation to the nucleus, where it binds to DNA and regulates target genes.(Villarino et al. 2015) STAT6 was found to be crucial for the inhibition of osteoclastogenesis by IL-4 and inhibits inflammatory bone erosion hence STAT6 is a possible target for the design of anti-erosive drugs. (Abu-Amer 2001).

1.5.3 Anti-Inflammatory Coating

The reaction of immune system after transplantation of prosthesis usually induce ‘rejection’ since the implant is considered as foreign matter (Anderson, Rodriguez, and Chang 2008). The addition of immunosuppressant, an agent that can slow down this defense reaction, can ultimately help to boost osseointegration process (Dawes et al. 2010). Therefore, the addition of anti-inflammatory agent such as corticosteroid or glucocorticoid that can act as immunosuppresant onto the coating layer for prosthetic device is beneficial.(Boehler, Graham, and Shea 2011; Dumont, Park, and Shea 2015) Dexamethasone, a glucocorticoid that interferes with NF-κB and AP-1, the main

inflammatory regulators, has been widely used as immunosuppressive agent for diseased soft tissues following organ transplant.(Coutinho and Chapman 2011)

1.5.4 Clinical Outcomes for Post-operative Inflammatory Management

Post-operative inflammatory management affects the clinical outcomes of surgical procedures, particularly for mobilization and functionalization of newly-implanted artificial joint (Anastase et al. 2014). Studies revealed that administration of dexamethasone as infiltration resulted in low severity of pain based on lower visual analogue scale (VAS) pain score, serum level of C-reactive protein (CRP), and IL-6.(Ikeuchi et al. 2014) Moreover, early mobility has been achieved two days post-operation when steroid anti-inflammatory was administered following the joint replacement (Ikeuchi et al. 2014). However, this administration technique only lasts for a few days, whereas encapsulation of anti-inflammatory agent into the surface of prosthesis can enhance the effect ten times longer (Dawes et al. 2010).

However, anti-inflammation agent has immunosuppressive activity, which is resulted from repressed transcription of genes that encode cytokines and chemokines that favours inflammation, and cell adhesion (Coutinho and Chapman 2011). Consequently, subjects that are given immunosuppressive agent after orthopedic procedure are in higher risk of developing infection, delayed wound healing, and slow rate of osseointegration (Scanzello et al. 2006). Moreover, long term use of TNF-α antagonist, a subclass of immunosuppressive agents, after orthopedic procedure for 30 days was reportedly to cause postoperative septic failure (Scanzello et al. 2006).

1.5.4.1 Effectivity of Anti-Inflammatory Coating

In order to achieve anti-inflammatory effect, the amount of anti-inflammatory agent released at all times must be within therapeutic range. Single dose of dexamethasone via intravenous route usually require 8 mg for post-operative inflammatory management (Anastase et al. 2014). Local injection containing 6.6 mg of dexamethasone into periarticular tissue has been shown to reduce local inflammation after total knee arthroplasty (Ikeuchi et al. 2013). The amount of dexamethasone required to be incorporated into prosthesis coating layer remains unknown and needs to be studied. In a study conducted by Dawes et al. (2010), 80 mg dexamethasone was coated onto Ti-6Al-7Nb alloy microspheres in combination with poly (lactide-co-glycolide (PLGA). Around thirty percent of dexamethasone was release within the first 60 minutes but 90% of the

drug was released in 23 days (Dawes et al. 2010). However, the anti-inflammatory effect that can be demonstrated by this system has not been studied.

1.6 Aims and Objectives

The antimicrobial agent needs to be released in a controlled manner so that a sufficient concentration of antimicrobial agent can be reached at all times to prevent biofilm formation during osseointegration process. Furthermore, another adverse event related to joint replacement is aseptic loosening; evidence revealed that anti-inflammatory drugs can reduce the risk such occurrence. In this study, simultaneous antibacterial and anti-inflammatory coatings were developed on model titanium alloy implant surfaces. These coatings were built employing LbL technique incorporating both an antimicrobial agent (chlorhexidine diacetate) and an anti-inflammatory drug (dexamethasone) between polyelectrolytes layers of alginate and poly-beta amino esters.

Chlorhexidine has been chosen in this study because this compound is a first-line topical antiseptic that has demonstrated to be highly effective to treat skin and soft-tissue infections caused by a broad range of bacteria, including methicillin-resistant *Stapylococcus aureus/*MRSA (Schlett et al. 2014). Long-term use of chlorhexidine has been established in many hospital settings therefore it is expected that chlorhexidine coatings on orthopedic prosthesis will not cause unwanted effects for the lifetime of the device. Dexamethasone has been chosen because it has both anti-inflammatory and immunosuppressive effect, which has positive impact on osseointegration (Coutinho and Chapman 2011). Other glucocorticoids including prednisolone and methyl-prednisolone are possible to use for their anti-inflammatory and immunosuppressive action but dexamethasone has greater bioavailability and it is retained in the body fluid for a longer period (Coutinho and Chapman 2011). The coating method in this study relies heavily on electrostatic interactions hence, the water-soluble form of drugs, which will largely dissociate into charged ions are used: chlorhexidine diacetate (CHX) and dexamethasone sodium phosphate (DEX-P).

A number of characterisations of developed system/coating were conducted:

- physico-chemical (TGA, TEM, zeta potential determination, particles size measurement);
- release profile of active molecules;
- antimicrobial activity testing;
- anti-inflammatory activity testing;

- cytocompatibility;
- durability and stability properties of the coatings.

1.7 Hypothesis

Several hypotheses for these studies were suggested:

- the number of polyelectrolyte layers will influence the physicochemical properties of the coating layer, drug release profile, the antibacterial effect and anti-inflammatory effect;
- drug release profile from the coating system will be controlled by layer erosion mechanism and follow zero-order kinetic model;
- no detrimental effects on titanium cytocompatibility will be caused by the coatings;
- both drugs will retain efficacy once released from the coatings.

Chapter 2: General Materials and Methods

This chapter refers to some of the common methods that have been used for the preparation of different titanium nanoparticles and coupons and testing their properties throughout this thesis. Later chapters will refer to these methods to reduce repetition by highlighting main differences in nanoparticle and coupons coating. Test methods that are specific to certain chapters will be described in detail in the appropriate chapter**.**

2.1 Chemicals

Titanium (IV) oxide (Anatase, <25nm, 99.7%), 3-Aminopropyl-triethoxysilane (APTS, 99%), chlorhexidine diacetate (CL) (Figure 16), Dexamethasone sodium phosphate (DEX-P, >97%) (Figure 17), phosphate buffer solution (PBS) tablets, sodium acetate trihydrate (≥99%), disodium phosphate (ACS reagent, ≥99%), sodium alginate (ALG) (Figure 18) were purchased from Sigma-Aldrich, UK.

HPLC grade acetonitrile, Glacial Acetic Acid, and Toluene were purchased from Fisher, UK. All other chemicals were reagent grade, stored according to manufacturer's guidelines and used as received.

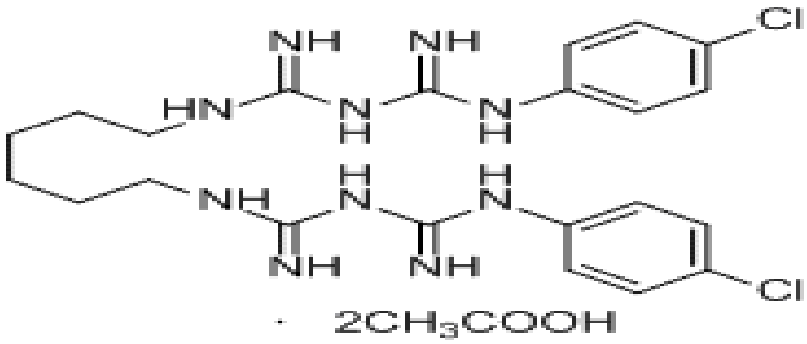

Figure 16. Chemical structure of chlorhexidine diacetate

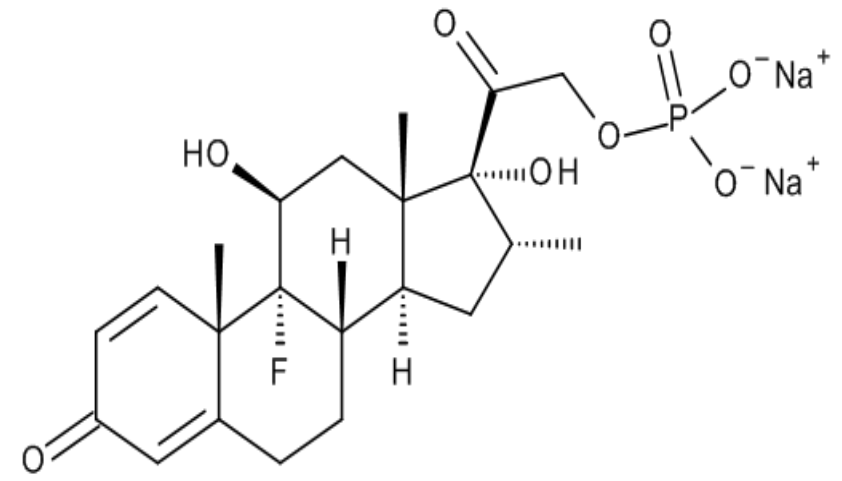

Figure 17. Chemical structure of Dexamethasone sodium monophosphate

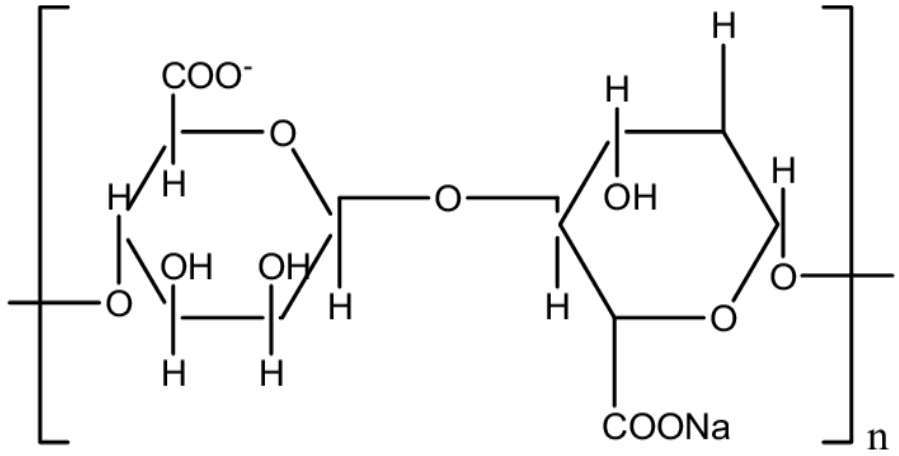

Figure 18. Chemical structure of Na alginate polymer

2.1.1 poly-beta-amino-ester synthesis

Amino-terminated poly(β-amino ester)s (PBAEs) (B1) a patented polymer were produced by mixing 1,6 hexanediol diacrylate and piperazine in a 1:1.1 ratio in DCM at a concentration of 5 ml of DCM for each 3.7 mmol of acrylate (Figure 19.a). The polymerization was performed under stirring at 50 C for 48 h. PBAEs was precipitated through pouring the mixture of the reaction in about ten times the volume of diethyl ether under vigorous mixing; the solvent was evaporated under vacuum. (Al Thaher et al. 2018).

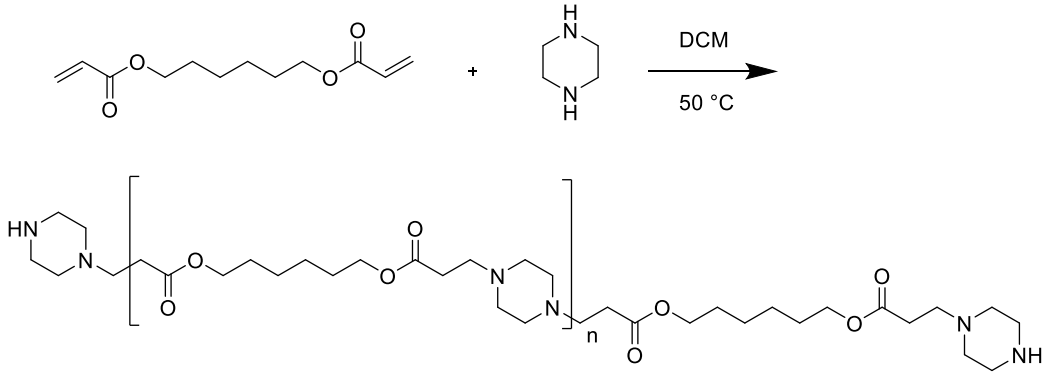

Figure 19. Synthesis of poly(β-amino ester)s using 1,6 hexanediol diacrylate and piperazine in 1:1.1 ratio in DCM.

By GPC, an average MW of B1 was determined to be 5600 kDa. This is confirmed with the patent data (Figure 20). Also, NMR has been conducted for B1, (Figure 21) represent an example of B1spectrum.

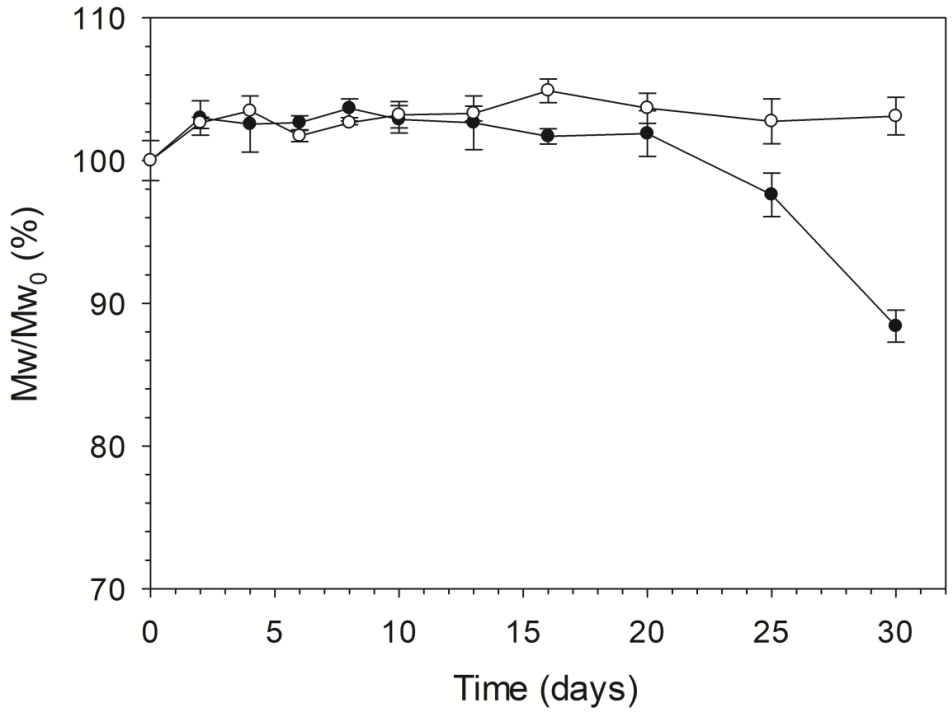

Figure 20. PBAE hydrolysis, B1 (mean ± SD n =3) at pH =7 (○) and pH =5 (●).

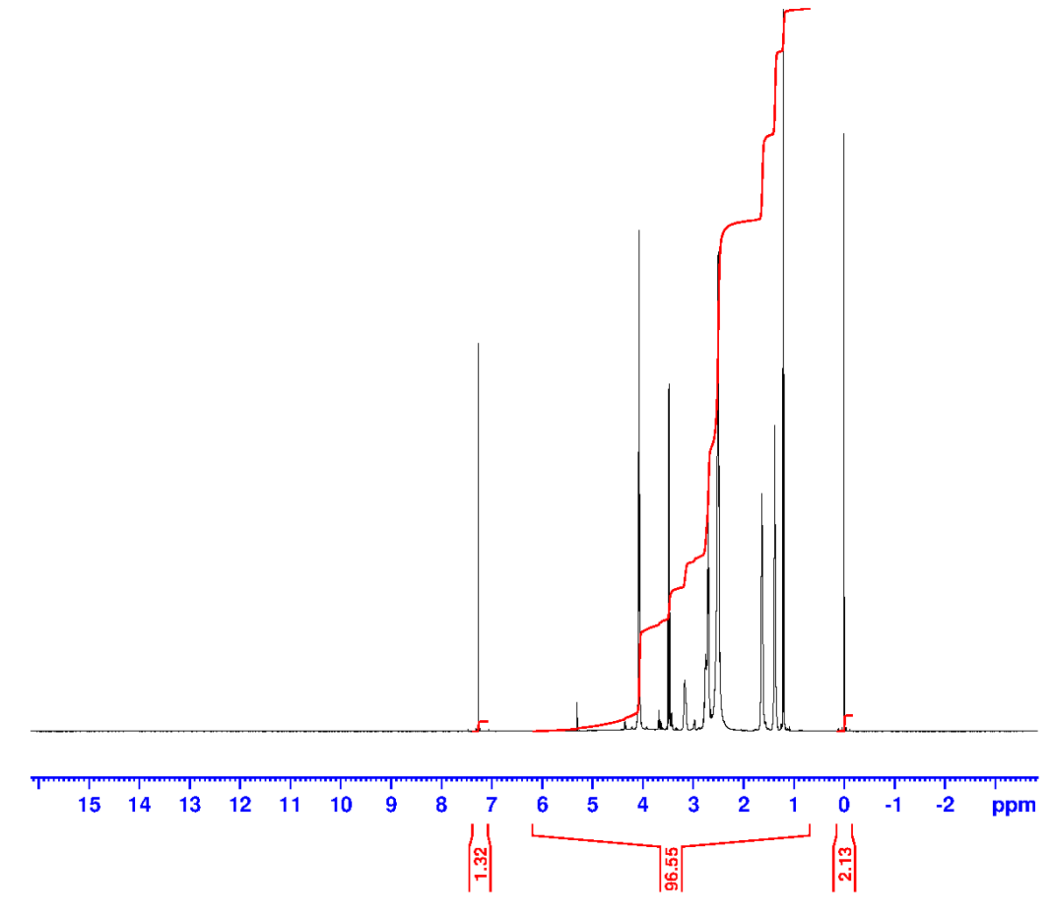

Figure 21. Example of NRM spectrum B1.

2.2 Nanoparticles preparation

2.2.1 Surface functionalisation of titanium nanoparticles

One gram of TiO_2 nanoparticles was dispersed in 15 mL of anhydrous toluene. 100 µl of APTS were added to the dispersion to functionalize the surface of TiO_2 nanoparticles. The dispersion was incubated for 24 hours at room Temperature under constant stirring. The amine functionalized TiO_2 (TiO_2-NH_2) nanoparticles were centrifuged at 14000 rpm and 20 °C for 5 minutes (LE-80K Ultracentrifuge, Beckman Coulter, UK). TiO_2-NH_2 nanoparticles were then redispersed in fresh toluene using a vortex mixer (WhirliMixer™, Fisherbrand, UK). Centrifugation and washing procedure were repeated for 3 times. After the final washing cycle, TiO_2-NH_2nanoparticles were collected and dried under fume hood for 24 hours.

2.2.2 Preparation of polyelectrolyte solutions

Polyanionic solutions were prepared by dissolving sodium alginate in acetate buffer 0.1 M, pH 5 (2 mg/ml). PBAE polymer (so called B1 polymer) was dissolved in acetate

buffer 0.1 M, pH 5 (2 mg/ml). Chlorhexidine diacetate and dexamethasone sodium phosphate (DEX-P) at a concentration of 10 mg/ml were separately dissolved in acetate buffer 0.1 M, pH 5. All solutions were stirred constantly using magnetic stirrer at 600 rpm for 2 hours at 20 °C.

2.2.3 Layer by layer (LbL) coating technique

TiO_2-NH_2 nanoparticles were coated with polyelectrolyte multilayers. The layers consisted of different numbers of repeating sequence as the following: ALG-CL-ALG-B1, ALG-B1-DEX-B1. One sequence containing these four layers were termed quadruple layer (Q).

TiO_2-NH_2 nanoparticles (250 mg) were placed into a test tube and with 20 ml of ALG (2mg/ml) solution. The mixture was homogenised for 10 min and the nanoparticles were collected by centrifuging at 5000 rpm, 20 °C for 2 minutes. The ALG-layered nanoparticles were washed with acetate buffer to remove the excess of ALG, centrifuged, and the supernatant removed. The second layer was applied onto ALG-layered nanoparticles by dispersing the nanoparticles in 10 ml of CL solution. The mixture was homogenised, centrifuged, and washed using a similar procedure to that for ALG layer. Polyelectrolyte coating, centrifugation, and washing steps were repeated for the third layer (ALG) and fourth layer (B1), resulting in the first quadruple layer. Layer-by-layer coating process was continued to achieve 10 quadruple layers. During the coating process, a small amount of coated nanoparticles were collected for evaluation: nanoparticles with one quadruple layer (Q1), three quadruple layers (Q3), five quadruple layers (Q5), seven quadruple layers (Q7), and ten quadruple layers (Q10). For DEX-coating, Layer-by-layer coating technique followed the previously mentioned steps except chlorhexidine solution was replaced with DEX.

After the final washing cycle, TiO_2-NH_2nanoparticles were collected and dried under fume hood for 24 hours.

2.3 Nanoparticles surface and material characterisation

2.3.1 Nanoparticles hydrodynamic size

The hydrodynamic size for the amino functionalized titanium nanoparticles and the LbL coated multilayer nanoparticles were measured by dynamic light scattering (DLS) using Malvern Zetasizer, Nano ZS particle characterization system (Malvern Instrument limited, UK). A 633 nm He–Ne laser with measurement angle of 17° was used to analyse the preparations. 1mg of nanoparticles was dispersed in 1mL of acetate buffer

pH 5, homogenised by vortex mixer and ultrasonic bath for 5min. The suspension was then transferred into square couvette.

2.3.2 Zeta potential measurements

The electrophoretic mobility of ALG, B1, chlorhexidine, DEX-P solutions and nanoparticles suspensions were determined with a Malvern Zetasizer, ZS particle characterization system (Malvern Instruments Limited, UK). Zeta potential (ζ) values were obtained from the Henry equation (Equation 1)

$$U_E = \frac{2\varepsilon\zeta f\mathrm{Ka}}{3\eta} \qquad (1)$$

where U_E describes electrophoretic mobility, ε denotes the dielectric constant, f (κa) is Henry's function, and η denotes viscosity. According to Smoluchowski´s approximation, the f(Ka) value was 1.5, a standard value for electrophoretic measurement in aqueous medium containing low concentration of electrolyte (Nita et al. 2013). Electrophoretic mobility was determined based on the measurement of velocity of particles within the fluid using Laser Doppler Velocimetry (LDV) technique. Following the washing step in each layer coating, 1mg of nanoparticles was dispersed in 1mL of acetate buffer pH 5, homogenised by vortex mixer and ultrasonic bath for 5min; for ALG, B1, chlorhexidine and DEX-P, the solutions used from LbL were employed. The suspension was then transferred into the capillary cell.

In each measurement, 1ml of the solution or suspension was placed into the capillary cell. The sample was irradiated and the ζ value was recorded. Measurements were performed in triplicate for each run and results are presented as the average ± standard deviation.

2.3.3 Transmission Electron microscopy – particle size determination

Images of particles were obtained using a Zeiss 902 transmission electron microscope (TEM) operating at a voltage of 80 kV. The aqueous dispersion of the particles was drop-cast onto a carbon-coated copper grid, and grid was dried at room temperature (20ºC) before loading into the microscope (direct deposition). The average particle size, size-distribution and morphology analysis of the samples was carried out from transmission electron micrographs using ImageJ for Windows (Version 1.50i).

2.3.4 Thermogravimetric Assay (TGA)

Thermogravimetric analysis (TGA) was performed using a Perkin-Elmer TGA 4000 instrument. Coated nanoparticles were initially weighed and heated from 50 to 750°C with a heating rate of 10 °C/min. Weight loss percentage of each sample at 100 °C and

750°C were determined relative to initial weight of sample. Organic and inorganic content was determined by subtracting the point at initial weight loss (%) up to when the line plateaus (approximately around 750°C).

2.3.5 Drug release study

Coated-particles were dispersed in two media, acetate buffer pH 5 and phosphate buffer pH 7 (10 mg/ml), and incubated statically at 37°C. The medium was withdrawn daily for quantification and the replaced with an equal volume of fresh buffer. All experiments were performed on 3 independent nanoparticles batches.

2.3.5.1 Drug concentration determination

The amount of chlorhexidine and DEX released from the coated nanoparticles was determined using reverse-phase High Performance Liquid Chromatography / with a Agilent Technologies® HPLC (1100 series) equipped with a Waters-Spherisorb ODS2 column (Pore size-80Å, 5 µm, and packing dimension of 4.6 mm X 150 mm). The injection volume was 10 µl in both cases. The quantification protocol for chlorhexidine used a mixture of acetate buffer-acetonitrile 58:42 as the mobile phase, flow rate of 1 mL/min, and a UV detector at 239 nm. Quantification procedure for DEX-P was as described in (Martín-Sabroso et al. 2013) using a mixture of PBS-acetonitrile-glacial acetic acid 70:26:4 as the mobile phase, flow rate of 1 mL/min, and a UV detector at 244 nm. Quantification procedure for DEX was adapted from (Martín-Sabroso et al. 2013) using the mobile phase mixture of PBS-acetonitrile-glacial acetic acid 70:26:4 as the mobile phase, flow rate of 1 mL/min, and a UV detector at 244 nm as retention times were ~4.5 min and ~18 min for DEX-P and DEX, respectively, and not overlapping of the two peak was observed.

Stock solutions of chlorhexidine, DEX-P and DEX with concentration of 1 mg/mL were prepared separately and a series of concentrations ranging from 0.4-25 µg/mL was prepared for calibration. A calibration curve that describes the relationship between peak area (mAu) and concentration of standard drug (µg/mL) was obtained for each drug from 3 independent stock solutions and the regression equation was derived (Figure 22, Figure 24).

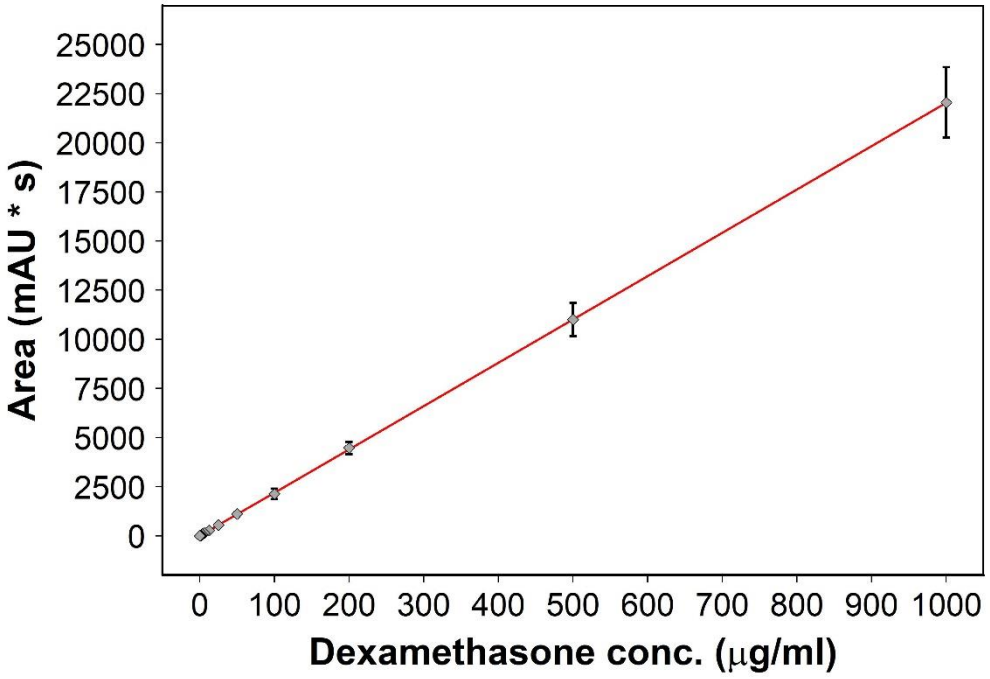

Figure 22. Calibration curve of dexamethasone employed (mean ± SD n =3).

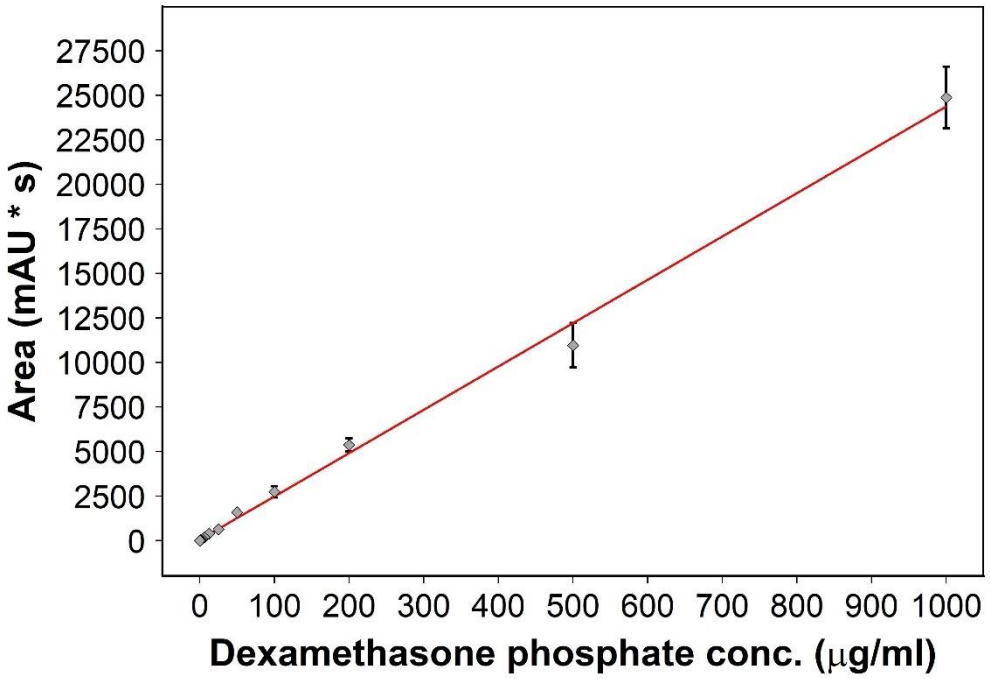

Figure 23. Calibration curve of DEX-P employed (mean ± SD n =3).

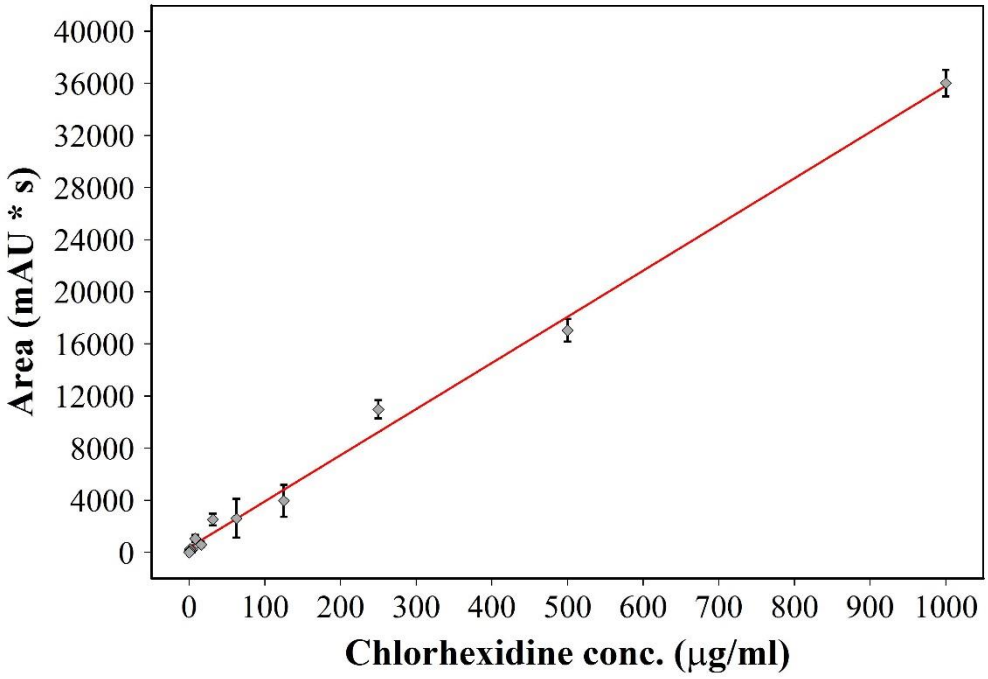

Figure 24. Calibration curve of chlorohexidine employed (mean ± SD n =3).

2.3.6 Drug loading estimation

The mass of DEX and chlorhexidine loaded into functionalized TiO_2 nanoparticles was estimated by analyzing the supernatant obtained during the centrifugation steps. The collected supernatant was analyzed using HPLC to measure the amount of DEX or chlorhexidine which was not loaded over the particles. DEX and chlorhexidine loading % were estimated based on the following equation (Papadimitriou and Bikiaris 2009).

$$\text{Drug loading (\%)} = \frac{initial\ drug\ mass - drug\ mass\ left\ in\ the\ supernatant}{initial\ particle\ mass} * 100$$

2.4 Antimicrobial testing

Brain heart infusion agar (BHI) was prepared by dissolving 47g of brain heart infusion agar powder in one litre of distilled water. The solution was shaken to suspend agar powder evenly, and then sterilized in an autoclave at 121 ºC for 15 minutes. The solution was allowed to cool to 50-55 ºC before being poured into Petri dishes (9 cm diameter). The Petri dishes were cooled to room temperature then stored at 8-15 ºC until use. BHI broth was prepared by dissolving 37g of BHI broth powder in one litre of distilled water, then sterilized in an autoclave at 121 ºC for 15 minutes. The sterilized broth was allowed

to cool to room temperature before being aliquoted into 15 ml sterile tubes and stored at 8-15 ºC until use.

Gram-positive bacteria methicillin-resistant *Staphylococcus aureus* (MRSA) 140, 924, and 275, *Staphylococcus epidermidis* 279, 189, 222, and *Enterococcus faecalis* along with Gram-negative bacterium *Acinetobacter baumannii* 640, 643, and 647, *Escherichia coli* were used. Bacteria frozen stokes were stored at -80°C; strains were streaked on BHI plates weekly and incubated for 18-24 hours at 37°C, then stored at 4°C.

Each bacterial strain was inoculated into BHI broth and incubated for 18-24 hours at 37ºC. Then, the inoculated growth was diluted 1000 times in fresh BHI broth, and 20 µl of the diluted broth were added into a sterile 96-well plate. After that, each well was filled with 100 µl of the release media from coated titanium nanoparticles or coupons, and the plates were incubated for 18-24 hours at 37ºC. On the next day, the growth in each well was evaluated visually. Each experiment was performed in triplicate for each individual strain, to determine the duration of the inhibitory activity of coated titanium coupons.

2.5 Cells culture

Human monocytic leukaemia cells (THP-1), Human osteoblast cells (Saos-2) were obtained from ATCC and grown in RPMI-1640 medium supplemented with 10% heat-inactivated foetal bovine serum (FBS) and 1% penicillin-streptomycin (PS) (Gibco by Life Technologies, US) at 37°C in a humidified 5% CO_2 atmosphere. Cell medium was changed twice per week.

2.5.1 Differentiation of THP-1 monocytes to macrophages

To initiate the differentiation of monocyte-derived macrophages, 30ng/mL of phorbol 12-myristate 13-acetate (PMA, Sigma-Aldrich) was added to the RPMI-1640 medium (10% FCS, 1% PS) for 3 days, where human monocytic leukemia cells (THP-1) were grown in suspension. Then adhered monocyte-derived macrophages were grown in RPMI-1640 medium supplemented with 10% heat-inactivated foetal bovine serum (FBS) and 1% penicillin-streptomycin (PS) (Gibco by Life Technologies, US) at 37°C in a humidified 5% CO_2 atmosphere. Cell medium were changed twice per week.

2.5.2 Exposure of cells to drug release media

The release buffer from the first 24 hours of either nanoparticles or titanium coupons at pH 7 was passed through 0.22µm syringe filter for sterilization.

Cells were seeded in 96-well plates (Thermo Fisher Scientific, Denmark) at a density of $5x10^4$ cells per well and incubated for 24 hours at 37°C in a humidified 5% CO_2 atmosphere to allow cell attachment. After removing the media and washing the cells with sterile PBS, cells were incubated with release media from nanoparticles or coupons for 3 hours at 37°C in a humidified 5% CO_2 atmosphere

1ug/mL of lipopolysaccharides (LPS, Sigma-Aldrich) was added to the macrophage cells in each well.

The cells incubated in cell medium only with neither 24h solute of nanoparticles nor LPS were used as blank control. The experiments were performed in triplicate wells to evaluate the cytokines produced by cells and cell mitochondrial activity at 2-time points, 6 hours and 24 hours.

2.5.2.1 Cell proliferation assay

MTT (3-4, 5-dimethylthiazol2,5-diphenyltetrazolium bromide, Sigma-Aldrich) assay was used to quantify metabolically active cells .Firstly, 5mg/mL of MTT stock solution was prepared by dissolving 100mg of MTT reagent in 20mL of PBS and filtered through a 0.22um syringe filter for sterilization. At each time point, cell medium was discarded. Then 20μL of MTT stock solution and 100uL of PBS were added to each well. The control well contains pure cell medium only without the addition of release medium, from this well the actual mitochondrial activity was detected. The rest of the wells contained cell medium plus the experimental sample. Then, the wells incubated in a humidified atmosphere at 37°C with 5% CO_2 for 4 hours. The supernatant was then removed and the precipitated formazan was dissolved in 100μL of dimethyl sulfoxide at 37°C for 30 minutes. The absorbance was measured by a spectrophotometer (Lab Tech LT5000MS) at 560nm. The absorbance of the walls that contain the release medium plus experimental samples was compared to the absorbance of the control medium which contains pure cells only. By following this protocol we measure the cytotoxic effect of our release medium.

2.5.2.2 Cytokines measurement

The quantity of TNF alpha (Thermo Fisher Scientific, Vienna, Austria) and IL-6 (Life Technologies, Frederick, MD, USA) secreted from individual samples by human THP-1/macrophages was detected by the enzyme-linked immunosorbent assay (ELISA) kit according to manufacturer's instructions. Briefly, 100uL of standards or samples diluted with the provided sample diluent were added in the appropriate wells of a 96-well plate coated with monoclonal antibody to human TNF alpha or IL-6, respectively. Standards

and samples were in triplicate. 50µL of biotin conjugate solution was then added to each well. The plate was covered by a plate cover and incubated at room temperature for 2 hours on a shaker. The supernatant was then removed and the wells were washed 4 times with wash buffer. 100µL of streptavidin-HRP solution was added to each well. The plate was covered by a new plate cover and incubated at room temperature for another 1 hour for TNF alpha or 30 minutes for IL-6 on a shaker. The supernatant was again removed and the wells were washed again 4 times with wash buffer. 100µL of 3,3',5,5'-Tetramethyl benzidine (TMB) substrate solution was added to each well and the plate was incubated at room temperature in the dark till the substrate solution began to turn bleu (about 15-20 min). Finally, 100uL of stop solution was added to each well to halt the reaction. The yellow coloured solution was then quantified by absorbance at 450nm with (TNF alpha) or without reference wavelength at 650nm (IL-6) in a multiwell microplate reader (LT-5000MS ELISA reader, Labtech). Calibration curves (Figure 25 and Figure 26) were obtained at each measurement to reduce variability between experiments.

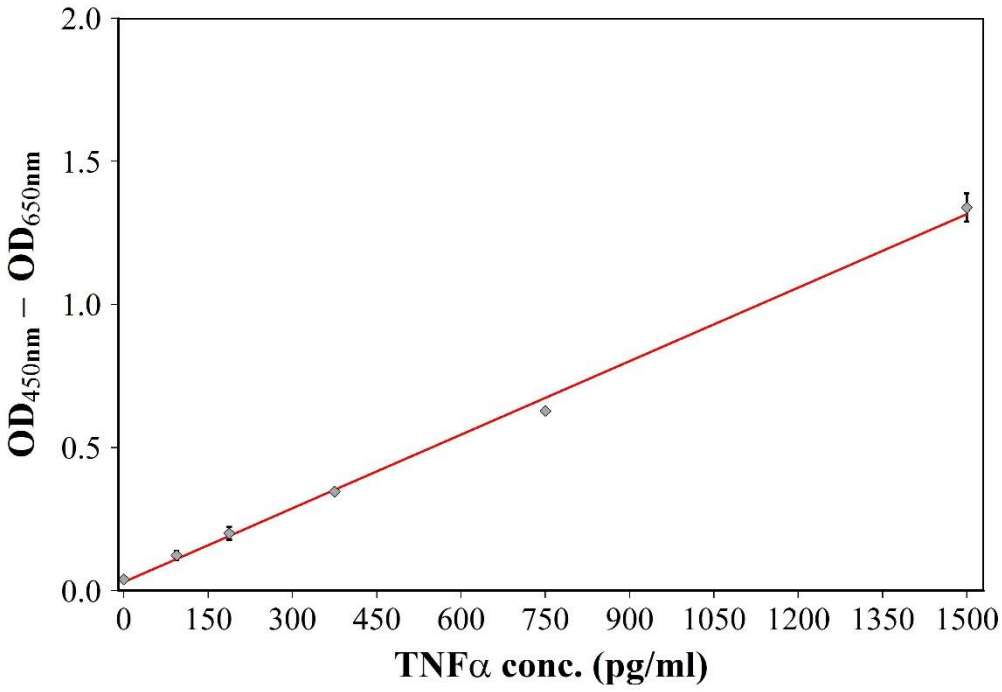

Figure 25. Example of calibration curve of TNFα (mean ± SD n =3).

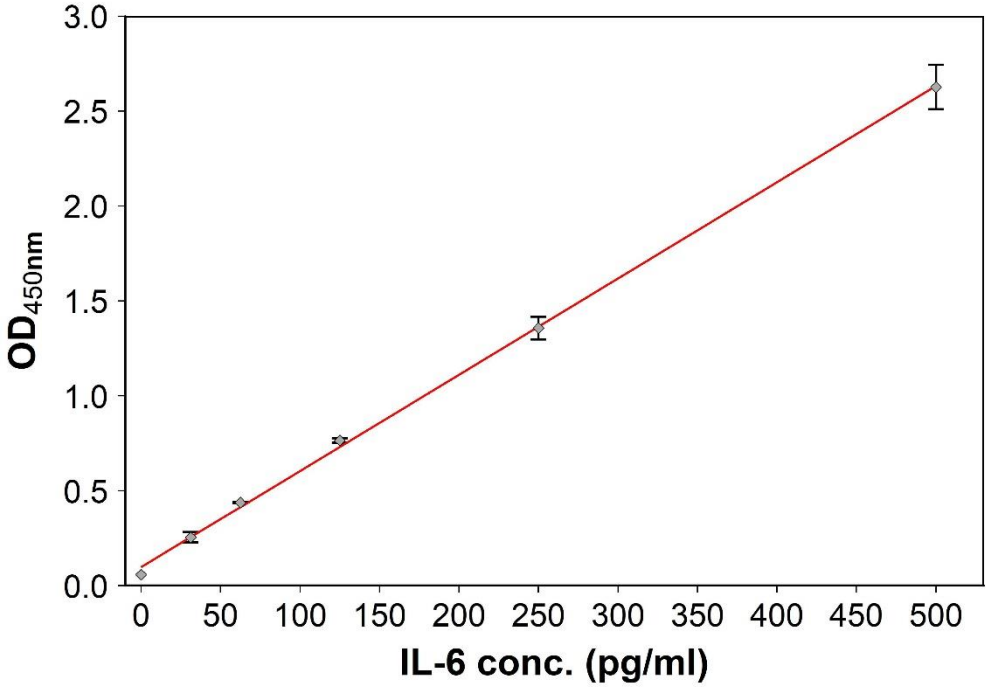

Figure 26. Example of calibration curve of IL-6 (mean ± SD n =3).

2.5.3 Epifluorescent imaging

Cells were fixed with 3.7% (w/v) formaldehyde in PBS at room temperature for 5 min and, then, permeabilised with 0.1% Triton X-100 for further 5 min at room temperature.

F-actin cytoskeleton was stained with 50 mg/L of tetramethyl rhodamine B isothiocyanate-conjugated phalloidin (Sigma-Aldrich, St. Louis, MO, USA) for 40 min at room temperature, followed by incubation with 5 mg/L of trihydrochloride Hoechst 33342 (Thermo Fisher Scientific, Eugene, OR, USA) for 10 min in the dark to stain cells nuclei. Samples were then washed with PBS, mounted and examined using LSM 880 upright confocal laser scanning microscope with Airyscan (Zeiss, Oberkochen, Germany) with a 63×magnification objective. The following settings were employed to excite the dyes and acquire the images: λex 540–545 nm and λex 340 nm; λem 570–573 nm and λem 488 nm for tetramethyl rhodamine B isothiocyanate-conjugated phalloidin and Hoechst, respectively. The obtained images were processed using ZEN imaging software (Zeiss).

2.6 Statistical analysis

One-way analysis of variance (ANOVA) was performed was performed using SPSS (12.0 to assess the statistical significance of results between groups at 95% confidence level ($p < 0.05$). All data were expressed as mean ± standard deviation (SD) from at least three independent values.

Chapter 3: Prolonged release of Dexamethasone from LbL coating for un-cemented joint replacement devices

3.1 Introduction

68 thousands primary hip and 71 thousand knee replacement procedures were performed by the National Health Service (NHS) in England and Wales in 2017 (National Joint Registry 2018). It is expected that these operations will be performed on an increasing number of patients because of the improvement in life quality they provide and the constantly aging population. There are two main methods of fixation, poly-(methyl methacrylate) based bone cement fixation and cementless fixation which aims towards the direct integration of the implant with the host tissue by bone in-growth into a porous or macroscopically textured implant surface. The two methods of fixation are used in a similar proportion of cases worldwide (although their relative popularity varies in different countries) and have similarly good clinical results (Maggs and Wilson 2017). In cementless fixation, integration is promoted by the local delivery of osseoinductive and/or osseoconductive drugs from the device surface. Despite the knowledge of effective molecules for such purpose, their controlled delivery remains a major challenge (Hammond 2012). The use of a dissolvable coating allows a sustained targeted release that cannot be achieved by simple adsorption or direct binding to the surface. Layer-by-layer (LbL) is a self-assembly technique employed to produce a coating and relies on the alternated deposition of positively and negatively charged polymers (polyelectrolytes) through electrostatic attraction (Chuang, Smith, and Hammond 2008; Hammond 2012; Macdonald et al. 2011; Smith et al. 2009; Wong et al. 2010). LbL has found medical applications when biocompatible polyelectrolytes are employed. LbL can be also used to release a drug from the coating, replacing one of the polyelectrolytes with the target molecule, whose only requirement is the presence of electrostatic charges. Additionally, to prolong the release of the target molecule, simply more layers are required. Scalability and ease of fabrication of LbL coating are further advantageous characteristics of such technique (Chuang, Smith, and Hammond 2008; Hammond 2012; Macdonald et al. 2011; Smith et al. 2009; Wong et al. 2010).

Inflammation is accompanied by the release of numerous makers in the surrounding tissues; interleukins (IL) and TNFα are released, and thus their quantification is employed for diagnostic purposes, including aseptic loosening (Vasconcelos et al. 2016; Jiranek et al. 1993; Goldring et al. 1983) and prosthetic joint infections (Randau et al.

2014). Aseptic loosening is a severe bone loss (osteolysis) in the tissue surrounding the implant and it is consequence of a prolonged inflammation (Landgraeber et al. 2014); it is the most likely cause of revision surgery for both hip ((Ulrich et al. 2008) and knee (Rozkydal et al. 2007) and it is responsible for about 40% of all revision procedures (Goriainov et al. 2014). Hence, the development of anti-inflammatory drugs releasing devices has been seen as tool in the fight towards the reduction of arthroplasty failure (Wu et al. 2016; Li et al. 2013) with the objective to improve on the current NICE guidelines that have set a maximum rate of revision after 10 years for failure of 10% (Utting et al. 2005). The administration of anti-inflammatory drugs does not treat osteolysis but aims at reducing the periprosthetic inflammation that leads to bone loss and consequent aseptic loosing of the device (Dang et al. 2011).

Dexamethasone (DEX) is well known anti-inflammatory steroidal drug widely used to manage swelling and pain after arthroplasty (Hickey et al. 2002; Zhou et al. 2018) and to reduce inflammation (Tsurufuji, Kurihara, and Ojima 1984). It is not water soluble, but the esterification of the hydroxyl moieties with phosphate groups results in dexamethasone phosphate (DEX-P) that is highly water soluble and is the main component of the medical formulations containing DEX.

We propose to develop an implant coating containing DEX-P fabricated using the LbL technique capable of prolonged release of the anti-inflammatory drug. The drugs will be embedded into a dissolvable coating, and such its release, will be controlled taking advantage of the negative charge of exhibited by DEX-P. The main benefits of this technology are the ease of fabrication and the scalability, thus making it easily translatable to a variety of orthopaedic implants offering successful and lasting joint repair.

3.2 Materials and Methods

3.2.1 Chemicals

Titanium (IV) oxide (Anatase, <25nm, 99.7%), (3-Aminopropyl) triethoxy-silane (APTS, 99%), phosphate buffer solution (PBS) tablets, sodium acetate trihydrate (≥99%), dexamethasone, dexamethasone phosphate, brain heart infusion agar, brain heart infusion broth, were purchased from Sigma-Aldrich, UK. HPLC grade acetonitrile, glacial acetic Acid, and toluene were purchased from Fisher, UK. All other chemicals were reagent grade, stored according to manufacturer's guidelines and used as received.

B1 polymer is a cationic polymer belongs to the class of poly(β-amino ester)s. the synthesis of this polymer detailed in 2.1.1.

3.2.2 Nanoparticles preparation

3.2.2.1 Surface functionalisation of titanium oxide nanoparticles

Titanium oxide nanoparticles were functionalized with amino groups ($TiO\text{-}NH_2$) via salinization, as described in section 2.2.1.

3.2.2.2 Layer by layer (LbL) coating technique

The amino functionalized titanium nanoparticles were coated with polyelectrolyte multilayers. The layers consisted of different numbers of repeating sequence as the following: Alginate-B1-DEX-B1. One sequence containing these four layers was termed quadruple layer (QL), up to ten quadruple layers were coated on the titanium nanoparticles, named as Q_n where n represents the number of quadruple layers. Table 7 and Figure 27 show the component of dexamethasone layer by layer coating on the amino functionalized titanium nanoparticles. The concentrations used were: 2 mg/ml for sodium alginate, 10 mg/ml for Dexamethasone phosphate, and 2 mg/ml for B1. (The procedure for LbL coating is described in section 2.2.3)

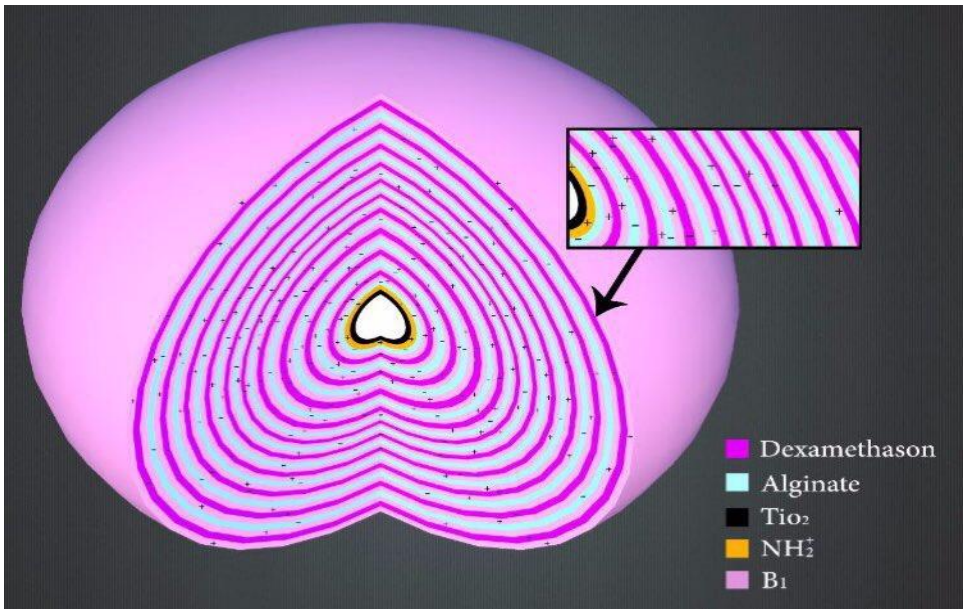

Figure 27. Components of DEX layer by layer coating on the titanium nanoparticles surface.

Number of quadruple layers	Abbreviation	Layer composite on the surface of amino functionalized nanoparticles
1	Q1	$TiONH_2$-Alginate-B1-DEX-B1
2	Q2	$TiONH_2$-Q_1-Alginate-B1-DEX-B1
3	Q3	$TiONH_2$-Q1-Q2-Alginate-B1-DEX-B1
4	Q4	$TiONH_2$-Q1-Q2-Q3-Alginate-B1-DEX-B1
5	Q5	$TiONH_2$-Q1-Q2-Q3-Q4-Alginate-B1-DEX-B1
6	Q6	$TiONH_2$-Q1-Q2-Q3-Q4-Q5-Alginate-B1-DEX-B1
7	Q7	$TiONH_2$-Q1-Q2-Q3-Q4-Q5-Q6-Alginate-B1-DEX-B1
8	Q8	$TiONH_2$-Q1-Q2-Q3-Q4-Q5-Q6-Q7-Alginate-B1-DEX-B1
9	Q9	$TiONH_2$-Q1-Q2-Q3-Q4-Q5-Q6-Q7-Q8-Alginate-B1-DEX-B1
10	Q10	$TiONH_2$-Q1-Q2-Q3-Q4-Q6-Q7-Q8-Q9-Alginate-B1-DEX-B1

Table 7. Components of DEX layer by layer coating on the titanium nanoparticles surface.

3.2.3 Nanoparticles surface and material characterisation

3.2.3.1 Nanoparticles size measurements

The hydrodynamic size for the amino functionalized titanium nanoparticles and the LbL coated multilayer nanoparticles were measured by dynamic light scattering (DLS) using Malvern Zetasizer, Nano ZS particle characterization system (Malvern Instrument limited, UK) as described in section 2.3.1.

3.2.3.2 Zeta potential measurements

Nanoparticles electrophoretic mobility was measured by dynamic light scattering (DLS), using Malvern Zetasizer, Nano ZS particle characterization system (Malvern instrument limited, UK), (described in section 2.3.2).

3.2.3.3 Transmission Electron microscopy – particle size determination

Images of particles were obtained using a Zeiss 902 transmission electron microscope (TEM) operating at a voltage of 80 kV as described in section 2.3.3. The average particle size, size-distribution and morphology analysis of the samples was carried out from transmission electron micrographs using ImageJ for Windows (Version 1.50i).

3.2.3.4 Thermogravimetric Assay (TGA)

Thermogravimetric assay was performed using a Perkin-Elmer TGA 4000 instrument (described in section 2.3.4).

3.2.4 Dexamethasone release quantification

Dexamethasone release was measured by dispersing the DEX coated nanoparticles (10 mg) into 1ml of a buffer media (acetate buffer pH 5, and phosphate buffer pH 7.3) and incubated at 37 °C.

An aliquot of 1 mL of the medium was withdrawn daily for quantification and the medium was replaced with an equal volume of fresh buffer. The amount of DEX/DEX-P released from the coating layer was determined using reverse-phase High Performance Liquid Chromatography/HPLC (1100 series Agilent Technologies®). The quantification procedure for dexamethasone is described in section 2.3.5.1.

3.3 Cell growth

Saos-2 and THP-1 cells were grown as described in 2.5.

3.3.1 Biological test

3.3.1.1 MTT

MTT assay was conducted to measure human macrophages (THP-1) and human osteoblasts (Saos-2) mitochondrial activity post-exposure to DEX coated titanium nanoparticles after 1, 2 and 3 days exposure as per the protocol described in section 2.5.2.1.

3.3.1.2 IL-6 and TNFα

The amount of IL-6 and TNFα released in the media after exposure to LPS and DEX for 6 and 24 hours was determined using appropriate ELISA kit (Sigma, UK) according to manufacturer's recommendations as per the protocol described in section 2.5.2.2.

3.3.1.3 Imaging

Epifluorescent images of human macrophages (THP-1) and human osteoblasts (Saos-2) were obtained staining F-actin cytoskeleton and nuclei. Cells were fixed with 3.7% (w/v) formaldehyde in PBS at room temperature for 5 min and permeabilised with 0.1%Triton X-100 at room temperature for 5 min. Tetramethyl rhodamine B isothiocyanate-conjugated phalloidin (50mg/L) (Sigma-Aldrich, St. Louis, MO, USA) was added at room temperature, after 40 minutes trihydrochloride Hoechst 33342 (5 mg/L) (Thermo Fisher Scientific, Eugene, OR, USA) was added and the cells stored for 10 minutes in the dark. Samples were washed with PBS, mounted and examined using LSM 880 upright confocal laser scanning microscope with Airyscan (Zeiss, Oberkochen, Germany) with a 63X magnification objective under the following conditions: λ_{ex} 540-545 nm and λ_{ex} 340 nm; λ_{em} 570-573 nm and λ_{em} 488 nm for tetramethyl rhodamine B isothiocyanate-conjugated phalloidin and Hoechst, respectively. ZEN imaging software (Zeiss) was employed for processing of the obtained images.

3.3.2 Statistical analysis

One-way analysis of variance (ANOVA) was performed to assess the statistical significance of results between groups at 95% confidence level ($p > 0.05$). All data were expressed as mean ± standard deviation (SD) from at least three independent values.

3.4 Results

The LbL DEX functionalised Ti nanoparticles were prepared and their physico-chemical and material properties were characterised employing zeta potential measurements and TGA techniques; drug release profile and biological evaluations.

3.4.1 Zeta potential measurements

The amino-functionalised titanium substrate presented a positive surface charge of +38.4±0.6 mV due to presence of protonated amino-groups on the surface.

Zeta potentials of the initial polyelectrolytes (Alginate and B1) and the drug (DEX) solutions were measured (Table 8); this is an important step to guarantee a successful LbL assembly.

Polyelectrolyte and drug solution	Zeta Potential (mV) ± SD
Alginate solution (2mg/mL)	-26.42±1.25
B1 solution (2mg/mL)	+10.25 ±1.66
DEX solution (10mg/mL)	-9.48±1.64

Table 8. Zeta potentials of the polyelectrolyte solutions (alginate and B1) and the drug (DEX-P) at pH =5

Alginate and B1 possessed opposite surface charges (Table 8), therefore, they were able to create a LbL assembly due to electrostatic interactions on the amino-functionalised titanium substrate (Ti-O-NH_2) used as a template for the LbL.

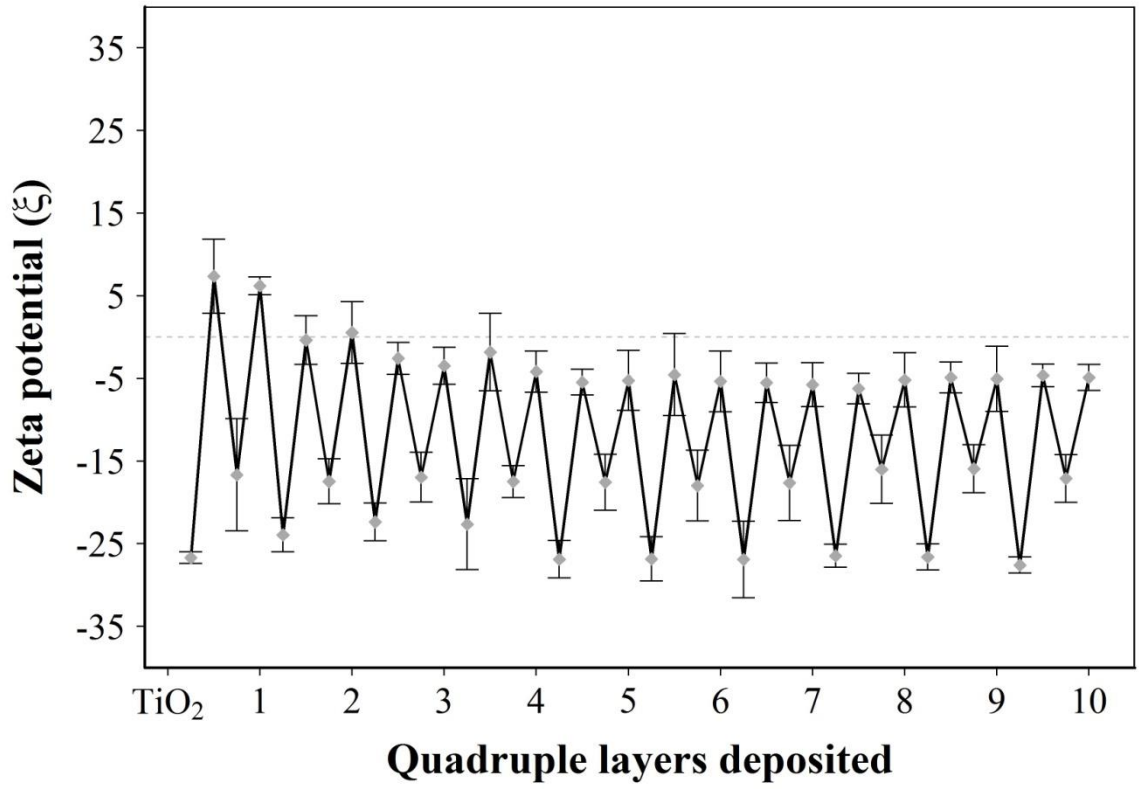

Figure 28. Zeta potential changes during the LbL assembly procedure of alginate/B1 and DEX layering on the amino functionalised titanium substrate. The layer 0 represented the bare (uncoated) Ti-O-NH_2 particles (mean ± SD n =3).

During the LbL procedure a zeta potential (Figure 28) was measured after each layer to ensure the polyelectrolyte deposition occurred. Zeta potentials alternated depending on the last adsorbed outer layer on the substrate: starting from a positively charged Ti-O-NH_2 template. Upon adsorption of the 1st layer (alginate) the surface charge turned to a negative value (~26 mV). Subsequently, when the cationic polyelectrolyte (B1) was layered the zeta potential turned to a positive value (~+7 mV). Then, when the DEX layer (anionic polyelectrolyte) was added, the surface charge of the surface changed to (~-15 mV).

When the outer layer of the LbL construct was either alginate or DEX-P, the zeta of the coated nanoparticles was close to zeta potential of the pure polyelectrolytes and drug; on the contrary when B1 was deposited the zeta potential reached a positive values only after the first layer, after that the deposition of B1 resulted in an increase of the nanoparticles zeta potential but did not reach values above 0 mV.

3.4.2 TEM and particles size

Particles appeared cubical and spherical-like shaped (Figure 29) with relatively narrow distributed diameters (Table 9). LbL did not noticeably impact the size of the particles; however, after 10 quadruple layers, some particles agglomeration could be observed.

Sample	**Average size (nm) ± SD**
TiO_2-particles	34±5
Amino-functionalised particles	34±6
Q10	40±8

Table 9. Average diameter size of TiO_2 nanoparticles bare, after functionalisation and LbL deposition determined from TEM images

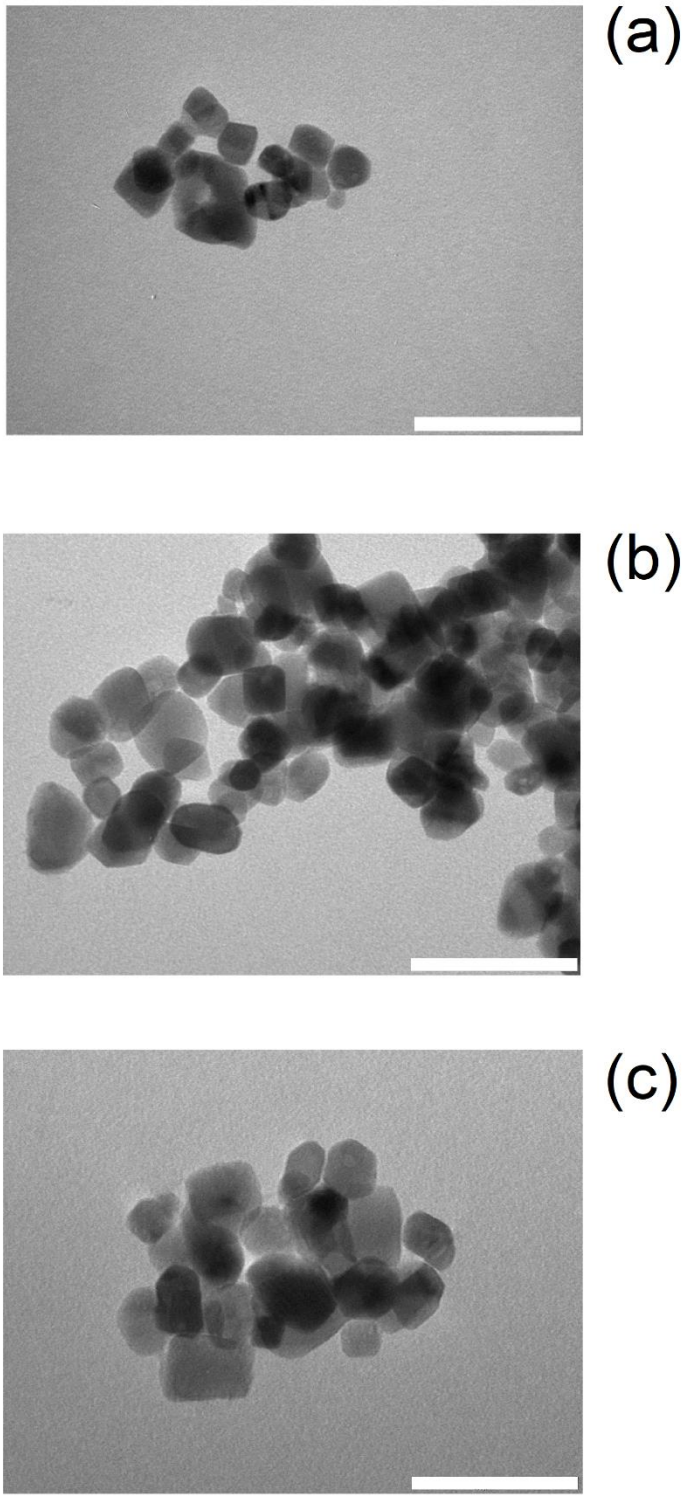

Figure 29. Example of Transmission Electron Microscopy images of (a) bare TiO_2 nanoparticles, (b) amino functionalised (TiO_2-NH_2) nanoparticles and LbL coated (Q10). Bar represents 100 nm.

3.4.3 Thermogravimetric analysis (TGA)

The amount of organic content (%) on the surface of multi-layered DEX-LbL loaded Ti-O-NH_2 particles, after the deposition of each quadruple layer (alginate, B1, DEX and B1) was evaluated by thermogravimetric analysis (TGA) (Figure 30).

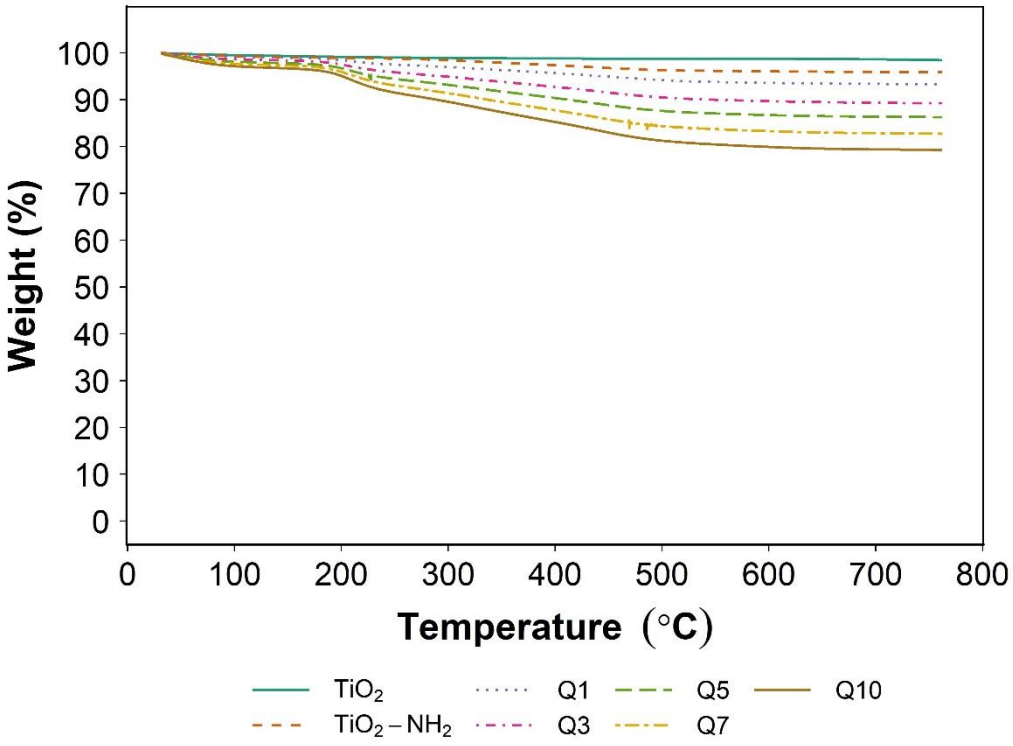

Figure 30. Thermograms of different LbL DEX coated Ti-O-NH_2 substrate.

The thermograms of LbL coated titanium nanoparticles exhibited a gradual weight loss with increasing temperature and they did not reveal further mass loss at temperature above 650 °C. We assumed that all the organic content present on the titanium surfaces has been lost at this point, and that the remaining mass was attributable to the inorganic core of the nanoparticles. A further mass loss was noticeable at about 100 °C and it represented the vaporization of the entrapped water moisture in nanoparticles and was not the result of degradation of organic compounds (alginate, B1 or DEX), therefore the total mass loss observed at 100 °C was subtracted to the mass loss observed at 750°C to determine the organic content.

The organic content (Table 10) of uncoated TiO_2 (bare) nanoparticles was the lowest (1.4±0.2%); while after amino functionalisation, the particles presented 4.2±0.9% of organic fraction. Moreover, in LbL coated particles, the weight loss at 750°C depended

on the number of quadruple layers deposited, from the highest for Q10 (17.5±1.4%) and the lowest for Q1 (6.6±0.4). As the organic content is a depended on the film thickness, Q10 was the highest film coating, followed by Q7, Q5, Q3, and Q1.

Quadruple Layer	Organic content (%)
Bare particles	1.4±0.2
TiO-NH_2	4.2±0.9
Q1	6.6±0.4
Q3	9.7±0.6
Q5	12.8±0.8
Q7	15.7±0.9
Q10	17.5±1.4

Table 10. Percentage of organic material in multi-layered DEX-LbL loaded Ti-O-NH_2 surface after addition of each quadruple layer (Q1, Q3, Q5, Q7 and Q10).

3.4.4 DEX release quantification

DEX-P and not DEX was detected in both the release media (pH5 and pH7.3). The amount of DEX released from the LbL coated Ti-O-NH_2 surfaces monotonically increased with increasing number if quadruple layers (from Q1 to Q10) at both pH5 and pH7.3 (Figure 31). Moreover, drug release was detectable for up to 20-30 days for both pH conditions (Figure 31). At pH=7.3 DEX was detected in the release buffer for up to 25 days compared to 30 days for drug release at pH=5; the same pattern (longer release at pH5 than pH7.3) was observed for the particles investigated regardless of number of layers. Furthermore, the total amount of DEX released was higher at pH=5 than the one released at pH=7.3 for comparable numbers of quadruples layers.

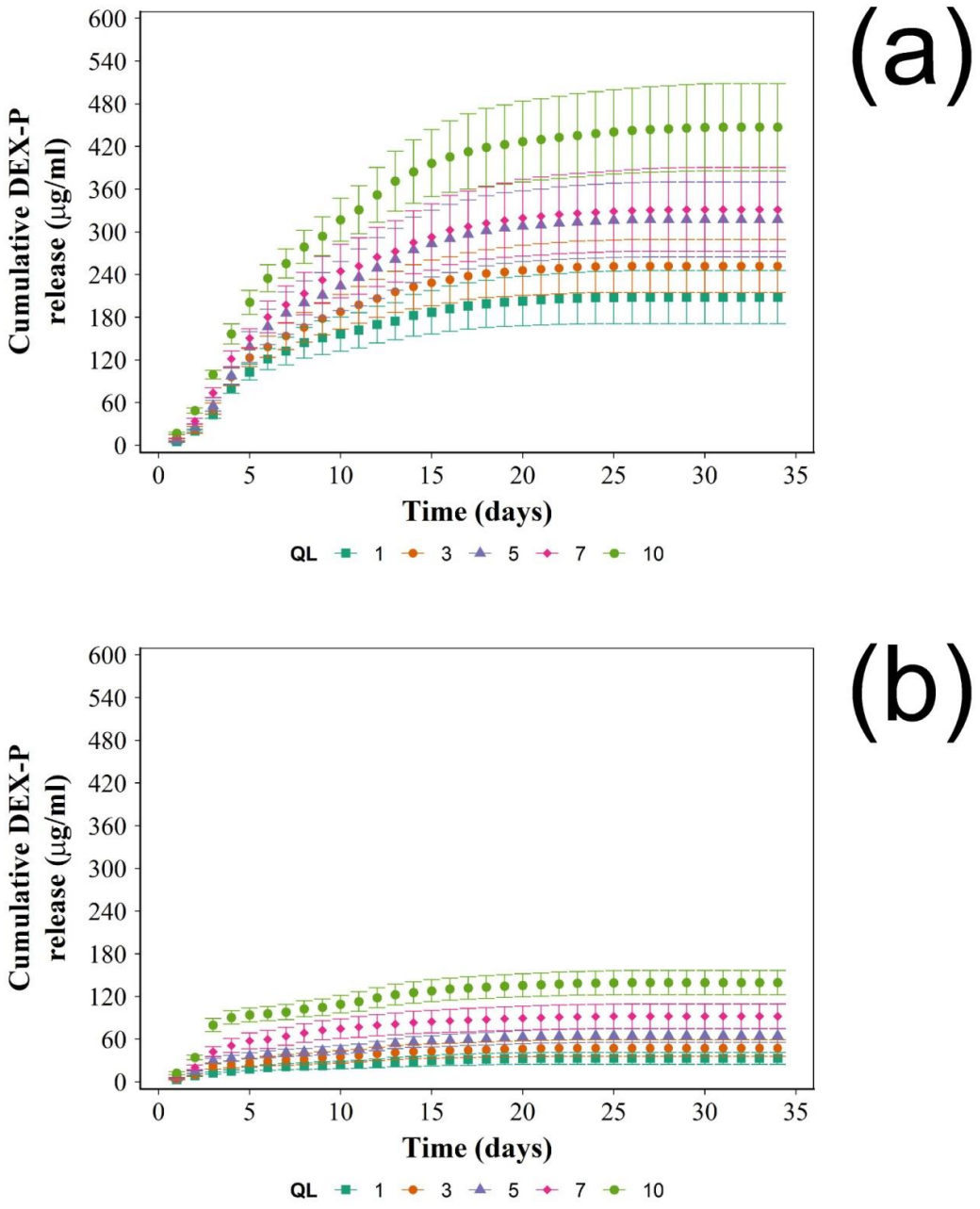

Figure 31. Cumulative release of DEX from LbL-Ti-O-NH_2 surfaces at pH=5 (A) and pH=7.3 (B) for different number of quadruple layers (Q1, Q3, Q5, Q7 and Q10) (mean ± SD n =3).

3.4.5 In-vitro inflammation model: LPS-activated human macrophages.

3.4.5.1 Mitochondrial activity

Cellular mitochondrial activity of macrophages after exposure for 6 and 24 hours to particle release buffer was assessed employing MTT assay and it did not reveal any detrimental effect (P>0.05) (Figure 32).

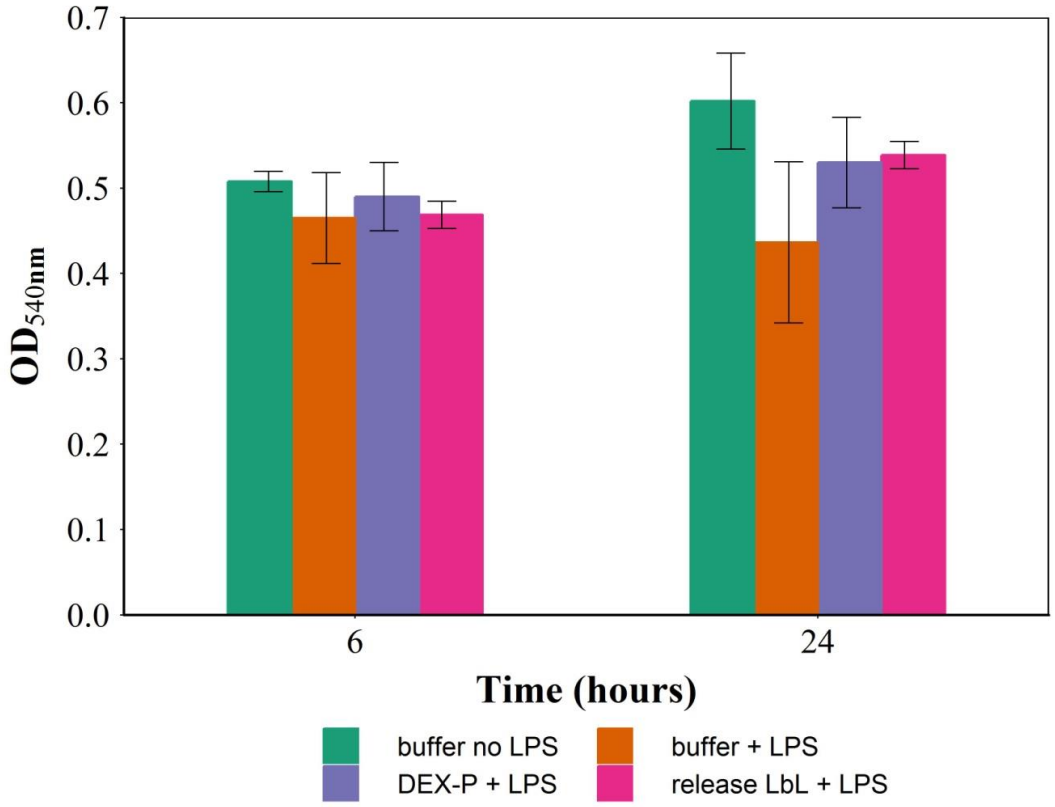

Figure 32. Mitochondrial activity of activated THP-1 cells exposed to media containing DEX-P or elutes from DEX released from LbL assembly for 6 and 24h. LPS concentration of 1µg/mL (mean ± SD n =6).

3.4.5.2 Inflammation markers (IL-6 and TNFα)

Activated human monocytes did not produce either noticeable amount of IL-6 or TNFα when not exposed to LPS. When inflammation was induced, IL-6 reached ~1.2 ng/ml and ~1.4 ng/ml after 6 and 24 h of exposure; similarly, TNFα concentration was about ~30 and ~33 ng/ml after the same exposure. The addition of DEX-P suppressed IL-6 production to about a third after both 6 and 24h; TNFα concentration was reduced to half after 6 h and about a third after 24 hours. The use of an equivalent dose of DEX release from LbL coating had similar reduction patterns for both inflammation markers but the efficacy of the release drug was about 20-30% inferior to pure DEX ($p<0.05$).

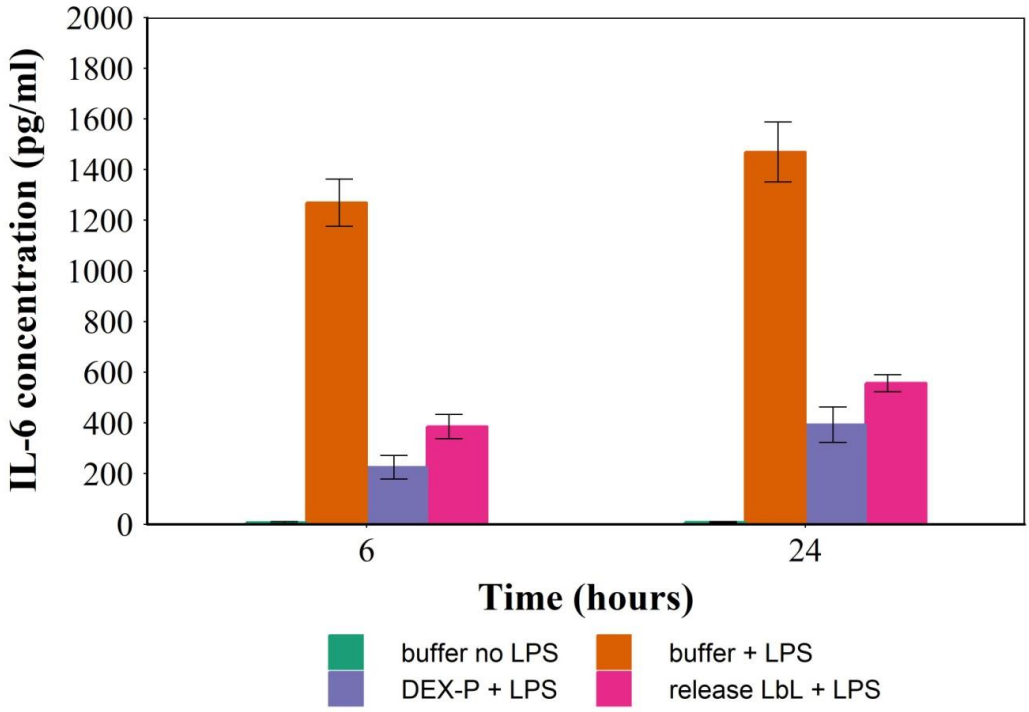

Figure 33. IL-6 expression of activated THP-1 cells post-exposure to media containing DEX-P or elutes from DEX released from LbL assembly for 6 and 24h. LPS concentration of 1µg/mL was used (mean ± SD n =3).

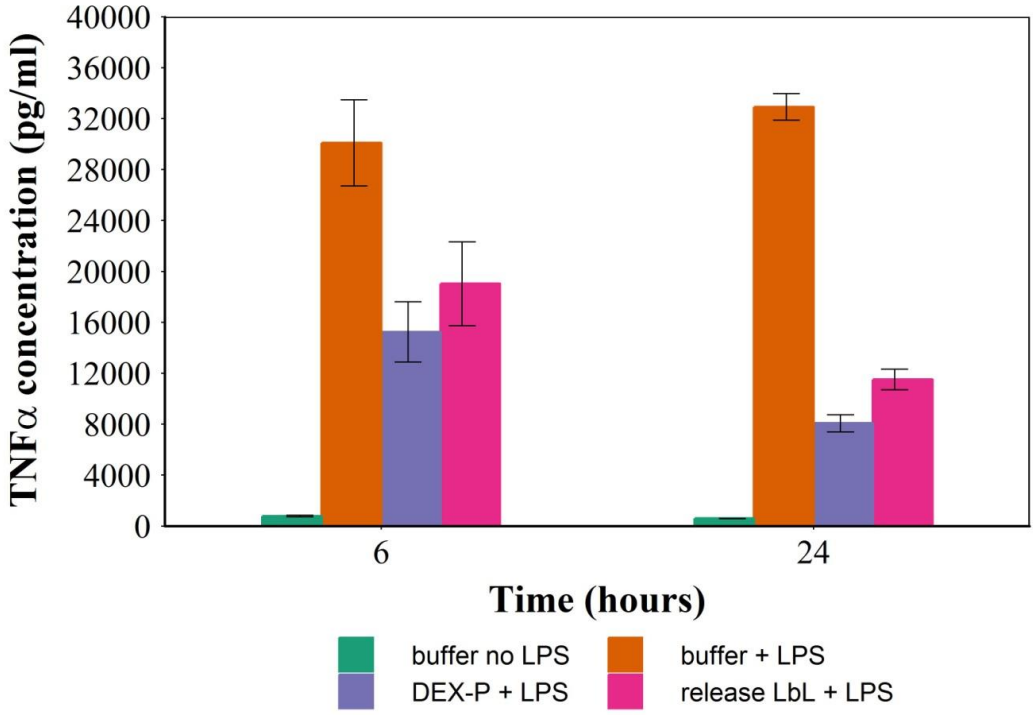

Figure 34. TNFα expression of activated THP-1 cells post-exposure to media containing DEX-P or elutes from DEX released from LbL assembly for 6 and 24h. LPS concentration of 1µg/mL was used (mean ± SD n =3).

3.4.5.3 Cell morphology

Additionally, cell morphology and cytoskeletal properties were evaluated by staining actin rings using confocal microscopy (Figure 35). The results showed that after 24h growth in media without LPS and DEX, the human macrophages were spread over the surface demonstrating a regular morphology. LPS exposure (1µg/mL), induced a reorganization in actin distribution of the macrophages resulting in evident difference in cell morphology: cells showed an oval-shaped configuration, after addition of DEX the cell size increased remaining oval shape.

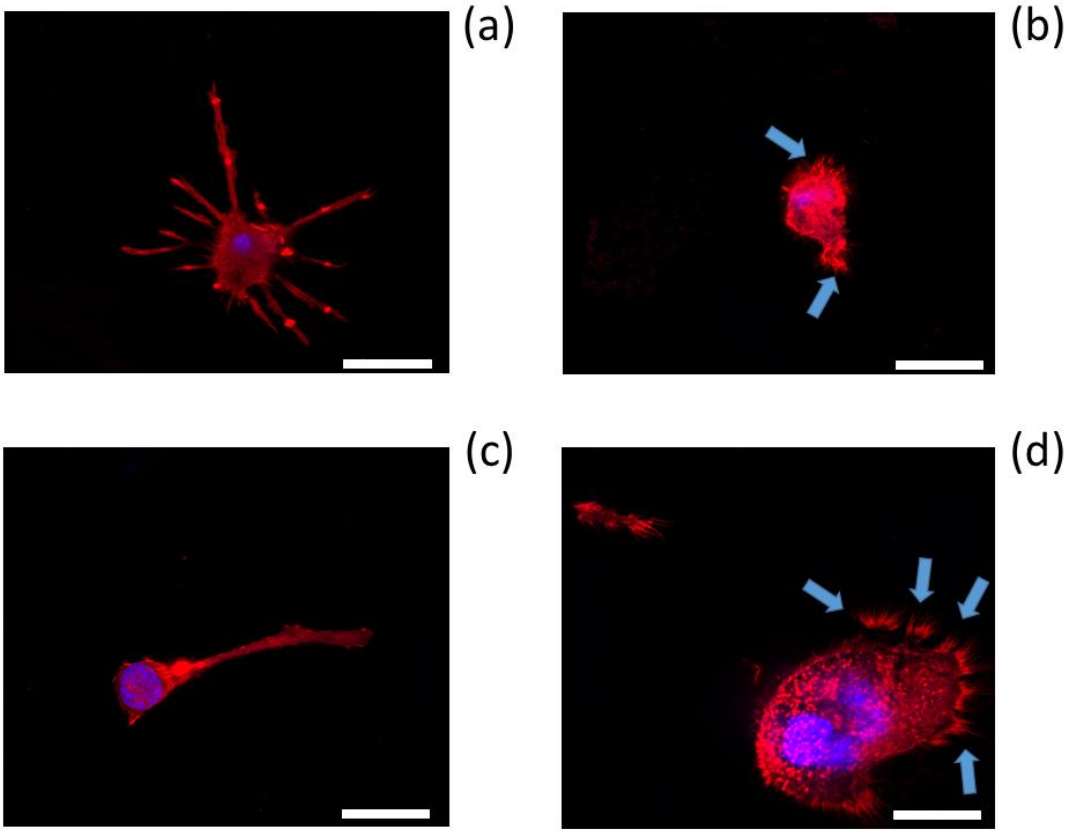

Figure 35. (a) Actin staining epifluorescent images of human macrophages LPS-DEX-; (b) LPS+DEX-; (c) LPS+DEX-P and (d) LPS+DEX from release buffer after 24hr exposure assessed by confocal microscopy. Actin rings and nuclei of cells were stained with phalloidin-FITC and DAPI, respectively; arrows indicate pseudopods. Bar corresponds to 20 µm.

3.4.6 Safety assessment for orthopaedic application using osteoblasts (Saos-2)

3.4.6.1 Mitochondrial activity

The mitochondrial activity of human osteoblasts exposed to DEX-P or the equivalent dose in release buffers at pH=7 increase with exposing time (Figure 36). No difference was observed when comparing control cells to either DEX-P or DEX in release buffers ($p<0.05$).

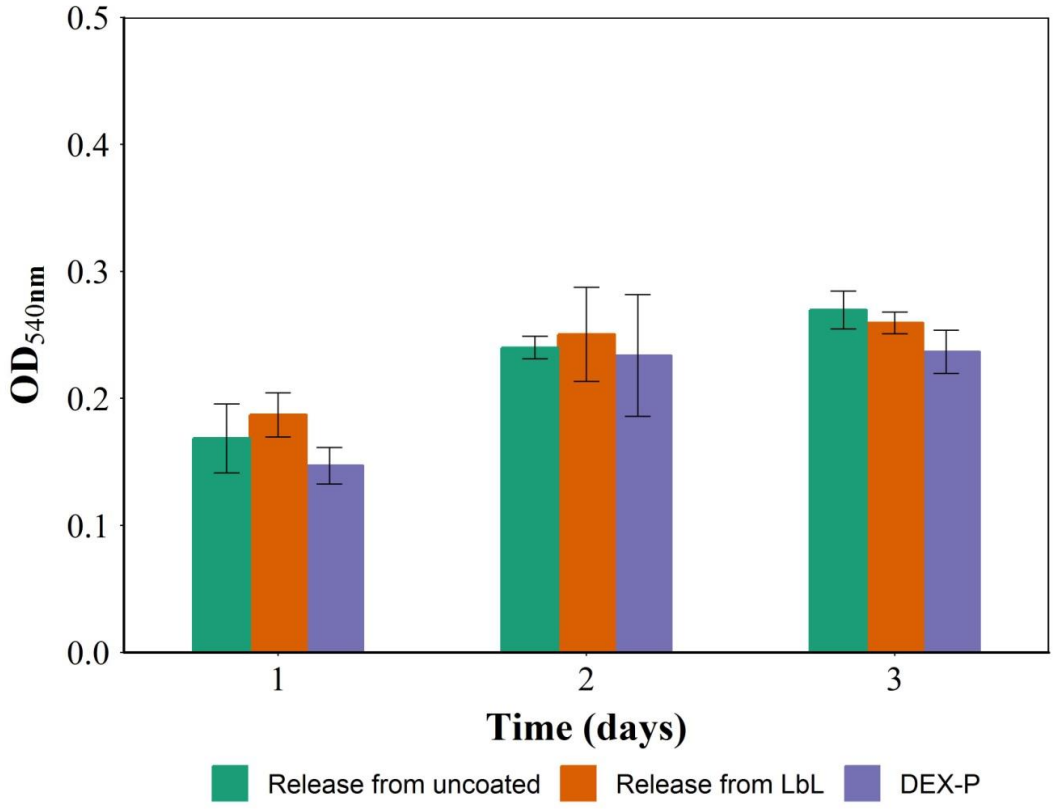

Figure 36. Mitochondrial activity of Saos-2 cells exposed to media containing DEX-P or elutes from LbL assembly for 1, 2 and 3 days (mean ± SD n =6).

3.4.6.2 Cell morphology

Already established osteoblast cultures to media containing either DEX-P or released DEX to the response to sterile PBS. Moreover, the tests were conducted only from release buffer pH7 as the acidic buffer (pH5) exhibited toxic activity. DEX released from the LbL coating did not negatively impact osteoblasts, it is clearly seen that the morphology of the actin rings and nuclei did not change after the addition of DEX-P or DEX from release buffer. In addition to that, Osteoblast cells appeared spread with well organised actin filaments regardless of the presence of DEX-P or DEX from release buffers (Figure 37).

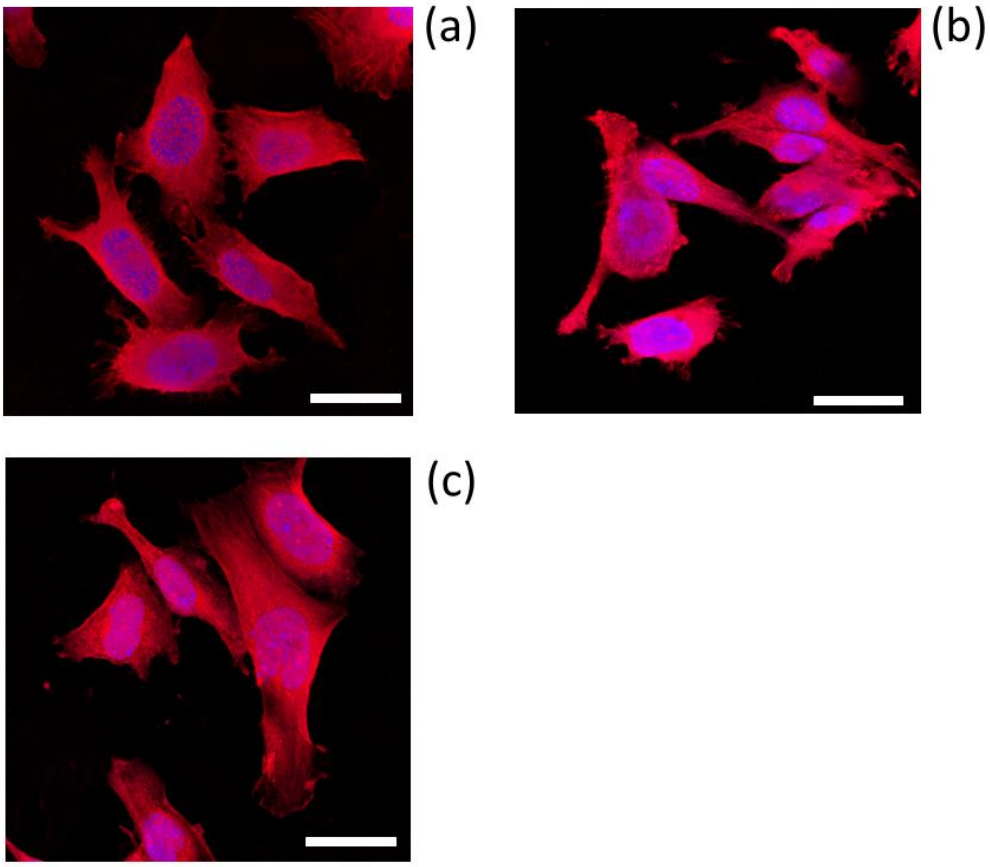

Figure 37. Actin staining epifluorescent images of human osteoblast (Saos-2) DEX-; (b) LPS+DEX-P and (c) DEX from release buffer after 24hr exposure assessed by confocal microscopy. Actin rings and nuclei of cells were stained with phalloidin-FITC and DAPI respectively. Bar corresponds to 20 μm.

3.5 Discussion

3.5.1 Size

The determined bare particle size is in agreement with the manufacturer stated dimensions; amino functionalisation did not impact on the nanoparticles size, while the small size increase calculated from TEM images observed after coating with 10 quadruple layers is consistent with under polyelectrolyte layers thickness under nanometre, similar to that reported in other studies (Feng et al. 2014; Al Thaher et al. 2018). As observed in other studies, polyelectrolyte deposition on nanoparticles surfaces originates agglomeration as the polyelectrolytes can deposit simultaneously over more than one particle during LbL assembly (Gosens et al. 2010).These aggregates during subsequent layer deposition behave as one individual particle leading to further agglomeration. However, agglomeration appears to be minimal as LbL protocol was optimised to minimise such occurrence through polyelectrolytes excess.

3.5.2 Zeta

The observed zig-zag of the zeta potential is typical of LbL deposition as the coated surface assumes the charge of the last layered polyelectrolyte, furthermore the negative potential observed after depositing DEX-P and alginate are very close to the values measured for the pure molecules leading to the conclusion that the surface was saturated by either compounds. On the contrary, the lack of symmetric inversion in zeta potential, observed after B1 deposition, could be attributed to the fact that B1 is a weaker charged polyelectrolyte compare to Alginate (Table 8). Moreover, no increase in the positive charge after B1 deposition despite attempts increasing B1 concentration and/or extending the contact time. However, deposition of B1 was accomplished as the zeta potential of the nanoparticles moved to higher values (less negative); this could only be achieved by positive charges neutralising the negative of the previous layer.

3.5.3 TGA

Thermogravimetric assay is typically conducted to confirm and quantify the attachment of organic molecules on surfaces either by conjugation (Gil-Tomás et al. 2007) or LbL (Al Thaher et al. 2018). As visible in Figure 30, the thermograms of all coated nanoparticles showed a plateau from around 650 °C that is due to the inorganic fraction (in this work made of TiO_2) of the nanoparticles remaining after the organic components have been burnt (Mai et al. 2014; Zhong et al. 2015). However the mass loss at this point does not correspond entirely to the amount of deposited polyelectrolyte and drug as the weight loss occurring around 100 °C is due to the vaporization of entrapped water not a result of degradation of organic compounds (alginate/B1/DEX-P) therefore this mass loss needs offsetting in the calculations (Du et al. 2015). Such water is due to the aqueous solution used during LbL that remains in the on the nanoparticles despite the drying process. Remarkably, the total moisture content increased with increasing numbers of layer.

The organic fraction of the particles for the amino functionalized nanoparticles (Table 10) was the results of the amino silanol conjugating to the titanium surfaces; moreover the organic fraction increased with growing number of quadruple layers: Q1, Q3, Q5, Q7, Q10 (Table 8). The organic content of the nanoparticles after each quadruple layer observed in this work was similar to LbL coated silica nanoparticles containing gentamicin (Al Thaher et al. 2018). The amount was almost linear with the number of quadruple layers up to Q7 but the rate of organic fraction deposition decreased after this, because, as already seen in TEM images, LbL is progressively hindered but agglomeration and the available surface diminish accordingly.

3.5.4 DEX release

in vitro release studies were performed at two different pHs to simulate different joint conditions: healthy joints (pH=7.3) (Goldie and Nachemson 1970) and inflamed joints, which are associated with local acidosis (de Nadai et al. 2013) (pH=5).

Drug release from LbL constructs is the sum of two simultaneous and independent processes; the progressive detachment of the coating layers (delamination) and the diffusion of the drug through the deposited layers (Smith et al. 2009). The kinetic of the two phenomena depends on nature of the polyelectrolytes employed and pH (Al Thaher et al. 2018); these two parameters directly influence the hydrolysis kinetic of the polyelectrolytes that govern the delamination process and the electrostatic attractions between layers that control the drug diffusion coefficient (Al Thaher et al. 2018; Smith et al. 2009). Moreover, if diffusion is the predominant mechanism of release the profile exhibits an exponential behaviour with the highest drug release at the beginning that gradually drops to zero. On the contrary delamination provides a zero order kinetic of release (constant rate until the LbL is fully degraded) (Smith et al. 2009; Al Thaher et al. 2018). The release profile observed in this work (Figure 31) is attributable to release mechanism dominated by diffusion, similar profiles where observed for similar coating prepared with the positive charged antibiotic gentamicin (Chuang, Smith, and Hammond 2008; Al Thaher et al. 2018) or an osseoinductive protein (Shah et al. 2013). However, DEX-P exhibited higher release at pH5 than pH7 while gentamicin exhibited the opposite behaviour (Al Thaher et al. 2018). Higher DEX release kinetic in acidic conditions compared to neutral were also observed (Wang et al. 2007) but determined by the hydrolysis of the ester bond employed to conjugate the steroid. Since only DEX-P was observed in the release buffers, the opposite impact of pH on the release of DEX-P and gentamicin can be assumed to depend on the charge of the two drugs at the pHs tested; DEX-P is negatively charged while chlorhexidine is positively charged. It has been demonstrated that the surface charge of the outer polyelectrolyte deposited is the key in controlling diffusion through all coating with lower diffusion for molecules exhibiting the same charge as the outer coating layer (Sato, Shiba, and Anzai 2013). B1 is almost completely deprotonated at pH7.3, with a charge close to zero, while in mild acidic conditions (pH5) is fully protonated and positively charged; DEX-P acid groups are deprotonated in both conditions and the drug is negatively charged hence the higher diffusion observed at pH5. Gentamicin, on the contrary, is positively charged at both pHs and such the higher diffusion observed at pH7.3. B1 hydrolysis is slow at pH5 (Al Thaher et al. 2018), more a month to reach a 80% reduction of the polyelectrolyte

molecular weight, thus higher delamination does not contribute to the release of DEX-P at pH=5 as it is also revealed by the release profile that is not zero order.

Moreover, drug release had been observed for about 4 weeks and it is length of time compatible to the requirements to prevent acute host inflammatory reaction that occurs immediately after device implantation and due to both the issue injury undergone during surgery to place the device and the response to the material itself (Anderson, Rodriguez, and Chang 2008). acute host inflammatory reaction can results in difficult device integration with compromised functionality and longevity (Bridges and García 2008).

3.5.5 Cytocompatibility and inflammatory activity towards human Monocytes

The mitochondrial activity (linked to cell viability) of human monocytes (THP-1)-derived macrophages exposed to DEX released from the LbL coated Ti-O-NH_2 surfaces was determined to exclude drug toxicity. Additionally, activated human monocytes (THP-1)-derived macrophages were used as model human macrophages. This cells line is very well established for studying functions and metabolism of human monocytes and macrophages (Qin 2012). LPS concentration of 1µg/mL is routinely employed to simulate inflammation in human macrophages (Glue et al. 2002; Moreira-Tabaka et al. 2012).

Cells were exposed to LPS and to either DEX-P or the same drug dose using the elutes collected from the DEX release studies at pH=7.3 to confirm that the anti-inflammatory activity of DEX, on inflammation markers such as TNFα and IL-6, was retained when released from the LbL construct. The elutes from the drug release studies performed at pH=5 were not considered due to the low cellular viability they caused when exposed to the cells as determined in preliminary studies. As we have shown (Figure 31) that DEX concentration in the release media varied according to the number of layers deposited onto the Ti-O-NH_2 surfaces, only elutes from DEX released from 10QL assembly was used as maximum concentration of released DEX was obtained.

In this study, inflammation was induced by exposure of monocyte-derived macrophages to LPS; specific measurable inflammatory markers produced by human macrophages such as IL-6 and tumour necrosis factor alpha (TNFα) were monitored (Qin 2012; Cochran and Finch-Arietta 1992). To be able obtain a reliable *in vitro* inflammation model, an appropriate cell density and an optimal LPS concentration should be utilized in cell cultures for quantification assays. This is mainly for the following reasons: if the cell density is not appropriate, IL-6 and TNFα production may not be detectable in the cell media and if LPS concentration is too high this could cause cell toxicity, and

oppositely, low LPS concentration may not be capable of activate macrophages inflammation.

LbL coating release not only DEX but also polyelectrolytes or the products of B1 hydrolysis, therefore we determined both whether DEX activity was retained once released and LbL decomposition products potential toxicity and inflammatory activity. DEX activity once released was marginally reduced compared to the equivalent amount of DEX-P likely as the drug was deposited and not conjugated to the surface, thus avoiding reactions for DEX active groups. Moreover, the coating conditions were mild (aqueous solution and room temperature) and thus unable to damage the molecules. B1 are a class of known biocompatible polyelectrolites hence the lack of toxic was expected.

Beside IL-6 and TNFα production (Figure 33 and Figure 34); LPS stimulation (1µg/mL) was shown to induce significant changes on the cytoskeletal properties and morphology of the cells (Figure 35) compared to the untreated cells (control group). Multiple pseudopods with abundant actin filaments were clearly visible only on cells exposed to LPS; these membrane features did not disappear when DEX was added. Pseudopodia are involved in cell movement and phagocytosis thus their presence is linked to the inflammation process. Similar images were presented by (Liu et al. 2008) and (Qin 2012). As monocytes phagocytosis is key in their immunological activity, structural changes may have negative impacts on monocytes ability to perform the assigned tasks (Dale, Boxer, and Liles 2008).

3.5.6 Cytocompatibility toward human osteoblast

The development and evaluation of any new biomaterial must comprise not only the assessment of functionally to the desired level, but also the demonstration of no adverse effects caused to tissues and cells that the material will be in contact with. The titanium coating presented here have demonstrated the ability to sustain dexamethasone release for prolonged periods of time with retained anti-inflammatory activity; however, their clinical utilisation is conditional to the ability of supporting osteoblast cells growth. They are the fundamental cells of bones and they are routinely employed in-vitro testing of novel orthopaedic materials (Mikulewicz and Chojnacka 2011; Baranowski et al. 2016). MTT assay assesses the mitochondrial activity of cells through the colorimetric quantification of the formazan produced by the oxidation of a tetrazolium dye in the cell mitochondria; MTT is therefore an indirect determination of the amount of viable cells (Mosmann 1983) under the assumption of constant mitochondrial activity among cells in the various conditions tested.

It was not possible to grow cells directly onto the LbL coated surfaces as we employed titanium nanoparticles as a model for titanium devices; hence we tested the response of already established osteoblast cultures to media containing either DEX-P or released DEX to the response to sterile PBS. Moreover, the tests were conducted only from release buffer pH7 as the acidic buffer (pH5) exhibited toxic activity.

DEX released from the LbL coating did not negatively impact osteoblasts (Figure 36 and Figure 37) and such these materials are not inferior to standard titanium in regards to osteoblasts growth. Because titanium exhibits sufficient cytocompatibility towards osteoblasts, it was not necessary for the LbL coating to improve such properties and non-inferiority was deemed sufficient.

Uncemented hip replacement devices have a porous or textured surface to allow mechanical interlocking with the bone; hence during insertion only the outer part of the surface contacts the bone. Because of this, our proposed coating deposited within the porous surface will not be subjected to friction and will remain unaffected by the handling and mechanical actions associated with the surgery

3.6 Conclusions

Longevity of joint replacement devices is severely impacted by inflammatory processes that can lead to bone loss and aseptic loosening of the prosthesis. We have successfully controlled the release of dexamethasone (a widely used anti-inflammatory steroidal drug) for about 20-30 days. This material did not impact on osteoblasts proliferation and the anti-inflammatory activity of the realised drug was retained. These materials therefore appear a potential tool for reducing the number of revision surgeries necessary when aseptic loosening develops.

Chapter 4: Chlorhexidine controlled release from layer-by-layer coated nanoparticles

4.1 Introduction

A successful preventive measure to encounter PJI requires multi-disciplinary considerations. Sterility during surgical procedure is of the utmost importance. However, prophylaxis treatment using antimicrobial agents is essential to further minimise bacterial attachment to prosthetic surface. Prosthetic devices can be designed to have antimicrobial property. This can be achieved by modifying the surface of implants or incorporating antimicrobial compound(s) onto the implants (Getzlaf et al. 2016).

Antimicrobial coating for prosthetic surface should be able to release the drug in a controlled manner to ensure optimum anti-infective activity in a determined period (Getzlaf et al. 2016; Al Thaher, Perni, and Prokopovich 2017). This is of the greatest importance since the failure to carry those tasks might potentially lead to development of antimicrobial resistance (Getzlaf et al. 2016). Although there is no 'gold standard' for local antibiotic release from antibiotic-coated prosthesis to date, antimicrobial activity should last for the lifetime of the device, roughly 20 years (Raphel et al. 2016) at least over the critical period after implantation (e.g. 2-3 months) (Lamagni 2014).

One of the most recent antibiotic eluting systems used in antimicrobial prosthetic devices is polyelectrolyte multilayer, a multiple coating layers that consist of multiply charged materials (Smith et al. 2009). Polyelectrolytes are deposited on the surface of implants through alternatively oppositely charged molecules in what is known as layer-by-layer (LbL) deposition technique (Alotaibi et al. 2018). The drug is entrapped in between the layer and is expected to be released via film-erosion mechanism (Smith et al. 2009). The film can consist of a single to hundreds of layer (Hsu, Hagerman, et al. 2014). The main advantage of polyelectrolyte multilayer coating system is that the amount of drug loaded into the film can be adjusted based on the total number of layering films and thus this approach is versatile for many therapeutic compounds (Hammond 2012).

The majority of studies in the field of anti-infective prosthesis focused on controlling the release of gentamicin. Nevertheless, in many cases, bacteria have become less susceptible to various antibiotics due to emerging resistance. Therefore, the use of alternative antimicrobial agents is encouraged (Williams, Mihok, and Murray 2016) and overuse of existing broad-spectrum antibiotic should be avoided (NICE 2015).

Chlorhexidine is a non- antibiotic antimicrobial agent; it is chemically classed a bisbiguanide and exists as a cationic form at physiological pH; its antimicrobial action is assumed to be caused by osmotic equilibrium of the bacterial cell alteration after electrostatic binding to the negatively charged bacterial cell wall (Lim and Kam 2008). Chlorhexidine is not water soluble; however, water soluble salts, found in commercial formulations, can be formed with gluconic acid (Lim and Kam 2008; Milstone, Passaretti, and Perl 2008). Chlorhexidine gluconate (CHG) is available in a variety of concentrations (0.5%-4%) and formulations (wipes, cloths, scrubs, solutions). It is available as either a single agent or in combination with alcohol (isopropyl alcohol or ethyl alcohol).

It is activity can be either bacteriostatic at low concentrations (0.0002% to 0.5%) or bactericidal at much higher concentrations (>0.5%) (Oosterwaal et al. 1989). At lower concentrations, it is capable of disrupting cellular membranes resulting in leakage of cell contents, while at higher concentrations, chlorhexidine can induce the coagulation of intracellular contents (Barrett-Bee, Newboult, and Edwards 1994). Although very high concentrations of chlorhexidine can result in ATPase inactivation, the lethal effects of chlorhexidine are primarily mediated by membrane disruptive properties. It has broad spectrum activity and is highly effective against a wide variety of organisms responsible for PJI, like *Staphylococcus aureus* (including methicillin-resistant *Staphylococcus aureus* (MRSA)) and coagulase negative *Staphylococcus*. It also demonstrates activity against Gram-negative bacteria, fungi and to a lesser extent, mycobacteria. It is sporostatic, but not sporicidal (Milstone, Passaretti, and Perl 2008). Chlorhexidine uptake by bacteria cells is extremely rapid as it has been shown that the maximum uptake occurs within the first 20 seconds of contact (Fitzgerald, Davies, and Russell 1989) and negligible further binding occurs with prolonged exposure times (Stinner et al. 2011). Such uptake is assumed to driven by passive diffusion and has been observed concentration dependent (McDonnell and Russell 1999). Once deposited on tissues chlorhexidine retains antimicrobial activity for long periods, for example on skin persistent antimicrobial activity has been observed for up to 48 hours (Hibbard 2005) .

Controlled release of anti-infective agents can be achieved by using biodegradable polymers such as alginate. Alginate is a naturally occurring anionic polymer typically obtained from brown seaweed, and has been extensively investigated and used for many biomedical applications, due to its biocompatibility, low toxicity, and relatively low cost (Lee and Mooney 2012).

In this chapter, LbL coating containing chlorhexidine will be prepared on titanium nanoparticles. The physical-chemical properties of the particles will be assessed through DLS, zeta potential and TGA. Drug release will be quantified along with the duration of antimicrobial activity; finally the impact of the media containing the released drug on human osteoblasts mitochondrial activity will be quantified through MTT assay.

4.2 Material and methods

4.2.1 Chemicals

Titanium (IV) oxide (Anatase, <25nm, 99.7%), (3-Aminopropyl) triethoxysilane (APTS, 99%), chlorhexidine diacetate (CL), phosphate buffer solution (PBS) tablets, sodium acetate trihydrate (≥99%), brain heart infusion agar, brain heart infusion broth, were purchased from Sigma-Aldrich, UK. HPLC grade acetonitrile, glacial acetic Acid, and toluene were purchased from Fisher, UK. All other chemicals were reagent grade, stored according to manufacturer's guidelines and used as received. B1 polymer which is a biocompatible, biodegradable cationic polymer of the poly(β-amino ester)s class as detailed in 2.1.1.

4.2.2 Nanoparticle preparation

4.2.2.1 Surface functionalization of titanium oxide nanoparticles

Titanium oxide nanoparticles were functionalized with amino groups ($TiO\text{-}NH_2$) via silanation, as described in section 2.2.1.

4.2.2.2 Layer by layer (LbL) coating technique

The amino fictionalized titanium nanoparticles were coated with polyelectrolyte multilayers. The layers consisted of different numbers of repeating sequence as the following: Alginate-Chlorhexidine-Alginate-B1. One sequence containing these four layers was termed quadruple layer (QL), up to ten quadruple layers were coated on the titanium nanoparticles, named as Qn where n represents the number of quadruple layers. Table 11 shows the component of chlorhexidine layer by layer coating on the amino functionalized titanium nanoparticles. The concentrations used were: 2mg/ml for sodium alginate, 10mg/ml for chlorhexidine, and 2mg/ml for B1. (The procedure for LbL coating is described in section 2.2.3).

Number of	Abbreviation	Layer composite on the surface of amino functionalized nanoparticles

quadruple layers		
1	Q1	TiO-NH_2-Alginate-Chlorhexidine-alginate-B1
2	Q2	TiO-NH_2-Q_{1-} Alginate-Chlorhexidine-alginate-B1
3	Q3	TiO-NH_2-Q1-Q2-Alginate-Chlorhexidine-alginate-B1
4	Q4	TiO-NH_2-Q1-Q2-Q3-Alginate-Chlorhexidine-alginate-B1
5	Q5	TiO-NH_2-Q1-Q2-Q3-Q4-Alginate- Chlorhexidine-alginate-B1
6	Q6	TiO-NH_2-Q1-Q2-Q3-Q4-Q5-Alginate-Chlorhexidine-alginate-B1
7	Q7	TiO-NH_2-Q1-Q2-Q3-Q4-Q5-Q6-Alginate-Chlorhexidine-alginate-B1
8	Q8	TiO-NH_2-Q1-Q2-Q3-Q4-Q5-Q6-Q7-Alginate-Chlorhexidine-alginate-B1
9	Q9	TiO-NH_2-Q1-Q2-Q3-Q4-Q5-Q6-Q7-Q8- Alginate-Chlorhexidine-alginate-B1
10	Q10	TiO-NH_2-Q1-Q2-Q3-Q4-Q6-Q7-Q8-Q9- Alginate-Chlorhexidine-alginate-B1

Table 11. Components of chlorhexidine layer by layer coating on the titanium nanoparticles surface.

4.2.3 Nanoparticles surface and material characterisation

4.2.3.1 Nanoparticles size measurements

The hydrodynamic size for the amino functionalized titanium nanoparticles and the LbL coated multilayer nanoparticles were measured by dynamic light scattering (DLS) using Malvern Zetasizer, Nano ZS particle characterization system (Malvern Instrument limited, UK) as described in section 2.3.1.

4.2.3.2 Zeta potential measurements

Nanoparticles electrophoretic mobility was measured by dynamic light scattering (DLS), using Malvern Zetasizer, Nano ZS particle characterization system (Malvern instrument limited, UK), (described in section 2.3.2).

4.2.3.3 Transmission Electron microscopy – particle size determination

Images of particles were obtained using a Zeiss 902 transmission electron microscope (TEM) operating at a voltage of 80 kV as described in section 2.3.3. The average particle size, size-distribution and morphology analysis of the samples was carried out from transmission electron micrographs using ImageJ for Windows (Version 1.50i).

4.2.3.4 Thermogravimetric Assay (TGA)

Thermogravimetric Assay was performed using a Perkin-Elmer TGA 4000 instrument (described in section 2.3.4).

4.2.4 Chlorhexidine release quantification

Chlorhexidine release was measured by dispersing the chlorhexidine coated nanoparticles (10mg) into 1ml of a buffer media and incubated at 37 °C. Two media: acetate buffer pH5, and phosphate buffer pH7.3, were used. pH7.3 represented healthy joint environment (Ribeiro, Monteiro, and Ferraz 2012) and pH5 represented infected joint condition (Kinnari et al. 2009; de Nadai et al. 2013).

An aliquot of 1 mL of the medium was withdrawn daily for quantification and the medium was replaced with equal volume of fresh buffer. The amount of CL released from the coating layer was determined using reverse-phase High Performance Liquid Chromatography/HPLC (1100 series Agilent Technologies®). The quantification procedure for chlorhexidine is described in section 2.3.5.1.

4.2.5 Antimicrobial testing

Antimicrobial testing was performed on chlorhexidine coated nanoparticles using the protocol described in section 2.4. The following clinical isolates from PJI were utilised: methicillin-resistant Methicillin resistant *Staphylococcus aureus* (MRSA) 275, 294; *Staphylococcus epidermidis* 272, 222, 199; Methicillin resistant *Staphylococcus epidermidis* (MRSE) 140, *Acinetobacter baumannii 646, 643, 640*; *Escherichia coli* 293, and *Enterococcus* 181.

4.2.6 Exposure of Osteoblast cells to release media

Human osteoblasts (Saos-2) were grown as described in section 2.5; MTT assay was conducted to measure cells' mitochondrial activity post-exposure to chlorhexidine

coated titanium nanoparticles after 1, 2 and 3 days exposure as per the protocol described in section 2.5.2.1.

4.2.7 Statistical analysis

One-way analysis of variance (ANOVA) was performed to assess the statistical significance of results between groups at 95% confidence level ($p < 0.05$). All data were expressed as mean ± standard deviation (SD) from at least three independent values.

4.3 Results

4.3.1 Surface functionalisation of TiO_2

The surface of TiO_2 nanoparticles carried neutral charge. In order to achieve successful deposition of the first layer, negatively charged ALG, the surface of TiO_2 nanoparticles were functionalized by APTS. The mechanism of this functionalisation has been proposed by (Howarter and Youngblood 2008), as illustrated in Figure 38. Initially, APTS were adsorbed onto TiO2 surface via hydrogen bond (Figure 38a). Next, more APTS were adsorbed and H-bonded APTS formed siloxane cross-links with each other (Figure 38b). The adsorbed APTS also formed siloxane bond with free APTS available in the solution during the treatment. As a result, multilayer build-up of APTS was formed, with NH_2 positioned at the surface (Figure 38c).

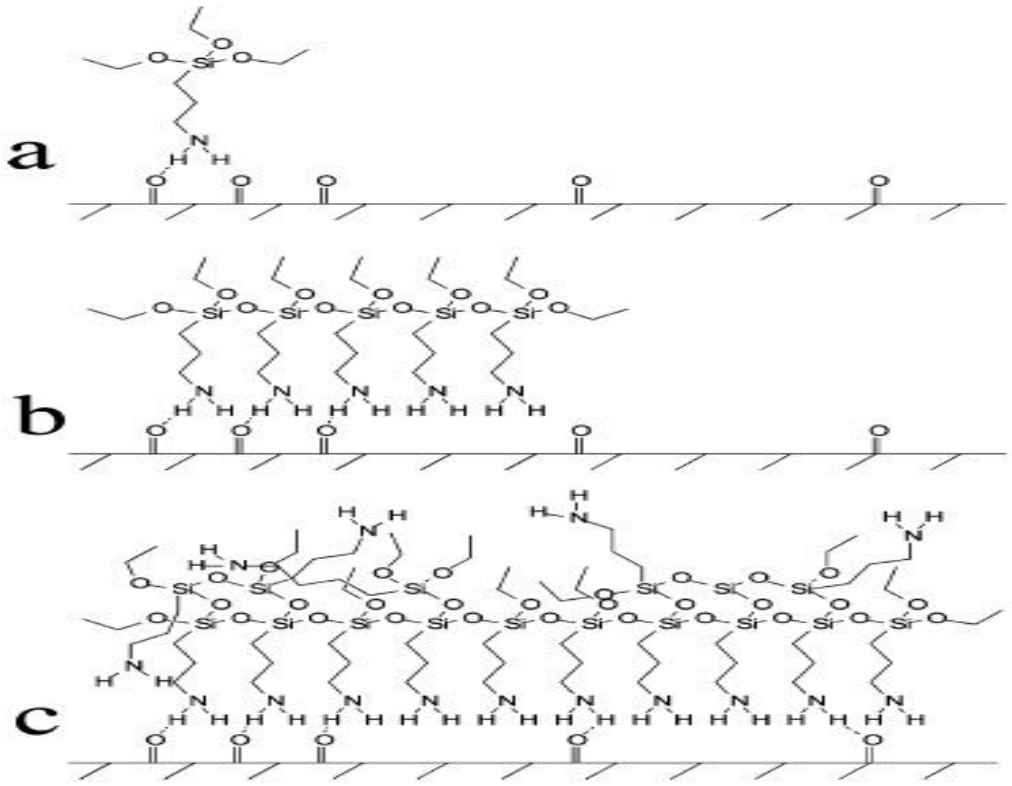

Figure 38. Amino-silanisation of TiO_2 nanoparticles. Initial adsorption of APTS onto TiO_2 surface (a) followed by siloxane cross-linking (b). Further crosslinking results in multilayer aminosilane build-up with NH2 groups positioned on the outermost layer (c). Figure adapted from (Howarter and Youngblood 2008).

4.3.2 Nanoparticles surface and material characterisation

4.3.2.1 Particle size measurements

The hydrodynamic size for amino functionalized titanium nanoparticles and nanoparticles layered with different number of quadruple layers are shown in Table 12. The diameter of the particles increased monotonically with progressively deposited layers from 504 nm for the bare functionalised particles (Ti-O-NH_2) to 2.2 μm after 10 quadruple layers.

Sample	Hydrodynamic diameter (nm)
TiO-NH_2 nanoparticles	504 ± 3.2
Q1	780.9 ± 5.1
Q3	1240 ± 9.7
Q5	1630 ± 8.4
Q7	1900 ± 6.5
Q10	2210 ± 10.5

Table 12. Hydrodynamic diameter measurement in acetate buffer pH5 for amino functionalised titanium nanoparticles and nanoparticles layered with different number of quadruple layer (n=3 ± SD).

4.3.2.2 Zeta potential measurements

Zeta potential measurements for amino functionalized titanium nanoparticles and for each layering step are shown in Figure 39.

Total 40 single layers were created to build ten quadruple layers. The amino functionalised titanium nanoparticles zeta potential was measured at +38.4±0.65 mV.

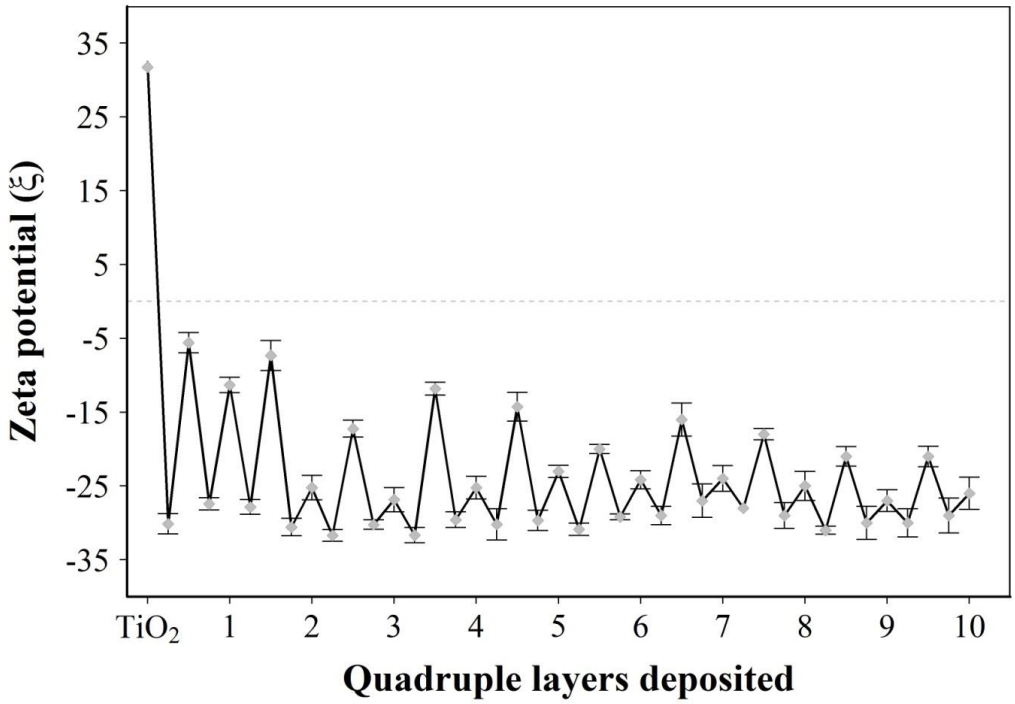

Figure 39. Zeta potential measurements for chlorhexidine coated amino functionalised titanium nanoparticles (mean ± SD n =3).

The coated nanoparticles generally exhibited a zig-zag pattern (alternating positive and negative value) after each coating step, as illustrated in Figure 39. The single repeated united was a sequence consisting of Alginate-Chlorhexidine-Alginate-B1 (quadruple films); this had a consistent zeta potential pattern (saw tooth) throughout the film deposition process as depicted in Figure 39. Coated particles exhibiting alginate as outer layer had zeta potential of around -30 mV regardless of the polyelectrolyte underneath (either chlorhexidine or B1); this value is very close to the zeta potential of pure alginate in the coating solution indicating a high coverage of the particles surface. The zeta potential turned to -5 mV after coating with chlorhexidine while coating of B1 onto these particles resulted in zeta potential of -11 mV.

4.3.3 TEM and particles size

Particles appeared cubical and spherical-like shaped (Figure 29) with relatively narrow distributed diameters (Table 9). LbL did not noticeably impact the size of the particles; however, after 10 quadruple layers, some particles agglomeration could be observed.

Sample	Average diameter (nm) ± SD
TiO_2-particles	34±5
Amino-functionalised particles	34±6
Q10	42±5

Table 13. Average diameter size of TiO_2 nanoparticles bare, after functionalisation and LbL deposition determined from TEM images.

4.3.3.1 Thermogravimetric analysis (TGA)

The TGA analysis of the various layers coated titanium nanoparticles are shown in Figure 41. Based on the TGA results, the percentage of organic content on the surface of the nanoparticles was calculated and it is presented in Table 14.

NP	% organic content (mean ± SD n =3).
Core	1.44 ± 0.08
Functionalised	4.48 ± 0.67
Q1	15.37 ± 0.01
Q3	21.55 ± 0.57
Q5	32.38 ± 0.06
Q7	36.41 ± 1.92
Q10	42.23 ± 5.84

Table 14. Organic content (%) in chlorhexidine layered titanium nanoparticles.

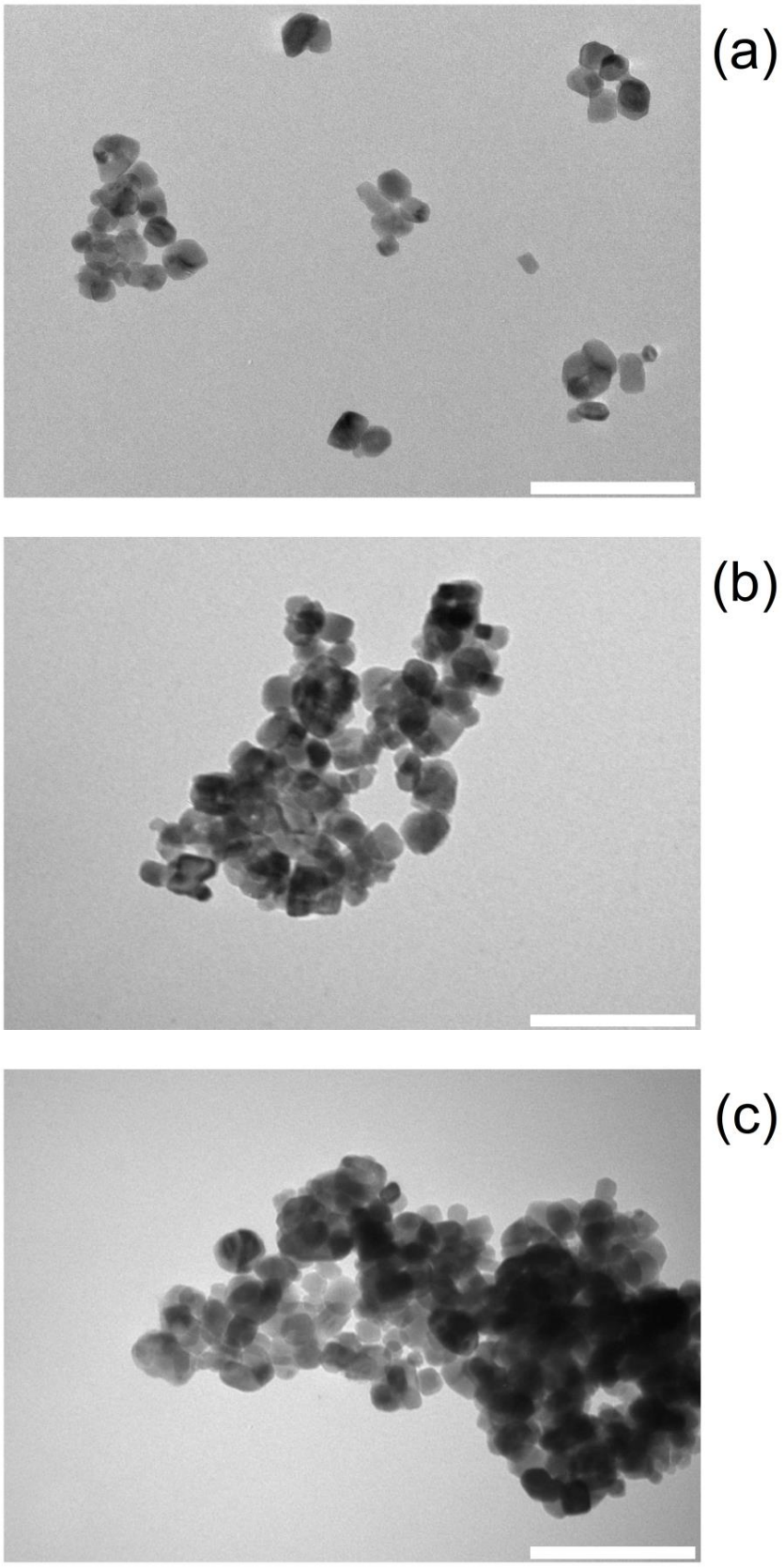

Figure 40. Example of Transmission Electron Microscopy images of (a) bare TiO_2 nanoparticles, (b) amino functionalised (TiO_2-NH_2) nanoparticles and LbL coated (Q10). Bar represents 100 nm.

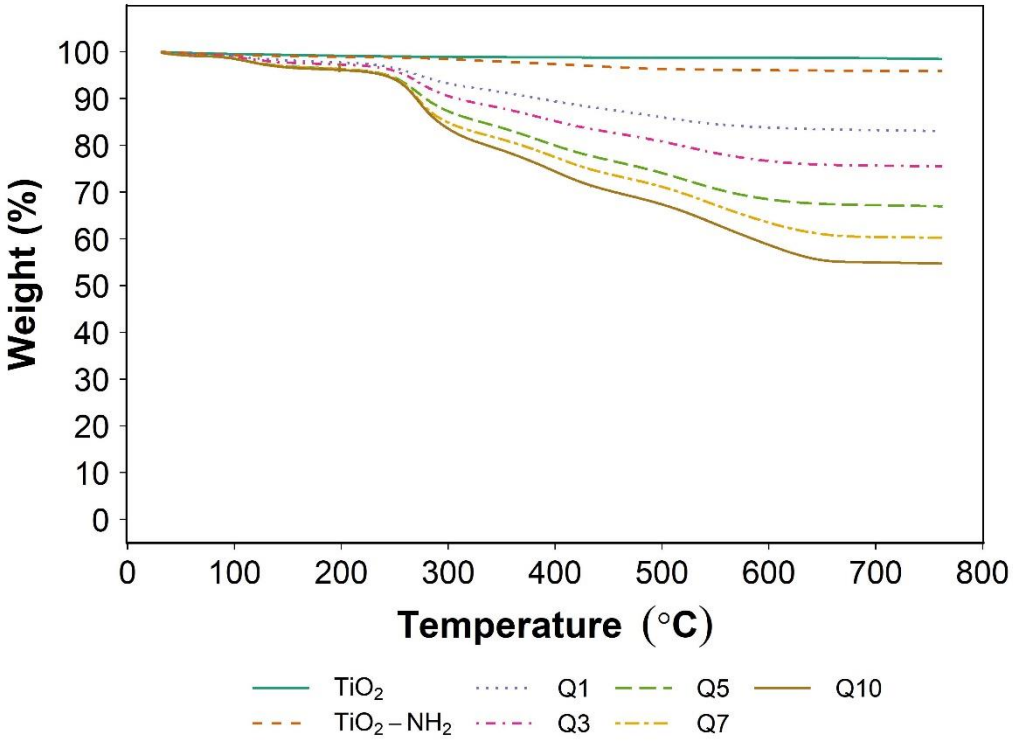

Figure 41. Thermogravimetric analysis for chlorhexidine layered titanium nanoparticles

As described in Figure 41, the thermograms of chlorhexidine coated titanium nanoparticles showed a plateau from about 650 °C. We presumed that the organic content has been lost at this point, and only the inorganic core of the nanoparticles remained. The total loss of weight at 100 °C represented vaporization of entrapped moisture in nanoparticles and was not the result of degradation of organic compounds (alginate, B1 or chlorhexidine). In contrast, the most dramatic weight loss occurred over the range 180 – 230 °C in chlorhexidine coated titanium nanoparticles indicated drug and polymers thermal decomposition. The weight loss of nanoparticles at 750°C was influenced by the number of quadruple layers. The order of weight loss from the highest to the lowest was as follow: Q10, Q7, Q5, Q3 and Q1. In contrast, the organic content of TiO_2 nanoparticles was the lowest, being 1.44 ± 0.08 %, increasing to 4.48 ± 0.67 % after amino-silanisation. This result indirectly indicated that the total organic content, which can indirectly indicate film thickness, of Q10 was the highest, followed by Q7, Q5, Q3, and Q1.

The slope of weight loss was sharp, confirming the higher content of coating organic material and its decomposition. The absolute value of the sloe also correlated with the number of quadruple layers as the thickest quadruple layer (Q10) had the greatest slope in comparison with Q1, Q3, Q5, and Q7, indicating the lowest degradation rate.

4.3.4 Chlorhexidine release study

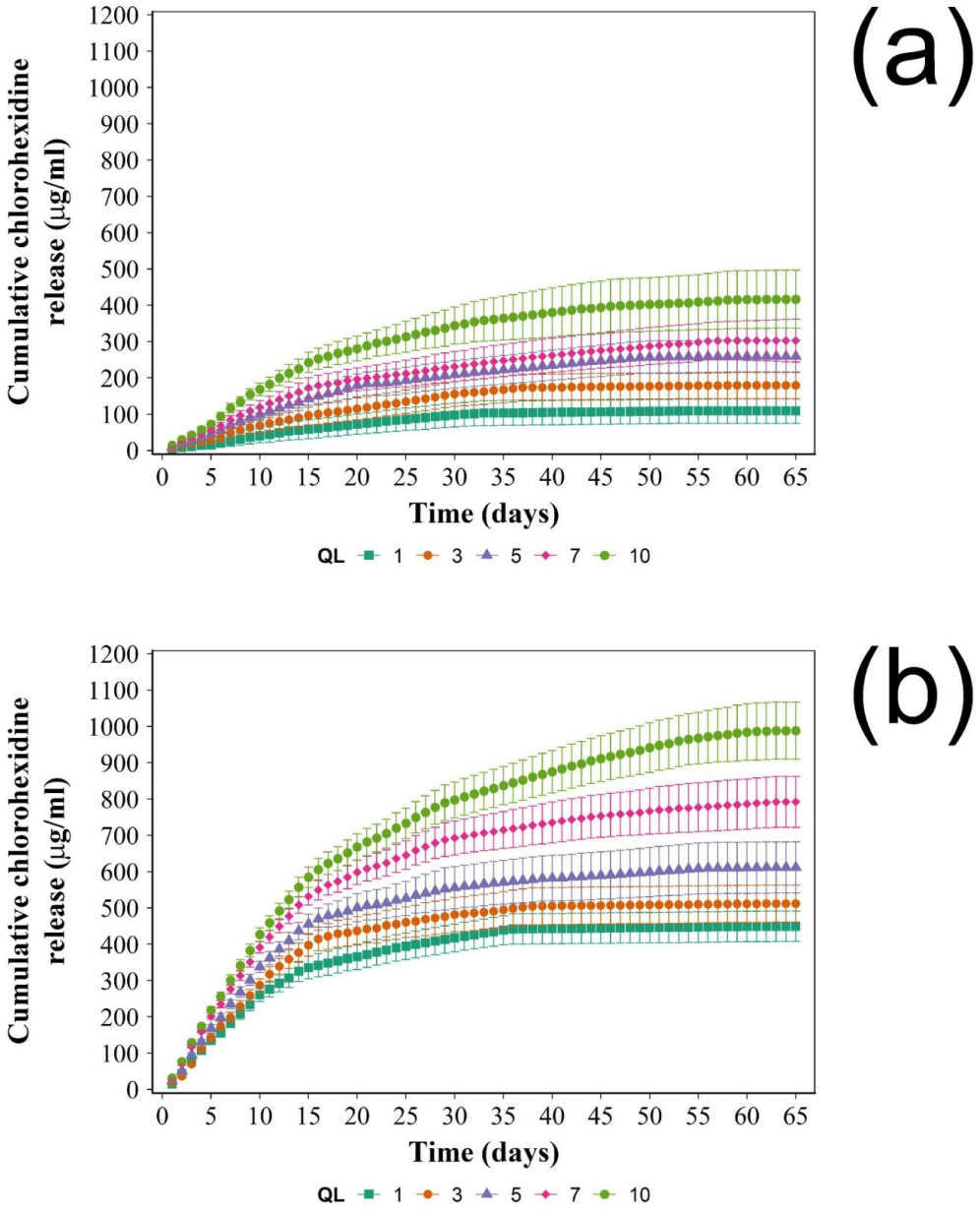

Figure 42. Chlorhexidine cumulative release in acetate buffer pH=7 (b) and pH=5 (a) from Q1, Q3, Q5, Q7, and Q10 (mean ± SD n =3).

Three major findings were identified in the release study of chlorhexidine coated titanium nanoparticles. Firstly, the total released amount of chlorhexidine was found to be monotonically increasing with the number of quadruple layers, which means that the highest drug content was found in Q10, while the lowest drug content was in Q1 (Figure 42). These findings indicated increased drug loaded after consecutive coating of quadruple layer. Also the release of Q10 and Q7 lasted more than 60 days in both conditions. Whereas Q5 released chlorhexidine up to 51 days in both pH5 and pH7; furthermore, Q1 and Q3 released chlorhexidine for less than 40 days in both release buffers. Secondly, chlorhexidine coated titanium nanoparticles showed monophasic release (zero order). Lastly, the release rate of chlorhexidine was higher at pH 5 than at pH 7.

4.3.5 Antimicrobial testing

Antimicrobial analysis against selected bacterial strains commonly encountered in PJIs was performed only on release media from 10Q coated titanium nanoparticles as these exhibited the longest release.

Figure 43 describes the antibacterial activities of chlorhexidine-coated titanium particles for certain Gram-negative (*E. coli* and *A. baumannii*) and Gram-positive (*S. epidermis*, MRSE, MRSA and *Enterococcus*) bacterial isolated from PJI. Generally, growth inhibition of these bacteria was achieved by the release media corresponding to 4-17 days of release for Gram negative bacteria and to 17-28 days for Gram-positive bacteria, indicating strongest susceptibility of Gram-positive bacteria towards chlorhexidine. The least sensitive bacteria towards were the three *A. baumannii* strains tested, where nanoparticles releasing chlorhexidine were able to inhibit growth of *A. baumannii* 643 for 4 days and *A. baumannii* 646 and 640 for 6 days. Growth of *E. coli* 293 and MRSA 140 was inhibited by media released up to 16 days. Growth of *Enterococcus* was inhibited by media released up to 18 days while MRSA 924 and MRSA 275, were successfully inhibited by media released up to 20 days and 28 days, respectively. *S. epidermidis* isolated 199, 222, and 275 were inhibited by media released up to 23, 25, and 22 days, respectively.

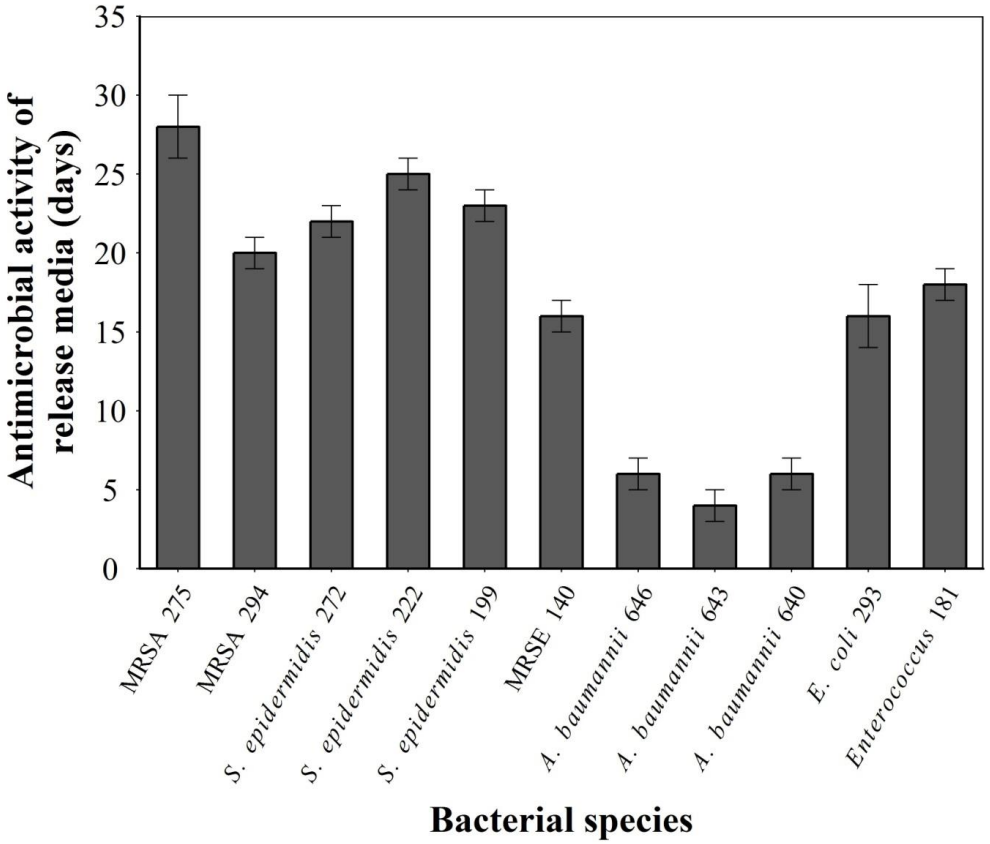

Figure 43. Antimicrobial testing for 10QL chlorhexidine coated titanium nanoparticles against various PJI clinical isolates (mean ± SD n =3).

4.3.6 MTT testing

MTT testing was employed to assess the cytocompatibility of chlorhexidine coated titanium nanoparticles.

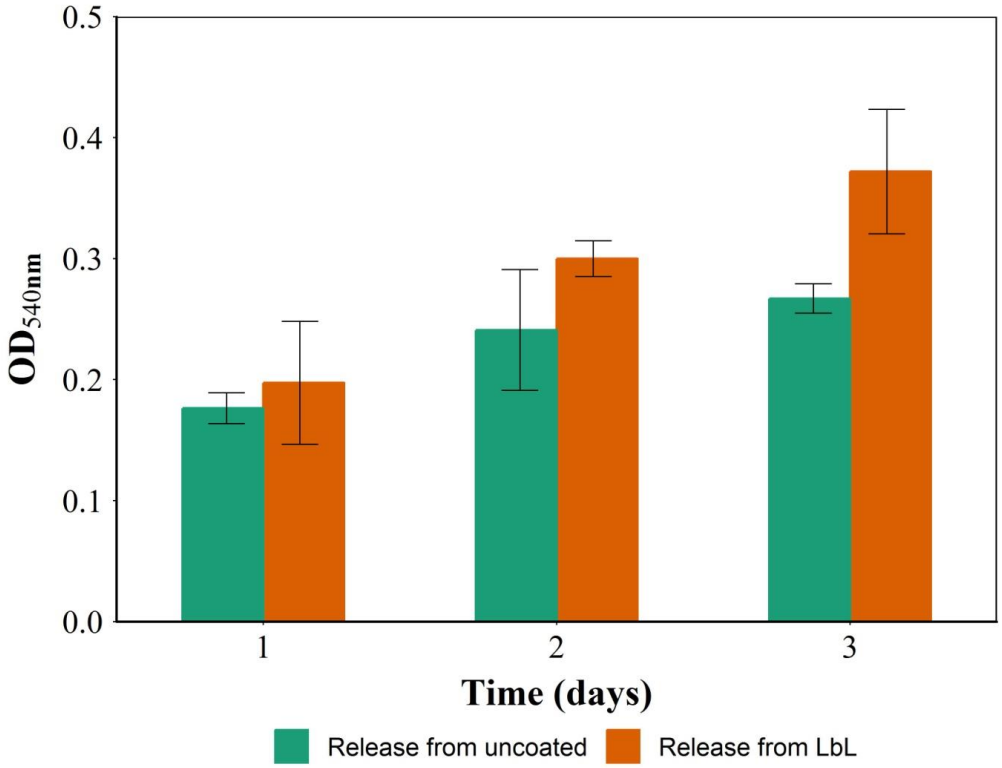

Figure 44. Mitochondrial activity of human osteoblasts (Saos-2) exposed to 1:10 dilutions of chlorhexidine coated titanium nanoparticles release buffer for 1, 2 and 3 days, assessed through MTT test (mean ± SD n =6).

Mitochondrial activity of Saos-2 increased with incubation time; when the release media containing chlorhexidine osteoblasts was added, no reduction ($p<0.05$) of mitochondrial activity was observed for incubation up to 3 days (Figure 44).

4.4 Discussion

4.4.1 Size measurements

Size for amino functionalized titanium nanoparticles and different quadruple layers containing B1 (polymer), alginate (polymer) and chlorhexidine (non antibiotic antimicrobial) were measured by dynamic light scattering (DLS) and TEM that are routinely applied techniques for such applications (Geißler et al. 2015). Titanium nanoparticles measured 34 nm, when analysed with TEM, compatible with the commercially stated dimension. After amino functionalisation the particle size increased significantly; furthermore, after layering different number of electrolytes there was a great increase in the size of nanoparticles up to 2.22 µm as seen in Q10 (Table 12).

When DLS was employed, the particles size estimated as 500 nm and about 5 folds increase was measured after deposition of 10 quadruple layers. This large increase in particle size is mainly due to the thickness of the deposited layers and by the agglomeration of the nanoparticles caused by the polyelectrolytes interacting simultaneously to more than one particle during LbL deposition (Gosens et al. 2010). The later mechanism has been suggested to be prevalent for the deposition of gentamicin on silica nanoparticles using LbL (Al Thaher et al. 2018). The hydrodynamic diameter increase observed here is likely due to aggregation as the increase would be too high to simply be the results of LbL that is generally in the order of nanometres (Ariga et al. 2011; Deshmukh et al. 2013; Gentile et al. 2015).

4.4.2 Zeta potential measurement

Chlorhexidine diacetate is a water-soluble antibacterial agent, but the solubility is affected by pH (do Amorim, Aun, and Mayer 2004). Solubility of chlorhexidine is higher in acidic pH (Anusavice, Zhang, and Shen 2006) but the activity is higher in slightly alkaline environment (do Amorim, Aun, and Mayer 2004). While only 3.3 mg/ml of CHX can be dissolved in pH 7 buffer, the dissolution of Chlorhexidine at pH 4 is three times higher, being more than 10 mg/ml (Anusavice, Zhang, and Shen 2006). In the preparation we used acetate buffer (pH 5) to ensure that B1 was positively charged (Al Thaher et al. 2018); in these conditions chlorhexidine ionizes and thus, it exhibits the desired positive charged that allowed the LbL deposition. The positive charge of chlorhexidine is due to chlorhexidine cations, the cationic group that is responsible for bacteriostatic activity (do Amorim, Aun, and Mayer 2004). At pH5, sodium alginate is negatively charged as the carboxyl groups are hydrogenated only at lower pH (Shinde and Nagarsenker 2009) as the pKa of carboxyl acids is about 4.5.

The adsorption of alginate rendered zeta potential (ζ) value negative, while the adsorption of chlorhexidine and B1 did not resulted in a positive ζ value; however the patterned exhibited a reduction of the negative charge on the nanoparticles surface after chlorhexidine and B1 deposition than after alginate (Figure 39). For example, after the first deposited alginate layer, ζ was -32.19 ± 3.99 mV. Deposition of chlorhexidine onto alginate-coated nanoparticles resulted in ζ equal -17.84 ± 10.51. This indicated that chlorhexidine had been successfully deposited onto the previous layer via electrostatic interaction between the cationic groups of chlorhexidine (the guanidium ion) and anionic groups of alginate (carboxyl acid). The third layer in each quadruple layer consisted of alginate and resulted in a negative ζ value at -34.76 ± 2.79, which indicates that the surface of nanoparticles has been entirely covered by this polyelectrolyte. Lastly, the

final coating layer in each quadruple layers unit was made of B1; when this polyelectrolyte was deposited the nanoparticles had a zeta potential ζ of -23.45 ± 6.15. This ζ value was less negative than that of the previous layer because the cationic groups in B1 were not capable to overcome the alginate charge; B1 belongs to a category of polymers whose zeta potential at pH 5 is about 10-15 mV, significantly smaller than alginate (absolute value ~ 30 mV) (Perni and Prokopovich 2017).

4.4.3 Thermogravimetric analysis

Thermogravimetric assay was conducted to confirm and quantify the attachment of polyelectrolytes and drug layers onto the surface of TiO_2 nanoparticles. As described in Figure 41, the thermograms of all coated nanoparticles showed a plateau line from around 650 °C. We presumed that the organic content has been lost at this point, and only the inorganic core of nanoparticles remained, such approach is the typical interpretation of thermograms (Mai et al. 2014; Zhong et al. 2015). The total loss of weight at 100 °C represented vaporization of entrapped moisture in nanoparticles and was not a result of degradation of organic compounds (alginate/B1/chlorhexidine). In contrast, the most dramatic weight loss occurred over the range 180-230 °C, indicating endothermic events of the drug and polymers, most likely as degradation.

In the LbL coating, the deposited polyelectrolytes were deposited through an aqueous medium. Despite the drying process, traces of water can still be present in the polyelectrolyte layers on the surface of the nanoparticles. Therefore, each layer carried some moisture content and, as the number of layer increases, the total moisture content became increased. In chlorhexidine coated with on quadruple layer (Q1) the weight loss at 100 °C, which indicated the moisture content, was 1.78 ± 0.06 %, this figure increased to 3.33 ± 0.04 % after 10 quadruple layers. Therefore, the weight loss at 100 °C was used as a correction in determining organic content (Du et al. 2015).

The thermograms of all coated nanoparticles (Figure 41) showed that the weight loss of Q1 to Q10 nanoparticles at 750°C from the highest to the lowest were in the following order: Q10, Q7, Q5, Q3, Q1 (Table 14). This result indirectly indicated that the total organic content, which is correlated to film thickness, of Q10 was the highest, followed by Q7, Q5, Q3, and Q1. These results demonstrated the progressive nature of the drug deposition through LbL; moreover the calculated organic matter percentage for the amino functionalized nanoparticles (Table 14) was caused by the amino silanol conjugating to the titanium surface. The organic fraction of the nanoparticles after each quadruple layer was close to the reported using the same LbL process on silica nanoparticles to deposit gentamicin (Al Thaher et al. 2018).

4.4.4 Chlorhexidine release quantification

Two opposite mechanisms concur to drug release from LbL coatings; one is the progressive detachment of the deposited layers (delamination) while the other is the diffusion of the drug through the deposited layers (Smith et al. 2009). The release profile is, therefore, the sum of these two simultaneous processes; moreover, as each of these two mechanisms have a distinctive release profile, from the observed profile it is possible to determine which mechanism is predominant (Smith et al. 2009; Al Thaher et al. 2018). For example, pure delamination, resulting from polyelectrolyte hydrolysis or detachment, causes a constant drug release rate up to full coating detachment when it drops to zero. On the contrary, diffusion returns a Fickian profile that has a maximum drug release rate at the beginning and monotonically decreasing down to zero (Smith et al. 2009; Al Thaher et al. 2018). Drug release rate from LbL coatings is influenced by numerous variables, i.e. number and polyelectrolytes used (Grech, Mano, and Reis 2008; Wong et al. 2010), the strength of the electrostatic interaction between polyelectrolytes layers (Al Thaher et al. 2018), and the kinetics of hydrolysis for the polyelectrolytes involved (Smith et al. 2009). The observed release kinetic (Figure 42) describes a drug release profile for chlorhexidine dominated by diffusion describes a drug release profile for chlorhexidine dominated by diffusion as the rate progressively decreases, this is consistent with the results presented for gentamicin (Al Thaher et al. 2018), furthermore the higher drug release at pH7 than at pH also confirms the previously hypothesised mechanism as B1 (and consequent delamination) would be predominant at pH5. The observed duration of chlorhexidine release from the LbL coated surfaces was ~ 2 months; hence the technology proposed would be fully capable of providing infection prevention for a period longer than about 1 week as it is currently available when antibiotic bone cement are employed (Swearingen et al. 2016). Moreover, when LbL coating similar to those employed here are fabricated with gentamicin, drug release had been observed for only 4 week (Al Thaher et al. 2018). The longer elution when chlorhexidine is considered is likely due to its higher charge than gentamicin and longer chain; both attributes would contribute to a lower diffusion through the deposited layers both electrostatically and sterically.

4.4.5 Antimicrobial testing

The release of chlorhexidine was studied in two different conditions (Figure 42). The first condition (pH5) was mimicking the slightly acidic conditions in infected joint (Kinnari et al. 2009). While the other condition (pH7.3) represented the healthy joint (Ribeiro, Monteiro, and Ferraz 2012).

Antimicrobial testing was carried out against clinical isolates of PJIs (Geipel 2009; Martinez-Pastor et al. 2009; Hsieh et al. 2009) directly incubating the release media from the coated nanoparticles with the tested bacteria. This simulates the real scenario in the prosthetic joint surgery. Also only the release media at pH7.3 was used as some of the strains were not able to grow sufficiently in the acidic buffer. As seen in Figure 42, chlorhexidine concentration in the media decreased with time, therefore the release media was capable of inhibit growth until chlorhexidine fell below MIC. The different efficacy observed is linked to species and strain variation of MIC; for example MIC for *E. coli* was reported 2.67 µg/ml (do Amorim, Aun, and Mayer 2004) while for MRSA the MIC was 4-8 µg/ml (Cookson, Bolton, and Platt 1991); *Pseudomonas aeruginosa* is much less susceptible to chlorhexidine 80 µg/ml (Thomas, Russell, and Maillard 2005).

In our study chlorhexidine was more effective in preventing the growth of Gram-positive bacteria than Gram-negative bacteria. Generally, bacteria are characterized as positive or negative based on a staining protocol that depends on the bacterium's chemical and physical cell wall properties (Madigan and Martinko 1997). Gram positive bacteria have a very thick cell wall made of peptidoglycan (a polymer of amino acids and sugars that create the cell wall of all bacteria in their cell membranes) (Madigan and Martinko 1997) that accounts for approximately 40% or more of the mass of the wall and it is capable of absorbing foreign material (Shockman and Barrett 1983). These bacteria retain the crystal violet dye (one of the two main chemicals used for Gram staining). While on the other hand, Gram negative bacteria have a very thin peptidoglycan layer which approximately 10 % or less that is between an inner cell membrane and a bacterial outer membrane (Madigan and Martinko 1997). Gram-negative bacteria do not retain the crystal violet stain because of the physical composition of the cell wall and are counter stained in pink (Madigan and Martinko 1997). Hence, they are termed as Gram-negative. Because of their thin but difficult-to-penetrate cell membrane, Gram-negative bacteria are often more resistant to antibiotics and other antibacterial interventions (Siu 2002); moreover the pathogenic capability of Gram-negative bacteria is often associated with certain components of their membrane, in particular the LPS (Salton and Kim 1996). The outer membrane protects the bacteria from several antibiotics, dyes, and detergents that would normally damage either the inner membrane or the cell wall (made of peptidoglycan); the outer membrane also provides Gram negative bacteria with resistance to lysozyme and penicillin (Madigan and Martinko 1997). The periplasmic space (space between the two cell membranes) also contains enzymes which break down or modify antibiotics (Munita and Arias 2016).

Hence, the higher sensitivity of the Gram-positive bacteria tested in this work is consistent with the general knowledge.

The opportunity of adding antibiotics to PMMA bone cement has allowed the treatment and prevention of infections post joint replacement surgery through a local delivery instead of through systemic administration of antibiotics. This opportunity is not available in un-cemented prosthesis that however possess other benefits such as a shorter operating room time, preservation of bone stock and ease of revision (Aprato et al. 2016); additionally un-cemented fixation is not affected by any of the possible complications associated with cemented fixation like third body wear, retained loose fragments and bone cement implantation syndrome (Aprato et al. 2016; Donaldson et al. 2009). Despite the numerous aforementioned benefits of un-cemented joint replacements, their instability was a major drawback that prevented the diffusion of these devices (Maggs and Wilson 2017). Modern designs have solved this problem hence the research focus has shifted towards providing antimicrobial activity. For example, vancomycin covalently bound to TiO rods strongly inhibited colonization and biofilm formation, the modified titanium surface exhibited potent antibacterial activity after pre-incubation for 45 days (Antoci et al. 2007). Similarly, gentamicin was deposited onto titanium devices but provided antimicrobial activity for a shorter period of time than antibiotic loaded bone cement 4 days and 7 days, respectively (Neut et al. 2011).

The rise of antibiotic resistance has driven research onto alternative techniques or molecules capable of antimicrobial activity without selecting resistant cells, silver ability to inactivate microorganisms has been widely researched (Besinis et al. 2017; Kuehl et al. 2016). However, there are growing concerns, both environmental safety and toxicity, associated to the use metal ions or nanoparticles. As alternative, chlorhexidine, which has been used in mouthwash solutions and topical treatment, has now been investigated for use in arthroplasty. Pins for external fixation coated with hydroxy apatite/chlorhexidine had large inhibition in *S. aureus* (DeJong et al. 2001). TiO_2 implants with chlorhexidine containing exerted potent bactericidal effect against *S. aureus* (Riool, Dirks, et al. 2017). However, 88% of the release occurred in the first 24 hours hence not providing prolong antimicrobial activity confirming the requirement for a delivery system in order to achieve antimicrobial properties for period of time that would protect patients from any type of PJI, not only early infections.

4.4.6 MTT assay

Any new biomaterial must demonstrate not only to functionally perform to the required level it has been developed for, but only not to hinder the contacting tissues and cells metabolic activity or induce cell death. The titanium coating presented here have demonstrated the ability to sustain chlorhexidine for prolong period of time; however, their clinical utilisation would be conditional to support osteoblast cells growth. These are the fundamental cells in bones and routinely employed in-vitro testing of novel orthopaedic materials (Mikulewicz and Chojnacka 2011; Baranowski et al. 2016). MTT assay is based on the determination of the mitochondrial activity of cell through the quantification of the formazan resulting from the oxidation of a tetrazolium dye and indirectly the amount of viable cells (Mosmann 1983).

Because titanium nanoparticles were employed as a model for titanium devices, it was not possible to grow cells directly onto the LbL coated surfaces; hence the response of already established osteoblast cultures to media containing released chlorhexidine was compared to the response to sterile PBS. Moreover, the tests were conducted only from release buffer pH7 as the acidic buffer (pH5) exhibited toxic activity.

Titanium surfaces are used in orthopaedic devices because osteoblast cells are capable of adhering and proliferating on such material hence the increasing mitochondrial activity observed in the controlled samples (Figure 44) was well expected; moreover the presence of chlorhexidine from the LbL coating did not negatively impact osteoblast and such these materials are not inferior to standard titanium in regards to osteoblast growth. Because titanium, as mentioned, exhibits sufficient cytocompatibility towards osteoblasts it was not necessary for the LbL coating to improve such properties and non-inferiority was deemed sufficient.

4.5 Conclusions

The ultimate goal of total joint replacement is to improve mobility of the patient. As prosthesis implants are semi-permanent, any harmful event such as aseptic loosening, infection, and hypersensitivity reaction should never occur for the lifetime of the devices. While bone cement in cemented prosthesis helps the fixation of the device and can provide a reservoir of antibiotics; un-cemented prosthesis only consists of inert materials that lacks osseoconductive properties. Without a good strategy, using un-cemented prosthesis will not reach its maximum benefits.

We constructed a drug eluting system for non-antibiotic agent (chlorhexidine) for un-cemented prosthesis using layer-by-layer technique. Our zeta potential determination and thermogravimetric assay indicated that each drug/polymer layer was stably deposited via electrostatic interactions. We have successfully controlled the release of chlorhexidine for more than two months without observing detrimental effects osteoblasts viability. Thus, this can be a solution to the problem of prolonged antimicrobial activity in un-cemented prostheses and antibiotic resistance.

Chapter 5: Chlorhexidine and dexamethasone controlled release from layer-by-layer coated nanoparticles

5.1 Introduction

Aseptic loosening and periprosthetic joint infection (PJI) are most common complication following joint replacement surgery (Postler et al. 2018), the consequences of these can range from the need to removal of the devices and insertion of the new one (revision surgery) to life threating and potentially life changing consequences (i.e. amputation). The incidence of PJI is, generally, lower than aseptic loosening (Ulrich et al. 2008), but the consequences can be more serious and complex (Li, Renz, and Trampuz 2018).

PJI are routinely treated with the use of antibiotics, either parenterally or though antibiotic laden bone cement (Anagnostakos 2017); however, the rise of resistance to these drugs among bacteria (Ravi et al. 2016) and the difficulties in controlling the release of the antimicrobial compounds are a serious limitation to this approach (Al Thaher, Perni, and Prokopovich 2017). Uncemented prosthesis are employed in a growing number of patients in light of a possible better long term integration of the device with the bone and the removal of the adverse events related to bone cement (Abdulkarim et al. 2013; Maggs and Wilson 2017). Despite these benefits, the instability un-cemented joint replacements was a major factor in preventing the wide use these devices (Maggs and Wilson 2017). Modern designs have solved this problem; however, the absence of bone cement removes the availability of the local antimicrobial delivery route. Hence the research focus in uncemented prosthetic devices has shifted towards providing antimicrobial activity. Antibiotics such as vancomycin and gentamicin have been covalently bound or deposited to titanium surfaces used in joint replacement devices (Antoci et al. 2007; Neut et al. 2011); however, the increase in antibiotic resistance poses a growing threat and novel delivery systems allowing prolonged and controlled release of non-antibiotic antimicrobial compounds for uncemented joint replacement devices are an urgent need. Chlorhexidine is well known antimicrobial compound that has been used in mouth washes and topical applications (Lim and Kam 2008), more recently it is use has been attempted in orthopaedic applications (DeJong et al. 2001) because of its wide range activity and ability to inactivate already antibiotic resistant bacteria (Cookson, Bolton, and Platt 1991).

Aseptic loosening is caused by the progressive destruction of the bone surrounding the device caused by an increased level of bone resorption by osteoclast cells; this process is

mediated by the immune system response that considers the implant a foreign matter (Sundfeldt, V Carlsson, et al. 2006; Greenfield et al. 2002) and, soon after transplantation induces 'rejection'. The addition of immune-suppressants, molecules capable of modulate the immune-system response, have been suggested as possible therapeutic approach to aseptic loosening (Ren et al. 2013) and dexamethasone, a steroidal drug, has been used to reduce osteolysis (Ren et al. 2014).

The layer-by-layer (LbL) technique has been investigated for prosthetic coating in various studies (Macdonald et al. 2011; Shah et al. 2013; Smith et al. 2009; Wong et al. 2010) incorporating antibiotic and bone morphogenic proteins in a eluting coating. The versatility of LbL in allowing the preparation of multidrug complexes is well known (Ramasamy et al. 2014) and the codelivery of drugs through coating prepared with this technique has been demonstrated (Deng et al. 2013).

In this chapter, coatings containing both dexamethasone phosphate (DEX-P) and chlorhexidine on the surface of amino functionalised titanium particles have been prepared. The role of the drugs distribution had been investigated in order to determine the most appropriate coating capable of simultaneously preventing PJI and reduce the risk of aseptic loosening through reducing the inflammatory response of the immunesystem.

5.2 Material and methods

5.2.1 Nanoparticles preparation

5.2.1.1 Surface functionalization of titanium nanoparticles

Titanium oxide nanoparticles were functionalized with amino groups ($TiO\text{-}NH_2$) via silanation, as described in section 2.2.1.

5.2.1.2 Layer by layer (LbL) coating technique

$TiO_2\text{-}NH_2$ nanoparticles were coated with polyelectrolyte multilayers as described in section 2.2.3. The layers consisted of different numbers of repeating sequence as the following: ALG-CL-ALG-B1, ALG-B1-DEX-B1. One sequence containing these four layers were termed quadruple layer (Q). Different combinations of quadruple layers containing chlorhexidine and DEX were prepared:

- ALG-B1-DEX-B1 from Q1 to 2 and ALG-CHL-ALG-B1 from Q3 to 10 denoted C20

- ALG-B1-DEX-B1 from Q1 to 4 and ALG-CHL-ALG-B1 from Q5 to 10 denoted C40
- ALG-B1-DEX-B1 for Q1-3-5-7-9 and ALG-CHL-ALG-B1 for Q2-4-6-8-10 denoted C50

After the final washing cycle, TiO_2-NH_2nanoparticles were collected and dried under fume hood for 24 hours.

5.2.2 Nanoparticles characterisation

5.2.2.1 Nanoparticles size measurements

The hydrodynamic size for the amino functionalized titanium nanoparticles and the LbL coated multilayer nanoparticles were measured by dynamic light scattering (DLS) using Malvern Zetasizer, Nano ZS particle characterization system (Malvern Instrument limited, UK) as described in section 2.3.1.

5.2.2.2 Zeta potential measurements

Nanoparticles electrophoretic mobility was measured by dynamic light scattering (DLS), using Malvern Zetasizer, Nano ZS particle characterization system (Malvern instrument limited, UK), (described in section 2.3.2).

5.2.2.3 Thermogravimetric Assay (TGA)

Thermogravimetric Assay was performed using a Perkin-Elmer TGA 4000 instrument (described in section 2.3.4).

5.2.3 Drug release study

Chlorhexidine and DEX release was measured by dispersing the chlorhexidine/DEX coated nanoparticles (10mg) into 1ml of a buffer media and incubated at 37 °C. Two media: acetate buffer pH5, and phosphate buffer pH7.3, were used. pH7.3 represented healthy joint environment (Ribeiro, Monteiro, and Ferraz 2012) and pH5 represented infected/ inflamed joint condition (Kinnari et al. 2009; de Nadai et al. 2013).

An aliquot of 1 mL of the medium was withdrawn daily for quantification and the medium was replaced with equal volume of fresh buffer. The amount of CL released from the coating layer was determined using reverse-phase High Performance Liquid Chromatography/HPLC (1100 series Agilent Technologies®). The quantification procedure for chlorhexidine and DEX is described in section 2.3.5.1.

5.2.4 Antimicrobial activity study

Antimicrobial testing was performed on chlorhexidine coated nanoparticles using the protocol described in section 2.4. Clinical isolates of PJI from were employed: Gram-positive bacteria methicillin-resistant *Staphylococcus aureus* (MRSA) 294 and 275, *Staphylococcus epidermidis* 279, 189 and 222, methicillin-resistant *Staphylococcus epidermidis* (MRSE) 140 and *Enterococcus* 181 along with Gram-negative bacteria *Escherichia coli* 293 and *Acinetobacter baumannii* 640, 643, and 646.

5.2.5 Cell culture and exposure to nanoparticles

Human monocytic leukaemia cells THP-1 cells were grown as described in 2.5.

5.2.5.1 MTT

MTT assay was conducted to measure human macrophages (THP-1) mitochondrial activity post-exposure to DEX coated titanium nanoparticles after 1, 2 and 3 days exposure as per the protocol described in section 2.5.2.1.

5.2.5.2 IL-6 and TNFα

The amount of IL-6 and TNFα released in the media after exposure to LPS and DEX for 6 and 24 hours was determined using appropriate ELISA kit (Sigma, UK) according to manufacturer's recommendations as per the protocol described in section 2.5.2.2.

5.2.6 Statistical analysis

One-way analysis of variance (ANOVA) was performed using SPSS (12.0) to assess the statistical significance of results between groups. At 95% confidence level ($p<0.05$) from at least three independent value all data were expressed as mean ± standard deviation (SD).

5.3 Results

5.3.1 Nanoparticle surface and material characterisation

5.3.1.1 Particle size measurement

The hydrodynamic size for amino functionalized titanium nanoparticles and nanoparticles layered with different number of quadruple layers are shown in Table 15. Particles diameters increased with increasing number of quadruple layers regardless of the drug deposited and each repeated unit. After the deposition of 10 quadruple layers

the hydrodynamic diameter of the nanoparticles was about 4 times greater than the functionalised nanoparticles.

a.

Sample	Hydrodynamic size (nm)
TiO_2-NH_2 nanoparticles	504 ± 3.2
Q1	651 ± 6.3
Q3	1056 ± 7.1
Q5	1487 ± 5.1
Q7	1856 ± 6.5
Q10	2160 ± 6.2

b.

Sample	Hydrodynamic size (nm)
TiO_2-NH_2 nanoparticles	504 ± 5.7
Q1	674 ± 3.6
Q3	859 ± 7.4
Q5	1260 ± 9.1
Q7	1669 ± 5.1
Q10	2081 ± 8.1

c.

Sample	Hydrodynamic size (nm)
TiO_2-NH_2 nanoparticles	504 ± 2.7
Q1	668 ± 9.5

Q3	840 ± 7.4
Q5	1050 ± 3.6
Q7	1455 ± 8.4
Q10	1875 ± 7.5

Table 15. Hydrodynamic diameter measurement in acetate buffer pH5 for amino functionalised titanium nanoparticles and nanoparticles layered with different number of quadruple layers (a) C20, (b) C40 and (c) C50 (mean ± SD n =3).

5.3.1.2 Zeta potential

Surface charge of all coated nanoparticles generally exhibited a zig-zag pattern, as illustrated in Figure 45. All three different LbL sequences had the first quadruple layer comprising of DEX-P and described the same pattern. Starting from the positive values of ~+38 mV of the uncoated amino functionalized nanoparticles to ~ -28 mV after the first layer deposited (alginate). Following the alginate layer B1 was deposited and the zeta potential reached +5 mV, the subsequent deposition of DEX-P resulted in a surface charge of -15 mV; a further layer of B1 (completing the first quadruple layer) resulted in the coated particle exhibiting a zeta potential of +5 mV.

Because C20 and C40 had also the same second quadruple layer, containing DEX-P, the zeta potential profile of these two nanoparticles continued to overlap; with negative potential after alginate (~-25 mV) and DEX-P (~-10 mV) and ~-3 mV after B1; on the contrary, a chlorhexidine containing quadruple layer was deposited in C50, hence the zeta potential of this type of nanoparticles differs from the other two.

Further layers alginate deposition resulted in particles with a zeta potential ~ -25 mV while deposition of B1or chlorhexidine returned a zeta potential of ~ -2 mV.

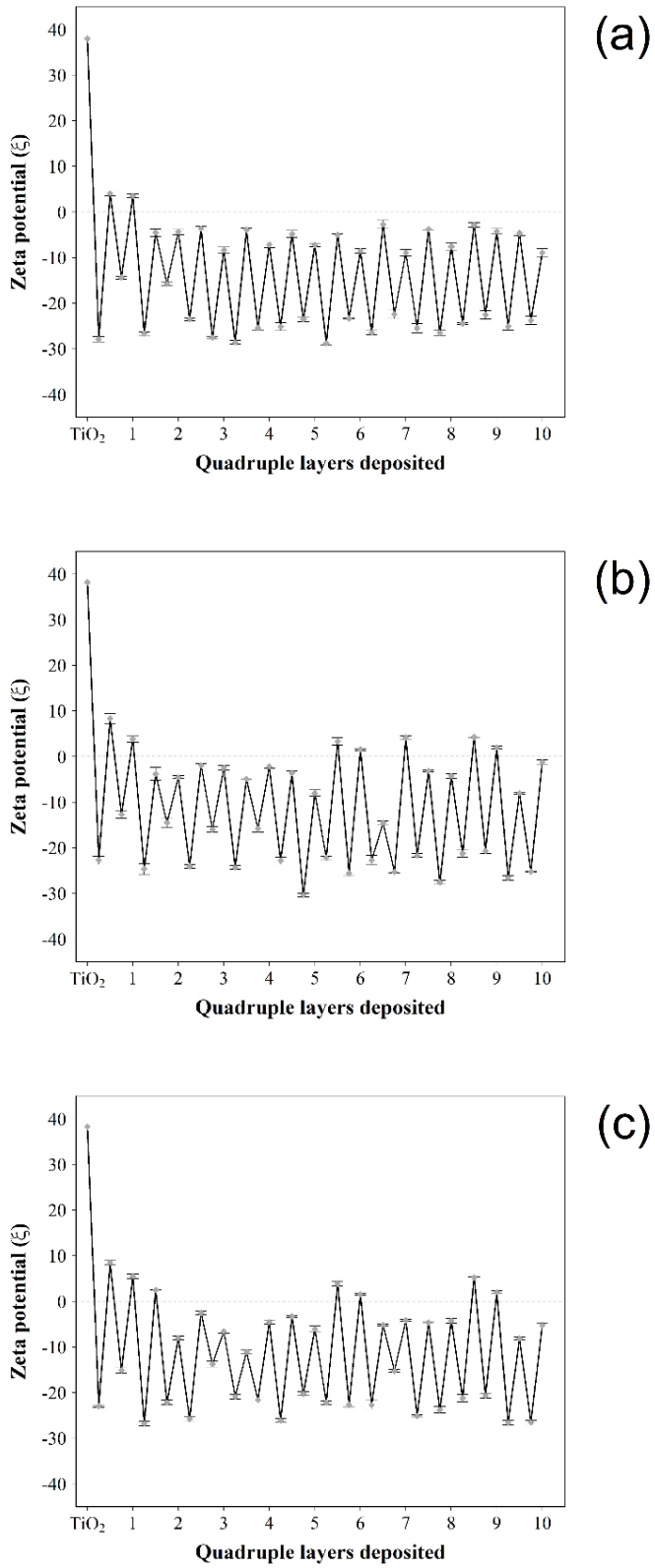

Figure 45. Zeta potential of DEX/chlorhexidine-coated nanoparticles after sequential coating of one quadruple layer (Q1), three quadruple layers (Q3), five quadruple layers (Q5), seven quadruple layers (Q7), and ten quadruple layers (Q10) for (a) C20, (b) C40, (c) C50 (mean ± SD n =3).

5.3.1.3 Thermogravimetric Analysis

The thermograms of all nanoparticles showed a mass loss at around 100°C, followed by a gradual weight decrease reaching a plateau starting at around 650 °C (Figure 46).

The weight loss of the nanoparticles at 750°C was influenced by the number of quadruple layers and by the sequence of drugs deposited. The greater the number of quadruple layers deposited the higher the weight loss; after the deposition of 10 quadruple layer the nanoparticles exhibited about 35% w/w of organic content regardless of the sequence employed ($p<0.05$). In contrast, the organic content of TiO_2 nanoparticles was the lowest, being 1.44 ± 0.08 %, increasing to 4.48 ± 0.67 % after amino-silanisation.

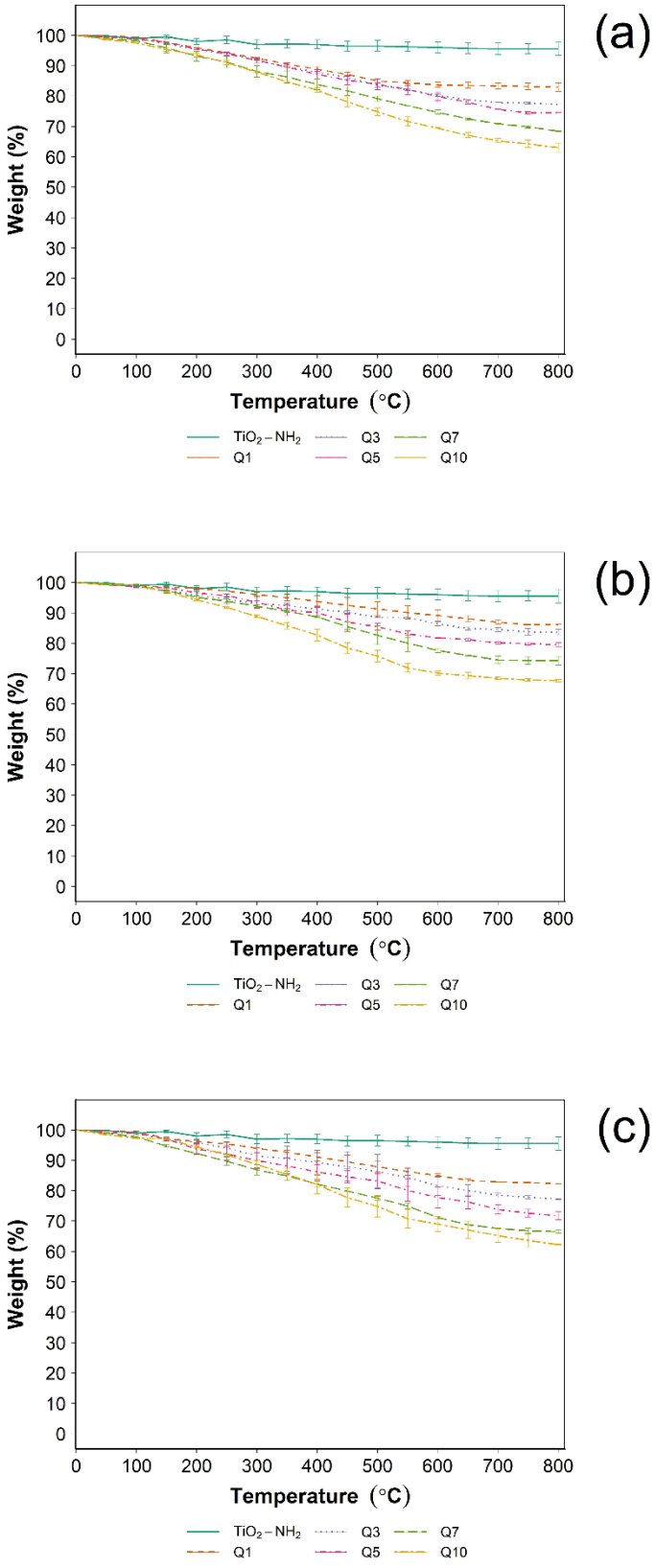

Figure 46. Thermograms of DEX/chlorhexidine-coated nanoparticles after sequential coating of one quadruple layer (Q1), three quadruple layers (Q3), five quadruple layers

(Q5), seven quadruple layers (Q7), and ten quadruple layers (Q10) for (a) C20, (b) C40, (c) C50 (mean ± SD n =3).

5.3.2 Drugs Release

For all three types of nanoparticles chlorhexidine release was maximum after the first day and the amount of drug released decreased gradually until it stopped; regardless of the LbL coating structure, chlorhexidine release at pH7.3 was greater than at pH5. The configuration of the LbL coating influenced the extent of the release period when chlorhexidine was detectable. For C20 the drug was released for about 45 days at pH5 and 60 days at pH7.3; chlorhexidine was released from C40 nanoparticles for 40 and 60 days at pH5 and 7.3, respectively. C50 sustained chlorhexidine release for 40 and 50 days at pH5 and 7.3, respectively (Figure 47, Figure 48 and Figure 49).

DEX-P release from C20 and C40 exhibited a maximum (an inflection in the cumulative amount of drug released) after 4 days in both pH conditions, this inflection was not observed in C50. Release continued for about 18 days in C20, 20 days in C40 and 12 days in C50. Overall DEX-P released was greater at pH5 than pH7.3 (Figure 47, Figure 48 and Figure 49) for C20 and C40 but not statistically different for C50 ($p<0.05$). Cumulatively the same amount of DEX-P was released from C20 or C40 ($p<0.05$); while a greater amount was observed in the release media from C50.

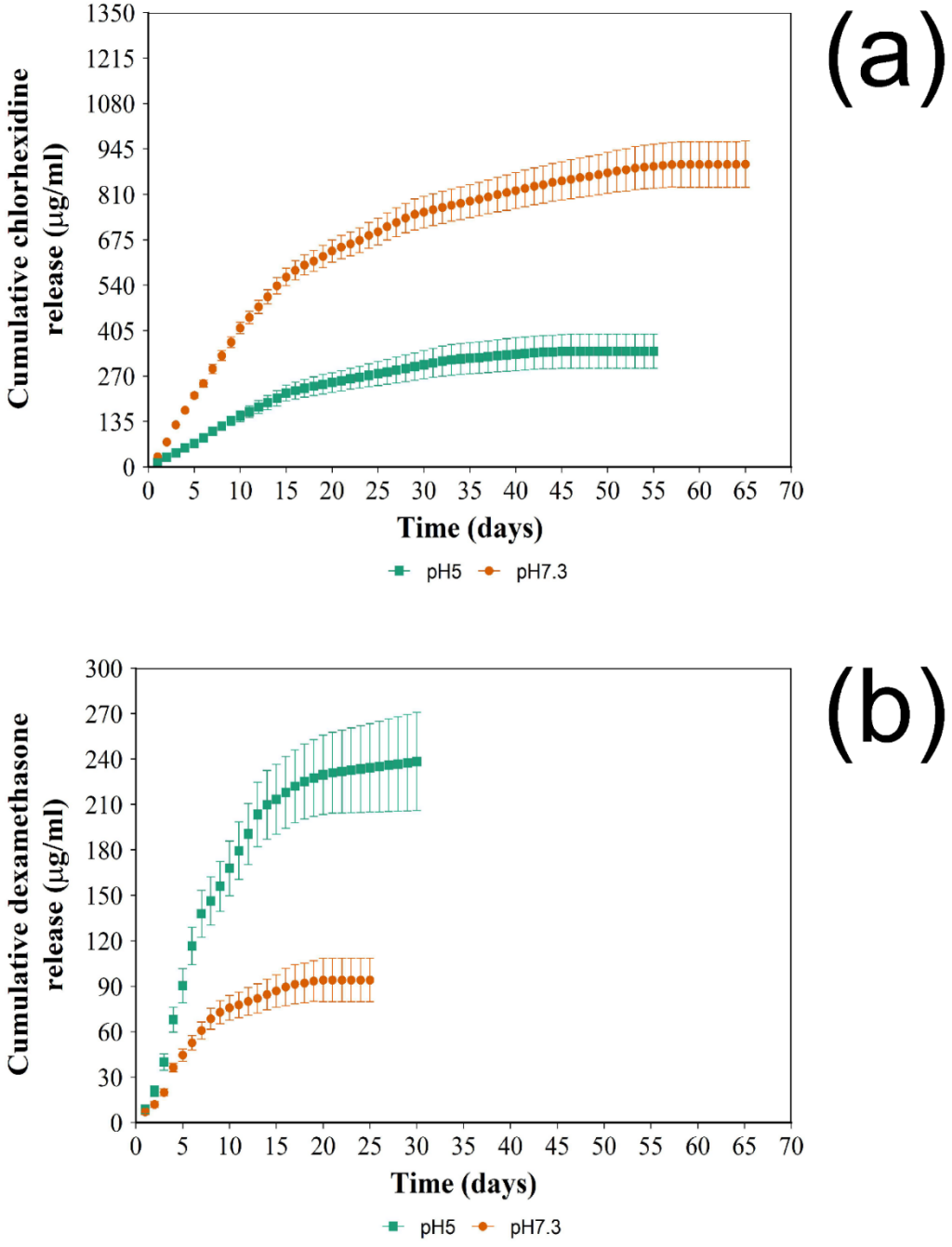

Figure 47. Cumulative release at pH5 and pH7.3 of chlorhexidine (a) and DEX-P (b) from coated nanoparticles C20 (mean ± SD n =3).

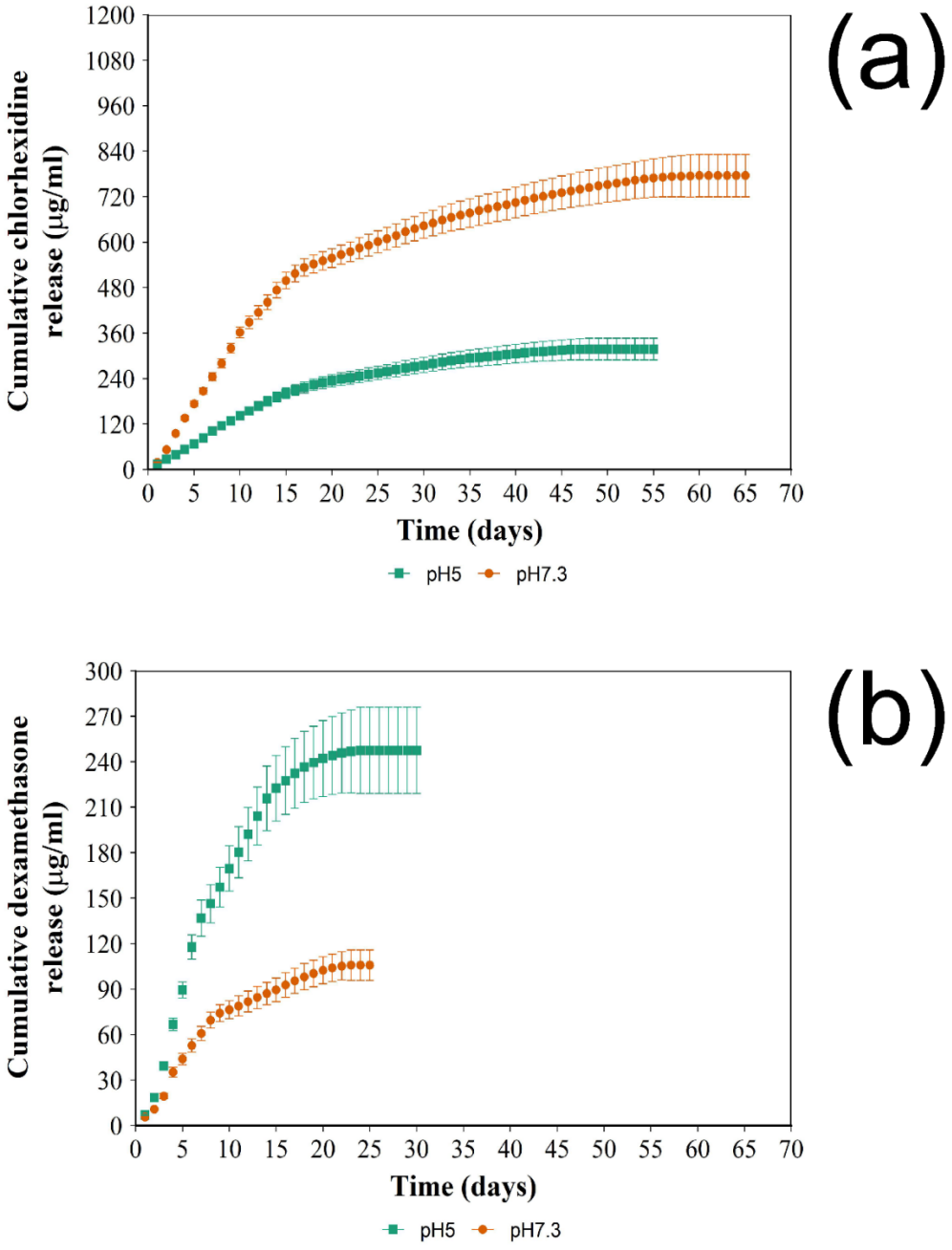

Figure 48. Cumulative release at pH5 and pH7.3 of chlorhexidine (a) and DEX-P (b) from coated nanoparticles C40 (mean ± SD n =3).

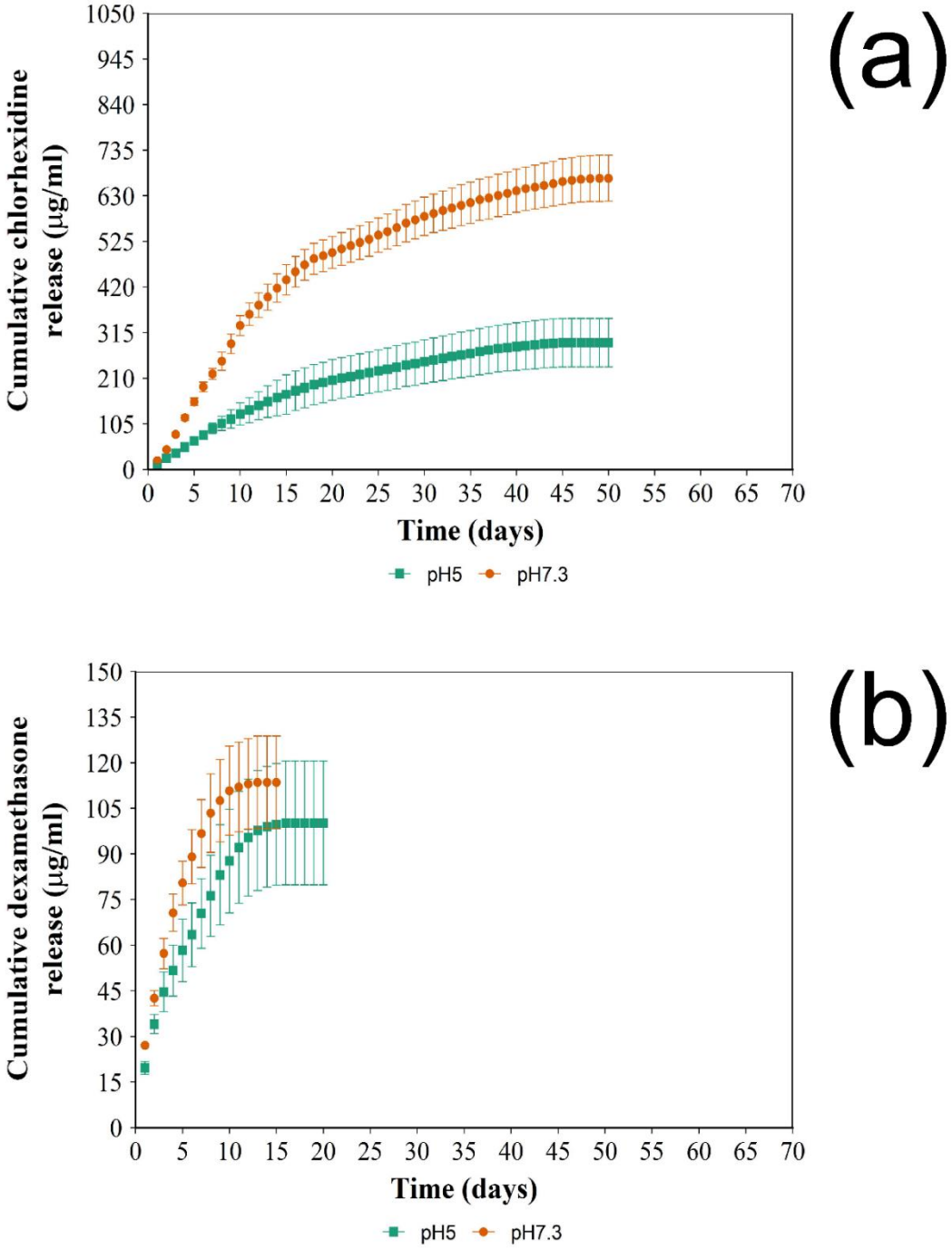

Figure 49. Cumulative release at pH5 and pH7.3 of chlorhexidine (a) and DEX-P (b) from coated nanoparticles C50 (mean ± SD n =3).

5.3.3 Antibacterial Activity

Generally, the growth inhibition of these bacteria was achieved in a period of 4-17 days for Gram negative (*E. coli* and *A. baumannii*) bacteria and 17-26 days for Gram-positive (*S. epidermis*, MRSA, MRSE and *Enterococcus*) bacteria, indicating strongest

susceptibility of Gram-positive bacteria towards chlorhexidine regardless of the type of DEX-P/chlorhexidine coating (Figure 46). The least sensitive bacteria were the three *A. baumannii* strains, where media containing chlorhexidine released from the coated nanoparticles were able to maintain growth inhibition of *A. baumannii* for 3 to 4 days. Buffers obtained after 17 days of release from were able to inhibit *E. coli* and MRSE 140 growth. On the other hand, the growth of *Enterococcus* was inhibited by media obtained after 19 days of release. Other MRSA isolates, MRSA 924 and MRSA 275, were successfully inhibited by buffers collected after 21 days and 26 days, respectively. Meanwhile, growth of S. epidermidis strain 189, 222, and 275 was inhibited by release buffers collected after 23, 25, and 26 days, respectively.

For most of the bacterial species tested the not statistical difference was observed between C20 and C40 ($p<0.05$); however, C50 had the shortest ability to inhibit bacterial growth.

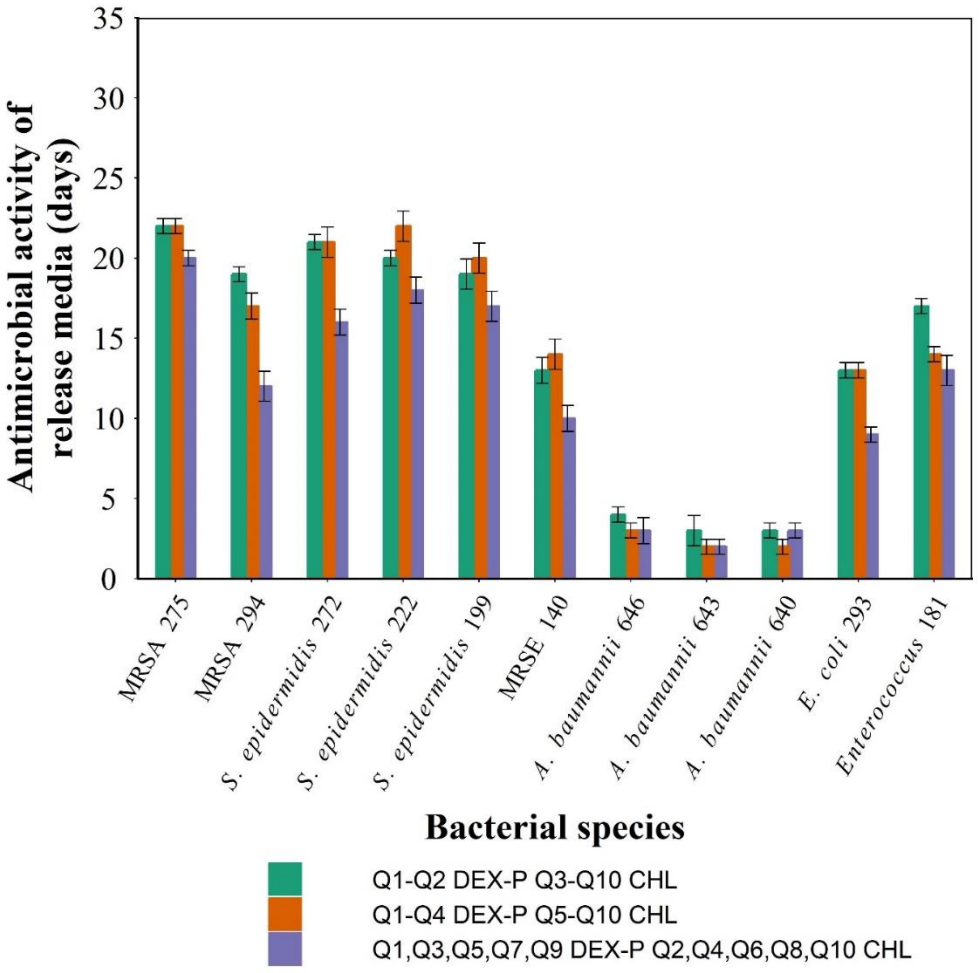

Figure 50. Antibacterial Activity of Chlorhexidine containing release media (a) C20, (b) C40 and (c) C50 (mean ± SD n =3).

5.3.4 Biological tests

5.3.4.1 Cell proliferation assay

Mitochondrial activity of activated THP-1 cells exposed to LPS was lower than in cells not exposed to LPS (control) ($p<0.05$) or exposed to LPS in release buffer from LbL coated titanium nanoparticles containing chlorhexidine and DEX-P) after both 6 and 24 hours of contact. After both periods of contact, no statistically significant differences were detected among the three type of LbL coating (Figure 51).

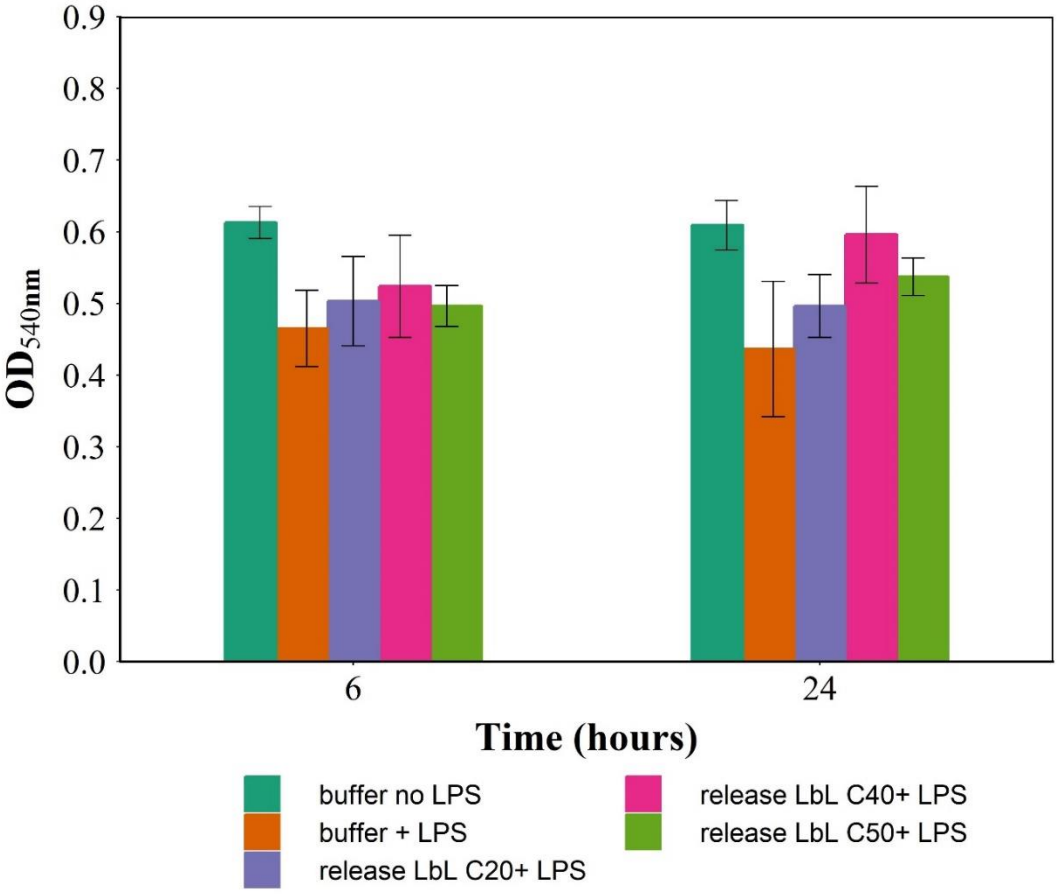

Figure 51. Mitochondrial activity of activated THP-1 after exposure to LPS and release buffer from LbL coated titanium nanoparticles (mean ± SD n =6).

5.3.4.2 Anti-inflammatory activity

Activated THP-1 cells did not release any IL-6 or TNFα when not exposed to LPS after 6 and 24 of contact with the medium (Figure 52 and Figure 53). On the contrary, when exposed to LPS without the release buffer from the LbL coating, an increasing amount

of both compounds was detected after 6 and 24 hours. The addition of the release buffer to LPS from the titanium coated nanoparticles reduced the amount of IL-6 and TNFα ($p<0.05$) compared to the pure LPS (Figure 52).

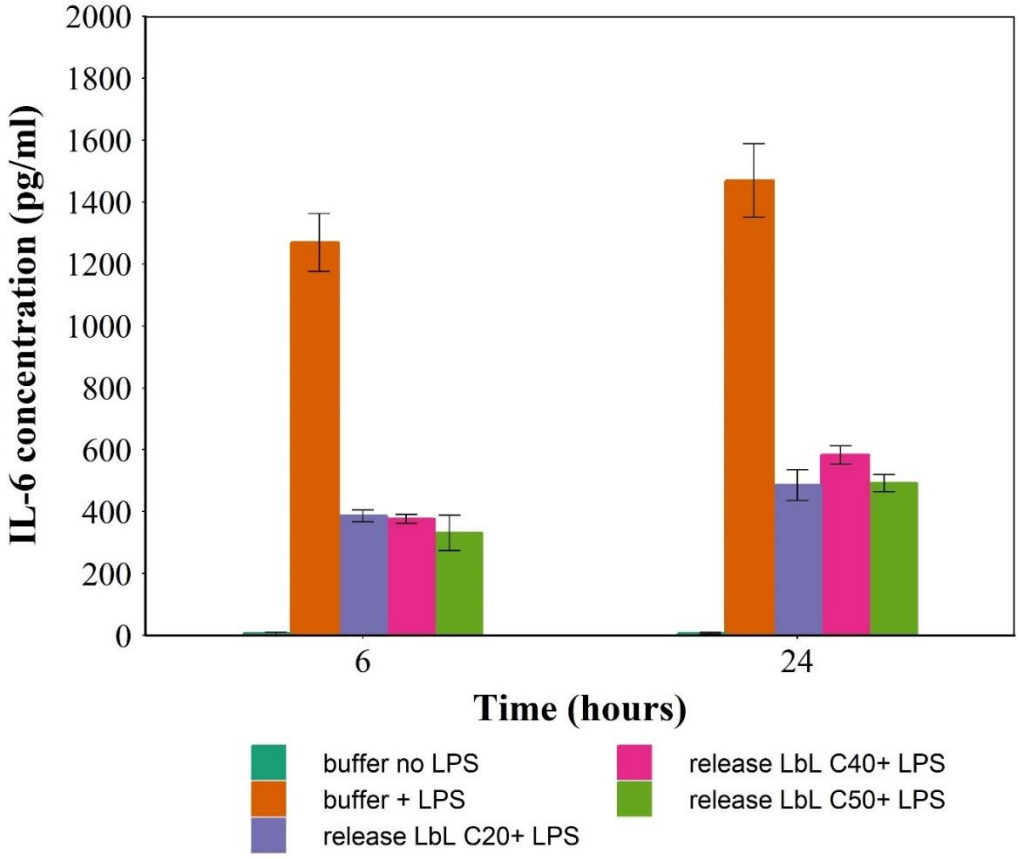

Figure 52. IL-6 produced by activated THP-1 after exposure to LPS and release buffer from LbL coated titanium nanoparticles (mean ± SD n =3).

No statistically significant difference was observed among the three type of LbL coating regarding the IL-6 release; while activated THP-1 cell exposed to LPS released a lower amount of TNFα when exposed to the release buffer from C50 then either C20 or C40 ($p<0.05$) (Figure 53).

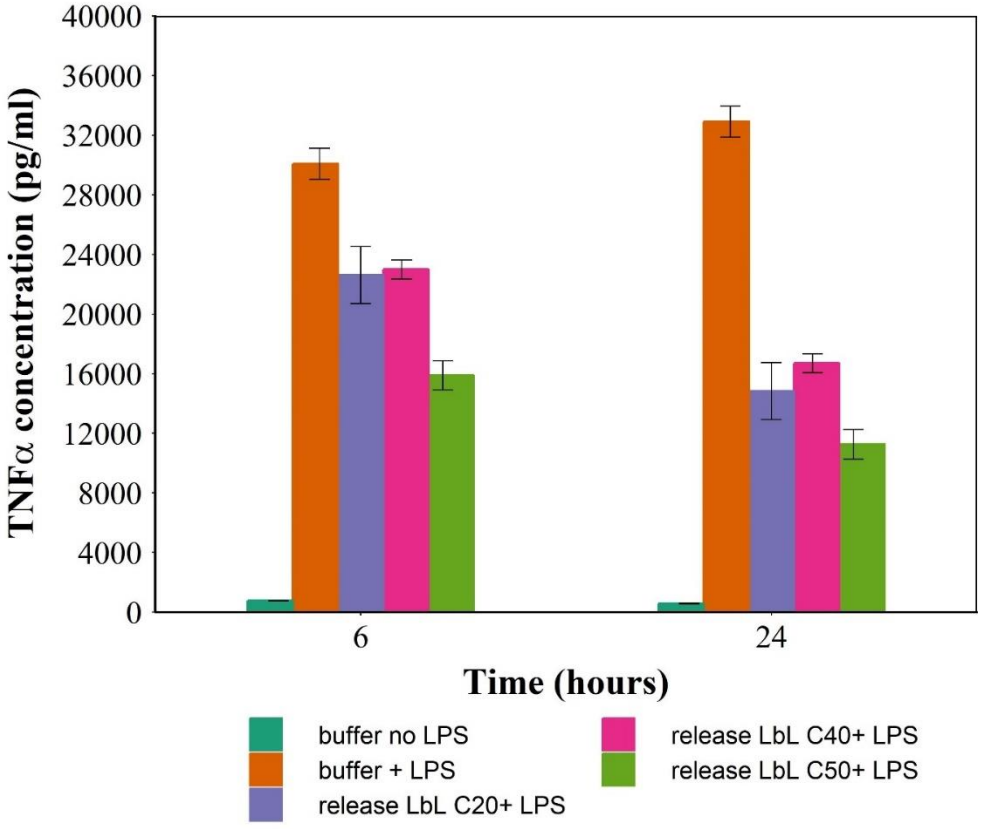

Figure 53. TNF-alpha produced by activated THP-1 after exposure to LPS and release buffer from LbL coated titanium nanoparticles (mean ± SD n =3).

5.4 Discussion

5.4.1 Nanoparticle surface functionalisation

The surface of TiO_2 nanoparticles has a charge close to neutrality. In order to achieve successful deposition of the first layer, negatively charged alginate, the surface of TiO_2 nanoparticles were functionalized by APTS. The mechanism of this functionalization has been proposed by (Howarter and Youngblood 2008). Initially, APTS was adsorbed onto TiO_2 surface via hydrogen bonds. Next, more APTS were adsorbed and H-bonded APTS formed siloxane cross-links with each other (Figure 11b). The adsorbed APTS also formed siloxane bond with free APTS available in the solution during the treatment. As a result, multilayer build-up of APTS was formed, with NH_2 moieties at the surface. The amine groups on the TiO_2 surface acted as anchoring points for alginate.

5.4.2 Nanoparticles characteristics

5.4.2.1 Size

Dynamic light scattering (DLS) is a widely applied technique for particles size determination (Geißler et al. 2015). The particles diameter was estimated at around 500 nm and about 5 folds increase was measured after deposition of 10 quadruple layers. The particles are stated to have a diameter about 50 nm, this large increase in particle size is mainly due to agglomeration of the nanoparticles; moreover the dimension of the coated nanoparticles would not agree with the general knowledge of LbL coating being a few nanometers (Ariga et al. 2011; Deshmukh et al. 2013; Gentile et al. 2015). This was the result of aggregation among particles caused by the polyelectrolytes interacting, during LbL deposition, simultaneously with more than one particle (Gosens et al. 2010; Al Thaher et al. 2018).

5.4.2.2 Zeta potential

Zeta potential during an LbL deposition presents a zig-zag pattern as the coated surface assumes the charge of the outer polyelectrolyte. The negative zeta potential values measured after depositing DEX-P and alginate were similar to the values of these pure molecules thus after deposition of these molecules the surface was saturated by either of these compounds. However, after B1 or chlorhexidine deposition, no positive zeta potential was measured particularly after the first quadruple layer, this likely the result of weak charges polyelectrolyte on these molecules compare to alginate or DEX-P. Attempts increasing B1 concentration and/or extending the contact time did not improve the outcome therefore the initially chosen protocol represented an optimal condition. However, successful deposition of B1 or chlorhexidine was obtained as the zeta potential of the nanoparticles moved to higher values (less negative).

5.4.3 Thermogravimetric Analysis

Thermogravimetric assay was conducted to confirm the deposition of polyelectrolyte and drug layers onto the surface of TiO_2 nanoparticles. We presumed that all the organic content had been lost at 750°C, and only the inorganic core of nanoparticles remained. The total loss of weight at 100 °C represented vaporization of entrapped moisture in nanoparticles and was not a result of degradation of organic compounds (alginate, B1, chlorhexidine, or DEX-P). The water originates from the aqueous medium used during the deposition that remained despite the drying process. Therefore, the weight loss at 100 °C was used as a correction in determining organic content. Thermograms demonstrated and increasing amount of organic matter with increasing number of

deposited quadruple layers confirming the progressive deposition of polyelectrolytes and drugs (Figure 46).

5.4.4 Drug Release

The pH surrounding joint replacement can vary from close to neutral conditions in heathy situations (Ribeiro, Monteiro, and Ferraz 2012; Goldie and Nachemson 1970) to acidic condition after PJI offset (Kinnari et al. 2009); similarly, inflammatory conditions are known to be accompanied by a drop in pH (de Nadai et al. 2013). Therefore, release studies of chlorohexidine and DEX-P were carried out in both acetate buffer pH5 reproducing the acidic conditions observed in infected or inflamed joint and phosphate buffer pH7.3 represented healthy joint environment.

The kinetic of drug release from LbL coatings is known to be pH dependent the level of protonation of amine groups and carboxylic acid present on the polyelectrolytes and consequently the diffusion of the molecules through the LbL layers (Smith et al. 2009). Moreover, pH also controls the kinetics of possible hydrolysis of the polyelectrolytes and such the second mechanisms of drug release from LbL coatings (Chuang, Smith, and Hammond 2008; Hammond 2012; Smith et al. 2009). The progressive reduction of chlorhexidine release observed (first order kinetic) in Figure 47, Figure 48 and Figure 49 confirms that for quadruple layers assembled with B1 diffusion is the predominant mechanism despite the hydrolytic properties of this polyelectrolyte; this can also be attributed to the slow hydrolysis of this polymer (Al Thaher et al. 2018).

As observed for LbL coating containing either pure DEX-P or chlorhexidine, the role of pH in controlling the drug release kinetics is opposite; DEX-P exhibited higher release at pH5 than pH7.3, on the other hand chlorhexidine exhibited higher release at pH7.3 than pH5 (Figure 47, Figure 48 and Figure 49). This pattern can be described by the role of surface charge of the outer layer of LbL constructs that has been shown to maximise the diffusion coefficient through the all coating when the diffusing molecule and outer layer exhibit opposite charges (Sato, Shiba, and Anzai 2013). DEX-P was negatively charged in the pH range tested and chlorhexidine was positively charged; at the same time the outer layer of the LbL coating, exhibiting B1, was positively charged at pH5 and close to neutrality at pH7.3. The greatest difference between charges of drug and LbL outer layer was, therefore, at pH7.3 for chlorhexidine and pH5 for DEX-P.

Chlorohexidine release from C20 and C40 was very similar to that observed for titanium particles coated with ten quadruple layers containing such drug (Chapter 4), at pH7.3,

while a lower amount of chlorhexidine, compared to coating prepared only with this molecule, was recorded for both type of DEX-P/chlorhexidine LbL coatings. In these particles, chlorhexidine was deposited on the six and eight outer layers hence the amount of drug that remained unreleased was the only difference particularly at pH7.3 where the counter diffusion of DEX-P was minimal. At pH5 instead, DEX-P diffusion was higher and this interfered with chlorhexidine diffusion.

When the two drugs were sequentially deposited (C50) chlorhexidine release was the lowest as the interference of the DEX-P was maximum. DEX-P release was the highest for the first few days as in this case the drug was closer to the coating surface and diffusion was the least obstacle; while as release continued chlorhexidine diffusion from the deeper layers prevented further steroidal drug release resulting in the lowest overall DEX-P release. Moreover, DEX-P concentration from C20 and C40 did not exhibit a maximum after the first day of release, but later, as in these coating DEX-P was deposited at the bottom of the LbL construct and the drug had to diffuse first through the chlorhexidine layers before reaching the surface.

5.4.5 Antibacterial Activity

Antimicrobial testing was carried out simulating the real scenario of an implanted prosthetic joint incubating the release media from the chlorhexidine LbL coated particles with clinical isolates of PJIs (Geipel 2009; Martinez-Pastor et al. 2009; Hsieh et al. 2009). Release media at pH7.3 was used only as some of the strains were not able to grow sufficiently in the acidic buffer. The protocol is based on the observation that chlorhexidine concentration in the media decreased with time hence the release media growth inhibition occurs until chlorhexidine fell below MIC. The differences in efficacy recorded are attributable to species and strain variation of MIC; for example MIC for *E. coli* was reported 2.67 µg/ml (do Amorim, Aun, and Mayer 2004) while for MRSA the MIC was 4-8 µg/ml (Cookson, Bolton, and Platt 1991); *Pseudomonas aeruginosa* is much less susceptible to chlorhexidine 80 µg/ml (Thomas, Russell, and Maillard 2005).

The longer activity of the C20 and C40 coatings depended on the higher concentration of chlorhexidine released from these LbL constructs compared to C50 (Figure 50).

Gram+ bacteria have a very thick cell wall made of a polymer of sugars and amino acids called peptidoglycan while Gram- bacteria have a very thin peptidoglycan layer between an inner cell membrane and a bacterial outer membrane (Madigan and Martinko 1997). Various antibacterial agents are more effective against Gram+ bacteria than Gram-

because of the more complex cell wall structure that reduces the ability of the agents to penetrate the cell (Siu 2002); therefore the higher sensitivity of the Gram positive bacteria tested (Figure 50) is consistent with established knowledge.

The rise of bacteria cells capable of surviving antibiotic is a growing concern for health operators and alternatives such as silver have been widely researched (Besinis et al. 2017; Kuehl et al. 2016). However, there are the use of metal ions or nanoparticles is now under close scrutiny for both environmental safety and toxicology. Chlorhexidine, used in mouthwash solutions and topical treatments for decades, has been recently investigated for use in arthroplasty coating the surface of external fixation pins with hydroxy apatite/chlorhexidine (DeJong et al. 2001). Chlorhexidine containing coatings on TiO_2 implants exhibited bactericidal activity against *S. aureus* (Riool, Dirks, et al. 2017). However, the antimicrobial activity was short as almost 90% of the drug was released in the first 24 hours hence the LbL coating developed here appeared better suited to help preventing PJI offset as these infection can establish weeks and months after surgery (Chen et al. 2014).

5.4.6 Biological test

The biological validation of the prepared coating was carried using activated human monocytes (THP-1)-derived macrophages as model human macrophages. This cells line is routinely employed to study the inflammation process of human monocytes and macrophages (Qin 2012). Activation of THP-1 cell was achieved using LPS at the concentration of 1µg/mL that is widely used to simulate inflammation in human macrophages (Glue et al. 2002; Moreira-Tabaka et al. 2012).

Cell were exposed to DEX-P, along with the chlorhexidine, released from the surface of the LbL coated titanium nanoparticles; only the release buffer collected at pH7.3 was used as the acidic buffer (pH5) resulted in high level of cell death; moreover the buffer was diluted 1:10 in fresh media as pure buffer was not able to sustain cell growth. Cell exposed to fresh PBS diluted in media 1:10 and not exposed to LPS served as positive control; furthermore pure DEX-P was not employed as each coating resulted in different concentration of the drug.

5.4.6.1 Cell proliferation assay

The mitochondrial activity is often measured as a surrogate outcome of cell viability, in order to ascertain that the LbL coatings were not cytotoxic to human monocytes (THP-1)-derived macrophages, the MTT assay was employed (Figure 51).

As seen in the previous chapter, LPS reduced the mitochondrial activity, thus cell viability, particularly at the longer exposure time (24 hours) as inflammation reduced cell metabolism. The expected absence of detrimental activity was observed when THP-1 cells were exposed to the release buffer containing both drugs and decomposition products of the polyelectrolytes as B1 and alginate are a known biocompatible polyelectrolites.

5.4.6.2 Anti-inflammatory activity testing

The anti-inflammatory activity of DEX-P released was assessed through the quantification of IL-6 and tumour necrosis factor alpha (TNFα) that are two specific inflammatory markers produced by human macrophages (Qin 2012; Cochran and Finch-Arietta 1992). Moreover, both IL-6 (Yoshitake et al. 2008; Udagawa et al. 1995) and TNFα (Kobayashi et al. 2000; Lam et al. 2000) have been known to induce osteoclastogesis. This process involves the differentiation of immune cells into osteoclast that are bone resorbing cells and act in the opposite direction of osteoblasts (bone forming cells). The imbalance of osteoclast leads to an overall osteolysis and potentially to aseptic loosening (Greenfield et al. 2002; Hartmann et al. 2017). Therefore, any technology capable of reducing these inflammation markers has the potential to prevent aseptic loosening.

None of these markers was detected when cells were not exposed to LPS as not inflammatory process was induced, on the contrary the concentration of these two molecules increased with time when THP-1 cells were stimulated by LPS; the buffers containing DEX-P achieved a significant reduction of the level of these two inflammation markers (Figure 52 and Figure 53) demonstrating the suitability of the LbL technology, moreover buffers collected from C50 had a greater anti-inflammatory activity as DEX-P concentration after 1 day of release was higher than C20 and C40.

5.5 Conclusions

The ultimate goal of total joint replacement is to improve mobility of the subjects. The prosthesis implanted at the joint area is permanent, which gives consequences that any harmful event such as aseptic loosening, infection, and hypersensitivity reaction should never occur for the lifetime of the devices. While the cement material in cemented prosthesis helps establishment of the device, uncemented prosthesis only consists of inert materials that lack of osseoconductive properties. Without a good strategy, bone procedures using uncemented prosthesis will not reach its maximum benefits.

We constructed a drugs elution system for antibacterial agent (chlorhexidine diacetate) and anti-inflammatory agent (dexamethasone sodium phosphate) from uncemented prosthesis using layer-by-layer technique. Our zeta potential determination and thermogravimetric assay indicated that each drug/polymer layer was stably deposited via electrostatic interaction despite the number of layers. We have successfully controlled the release of chlorhexidine for more than one month and DEX-P for about 15 days. The release of chlorhexidine was accompanied by antimicrobial activity towards a variety of clinical isolates of PJI. DEX-P released was also capable of reducing inflammation markers such as IL-6 and TNFα. Depending on the distribution of the two drug different release profiles and subsequent antimicrobial and anti-inflammatory activity was achieved, coatings made with DEX-P in the initial deposited layers and chlorhexidine on the outer layers appeared better suited for the prevention of PJI and aseptic loosening.

Chapter 6: Dual release of dexamethasone and chlorhexidine from coated titanium coupon for hip joint arthroplasty

6.1 Introduction

Joints are parts of the musculoskeletal system that allow reciprocal movement of body parts; as they are subjected to "wear and tear" patients can progressively experience diminished and painful ability to use such articulation; trauma is another source of joint damage. When joint functionality is affected beyond the natural ability to self-repair, replacement devices are inserted to restore mobility and improve patient quality of life; such procedures are called arthroplasty (Siopack and Jergesen 1995). Osteoarthritis is the leading cause of joint replacement (Singh 2011) and the number of procedure is expected to more than double by 2030 (Inacio, Paxton, et al. 2017; Culliford et al. 2015)

Prosthesis are usually made of metal, ceramic, or high-density polyethylene (Santavirta et al. 1998; Kunčická, Kocich, and Lowe 2017). Fixation of the prosthesis can be cemented or uncemented; in the former case bone cement, generally PMMA based, is applied to rapidly secure the device in the correct place (Breusch S.J. and H. 2005), while in the later the device is mechanically inserted into the bone socket.

Uncemented prosthetic outperform cemented devices in terms of operating room time, preservation of bone stock and ease of revision (Aprato et al. 2016); moreover, bone cement implantation syndrome (Aprato et al. 2016; Donaldson et al. 2009) is completely avoided. Historically uncemented joint replacements were not favoured because of their instability (Maggs and Wilson 2017); nevertheless modern design have been shown to be as successful as cemented devices (Prudhon and Verdier 2017; Abdulkarim et al. 2013). Modern designs have solved this problem hence the research focus has shifted towards providing antimicrobial activity.

The main complications of joint replacement are aseptic loosening and prosthetic joint infections (PJIs); aseptic loosening is the severe bone loss (osteolysis) in the area nearby the implant and it is the results after a prolonged local inflammation (Landgraeber et al. 2014). Aseptic loosening is the cause of approximately 40% of all revision procedures (Goriainov et al. 2014). PJI incidence rates are around 1-2%, the management of these infections is complex and can involve debridement, antibiotics and implant retention (DAIR); unfortunately about 50% of patients undergoing DAIR require revision surgery (the removal of the implanted device and the insertion of a new one) (Romanò et al.

2012). More extreme PJI cases can require amputation (Tande and Patel 2014) or lead to death (McPherson et al. 2002). Revision surgeries performed as a consequence of PJI in England and Wales increased from 378 in 2005 to 1048 in 2014; this increase (a 2.8-fold) is higher than the 2.1-fold increase in primary knee replacements observed in the same period (Lenguerrand et al. 2017). Consequently, PJIs do not only pose a threat to patients' life or quality of life but also constitute a considerable economic burden to health services it has also been forecasted that, the volume of primary and revision TKAs in England and Wales will have increased by 117% and 332%, respectively between 2012 and 2030 (Patel et al. 2015). For the National Health Service, a revision knee replacement due to PJI have been shown to cost over £30,000 per case, more than three time the cost of aseptic revision (Kallala et al. 2015), similar ratios have been observed in the USA (Lavernia, Lee, and Hernandez 2006).

While the use of antibiotic laden bone cements is partially capable of reducing early PJI (Al Thaher, Perni, and Prokopovich 2017), no effective treatments are available to reduce the inflammation causing aseptic loosening or late PJI (Apostu et al. 2018). Raising rates of antibiotic resistance are further reducing antibiotic laden bone cement efficacy (Tyas et al. 2016). It is, therefore, evident how the development of novel strategies to tackle these two problems is urgent as the number of joint replacement devices is expected to grow (Kurtz et al. 2007; Kurtz et al. 2009).

Layer-by-layer (LbL) deposition is a coating technique consisting of polyelectrolytes deposited on a surface through alternatively exposing it to oppositely charged molecules (Alotaibi et al. 2018). This technique has found numerous applications in medical devices in virtue of its scalability, versatility and, because of the mild aqueous conditions employed, ability to handle chemically sensitive active molecules such as growth factors (Macdonald et al. 2011; Wu et al. 2016; Hammond 2012).

In this study, we developed antibacterial and anti-inflammatory coating on titanium alloy implant. The coating was built employing the LbL technique incorporating an antimicrobial agent (chlorhexidine diacetate) and an anti-inflammatory drug (dexamethasone) using patented polymer, B1. Through the use of titanium nanoparticles as model for devices surfaces, in the previous chapter, the use of 4 quadruple layers containing DEX-P followed by 6 quadruple layers containing chlorhexidine appeared to fulfil both the requirement related to prolong antimicrobial activity and anti-inflammatory capability; therefore these type of coating will prepared on titanium coupons to validate the technology on a system more closely resembling in vivo situations. The surfaces were characterised and the antimicrobial activity determined

against a variety of prosthetic infection clinical isolates. Moreover, the absence of detrimental effects of the coating on osteoblasts growth and the retention of anti-inflammatory activity of DEX after release was assessed.

6.2 Materials and Method

6.2.1 Materials

Titanium coupon, Piranha solution. (3-Aminopropyl) triethoxysilane (APTS, 99%), Chlorhexidine diacetate (CL), Dexamethasone sodium phosphate (DEX, >97%), Phosphate buffer solution (PBS) tablets, Sodium acetate trihydrate (≥99%), citric acid monohydrate (ACS reagent, ≥99%), disodium phosphate (ACS reagent, ≥99% were purchased from Sigma-Aldrich, UK. HPLC grade acetonitrile, Glacial Acetic Acid, and Toluene were purchased from Fisher, UK. All other chemicals were reagent grade, stored according to manufacturer's guidelines and used as received.

6.2.2 Titanium coupon functionalization

Titanium coupons were immersed in 20 mL of piranha solution for one hour washed three times in PBS. Then the coupons were dispersed in 15 mL of anhydrous toluene. One hundred microliters of APTS were added and the suspension was incubated for 24 hours at room temperature. The amine functionalized titanium coupons were washed using toluene to purify the surface of the functionalize titanium coupons from unreacted APTS. The washing procedure was repeated for 3 times. After the final washing cycle, titanium coupons were collected and dried under fume hood for 24 hours.

6.2.3 Preparation of polyelectrolyte solution

Polyanionic solution was prepared as described in section 2.2.2.

6.2.4 Determination of polyelectrolyte solution charge

The electrophoretic mobility of ALG, B1, CHX, and DEX solutions were determined by Dynamic Light Scattering (DLS) as described in section 2.3.2.

6.2.5 Layer by layer (LbL) coating technique for Titanium coupon.

The titanium coupons were coated with polyelectrolyte multilayers containing either only chlorohexidine, only DEX-P or both chlorohexidine and DEX-P. The layers consisted of different numbers of repeated fundamental sequences: ALG-CHX-ALG-B1 or ALG-B1-DEX-B1; a sequence containing these four layers were termed quadruple layer (Q).

The titanium coupons were placed into a test tube with 20 ml of ALG solution for 10 min, then the coupons were collected. The ALG-layered coupons were washed with acetate buffer to remove the excess of ALG. The second layer was applied onto ALG-layered coupons by placing them in 10 ml of CHX or DEX-P solution for 10 min. The coupons were then washed using similar procedure to that for ALG layer. Polyelectrolyte coating, and washing steps were repeated for the third layer (ALG) and fourth layer (B1), resulting in the first quadruple layer. Layer-by-layer coating process was continued to achieve a total of 10 quadruple layers. For coupons containing both DEX-P and chlorhexidine, the first 4 quadruple layers contained DEX-P and the remaining 6 chlorohexidine. The entire LbL coating was carried out at room temperature.

6.2.6 SEM imaging

To identify the difference between the morphology of the surfaces and coating thickness between the coated and uncoated titanium coupons SEM was employed. Images of titanium coupons (uncoated and LbL coated) were obtained using SEM [ZEISS, 1540XB].

6.2.7 Coated Titanium coupon release study

Coated- coupons were dispersed in two media (1.5ml each), acetate buffer pH 5 and phosphate buffer pH 7, and incubated at 37°C. An aliquot of 1.5 ml of the medium was withdrawn daily for quantification and the medium was replaced with equal volume of fresh buffer.

The amount of chlorhexidine and DEX released from the coating layer was determined using reverse-phase High Performance Liquid Chromatography / HPLC (1100 series Agilent Technologies®) as described in section 2.3.5.1.

6.2.8 Coated Titanium coupon antimicrobial activity testing

Gram-positive bacteria methicillin-resistant *Staphylococcus aureus* (MRSA) 294 and 275, methicillin-resistant *Staphylococcus epidermidis* (MRSE) 140, *Staphylococcus epidermidis* 272, 222, 199, and *Enterococcus faecalis* along with Gram-negative bacterium *Acinetobacter baumannii* 640, 643, and 646, *Escherichia coli* 293 were used. All these were clinical isolates of PJIs and antimicrobial testing was performed on chlorhexidine coated nanoparticles using the protocol described in section 2.4.

6.2.9 Cell culture

Human monocytic leukaemia cells THP-1 cells were grown as described in 2.5.

6.2.9.1 MTT

MTT assay was conducted to measure human macrophages (THP-1) mitochondrial activity post-exposure to DEX coated titanium coupons after 1, 2 and 3 days exposure as per the protocol described in section 2.5.2.1.

6.2.9.2 IL-6 and TNFα

The amount of IL-6 and TNFα released in the media after exposure to LPS and DEX for 6 and 24 hours was determined using appropriate ELISA kit (Sigma, UK) according to manufacturer's recommendations as per the protocol described in section 2.5.2.2.

6.2.10 Statistical analysis

Statistical analysis was performed using the one-way analysis of variance (ANOVA) test with Tukey's multiple-comparison as a post hoc test after confirming normal distribution by Kolmogorov-Smirnov test. Value with $p<0.05$ were considered as statistically significant

6.3 Results

SEM images clearly showed the difference between uncoated and coated titanium samples, showing layers of polymer coatings on LbL coated coupons (Figure 54 to Figure 55).

6.3.1 Coated Titanium coupon imaging

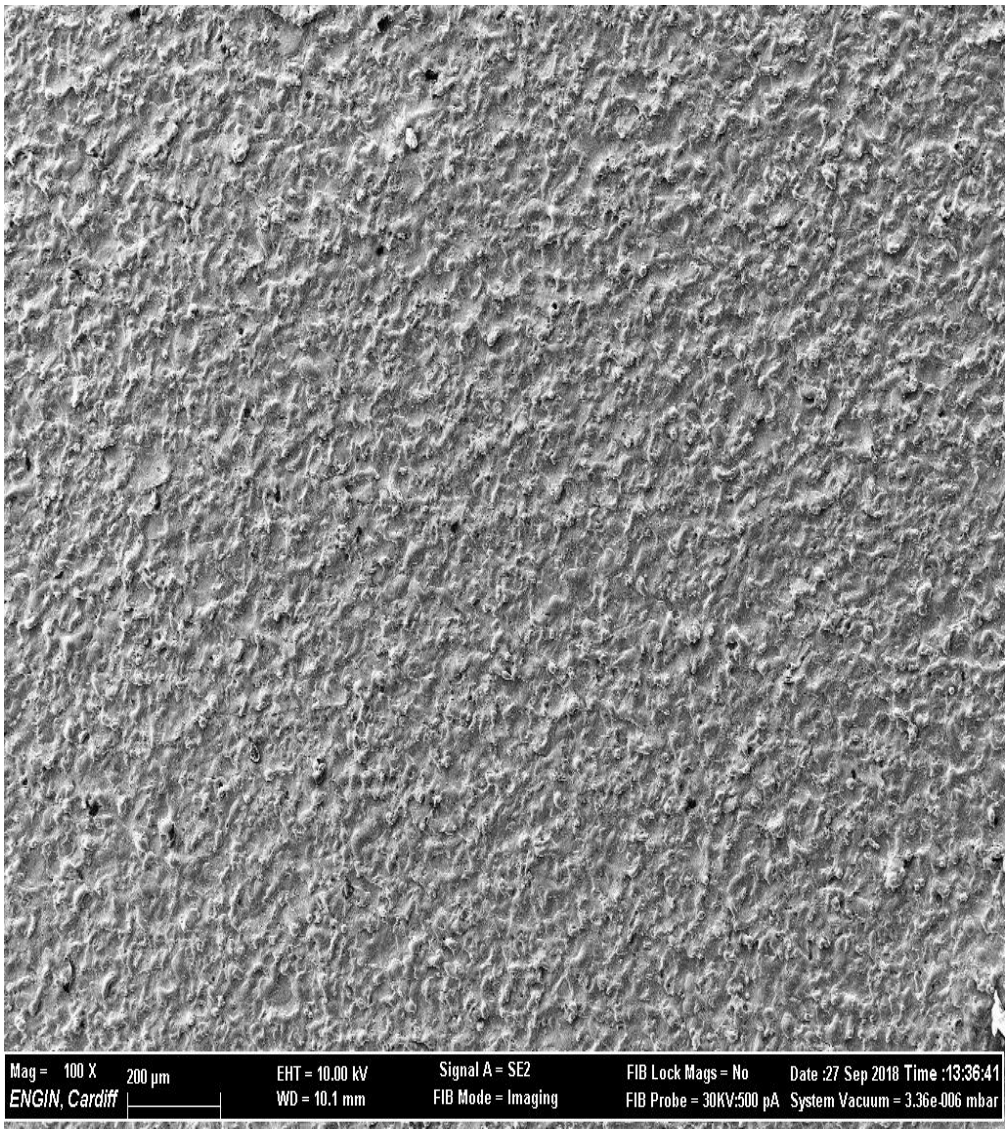

Figure 54. Example if SEM image of uncoated titanium coupon

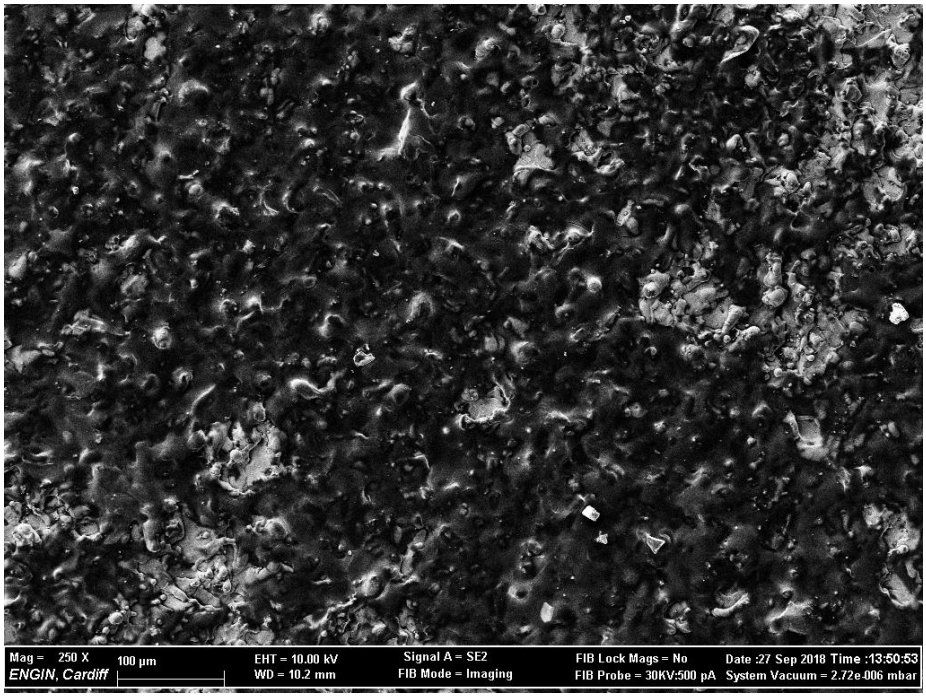

(a)

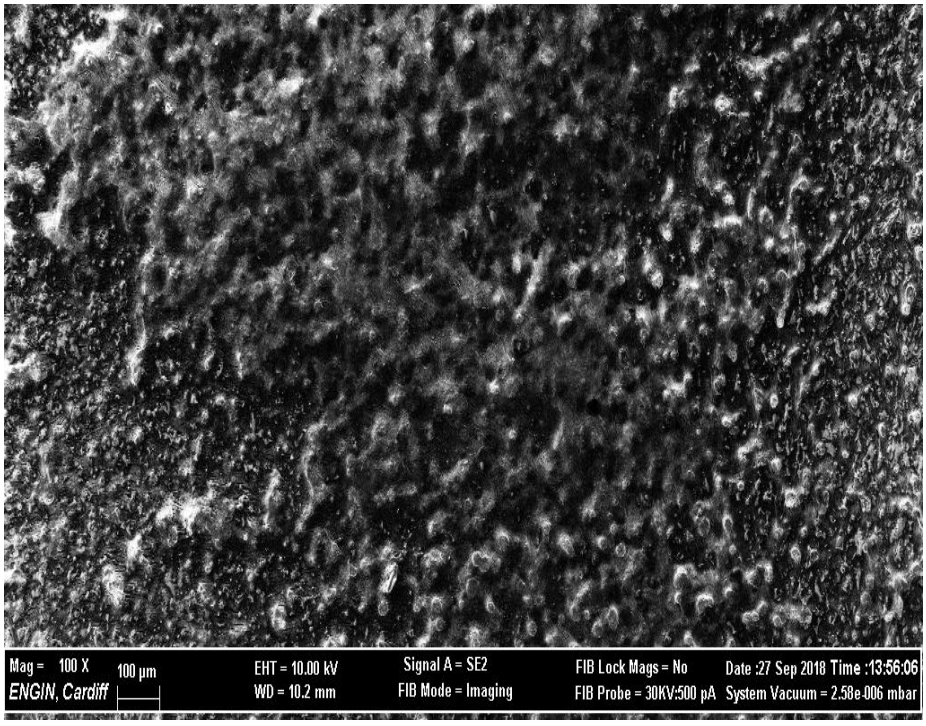

(b)

Figure 55. Example of SEM image of coated titanium coupon (a) and after shear force applied (b).

6.3.2 Release study

Drug release for both chlorohexidine and DEX-P from LbL coating containing only one single therapeutic agents was continuous for about 14 days in case of chlorhexidine and 5 days for DEX-P, after this release decreased and stopped after a further 2-3 days

(Figure 56 and Figure 57). The amount of chlorhexidine released was about 3 times higher than DEX-P and the pH of the media had not impact on chlorhexidine release kinetics while DEX-P had faster release at pH =5.

Release from coatings containing both chlorhexidine and DEX-P (Figure 58 and Figure 59) exhibited the same patterns that were observed for coating containing a single drug. However, the amount of DEX-P release was about 10% of that released from coating made with only this molecule, the amount of chlorhexidine released was comparable to that of pure coatings instead.

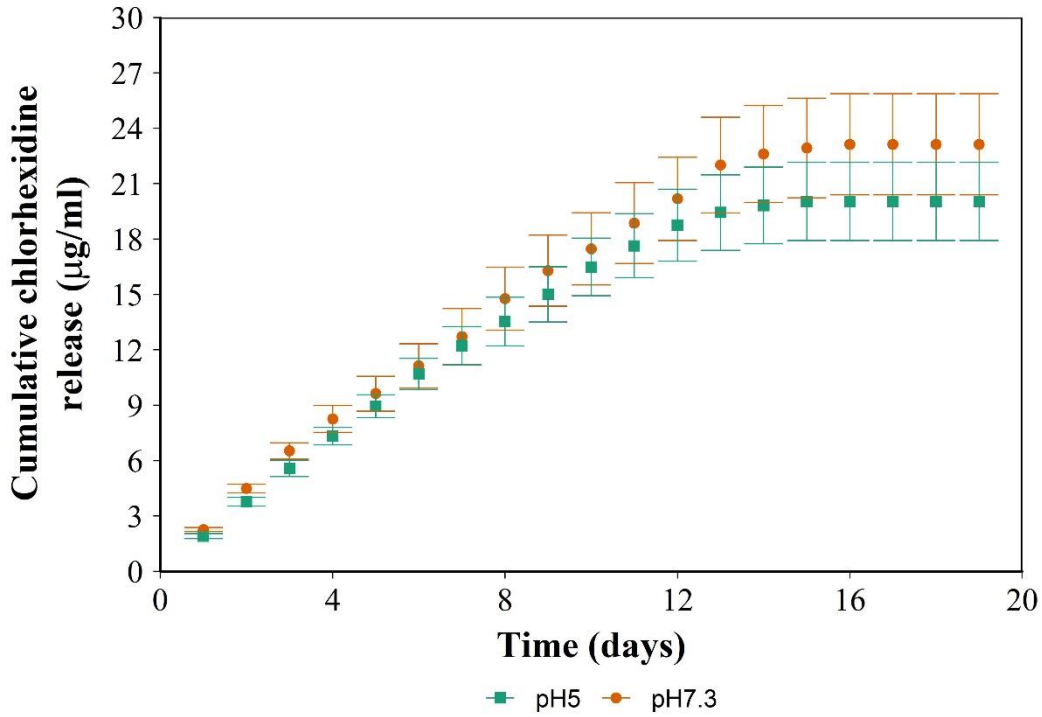

Figure 56. Chlorhexidine cumulative release in ug/ml from Q10 coated titanium coupon (mean ± SD n =3).

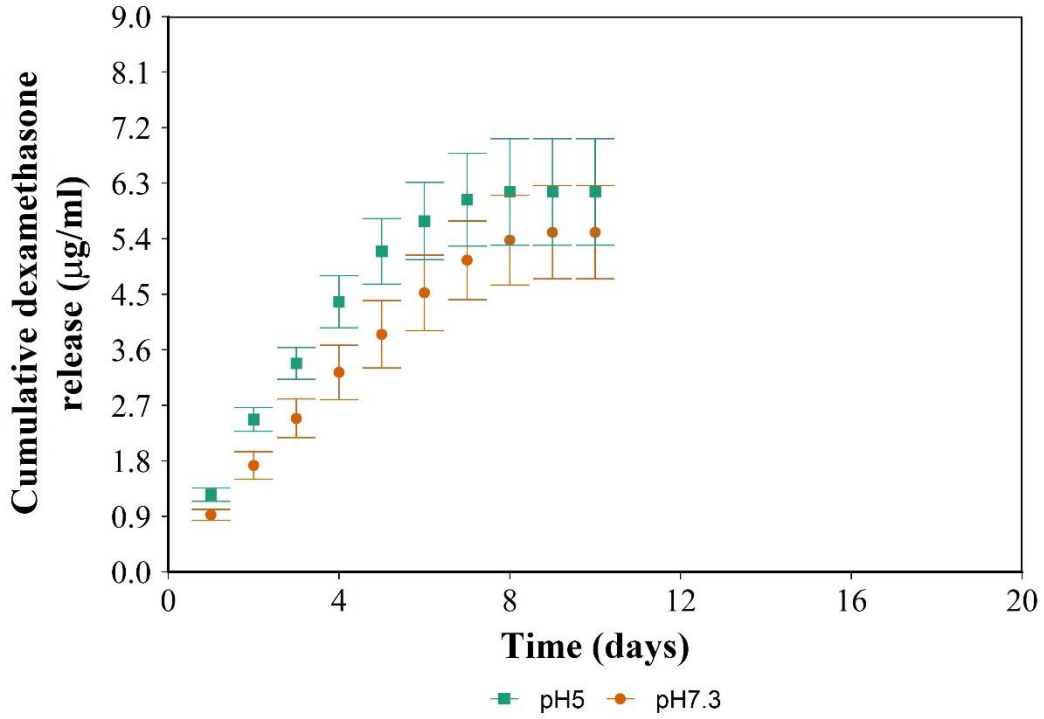

Figure 57. DEX cumulative release in µg/ml from Q10 coated titanium coupon (mean ± SD n =3).

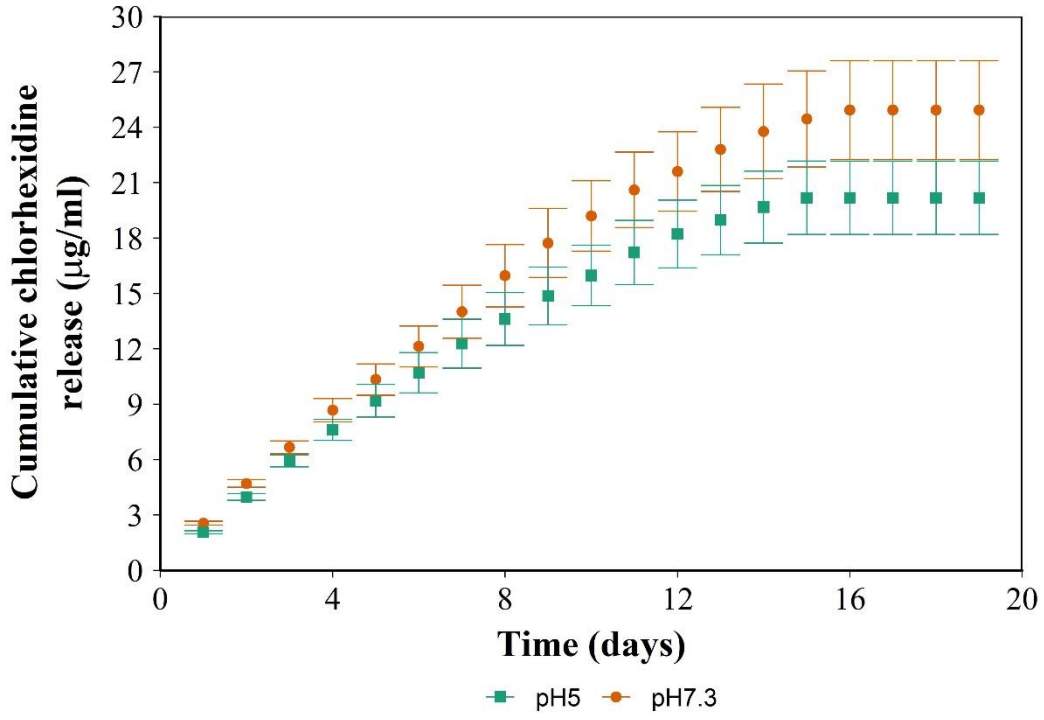

Figure 58. Chlorhexidine cumulative release in µg/ml from Q4 DEX and Q6 CHX combined coated titanium coupons (mean ± SD n =3).

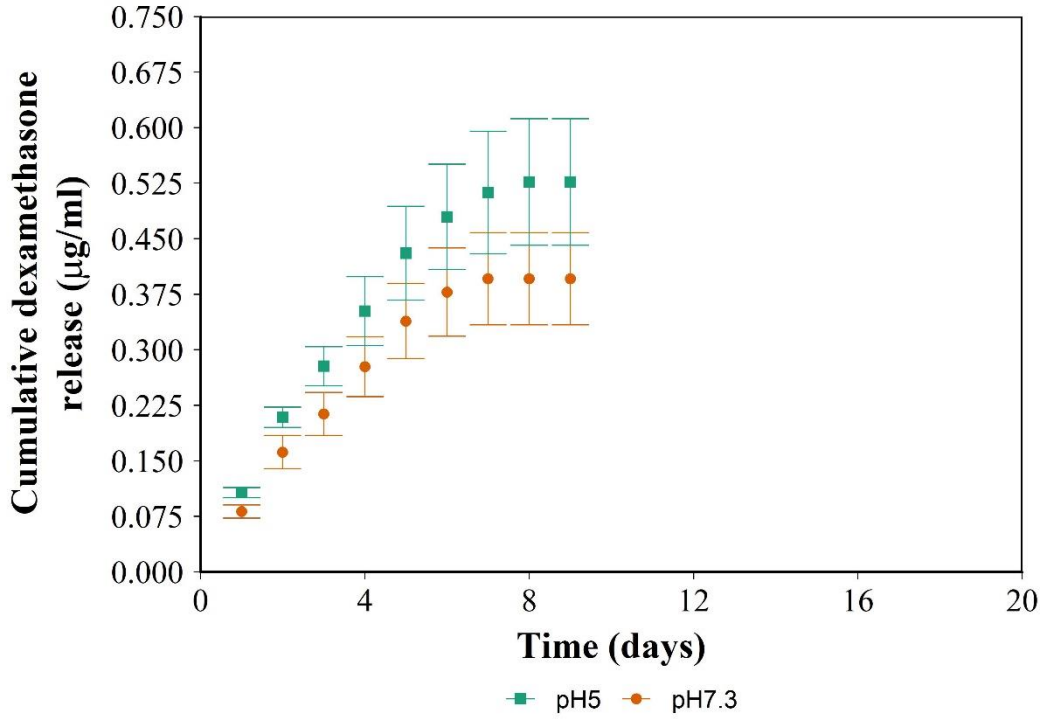

Figure 59. DEX cumulative release in µg/ml from Q4 DEX and Q6 CHX combined coated titanium coupons (mean ± SD n =3).

6.3.3 Antimicrobial activity testing

Release media at pH 7.3 from samples containing chlorhexidine only and chlorohexidine and DEX-P were capable of preventing growth of numerous pathogenic bacteria species (Figure 60).

Most of the bacteria were inhibited by buffer released after 3-4 days; *Acinetobacter baumannii* isolated were the most resistant as they were not inhibited by samples costed with chlorohexidine and DEX-P and growth of 2 out of the three strains was prevented only by the media corresponding to the first day of release. *S. epidermidis 222* was the isolated inhibited by the media corresponding to the longer release,

Generally, the inhibitor activity of the media containing release drugs from pure chlorohexidine or chlorohexidine and DEX-P, was the same; for Enterococcus, *E. coli*, *S. epidermidis* 325 and *Acinetobacter baumannii* 646 and 645 the samples containing only chlorhexidine corresponding to one further day of release prevented bacterial growth compared to chlorohexidine and DEX-P coating.

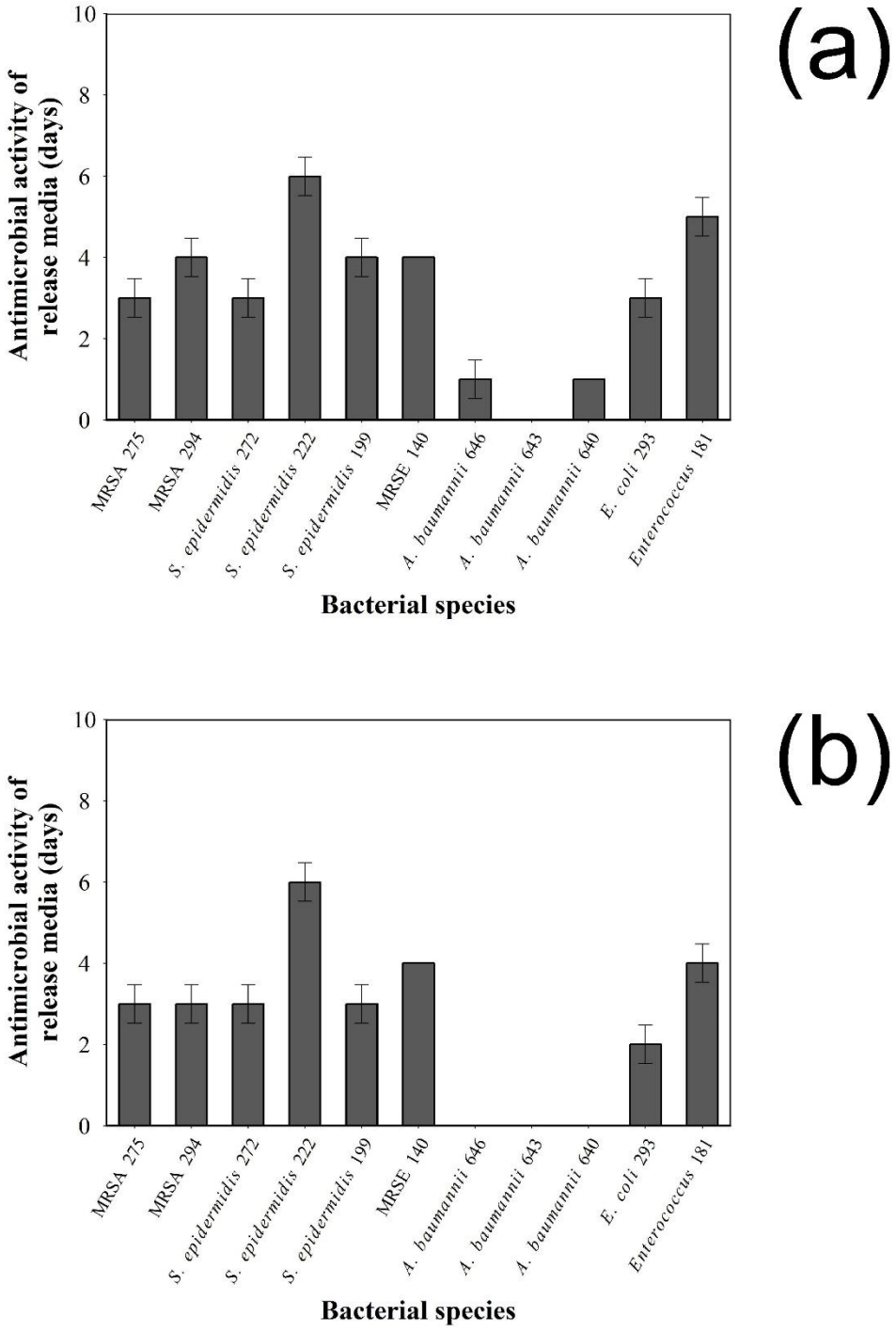

Figure 60. Antimicrobial activity for the daily release of Q10 pure chlorohexidine (a) chlorohexidine/DEP-P (b) coated titanium coupon (mean ± SD n =3).

6.3.4 Cytotoxicity testing

The media containing release compounds from coated coupons did not affect the mitochondrial activity of monocytes for up to 24 hours of contact. On the contrary

addition of LPS to media originated from contact with uncoated titanium surfaces reduced mitochondrial activity compared to media not containing LPS ($p < 0.05$). When LPS was added to release media obtained from coated titanium coupons the mitochondrial activity was reduced compared to the same media without LPS, but after 24 hours of contact, mitochondrial activity was greater for media that was in contact with coated surfaces than uncoated ($p<0.05$).

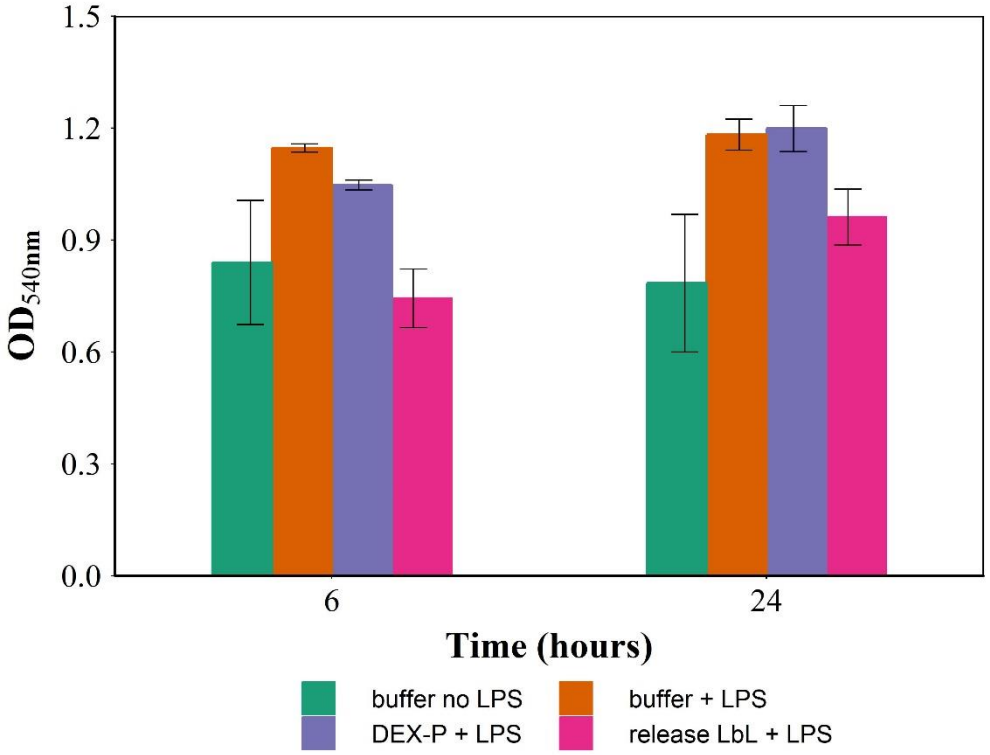

Figure 61. Mitochondrial activity of Macrophages after 6 and 24 hours in contact with media exposed to coated and uncoated coupons for 24 h (mean ± SD n =6).

6.3.5 Anti-inflammatory testing

No effect on inflammation markers was detected when macrophages were in contact with the coated samples compared to uncoated titanium ($p<0.05$); when LPS was added to cells grown on uncoated surfaces both IL-6 and TNFα levels increased considerably after 6 hours of exposure, in case of IL-6 concentration increased further during the subsequent incubation period. DEX-P containing coating reduced the levels of both inflammatory markers compared to uncoated surfaces ($p<0.05$) (Figure 62).

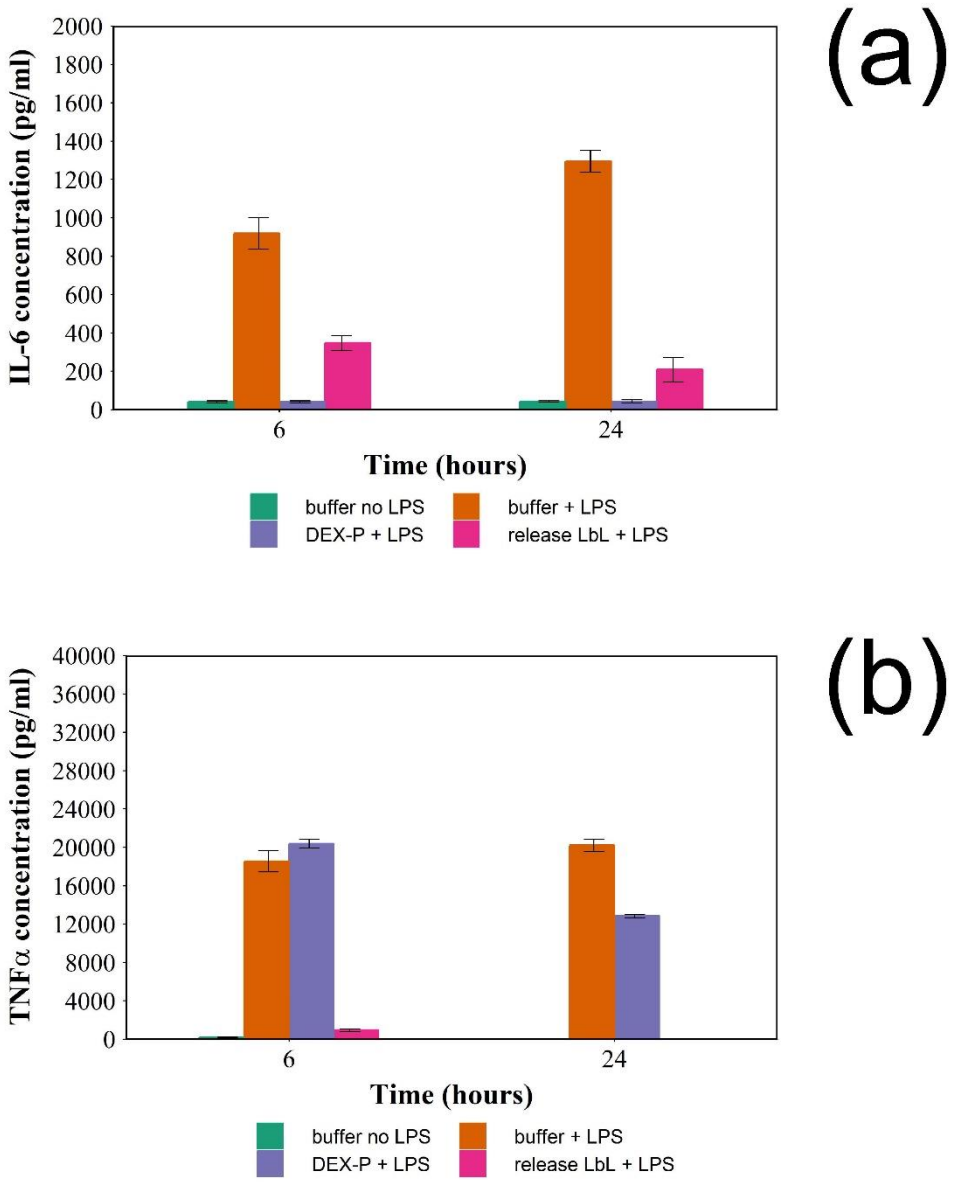

Figure 62. Anti-inflammatory effect of combined coated Q4 DEX and Q6 CHX on IL-6 (a) and TNFα (b) released from Macrophages (mean ± SD n =3).

6.4 Discussion

Chlorhexidine was chosen in this study because this compound is a first-line topical antiseptic that has demonstrated to be highly effective to treat skin and soft-tissue infection caused by a broad range of bacteria, including methicillin-resistant *Staphylococcus aureus*/MRSA (Schlett et al. 2014). Recently, chlorhexidine has shown promising results when employed in orthopaedic materials such as fixation pins (DeJong et al. 2001) and titanium surfaces (Riool, Dirks, et al. 2017). Dexamethasone was chosen

because it has both anti-inflammatory and immunosuppressive properties, which has positive impact on osseointegration (Coutinho and Chapman 2011). Other glucocorticoids including prednisolone and methylprednisolone are possible to use for their anti-inflammatory and immunosuppressive actions but dexamethasone has greater bioavailability and it remains in the body fluid for a longer period (Coutinho and Chapman 2011).

6.4.1 Release study

Chlorohexidine and DEX-P release was carried out in two different media: acetate buffer pH5 to mimic the acidic conditions observed in infected (Kinnari et al. 2009) or inflamed (de Nadai et al. 2013); phosphate buffer pH7.3 represented healthy joint environment (Ribeiro, Monteiro, and Ferraz 2012; Goldie and Nachemson 1970).

Drug release from LbL coating is pH dependent as this parameter is pivotal in controlling the level of protonation of amine and carboxylic acid present on the polyelectrolytes and such the electrostatic field. It has been hypothesised that delamination due to B1 hydrolysis would contribute to drug release (Chuang, Smith, and Hammond 2008; Hammond 2012; Smith et al. 2009), however recent evidence has revealed that drug diffusion is the governing phenomena of release from the coating prepared in this work (Al Thaher et al. 2018). DEX-P exhibited higher release at pH5 than pH7.3 while chlorhexidine exhibited the opposite behaviour (Figure 56 to Figure 59). This difference can be attributed to the different charge of the two drugs as DEX-P is negatively charged in the pH range tested while chlorhexidine is positively charged. It has been demonstrated that the surface charge of the outer layer of LbL constructs is the key in controlling diffusion through the all coating and that diffusion is hindered when molecule and outer layer exhibit the same charge (Sato, Shiba, and Anzai 2013). Release results for DEX-P and chlorohexidine follow this as the outer layer of the LbL coating was made with B1 that is positively charged at pH5 and close to neutrality at pH7.3 thus favouring chlorhexidine diffusion at pH7.3 and DEX-P at pH5, the conditions that return the greater difference between drug and outer layer charge.

Chlorohexidine release was very similar between the coating containing only this drug or a combination with DEX-P, this is because chlorohexidine was deposited on the outer layers of the LbL coating and it is possible that the majority of drug deposited on the initial layers remains entrapped in the coating. This also explains the observation that the concentration of DEX-P is about 90% smaller from the mixed coating than from the pure samples despite the number of layers containing the steroidal drug being 40%.

Overall drug release observed from coupons is detectable for a shorter period of time and the concentration of drug is lower than from NP coated with the same LbL constructs because the ratio between sample surface to release media volume is smaller with coupons.

6.4.2 Antimicrobial activity

Antimicrobial testing was carried out against clinical isolates of PJIs (Geipel 2009; Martinez-Pastor et al. 2009; Hsieh et al. 2009); the protocol involved the incubation of the release media from the coated coupons with the tested bacteria simulating the scenario in the prosthetic joint surgery. Chlorhexidine concentration in the media decreased with time (Figure 56 and Figure 58), therefore the release inhibitory activity was expected until chlorhexidine fell below MIC. The different efficacy observed is linked to species and strain variation of MIC; for example MIC for *E. coli* was reported 2.67 µg/ml (do Amorim, Aun, and Mayer 2004) while for MRSA the MIC was 4-8 µg/ml (Cookson, Bolton, and Platt 1991); *Pseudomonas aeruginosa* is much less susceptible to chlorhexidine 80 µg/ml (Thomas, Russell, and Maillard 2005).

As currently no antibacterial releasing uncemented prosthetic devices are available no control sample was clearly identifiable, and it could be assumed that uncoated titanium surfaces were not able to prevent microbial growth.

Chlorhexidine was generally more effective in preventing the growth of Gram positive bacteria (i.e. MRSA and *S. epidermidis*) than Gram negative bacteria (*E. coli* and *A. baumannii*) (Figure 60 and Figure 61). Generally, bacteria are classified as either Gram positive or negative according to the outcome of a staining protocol (Madigan and Martinko 1997). Gram positive bacteria present a very thick cell wall made of a protein called peptidoglycan (Madigan and Martinko 1997); while Gram negative bacteria exhibit thin peptidoglycan layers and a bacterial outer membrane (Madigan and Martinko 1997). Gram negative bacteria are often found to be more resistant to antibiotics and other antibacterial interventions than Gram positive spp. (Siu 2002); hence, the higher sensitivity of the gram positive bacteria tested in this work is consistent with the general knowledge.

Antimicrobial activity was comparable between pure chlorhexidine and chlorhexidine/DEX-P samples; this is in agreement with the release profile of the two type of samples that was very similar (Figure 56 and Figure 58).

Chlorohexidine embedded epoxy-based coatings on titanium implants exhibited bactericidal activity against *S. aureus;* however almost 90% of the drug was released in

the first day (Riool, Dirks, et al. 2017) limiting the efficacy window of this approach; while the release and antimicrobial activity shown by the LbL coating developed in this work was more prolonged.

6.4.3 Coated Titanium coupon imaging and durability

SEM of the LbL coated sample demonstrated that the polymer coating was applied on the titanium surface successfully. Moreover, the coating was remained on the surface during a removal force applied by the brush confirming that the coating is capable to withstand the removal forces applied during insertion of the device. Durability of the surface modification applied on material for uncemented devices is critical as strong forces are exerted on the during the surgery and in case the coating is scratched it would not be able to accomplish the planned objective of providing antimicrobial and anti-inflammatory activity (Riool, Dirks, et al. 2017; Mansell et al. 2012).

6.4.4 Cytotoxicity and Anti-inflammatory testing

Human monocytes (THP-1)-derived macrophages activated with PMA were used as model of human macrophages that are cells of the immune system involved in inflammation. Cells were exposed to LPS and to elutes collected from the DEX release studies at pH=7.3 to confirm that the anti-inflammatory activity of DEX was retained and that no cytotoxic activity was induced. Elutes in buffer pH=5 were not investigated because they cells exposed to these media exhibited low cellular viability. LPS was used to induce as inflammatory response in from the activated monocytes and two specific inflammatory markers produced by human macrophages (IL-6 and tumour necrosis factor alpha (TNFα)) were quantified (Qin 2012; Cochran and Finch-Arietta 1992). Appropriate cell density and an optimal LPS concentration were determined in preliminary experiments and are similar to other published research (Glue et al. 2002; Moreira-Tabaka et al. 2012).

Polyelectrolytes and the products of B1 hydrolysis are released from LbL coatings beside DEX; therefore, we determined both whether anti-inflammatory activity was retained but also the decomposition products of the LbL coating do not pose a cytotoxic risk. MTT measures mitochondrial activity that is linked to cell viability, coating does not impact on monocytes metabolism highlighting the compatibility of the coating towards this type of cells. B1 belongs to a class of known biocompatible polyelectrolytes thus the lack of toxic was expected. However, LPS caused a significant reduction linked to the induction of inflammation (Figure 61).

DEX activity once released was retained as the level of both inflammation markers (IL-6 and TNFα) after LPS exposure were lower when elutes from coated coupons where used compared to uncoated samples. The mild coating conditions employed for the LbL deposition (aqueous solution and room temperature) do not inactivate the steroidal drug similarly to diclofenac when released from LbL coatings (Hsu, Park, et al. 2014).

6.5 Conclusions

The coating developed here is the first capable of providing both antimicrobial and anti-inflammatory activity hence it has the characteristics necessary to tackle the two main sources of joint replacement device failure: PJIs and aseptic loosening.

Chapter 7: General conclusions

Cementless prostheses were introduced in the early 1980s in an attempt to prevent aseptic loosening of the acetabular cup and the difficulties associated with revision of cemented THAs. Uncemented prosthesis considered the best choice for a younger patient who undergoes total joint arthroplasty (TJA). Failure rates for cementless acetabular and femoral components were not dramatically better than failure rates for cemented components. Increased wear rates have been associated with cementless acetabular fixation, which is a concern, as survival curves in cemented THAs demonstrated an increase in rates of loosening and revision in the second decade. Stress shielding, aseptic loosening, osteolysis, and thigh pain remain problems with certain models as well. Also, prosthetic joint infection still one of the major limitations associated with cementless fixation.

Osseointegration, the condition where osteoblast cells are attached and started to grow on the surface of the prosthesis, should be achieved without being interfered by microbial infection or inflammation. Therefore, there has been growing attention on the development of prosthesis with antimicrobial and anti-inflammatory activity (Goodman et al. 2013; Raphel et al. 2016; Zhang et al. 2008). The currently available uncemented prosthesis in the United Kingdom is often coated with osteoconductive materials. Pressfit® (Waldemar), CSF® (Joint Replacement Instrumentation Ltd.), Trident® and ABG II® (Stryker) are a few hip joint implants that are coated with hydroxyapatite. Metha® (B Braun), Cerafit® (Corin) prostheses are coated with pure calcium phosphate. The antibacterial and anti-inflammatory agents-coated prosthesis is not available in the market yet, but ongoing research showed promising results (Gallo, Holinka, and Moucha 2014; Getzlaf et al. 2016; Raphel et al. 2016; Tamanna, Bulitta, and Yu 2015).

The goal of this research was to develop a novel coating system that contains anti-inflammatory and antimicrobial agents, as a prophylaxis to prevent (PJI) and aseptic loosening after total joint replacement. To achieve this, a new layer by layer (LbL) coating films was developed for loading dexamethasone as an anti-inflammatory drug and chlorhexidine as a non-antibiotic antimicrobial agent; the later has been chosen due to the low risk of bacterial resistance. Initially titanium nanoparticles were used as a model system for larger surfaces; the two drugs were initially deposited separately and then in various combinations.

We have successfully controlled the release of dexamethasone for about a week. This material did not impact on osteoblasts proliferation and the anti-inflammatory activity of the realised drug was retained.

LbL Dexamethasone coated titanium nanoparticles (chapter 3) have controlled and sustained drug release for more than three weeks. The release profile was attributable to the release mechanism dominated by diffusion. The daily dexamethasone release from coated titanium nanoparticles did not impact on macrophages and osteoblasts proliferation. The addition of DEX-P suppressed IL-6 production to about a third after both 6 and 24h; TNF-concentration was reduced to half after 6 hands about a third after 24 hours. The use of an equivalent dose of DEX release from LbL coating had similar reduction patterns for both inflammation markers, but the efficacy of the released drug was about 20-30% inferior to pure DEX.

We loaded individually (chapter 4), chlorhexidine has been successfully released for up to 60 days, the observed release kinetic describes a drug release profile for chlorhexidine dominated by diffusion as the rate progressively decreases. Also, it prevented bacterial growth for about one month. Cytocompatibility testing indicates that the coating film was not toxic to osteoblast.

In the same way, the nanoparticles with different combination ratios of chlorhexidine and dexamethasone (chapter 5) controlled and prolonged the release of chlorhexidine for more than six weeks and dexamethasone for about three weeks. The antibacterial activity against a variety of clinical isolates of PJI of the coated nanoparticles lasted for more than two weeks. The combined coated films did not have a negative impact on osteoblasts mitochondrial activity, and this indicates that the produced coating systems are cytocompatible. In addition to particles coated with alternated quadruple layers of chlorhexidine and DEX had a higher anti-inflammatory activity as DEX-P concentration after one day of release was higher than in case the quadruples layers containing the steroidal drug were deposited in only in layers closer to the titanium surface.

The most promising coating in terms of both antimicrobial and anti-inflammatory activity determined from the investigation on nanoparticles was applied on titanium

coupons (chapter 6); the release of chlorhexidine was controlled for up to 14 days and dexamethasone for 5 days while the antibacterial activity of the coated coupons lasts for six days. The shorter release and antimicrobial activity observed from the coatings compared to the nanoparticles was the results of a reduced surface to release media in case of coupons in the experimental set-up. The media containing release compounds from the coated coupons did not affect the mitochondrial activity of monocytes for up to 24 hours of contact. For anti-inflammatory activity, DEX-P containing coating reduced the levels of both inflammatory markers (TNF-α, IL-6) compared to uncoated surfaces

In conclusion, this study helps to examine single anti-inflammatory and antimicrobial agents or in combination over titanium nanoparticles and titanium coupons. The coatings developed here are the first capable of providing both antimicrobial and anti-inflammatory activity hence they possess the characteristics necessary to tackle the two main sources of joint replacement device failure: PJI and aseptic loosening.

Chapter 8: Future work

Even though the different coating systems in this study were assessed for cytocompatibility using cell line Saos-2 and activated THP-1, the biocompatibility of these coatings must be questioned in more details. More in vitro tests measuring the toxicity of the coating films on tissue and cells is needed and direct contact and indirect contact cytotoxicity testing is suggested for all the coatings following the International Organization for Standardization 109993-5 to define their clinical applicability (Li, Zhou, and Xu 2015).

If the results of such experiments indicate the coatings cytocompatibility, animal testing may then be valid to assess the extent of their biocompatibility and bioactivity. The antibacterial and anti-inflammatory activity of all coating films could be studied in vivo by using dummy implants (titanium disks). After developing the coating over the titanium disk, it should be inserted into the subcutaneous pocket of the animal model. The inflammatory response (redness, swelling and extent of any abscess in mm^2) should be monitored daily to measure the anti-inflammatory effect of the coating. In addition to that, after sacrifice, the disk/implant and associated tissue surrounding the samples should be carefully removed from each implantation site and the number of bacteria on the disks/implants or in the tissues determined by serial dilution (Chen et al. 2016).

Other suggestion would be to model an orthopaedic implant infection, and this could be done by using medical-grade titanium-wire implant, precoated with the coating film, surgically placed into the distal aspect of the right femur of the mice. The joint is challenged with a bioluminescent bacterial strain that contains a bioluminescent lux operon construct integrated into a stable bacterial plasmid that naturally produces a blue-green light emitted only by active bacteria. After that, in vivo bioluminescence imaging should be performed by using the IVIS Lumina II in vivo imaging system. To confirm that bioluminescence signals corresponds to the bacterial burden in vivo, bacteria adherent to the implants and surrounding tissue must be quantified through sonication and colony-forming unit (CFU) counting (Stavrakis et al. 2016).

The development of the LbL coating films has generated opportunities for the delivery of different active compounds from the surface of the implantable devices. The drugs that can be loaded into the polymeric films are not restricted to dexamethasone and chlorhexidine; generally, any drug molecule with a suitable charge and size for LbL coating can be used instead of the model compounds. Other therapeutic agents, for

example, another antimicrobial, anti-inflammatory, and osteoconductive agents can also be incorporated in LbL coatings. Common antimicrobial agents that we suggest using in coating films are vancomycin and ciprofloxacin due to their broad spectrum and low bacterial resistance. In the case of anti-inflammatory coating, non-steroidal anti-inflammatory such as naproxen and diclofenac could be used to compare their anti-inflammatory effect to dexamethasone (steroidal anti-inflammatory). Also, hydroxyapatite is an osteoconductive material that has been shown, in both *in vivo* and *in vitro* models, to induce osteoblast adhesion and in some studies differentiation could be tested as polyelectrolyte (Zhang et al., 2014).

Furthermore, other polymers can be used instead of alginate and B1 to build up the LBL system. For example, hyaluronic acid could be used instead of alginate because of its higher cytocompatibility and its negative charge. Overall, to optimize drug loading and release profile, polymers with different molecular weight, chemical structure, charge, and hydrolysis kinetic can be studied for promoting the biocompatibility and bioactivity performance of LbL films.

References

Abbas, Sabiha, and Yousef Abu-Amer. 2003. Dominant-negative IκB Facilitates Apoptosis of Osteoclasts by Tumor Necrosis Factor-α.

Abdulkarim, Ali, Prasad Ellanti, Nicola Motterlini, Tom Fahey, and John M. O'Byrne. 2013. 'Cemented versus uncemented fixation in total hip replacement: a systematic review and meta-analysis of randomized controlled trials', *Orthopedic reviews*, 5: e8-e8.

Abu-Amer, Y. 2001. 'IL-4 abrogates osteoclastogenesis through STAT6-dependent inhibition of NF-kappaB', *J Clin Invest*, 107: 1375-85.

Abu-Amer, Yousef, Isra Darwech, and John C. Clohisy. 2007. 'Aseptic loosening of total joint replacements: mechanisms underlying osteolysis and potential therapies', *Arthritis research & therapy*, 9 Suppl 1: S6-S6.

Al Thaher, Y., S. Perni, and P. Prokopovich. 2017. 'Nano-carrier based drug delivery systems for sustained antimicrobial agent release from orthopaedic cementous material', *Adv Colloid Interface Sci*, 249: 234-47.

Al Thaher, Yazan, Silvia Latanza, Stefano Perni, and Polina Prokopovich. 2018. 'Role of poly-beta-amino-esters hydrolysis and electrostatic attraction in gentamicin release from layer-by-layer coatings', *Journal of Colloid and Interface Science*, 526: 35-42.

Alotaibi, Hadil Faris, Yazan Al Thaher, Stefano Perni, and Polina Prokopovich. 2018. 'Role of processing parameters on surface and wetting properties controlling the behaviour of layer-by-layer coated nanoparticles', *Current Opinion in Colloid & Interface Science*, 36: 130-42.

Alt, V., A. Bitschnau, F. Bohner, K. E. Heerich, E. Magesin, A. Sewing, T. Pavlidis, G. Szalay, C. Heiss, U. Thormann, S. Hartmann, W. Pabst, S. Wenisch, and R. Schnettler. 2011. 'Effects of gentamicin and gentamicin-RGD coatings on bone ingrowth and biocompatibility of cementless joint prostheses: an experimental study in rabbits', *Acta Biomater*, 7: 1274-80.

Alt, Volker. 2017. 'Antimicrobial coated implants in trauma and orthopaedics–A clinical review and risk-benefit analysis', *Injury*, 48: 599-607.

Amarasekara, Dulshara Sachini, Hyeongseok Yun, Sumi Kim, Nari Lee, Hyunjong Kim, and Jaerang Rho. 2018. 'Regulation of Osteoclast Differentiation by Cytokine Networks', *Immune network*, 18: e8-e8.

Ambrose, C. G., T. A. Clyburn, J. Mika, G. R. Gogola, H. B. Kaplan, A. Wanger, and A. G. Mikos. 2014. 'Evaluation of antibiotic-impregnated microspheres for the prevention of implant-associated orthopaedic infections', *J Bone Joint Surg Am*, 96: 128-34.

Anagnostakos, K. 2017. 'Therapeutic Use of Antibiotic-loaded Bone Cement in the Treatment of Hip and Knee Joint Infections', *J Bone Jt Infect*, 2: 29-37.

Anastase, Denisa Madalina, Simona Cionac Florescu, Ana Maria Munteanu, Traian Ursu, and Cristian Ioan Stoica. 2014. 'Analgesic techniques in hip and knee arthroplasty: from the daily practice to evidence-based medicine', *Anesthesiology research and practice*, 2014: 569319-19.

Anderson, James M., Analiz Rodriguez, and David T. Chang. 2008. 'Foreign body reaction to biomaterials', *Seminars in Immunology*, 20: 86-100.

Ansari, Juned Salam, Tsuneari Takahashi, and Hemant Pandit. 2018. 'Uncemented hips: current status', *Orthopaedics and Trauma*, 32: 20-26.

Antoci, V., Jr., C. S. Adams, J. Parvizi, H. M. Davidson, R. J. Composto, T. A. Freeman, E. Wickstrom, P. Ducheyne, D. Jungkind, I. M. Shapiro, and N. J. Hickok. 2008. 'The inhibition of Staphylococcus epidermidis biofilm formation by vancomycin-modified titanium alloy and implications for the treatment of periprosthetic infection', *Biomaterials*, 29: 4684-90.

Antoci, V., Jr., S. B. King, B. Jose, J. Parvizi, A. R. Zeiger, E. Wickstrom, T. A. Freeman, R. J. Composto, P. Ducheyne, I. M. Shapiro, N. J. Hickok, and C. S. Adams. 2007. 'Vancomycin covalently bonded to titanium alloy prevents bacterial colonization', *J Orthop Res*, 25: 858-66.

Anusavice, K. J., N. Z. Zhang, and C. Shen. 2006. 'Controlled release of chlorhexidine from UDMA-TEGDMA resin', *J Dent Res*, 85: 950-4.

Apostu, D., O. Lucaciu, C. Berce, D. Lucaciu, and D. Cosma. 2018. 'Current methods of preventing aseptic loosening and improving osseointegration of titanium implants in cementless total hip arthroplasty: a review', *J Int Med Res*, 46: 2104-19.

Aprato, Alessandro, Salvatore Risitano, Luigi Sabatini, Matteo Giachino, Gabriele Agati, and Alessandro Massè. 2016. 'Cementless total knee arthroplasty', *Annals of translational medicine*, 4: 129-29.

Arciola, C. R., D. Campoccia, P. Speziale, L. Montanaro, and J. W. Costerton. 2012. 'Biofilm formation in Staphylococcus implant infections. A review of molecular mechanisms and implications for biofilm-resistant materials', *Biomaterials*, 33: 5967-82.

Arend, W. P., and C. Gabay. 2000. 'Physiologic role of interleukin-1 receptor antagonist', *Arthritis research*, 2: 245-48.

Ariga, K., Y. M. Lvov, K. Kawakami, Q. Ji, and J. P. Hill. 2011. 'Layer-by-layer self-assembled shells for drug delivery', *Adv Drug Deliv Rev*, 63: 762-71.

Bahna, P., T. Dvorak, H. Hanna, A. W. Yasko, R. Hachem, and I. Raad. 2007. 'Orthopaedic metal devices coated with a novel antiseptic dye for the prevention of bacterial infections', *Int J Antimicrob Agents*, 29: 593-6.

Baranowski, Andreas, Anja Klein, Ulrike Ritz, Angelika Ackermann, Joris Anthonissen, Kerstin B. Kaufmann, Christian Brendel, Hermann Götz, Pol M. Rommens, and Alexander Hofmann. 2016. 'Surface Functionalization of Orthopedic Titanium Implants with Bone Sialoprotein', *PLOS ONE*, 11: e0153978.

Barrett-Bee, K., L. Newboult, and S. Edwards. 1994. 'The membrane destabilising action of the antibacterial agent chlorhexidine', *FEMS Microbiol Lett*, 119: 249-53.

Berry, D.J. . 2001. Primary total hip arthroplasty. In:, editor. Chapman's Orthopaedic Surgery (Lippincott: Williams and Wilkins: Philadelphia).

Bertazzoni Minelli, E., A. Benini, E. Samaila, M. Bondi, and B. Magnan. 2015. 'Antimicrobial activity of gentamicin and vancomycin combination in joint fluids after antibiotic-loaded cement spacer implantation in two-stage revision surgery', *J Chemother*, 27: 17-24.

Besinis, A., S. D. Hadi, H. R. Le, C. Tredwin, and R. D. Handy. 2017. 'Antibacterial activity and biofilm inhibition by surface modified titanium alloy medical implants following application of silver, titanium dioxide and hydroxyapatite nanocoatings', *Nanotoxicology*, 11: 327-38.

Boehler, Ryan M., John G. Graham, and Lonnie D. Shea. 2011. 'Tissue engineering tools for modulation of the immune response', *BioTechniques*, 51: 239-passim.

Breusch S.J., and Malchau H. 2005. *The Well-cemented Total Hip Arthroplasty: Theory and Practice.* (Springer–Berlin: New York).

Bridges, Amanda W., and Andrés J. García. 2008. 'Anti-Inflammatory Polymeric Coatings for Implantable Biomaterials and Devices', *Journal of Diabetes Science and Technology*, 2: 984-94.

Bucay, N., I. Sarosi, C. R. Dunstan, S. Morony, J. Tarpley, C. Capparelli, S. Scully, H. L. Tan, W. Xu, D. L. Lacey, W. J. Boyle, and W. S. Simonet. 1998. 'osteoprotegerin-deficient mice develop early onset osteoporosis and arterial calcification', *Genes Dev*, 12: 1260-8.

Cai, Kaiyong, Annett Rechtenbach, Jianyuan Hao, Jörg Bossert, and Klaus D. Jandt. 2005. 'Polysaccharide-protein surface modification of titanium via a layer-by-

layer technique: Characterization and cell behaviour aspects', *Biomaterials*, 26: 5960-71.
Cai, Xinjie, Kena Ma, Yi Zhou, Tao Jiang, and Yining Wang. 2016. 'Surface functionalization of titanium with tetracycline loaded chitosan–gelatin nanosphere coatings via EPD: fabrication, characterization and mechanism', *RSC Advances*, 6: 7674-82.
Catelas, I., M. A. Wimmer, and S. Utzschneider. 2011. 'Polyethylene and metal wear particles: characteristics and biological effects', *Semin Immunopathol*, 33: 257-71.
Cenni, E., D. Granchi, G. Ciapetti, L. Savarino, A. Corradini, M. Vancini, and A. Giunti. 2002. 'Gene expression of bone-associated cytokines in MG63 osteoblast-like cells incubated with acrylic bone cement extracts in minimum essential medium', *J Biomater Sci Polym Ed*, 13: 1283-94.
Chang, Y., C-L. Tai, P-H. Hsieh, and S. W. N. Ueng. 2013. 'Gentamicin in bone cement', *Bone & Joint Research*, 2: 220-26.
Chen, A., F. Haddad, P. Lachiewicz, M. Bolognesi, L. E. Cortes, M. Franceschini, J. Gallo, A. Glynn, A. G. Della Valle, A. Gahramanov, M. Khatod, S. Lazarinis, G. Lob, A. Nana, P. Ochsner, I. Tuncay, T. Winkler, and Y. Zeng. 2014. 'Prevention of late PJI', *J Orthop Res*, 32 Suppl 1: S158-71.
Chen, L., and Y. M. Wen. 2011. 'The role of bacterial biofilm in persistent infections and control strategies', *Int J Oral Sci*, 3: 66-73.
Chen, R., M. D. Willcox, K. K. Ho, D. Smyth, and N. Kumar. 2016. 'Antimicrobial peptide melimine coating for titanium and its in vivo antibacterial activity in rodent subcutaneous infection models', *Biomaterials*, 85: 142-51.
Chua, P. H., K. G. Neoh, E. T. Kang, and W. Wang. 2008. 'Surface functionalization of titanium with hyaluronic acid/chitosan polyelectrolyte multilayers and RGD for promoting osteoblast functions and inhibiting bacterial adhesion', *Biomaterials*, 29: 1412-21.
Chuang, H. F., R. C. Smith, and P. T. Hammond. 2008. 'Polyelectrolyte multilayers for tunable release of antibiotics', *Biomacromolecules*, 9: 1660-8.
Claassen, L., M. Ettinger, C. Plaass, K. Daniilidis, T. Calliess, and M. Ezechieli. 2014. 'Diagnostic value of bone scintigraphy for aseptic loosening after total knee arthroplasty', *Technol Health Care*, 22: 767-73.
Cochran, F. R., and M. B. Finch-Arietta. 1992. 'Interleukin-6 can prime THP-1 macrophages for enhanced production of tumor necrosis factor-alpha in response to LPS', *Immunopharmacology*, 23: 97-103.
Coelho, Jorge F., Paula C. Ferreira, Patricia Alves, Rosemeyre Cordeiro, Ana C. Fonseca, Joana R. Góis, and Maria H. Gil. 2010. 'Drug delivery systems: Advanced technologies potentially applicable in personalized treatments', *The EPMA journal*, 1: 164-209.
Cookson, B. D., M. C. Bolton, and J. H. Platt. 1991. 'Chlorhexidine resistance in methicillin-resistant Staphylococcus aureus or just an elevated MIC? An in vitro and in vivo assessment', *Antimicrob Agents Chemother*, 35: 1997-2002.
Costerton, J. W., P. S. Stewart, and E. P. Greenberg. 1999. 'Bacterial biofilms: a common cause of persistent infections', *Science*, 284: 1318-22.
Coutinho, Agnes E., and Karen E. Chapman. 2011. 'The anti-inflammatory and immunosuppressive effects of glucocorticoids, recent developments and mechanistic insights', *Molecular and cellular endocrinology*, 335: 2-13.
Culliford, D. J., J. Maskell, D. J. Beard, D. W. Murray, A. J. Price, and N. K. Arden. 2010. 'Temporal trends in hip and knee replacement in the United Kingdom: 1991 to 2006', *J Bone Joint Surg Br*, 92: 130-5.
Culliford, D., J. Maskell, A. Judge, C. Cooper, D. Prieto-Alhambra, and N. K. Arden. 2015. 'Future projections of total hip and knee arthroplasty in the UK: results from the UK Clinical Practice Research Datalink', *Osteoarthritis and Cartilage*, 23: 594-600.

D'Antonio, J. A., W. N. Capello, and M. Naughton. 2012. 'Ceramic bearings for total hip arthroplasty have high survivorship at 10 years', *Clin Orthop Relat Res*, 470: 373-81.
Dai, S., T. Hirayama, S. Abbas, and Y. Abu-Amer. 2004. 'The IkappaB kinase (IKK) inhibitor, NEMO-binding domain peptide, blocks osteoclastogenesis and bone erosion in inflammatory arthritis', *J Biol Chem*, 279: 37219-22.
Dale, David C., Laurence Boxer, and W. Conrad Liles. 2008. 'The phagocytes: neutrophils and monocytes', *Blood*, 112: 935-45.
Dang, Tram T., Kaitlin M. Bratlie, Said R. Bogatyrev, Xiao Y. Chen, Robert Langer, and Daniel G. Anderson. 2011. 'Spatiotemporal effects of a controlled-release anti-inflammatory drug on the cellular dynamics of host response', *Biomaterials*, 32: 4464-70.
Das, Kakoli, Susmita Bose, Amit Bandyopadhyay, Balu Karandikar, and Bruce L. Gibbins. 2008. 'Surface coatings for improvement of bone cell materials and antimicrobial activities of Ti implants', *Journal of Biomedical Materials Research Part B: Applied Biomaterials*, 87B: 455-60.
Davies, N., W. Jackson, A. Price, J. Rees, and C. Lavy. 2012. *FRCS Trauma and Orthopaedics Viva.* (Oxford University Press,: Oxford).
Dawes, G. J. S., L. E. Fratila-Apachitei, B. S. Necula, I. Apachitei, G. J. Witkamp, and J. Duszczyk. 2010. 'Release of PLGA-encapsulated dexamethasone from microsphere loaded porous surfaces', *J Mater Sci Mater Med*, 21: 215-21.
de Nadai, T. R., M. N. de Nadai, A. A. Albuquerque, M. T. de Carvalho, A. C. Celotto, and P. R. Evora. 2013. 'Metabolic acidosis treatment as part of a strategy to curb inflammation', *Int J Inflam*, 2013: 601424.
Decher, Gero. 1997. 'Fuzzy Nanoassemblies: Toward Layered Polymeric Multicomposites', *Science*, 277: 1232-37.
DeJong, E. S., T. M. DeBerardino, D. E. Brooks, B. J. Nelson, A. A. Campbell, C. R. Bottoni, A. E. Pusateri, R. S. Walton, C. H. Guymon, and A. T. McManus. 2001. 'Antimicrobial efficacy of external fixator pins coated with a lipid stabilized hydroxyapatite/chlorhexidine complex to prevent pin tract infection in a goat model', *J Trauma*, 50: 1008-14.
Del Pozo, J. L., and R. Patel. 2009. 'Clinical practice. Infection associated with prosthetic joints', *N Engl J Med*, 361: 787-94.
Deng, Zhou J., Stephen W. Morton, Elana Ben-Akiva, Erik C. Dreaden, Kevin E. Shopsowitz, and Paula T. Hammond. 2013. 'Layer-by-Layer Nanoparticles for Systemic Codelivery of an Anticancer Drug and siRNA for Potential Triple-Negative Breast Cancer Treatment', *ACS Nano*, 7: 9571-84.
Deshmukh, P. K., K. P. Ramani, S. S. Singh, A. R. Tekade, V. K. Chatap, G. B. Patil, and S. B. Bari. 2013. 'Stimuli-sensitive layer-by-layer (LbL) self-assembly systems: targeting and biosensory applications', *J Control Release*, 166: 294-306.
do Amorim, C.V., C.E. Aun, and M.P. Mayer. 2004. 'Susceptibility of some oral microorganisms to chlorhexidine and paramonochlorophenol', *Braz Oral Res*, 18: 242-6.
Donaldson, A. J., H. E. Thomson, N. J. Harper, and N. W. Kenny. 2009. 'Bone cement implantation syndrome', *Br J Anaesth*, 102: 12-22.
Dougall, W. C. 2012. 'Molecular pathways: osteoclast-dependent and osteoclast-independent roles of the RANKL/RANK/OPG pathway in tumorigenesis and metastasis', *Clin Cancer Res*, 18: 326-35.
Drago, L., W. Boot, K. Dimas, K. Malizos, G. M. Hansch, J. Stuyck, D. Gawlitta, and C. L. Romano. 2014. 'Does implant coating with antibacterial-loaded hydrogel reduce bacterial colonization and biofilm formation in vitro?', *Clin Orthop Relat Res*, 472: 3311-23.
Du, Pengcheng, Xubo Zhao, Jin Zeng, Jinshan Guo, and Peng Liu. 2015. 'Layer-by-layer engineering fluorescent polyelectrolyte coated mesoporous silica nanoparticles

as pH-sensitive nanocarriers for controlled release', *Applied Surface Science*, 345: 90-98.
Dumont, C. M., J. Park, and L. D. Shea. 2015. 'Controlled release strategies for modulating immune responses to promote tissue regeneration', *J Control Release*, 219: 155-66.
Dunne, W. Michael, Jr. 2002. 'Bacterial adhesion: seen any good biofilms lately?', *Clin Microbiol Rev*, 15: 155-66.
Engh, C. A., D. O'Connor, M. Jasty, T. F. McGovern, J. D. Bobyn, and W. H. Harris. 1992. 'Quantification of implant micromotion, strain shielding, and bone resorption with porous-coated anatomic medullary locking femoral prostheses', *Clin Orthop Relat Res*: 13-29.
Etienne, O., C. Picart, C. Taddei, Y. Haikel, J. L. Dimarcq, P. Schaaf, J. C. Voegel, J. A. Ogier, and C. Egles. 2004. 'Multilayer polyelectrolyte films functionalized by insertion of defensin: a new approach to protection of implants from bacterial colonization', *Antimicrob Agents Chemother*, 48: 3662-69.
Eze, Emmanuel C., Hafizah Y. Chenia, and Mohamed E. El Zowalaty. 2018. 'Acinetobacter baumannii biofilms: effects of physicochemical factors, virulence, antibiotic resistance determinants, gene regulation, and future antimicrobial treatments', *Infection and drug resistance*, 11: 2277-99.
Feng, Wei, Wei Nie, Chuanglong He, Xiaojun Zhou, Liang Chen, Kexin Qiu, Weizhong Wang, and Zhiqi Yin. 2014. 'Effect of pH-Responsive Alginate/Chitosan Multilayers Coating on Delivery Efficiency, Cellular Uptake and Biodistribution of Mesoporous Silica Nanoparticles Based Nanocarriers', *ACS Applied Materials & Interfaces*, 6: 8447-60.
Fitzgerald, K. A., A. Davies, and A. D. Russell. 1989. 'Uptake of 14C-chlorhexidine diacetate to Escherichia coli and Pseudomonas aeruginosa and its release by azolectin', *FEMS Microbiol Lett*, 51: 327-32.
Gallardo-Moreno, A. M., M. A. Pacha-Olivenza, M. C. Fernandez-Calderon, C. Perez-Giraldo, J. M. Bruque, and M. L. Gonzalez-Martin. 2010. 'Bactericidal behaviour of Ti6Al4V surfaces after exposure to UV-C light', *Biomaterials*, 31: 5159-68.
Gallardo-Moreno, A. M., M. A. Pacha-Olivenza, L. Saldana, C. Perez-Giraldo, J. M. Bruque, N. Vilaboa, and M. L. Gonzalez-Martin. 2009. 'In vitro biocompatibility and bacterial adhesion of physico-chemically modified Ti6Al4V surface by means of UV irradiation', *Acta Biomater*, 5: 181-92.
Gallo, J., M. Holinka, and C. S. Moucha. 2014. 'Antibacterial surface treatment for orthopaedic implants', *Int J Mol Sci*, 15: 13849-80.
Gao, Jing, N. Eric Huddleston, Evan M. White, Jitendra Pant, Hitesh Handa, and Jason Locklin. 2016. 'Surface Grafted Antimicrobial Polymer Networks with High Abrasion Resistance', *ACS Biomaterials Science & Engineering*, 2: 1169-79.
Gbejuade, Herbert O., Andrew M. Lovering, and Jason C. Webb. 2015. 'The role of microbial biofilms in prosthetic joint infections', *Acta Orthopaedica*, 86: 147-58.
Geipel, Udo. 2009. 'Pathogenic organisms in hip joint infections', *International journal of medical sciences*, 6: 234-40.
Geißler, D., C. Gollwitzer, A. Sikora, C. Minelli, M. Krumrey, and U. Resch-Genger. 2015. 'Effect of fluorescent staining on size measurements of polymeric nanoparticles using DLS and SAXS', *Analytical Methods*, 7: 9785-90.
Gentile, P., I. Carmagnola, T. Nardo, and V. Chiono. 2015. 'Layer-by-layer assembly for biomedical applications in the last decade', *Nanotechnology*, 26: 422001.
Getzlaf, M. A., E. A. Lewallen, H. M. Kremers, D. L. Jones, C. A. Bonin, A. Dudakovic, R. Thaler, R. C. Cohen, D. G. Lewallen, and A. J. van Wijnen. 2016. 'Multi-disciplinary antimicrobial strategies for improving orthopaedic implants to prevent prosthetic joint infections in hip and knee', *J Orthop Res*, 34: 177-86.

Giebaly, Dia Eldean, Haider Twaij, Mazin Ibrahim, and Fares S. Haddad. 2016. 'Cementless Hip Implants: An Expanding Choice', *HIP International*, 26: 413-23.
Gil-Tomás, Jesús, Sarah Tubby, Ivan P. Parkin, Naima Narband, Linda Dekker, Sean P. Nair, Michael Wilson, and Cale Street. 2007. 'Lethal photosensitisation of Staphylococcus aureus using a toluidine blue O–tiopronin–gold nanoparticle conjugate', *Journal of Materials Chemistry*, 17: 3739-46.
Glue, C., J. B. Hansen, P. Schjerling, T. Jinquan, and L. K. Poulsen. 2002. 'LPS-induced cytokine production in the monocytic cell line THP-1 determined by multiple quantitative competitive PCR (QC-PCR)', *Scand J Clin Lab Invest*, 62: 405-12.
Goldie, Ian, and Alf Nachemson. 1970. 'Synovial pH in Rheumatoid Knee Joints: II. The Effect of Local Corticosteroid Treatment', *Acta Orthopaedica Scandinavica*, 41: 354-62.
Goldring, S. R., A. L. Schiller, M. Roelke, C. M. Rourke, D. A. O'Neil, and W. H. Harris. 1983. 'The synovial-like membrane at the bone-cement interface in loose total hip replacements and its proposed role in bone lysis', *J Bone Joint Surg Am*, 65: 575-84.
Gong, He, Wei Wu, Juan Fang, Xin Dong, Meisheng Zhao, and Tongtong Guo. 2012. 'Effects of Materials of Cementless Femoral Stem on the Functional Adaptation of Bone', *Journal of Bionic Engineering*, 9: 66-74.
Goodman, Stuart B., Zhenyu Yao, Michael Keeney, and Fan Yang. 2013. 'The future of biologic coatings for orthopaedic implants', *Biomaterials*, 34: 3174-83.
Goriainov, Vitali, R. B. Cook, Jeremy Latham, Doug Dunlop, and Richard Oreffo. 2014. *Bone and Metal - an Orthopaedic Perspective on Osseointegration of Metals*.
Gosens, I., J. A. Post, L. J. de la Fonteyne, E. H. Jansen, J. W. Geus, F. R. Cassee, and W. H. de Jong. 2010. 'Impact of agglomeration state of nano- and submicron sized gold particles on pulmonary inflammation', *Part Fibre Toxicol*, 7: 37.
Grech, Jessica M.R., Joao F. Mano, and Rui L. Reis. 2008. 'Chitosan Beads as Templates for Layer-by-Layer Assembly and their Application in the Sustained Release of Bioactive Agents', *Journal of Bioactive and Compatible Polymers*, 23: 367-80.
Green, T. R., J. Fisher, M. Stone, B. M. Wroblewski, and E. Ingham. 1998. 'Polyethylene particles of a 'critical size' are necessary for the induction of cytokines by macrophages in vitro', *Biomaterials*, 19: 2297-302.
Greenfield, E. M., Y. Bi, A. A. Ragab, V. M. Goldberg, and R. R. Van De Motter. 2002. 'The role of osteoclast differentiation in aseptic loosening', *J Orthop Res*, 20: 1-8.
Hall-Stoodley, L., and P. Stoodley. 2005. 'Biofilm formation and dispersal and the transmission of human pathogens', *Trends Microbiol*, 13: 7-10.
Hammond, Paula T. 2012. 'Building biomedical materials layer-by-layer', *Materials Today*, 15: 196-206.
Harris, Andrew, Joey Johnson, P. Kaveh Mansuripur, and Richard Limbird. 2015. 'Cobalt toxicity after revision to a metal-on-polyethylene total hip arthroplasty for fracture of ceramic acetabular component', *Arthroplasty Today*, 1: 89-91.
Hartmann, E. S., M. I. Kohler, F. Huber, J. I. Redeker, B. Schmitt, M. Schmitt-Sody, B. Summer, A. Fottner, V. Jansson, and S. Mayer-Wagner. 2017. 'Factors regulating bone remodeling processes in aseptic implant loosening', *J Orthop Res*, 35: 248-57.
Havelin, Leif, Birgitte Espehaug, and L. B Engesaeter. 2002. The performance of two hydroxyapatite-coated acetabular cups compared with Charnley cups. From the Norwegian Arthroplasty Register.
Hedia, H. S. 2007. 'Effect of coating thickness and its material on the stress distribution for dental implants', *Journal of Medical Engineering & Technology*, 31: 280-87.

Hernigou, Philippe, François Roubineau, Charlie Bouthors, and Charles-Henri Flouzat-Lachaniette. 2016. 'What every surgeon should know about Ceramic-on-Ceramic bearings in young patients', *EFORT open reviews*, 1: 107-11.
Hibbard, J. S. 2005. 'Analyses comparing the antimicrobial activity and safety of current antiseptic agents: a review', *J Infus Nurs*, 28: 194-207.
Hickey, T., D. Kreutzer, D. J. Burgess, and F. Moussy. 2002. 'Dexamethasone/PLGA microspheres for continuous delivery of an anti-inflammatory drug for implantable medical devices', *Biomaterials*, 23: 1649-56.
Hickok, N. J., and I. M. Shapiro. 2012. 'Immobilized antibiotics to prevent orthopaedic implant infections', *Adv Drug Deliv Rev*, 64: 1165-76.
Holmberg, Kyle V., Mahsa Abdolhosseini, Yuping Li, Xi Chen, Sven-Ulrik Gorr, and Conrado Aparicio. 2013. 'Bio-inspired stable antimicrobial peptide coatings for dental applications', *Acta Biomater*, 9: 8224-31.
Hooper, Gary. 2013. The ageing population and the increasing demand for joint replacement.
Howarter, John A., and Jeffrey P. Youngblood. 2008. 'Self-Cleaning and Next Generation Anti-Fog Surfaces and Coatings', *Macromolecular Rapid Communications*, 29: 455-66.
Hsieh, P. H., M. S. Lee, K. Y. Hsu, Y. H. Chang, H. N. Shih, and S. W. Ueng. 2009. 'Gram-negative prosthetic joint infections: risk factors and outcome of treatment', *Clin Infect Dis*, 49: 1036-43.
Hsu, Bryan B., Samantha R. Hagerman, Kelsey Jamieson, Jovana Veselinovic, Nicholas O'Neill, Eggehard Holler, Julia Y. Ljubimova, and Paula T. Hammond. 2014. 'Multilayer Films Assembled from Naturally-Derived Materials for Controlled Protein Release', *Biomacromolecules*, 15: 2049-57.
Hsu, Bryan B., Myoung-Hwan Park, Samantha R. Hagerman, and Paula T. Hammond. 2014. 'Multimonth controlled small molecule release from biodegradable thin films', *Proceedings of the National Academy of Sciences of the United States of America*, 111: 12175-80.
Hu, H., W. Zhang, Y. Qiao, X. Jiang, X. Liu, and C. Ding. 2012. 'Antibacterial activity and increased bone marrow stem cell functions of Zn-incorporated TiO2 coatings on titanium', *Acta Biomater*, 8: 904-15.
Hu, X., K. G. Neoh, Z. Shi, E. T. Kang, C. Poh, and W. Wang. 2010. 'An in vitro assessment of titanium functionalized with polysaccharides conjugated with vascular endothelial growth factor for enhanced osseointegration and inhibition of bacterial adhesion', *Biomaterials*, 31: 8854-63.
Ikeuchi, M., Y. Kamimoto, M. Izumi, K. Fukunaga, K. Aso, N. Sugimura, M. Yokoyama, and T. Tani. 2014. 'Effects of dexamethasone on local infiltration analgesia in total knee arthroplasty: a randomized controlled trial', *Knee Surg Sports Traumatol Arthrosc*, 22: 1638-43.
Ikeuchi, M., Y. Kamimoto, M. Izumi, N. Sugimura, M. Takemura, K. Fukunaga, M. Yokoyama, and T. Tani. 2013. 'Local infusion analgesia using intra-articular double lumen catheter after total knee arthroplasty: a double blinded randomized control study', *Knee Surg Sports Traumatol Arthrosc*, 21: 2680-4.
Inacio, M. C. S., E. W. Paxton, S. E. Graves, R. S. Namba, and S. Nemes. 2017. 'Projected increase in total knee arthroplasty in the United States - an alternative projection model', *Osteoarthritis Cartilage*, 25: 1797-803.
Inacio, Maria C. S., Stephen E. Graves, Nicole L. Pratt, Elizabeth E. Roughead, and Szilard Nemes. 2017. 'Increase in Total Joint Arthroplasty Projected from 2014 to 2046 in Australia: A Conservative Local Model With International Implications', *Clin Orthop Relat Res*, 475: 2130-37.
Israël, Alain. 2010. 'The IKK complex, a central regulator of NF-kappaB activation', *Cold Spring Harb Perspect Biol*, 2: a000158-a58.
J., Webb J. C., and Spencer R. F. 2007. 'The role of polymethylmethacrylate bone cement in modern orthopaedic surgery', *J Bone Joint Surg Br*, 89-B: 851-57.

Jasty, M., C. Bragdon, D. Burke, D. O'Connor, J. Lowenstein, and W. H. Harris. 1997. 'In vivo skeletal responses to porous-surfaced implants subjected to small induced motions', *J Bone Joint Surg Am*, 79: 707-14.

Jayasuriya, Raveen L., Simon C. Buckley, Andrew J. Hamer, Robert M. Kerry, Ian Stockley, Mohamed W. Tomouk, and Jeremy Mark Wilkinson. 2013. 'Effect of Sliding-Taper Compared with Composite-Beam Cemented Femoral Prosthesis Loading Regime on Proximal Femoral Bone Remodeling: A Randomized Clinical Trial', *JBJS*, 95: 19-27.

Jin, G., H. Cao, Y. Qiao, F. Meng, H. Zhu, and X. Liu. 2014. 'Osteogenic activity and antibacterial effect of zinc ion implanted titanium', *Colloids Surf B Biointerfaces*, 117: 158-65.

Jiranek, W. A., M. Machado, M. Jasty, D. Jevsevar, H. J. Wolfe, S. R. Goldring, M. J. Goldberg, and W. H. Harris. 1993. 'Production of cytokines around loosened cemented acetabular components. Analysis with immunohistochemical techniques and in situ hybridization', *J Bone Joint Surg Am*, 75: 863-79.

Johnson, G.R. 2014. 'Developments in joint replacement technology.' in P. A. Revell (ed.), *Joint Replacement Technology* (Woodhead Publishing).

Kallala, R. F., I. S. Vanhegan, M. S. Ibrahim, S. Sarmah, and F. S. Haddad. 2015. 'Financial analysis of revision knee surgery based on NHS tariffs and hospital costs: does it pay to provide a revision service?', *Bone Joint J*, 97-b: 197-201.

Kazemzadeh-Narbat, Mehdi, Benjamin Lai, Chuanfan Ding, Jayachandran Kizhakkedathu, Robert E.W. Hancock, and Rizhi Wang. 2013. Multilayered coating on titanium for controlled release of antimicrobial peptides for the prevention of implant-associated infections.

Kazemzadeh-Narbat, Mehdi, Shahryar Noordin, Bassam Masri, Donald Garbuz, Clive P Duncan, Robert E W Hancock, and Rizhi Wang. 2012. *Drug release and bone growth studies of antimicrobial peptide-loaded calcium phosphate coating on titanium*.

Kearns, Kenneth A., Dan Witmer, Junaid Makda, Javad Parvizi, and Donald Jungkind. 2011. 'Sterility of the personal protection system in total joint arthroplasty', *Clin Orthop Relat Res*, 469: 3065-69.

Keravala, Annahita, Eric R. Lechman, Joan Nash, Zhibao Mi, and Paul D. Robbins. 2006. 'Human, viral or mutant human IL-10 expressed after local adenovirus-mediated gene transfer are equally effective in ameliorating disease pathology in a rabbit knee model of antigen-induced arthritis', *Arthritis research & therapy*, 8: R91-R91.

Khanuja, H. S., J. J. Vakil, M. S. Goddard, and M. A. Mont. 2011. 'Cementless femoral fixation in total hip arthroplasty', *J Bone Joint Surg Am*, 93: 500-9.

Kim, Inje, Hyun Ah Kim, Young-Il Seo, Yeong Wook Song, Jin-Young Jeong, and Dong Hyun Kim. 2010. 'The prevalence of knee osteoarthritis in elderly community residents in Korea', *Journal of Korean medical science*, 25: 293-98.

Kinnari, Teemu J., Jaime Esteban, Nieves Z. Martin-de-Hijas, Orlando Sánchez-Muñoz, Sandra Sánchez-Salcedo, Montserrat Colilla, María Vallet-Regí, and Enrique Gomez-Barrena. 2009. 'Influence of surface porosity and pH on bacterial adherence to hydroxyapatite and biphasic calcium phosphate bioceramics', *Journal of Medical Microbiology*, 58: 132-37.

Klose, D., F. Siepmann, K. Elkharraz, and J. Siepmann. 2008. 'PLGA-based drug delivery systems: Importance of the type of drug and device geometry', *Int J Pharm*, 354: 95-103.

Kobayashi, K., N. Takahashi, E. Jimi, N. Udagawa, M. Takami, S. Kotake, N. Nakagawa, M. Kinosaki, K. Yamaguchi, N. Shima, H. Yasuda, T. Morinaga, K. Higashio, T. J. Martin, and T. Suda. 2000. 'Tumor necrosis factor alpha stimulates osteoclast differentiation by a mechanism independent of the ODF/RANKL-RANK interaction', *J Exp Med*, 191: 275-86.

Kong, Y. Y., H. Yoshida, I. Sarosi, H. L. Tan, E. Timms, C. Capparelli, S. Morony, A. J. Oliveira-dos-Santos, G. Van, A. Itie, W. Khoo, A. Wakeham, C. R. Dunstan, D. L. Lacey, T. W. Mak, W. J. Boyle, and J. M. Penninger. 1999. 'OPGL is a key regulator of osteoclastogenesis, lymphocyte development and lymph-node organogenesis', *Nature*, 397: 315-23.

Kretzer, Jan Philippe, Joern Reinders, Robert Sonntag, Sebastien Hagmann, Marcus Streit, Sebastian Jeager, and Babak Moradi. 2014. 'Wear in total knee arthroplasty--just a question of polyethylene?: Metal ion release in total knee arthroplasty', *International orthopaedics*, 38: 335-40.

Kuehl, Richard, Priscilla S. Brunetto, Anne-Kathrin Woischnig, Massimo Varisco, Zarko Rajacic, Juerg Vosbeck, Luigi Terracciano, Katharina M. Fromm, and Nina Khanna. 2016. 'Preventing Implant-Associated Infections by Silver Coating', *Antimicrob Agents Chemother*, 60: 2467-75.

Kunčická, Lenka, Radim Kocich, and Terry C. Lowe. 2017. 'Advances in metals and alloys for joint replacement', *Progress in Materials Science*, 88: 232-80.

Kurtz, S. M., E. Lau, K. Ong, K. Zhao, M. Kelly, and K. J. Bozic. 2009. 'Future young patient demand for primary and revision joint replacement: national projections from 2010 to 2030', *Clin Orthop Relat Res*, 467: 2606-12.

Kurtz, S., K. Ong, E. Lau, F. Mowat, and M. Halpern. 2007. 'Projections of primary and revision hip and knee arthroplasty in the United States from 2005 to 2030', *J Bone Joint Surg Am*, 89: 780-5.

Lam, J., S. Takeshita, J. E. Barker, O. Kanagawa, F. P. Ross, and S. L. Teitelbaum. 2000. 'TNF-alpha induces osteoclastogenesis by direct stimulation of macrophages exposed to permissive levels of RANK ligand', *J Clin Invest*, 106: 1481-8.

Lamagni, Theresa. 2014. 'Epidemiology and burden of prosthetic joint infections', *Journal of Antimicrobial Chemotherapy*, 69: i5-i10.

Landgraeber, Stefan, #xe4, Marcus ger, Joshua J. Jacobs, and Nadim James Hallab. 2014. 'The Pathology of Orthopedic Implant Failure Is Mediated by Innate Immune System Cytokines', *Mediators of Inflammation*, 2014: 9.

Lavernia, C., D. J. Lee, and V. H. Hernandez. 2006. 'The increasing financial burden of knee revision surgery in the United States', *Clin Orthop Relat Res*, 446: 221-6.

Lechman, E. R., D. Jaffurs, S. C. Ghivizzani, A. Gambotto, I. Kovesdi, Z. Mi, C. H. Evans, and P. D. Robbins. 1999. 'Direct adenoviral gene transfer of viral IL-10 to rabbit knees with experimental arthritis ameliorates disease in both injected and contralateral control knees', *J Immunol*, 163: 2202-8.

Lee, D. W., Y. P. Yun, K. Park, and S. E. Kim. 2012. 'Gentamicin and bone morphogenic protein-2 (BMP-2)-delivering heparinized-titanium implant with enhanced antibacterial activity and osteointegration', *Bone*, 50: 974-82.

Lee, K. Y., and D. J. Mooney. 2012. 'Alginate: properties and biomedical applications', *Prog Polym Sci*, 37: 106-26.

Lenguerrand, E., M. R. Whitehouse, A. D. Beswick, A. D. Toms, M. L. Porter, and A. W. Blom. 2017. 'Description of the rates, trends and surgical burden associated with revision for prosthetic joint infection following primary and revision knee replacements in England and Wales: an analysis of the National Joint Registry for England, Wales, Northern Ireland and the Isle of Man', *BMJ Open*, 7: e014056.

Li, Cheng, Nora Renz, and Andrej Trampuz. 2018. 'Management of Periprosthetic Joint Infection', *Hip Pelvis*, 30: 138-46.

Li, D., G. Guo, R. Fan, J. Liang, X. Deng, F. Luo, and Z. Qian. 2013. 'PLA/F68/dexamethasone implants prepared by hot-melt extrusion for controlled release of anti-inflammatory drug to implantable medical devices: I. Preparation, characterization and hydrolytic degradation study', *Int J Pharm*, 441: 365-72.

Li, J., G. Wang, D. Wang, Q. Wu, X. Jiang, and X. Liu. 2014. 'Alkali-treated titanium selectively regulating biological behaviors of bacteria, cancer cells and mesenchymal stem cells', *J Colloid Interface Sci*, 436: 160-70.
Li, Weijia, Jing Zhou, and Yuyin Xu. 2015. 'Study of the in vitro cytotoxicity testing of medical devices', *Biomedical reports*, 3: 617-20.
Lim, K. S., and P. C. Kam. 2008. 'Chlorhexidine--pharmacology and clinical applications', *Anaesth Intensive Care*, 36: 502-12.
Lin, T. H., J. Pajarinen, L. Lu, A. Nabeshima, L. A. Cordova, Z. Yao, and S. B. Goodman. 2017. 'NF-kappaB as a Therapeutic Target in Inflammatory-Associated Bone Diseases', *Adv Protein Chem Struct Biol*, 107: 117-54.
Liu, Dan-Qing, Li-Min Li, Ya-Lan Guo, Rui Bai, Chen Wang, Zhen Bian, Chen-Yu Zhang, and Ke Zen. 2008. 'Signal Regulatory Protein α Negatively Regulates β2 Integrin-Mediated Monocyte Adhesion, Transendothelial Migration and Phagocytosis', *PLOS ONE*, 3: e3291.
López-López, José A, Rachel L Humphriss, Andrew D Beswick, Howard H Z Thom, Linda P Hunt, Amanda Burston, Christopher G Fawsitt, William Hollingworth, Julian P T Higgins, Nicky J Welton, Ashley W Blom, and Elsa M R Marques. 2017. 'Choice of implant combinations in total hip replacement: systematic review and network meta-analysis', *BMJ*, 359: j4651.
Luan, X., Q. Lu, Y. Jiang, S. Zhang, Q. Wang, H. Yuan, W. Zhao, J. Wang, and X. Wang. 2012. 'Crystal structure of human RANKL complexed with its decoy receptor osteoprotegerin', *J Immunol*, 189: 245-52.
Luo, Gang, Fangfei Li, Xiaoming Li, Zheng-Guo Wang, and Bo Zhang. 2018. 'TNF-α and RANKL promote osteoclastogenesis by upregulating RANK via the NF-κB pathway', *Molecular medicine reports*, 17: 6605-11.
Macdonald, M. L., R. E. Samuel, N. J. Shah, R. F. Padera, Y. M. Beben, and P. T. Hammond. 2011. 'Tissue integration of growth factor-eluting layer-by-layer polyelectrolyte multilayer coated implants', *Biomaterials*, 32: 1446-53.
Madigan, Michael, and John Martinko. 1997. *Brock Biology of Micro-Organisms*.
Maggs, Joanna, and Matthew Wilson. 2017. 'The Relative Merits of Cemented and Uncemented Prostheses in Total Hip Arthroplasty', *Indian journal of orthopaedics*, 51: 377-85.
Mai, Thanh Binh, Thi Nga Tran, Md. Rafiqul Islam, Jong Myung Park, and Kwon Taek Lim. 2014. 'Covalent functionalization of silica nanoparticles with poly(N-isopropylacrylamide) employing thiol-ene chemistry and activator regenerated by electron transfer ATRP protocol', *Journal of Materials Science*, 49: 1519-26.
Makino, Takahiro, Takashi Kaito, Yusuke Sakai, Shota Takenaka, and Hideki Yoshikawa. 2018. 'Computed tomography color mapping for evaluation of bone ongrowth on the surface of a titanium-coated polyetheretherketone cage in vivo: A pilot study', *Medicine*, 97: e12379-e79.
Mansell, J. P., J. Brown, J. G. Knapp, C. F. Faul, and A. W. Blom. 2012. 'Lysophosphatidic acid-functionalised titanium as a superior surface for supporting human osteoblast (MG63) maturation', *Eur Cell Mater*, 23: 348-61.
Martín-Sabroso, Cristina, Daniel Filipe Tavares-Fernandes, Juan Ignacio Espada-García, and Ana Isabel Torres-Suárez. 2013. 'Validation protocol of analytical procedures for quantification of drugs in polymeric systems for parenteral administration: Dexamethasone phosphate disodium microparticles', *Int J Pharm*, 458: 188-96.
Martin, John R., Luke Spencer-Gardner, Christopher L. Camp, John M. Stulak, and Rafael J. Sierra. 2015. 'Cardiac cobaltism: a rare complication after bilateral metal-on-metal total hip arthroplasty', *Arthroplasty Today*, 1: 99-102.
Martinez-Pastor, J. C., E. Munoz-Mahamud, F. Vilchez, S. Garcia-Ramiro, G. Bori, J. Sierra, J. A. Martinez, L. Font, J. Mensa, and A. Soriano. 2009. 'Outcome of acute prosthetic joint infections due to gram-negative bacilli treated with open

debridement and retention of the prosthesis', *Antimicrob Agents Chemother*, 53: 4772-7.
Masse, A., A. Bruno, M. Bosetti, A. Biasibetti, M. Cannas, and P. Gallinaro. 2000. 'Prevention of pin track infection in external fixation with silver coated pins: clinical and microbiological results', *J Biomed Mater Res*, 53: 600-4.
Matharu, Gulraj S., Antti Eskelinen, Andrew Judge, Hemant G. Pandit, and David W. Murray. 2018. 'Revision surgery of metal-on-metal hip arthroplasties for adverse reactions to metal debris', *Acta Orthopaedica*, 89: 278-88.
Matsuno, H., A. Yokoyama, F. Watari, M. Uo, and T. Kawasaki. 2001. 'Biocompatibility and osteogenesis of refractory metal implants, titanium, hafnium, niobium, tantalum and rhenium', *Biomaterials*, 22: 1253-62.
Mattioli-Belmonte, M., S. Cometa, C. Ferretti, R. Iatta, A. Trapani, E. Ceci, M. Falconi, and E. De Giglio. 2014. 'Characterization and cytocompatibility of an antibiotic/chitosan/cyclodextrins nanocoating on titanium implants', *Carbohydr Polym*, 110: 173-82.
McDonnell, G., and A. D. Russell. 1999. 'Antiseptics and disinfectants: activity, action, and resistance', *Clin Microbiol Rev*, 12: 147-79.
McPherson, Edward J., Chris Woodson, Paul Holtom, Nikolaos Roidis, Chrissandra Shufelt, and Michael Patzakis. 2002. 'Periprosthetic Total Hip Infection: Outcomes Using a Staging System', *Clinical Orthopaedics and Related Research (1976-2007)*, 403: 8-15.
Merollini, K. M., R. W. Crawford, and N. Graves. 2013. 'Surgical treatment approaches and reimbursement costs of surgical site infections post hip arthroplasty in Australia: a retrospective analysis', *BMC Health Serv Res*, 13: 91.
Mikulewicz, Marcin, and Katarzyna Chojnacka. 2011. 'Cytocompatibility of Medical Biomaterials Containing Nickel by Osteoblasts: a Systematic Literature Review', *Biological Trace Element Research*, 142: 865-89.
Miller, Robert E., Daniel Branstetter, Allison Armstrong, Bryan Kennedy, Jon Jones, Laine Cowan, Jeanine Bussiere, and William C. Dougall. 2007. 'Receptor Activator of NF-κB Ligand Inhibition Suppresses Bone Resorption and Hypercalcemia but Does Not Affect Host Immune Responses to Influenza Infection', *The Journal of Immunology*, 179: 266-74.
Milstone, A. M., C. L. Passaretti, and T. M. Perl. 2008. 'Chlorhexidine: expanding the armamentarium for infection control and prevention', *Clin Infect Dis*, 46: 274-81.
Molina-Manso, D., G. del Prado, A. Ortiz-Perez, M. Manrubia-Cobo, E. Gomez-Barrena, J. Cordero-Ampuero, and J. Esteban. 2012. 'In vitro susceptibility of Staphylococcus aureus and Staphylococcus epidermidis isolated from prosthetic joint infections', *J Antibiot (Tokyo)*, 65: 505-8.
Moreira-Tabaka, Helena, Jean Peluso, Jean-Luc Vonesch, Didier Hentsch, Pascal Kessler, Jean-Marie Reimund, Serge Dumont, and Christian D. Muller. 2012. 'Unlike for Human Monocytes after LPS Activation, Release of TNF-α by THP-1 Cells Is Produced by a TACE Catalytically Different from Constitutive TACE', *PLOS ONE*, 7: e34184.
Moskal, Joseph T., Susan G. Capps, and John A. Scanelli. 2016. 'Still no single gold standard for using cementless femoral stems routinely in total hip arthroplasty', *Arthroplasty Today*, 2: 211-18.
Mosmann, Tim. 1983. 'Rapid colorimetric assay for cellular growth and survival: Application to proliferation and cytotoxicity assays', *Journal of Immunological Methods*, 65: 55-63.
Munita, Jose M., and Cesar A. Arias. 2016. 'Mechanisms of Antibiotic Resistance', *Microbiology spectrum*, 4: 10.1128/microbiolspec.VMBF-0016-2015.
Muszanska, Agnieszka K., M. Reza Nejadnik, Yun Chen, Edwin R. van den Heuvel, Henk J. Busscher, Henny C. van der Mei, and Willem Norde. 2012. 'Bacterial

Adhesion Forces with Substratum Surfaces and the Susceptibility of Biofilms to Antibiotics', *Antimicrob Agents Chemother*, 56: 4961-64.
Naiyer, M. M., S. Saha, V. Hemke, S. Roy, S. Singh, K. V. Musti, and B. Saha. 2013. 'Identification and characterization of a human IL-10 receptor antagonist', *Hum Immunol*, 74: 28-31.
Nam, D., R. L. Barrack, and H. G. Potter. 2014. 'What are the advantages and disadvantages of imaging modalities to diagnose wear-related corrosion problems?', *Clin Orthop Relat Res*, 472: 3665-73.
National Joint Registry. 2017. "UK National joint registry 14th annual report." In.
———. 2018. "UK National joint registry 15th annual report." In.
Neut, D., R. J. Dijkstra, J. I. Thompson, H. C. van der Mei, and H. J. Busscher. 2011. 'Antibacterial efficacy of a new gentamicin-coating for cementless prostheses compared to gentamicin-loaded bone cement', *J Orthop Res*, 29: 1654-61.
NICE. 2015. 'Antimicrobial stewardship: systems and processes for effective antimicrobial medicine use. NG15'.
Nita, L. E., A. Chiriac, M. Bercea, and B. A. Wolf. 2013. 'Synergistic behavior of poly(aspartic acid) and Pluronic F127 in aqueous solution as studied by viscometry and dynamic light scattering', *Colloids Surf B Biointerfaces*, 103: 544-9.
Oeckinghaus, A., and S. Ghosh. 2009. 'The NF-kappaB family of transcription factors and its regulation', *Cold Spring Harb Perspect Biol*, 1: a000034.
Oosterbos, C. J. M., H. Ch. Vogely, M. W. Nijhof, A. Fleer, A. J. Verbout, A. J. Tonino, and W. J. A. Dhert. 2002. 'Osseointegration of hydroxyapatite-coated and noncoated Ti6Al4V implants in the presence of local infection: A comparative histomorphometrical study in rabbits', *J Biomed Mater Res*, 60: 339-47.
Oosterwaal, P. J., F. H. Mikx, M. E. van den Brink, and H. H. Renggli. 1989. 'Bactericidal concentrations of chlorhexidine-digluconate, amine fluoride gel and stannous fluoride gel for subgingival bacteria tested in serum at short contact times', *J Periodontal Res*, 24: 155-60.
Ordikhani, Farideh, Marzieh Ramezani Farani, Mehdi Dehghani, Elnaz Tamjid, and A. Simchi. 2015. Physicochemical and biological properties of electrodeposited graphene oxide/chitosan films with drug-eluting capacity.
P., Mihok, Hassaballa M., Robinson J., Porteous A., Bowker K., Lovering A., and Murray J. 2014. 'Antimicrobial properties of local anaesthetic bupivacaine in combination with gentamicin', *Orthopaedic Proceedings*, 96-B: 2-2.
Papadimitriou, S., and D. Bikiaris. 2009. 'Novel self-assembled core-shell nanoparticles based on crystalline amorphous moieties of aliphatic copolyesters for efficient controlled drug release', *J Control Release*, 138: 177-84.
Parvizi, J., N. Shohat, and T. Gehrke. 2017. 'Prevention of periprosthetic joint infection: new guidelines', *Bone Joint J*, 99-b: 3-10.
Patel, A., G. Pavlou, R. E. Mujica-Mota, and A. D. Toms. 2015. 'The epidemiology of revision total knee and hip arthroplasty in England and Wales: a comparative analysis with projections for the United States. A study using the National Joint Registry dataset', *Bone Joint J*, 97-b: 1076-81.
Penner M.J., Almousa S.A., and Kolla L. *Aseptic Loosening*, .
Perni, Stefano, and Polina Prokopovich. 2017. 'Poly-beta-amino-esters nano-vehicles based drug delivery system for cartilage', *Nanomedicine : nanotechnology, biology, and medicine*, 13: 539-48.
Pijls, B. G., J. M. Meessen, J. W. Schoones, M. Fiocco, H. J. van der Heide, A. Sedrakyan, and R. G. Nelissen. 2016. 'Increased Mortality in Metal-on-Metal versus Non-Metal-on-Metal Primary Total Hip Arthroplasty at 10 Years and Longer Follow-Up: A Systematic Review and Meta-Analysis', *PLOS ONE*, 11: e0156051.

Pilliar, R. M., J. M. Lee, and C. Maniatopoulos. 1986. 'Observations on the effect of movement on bone ingrowth into porous-surfaced implants', *Clin Orthop Relat Res*: 108-13.
Popat, K. C., M. Eltgroth, T. J. Latempa, C. A. Grimes, and T. A. Desai. 2007. 'Decreased Staphylococcus epidermis adhesion and increased osteoblast functionality on antibiotic-loaded titania nanotubes', *Biomaterials*, 28: 4880-8.
Postler, Anne, Cornelia Lützner, Franziska Beyer, Eric Tille, and Jörg Lützner. 2018. 'Analysis of Total Knee Arthroplasty revision causes', *BMC Musculoskeletal Disorders*, 19: 55.
Prieto-Alhambra, D., A. Judge, M. K. Javaid, C. Cooper, A. Diez-Perez, and N. K. Arden. 2014. 'Incidence and risk factors for clinically diagnosed knee, hip and hand osteoarthritis: influences of age, gender and osteoarthritis affecting other joints', *Ann Rheum Dis*, 73: 1659-64.
Prudhon, Jean-Louis, and Régis Verdier. 2017. 'Cemented or cementless total knee arthroplasty? - Comparative results of 200 cases at a minimum follow-up of 11 years', *SICOT-J*, 3: 70-70.
Qasim, Sultan Naseer, Andrew Swann, and Robert Ashford. 2017. 'The DAIR (debridement, antibiotics and implant retention) procedure for infected total knee replacement - a literature review', *SICOT-J*, 3: 2-2.
Qin, Z. 2012. 'The use of THP-1 cells as a model for mimicking the function and regulation of monocytes and macrophages in the vasculature', *Atherosclerosis*, 221: 2-11.
Ramasamy, T., Z. S. Haidar, T. H. Tran, J. Y. Choi, J. H. Jeong, B. S. Shin, H. G. Choi, C. S. Yong, and J. O. Kim. 2014. 'Layer-by-layer assembly of liposomal nanoparticles with PEGylated polyelectrolytes enhances systemic delivery of multiple anticancer drugs', *Acta Biomater*, 10: 5116-27.
Rammelt, Stefan, Till Illert, Susanne Bierbaum, Dieter Scharnweber, Hans Zwipp, and Wolfgang Schneiders. 2006. *Coating of titanium implants with collagen, RGD peptide and chondroitin sulfate*.
Randau, Thomas M., Max J. Friedrich, Matthias D. Wimmer, Ben Reichert, Dominik Kuberra, Birgit Stoffel-Wagner, Andreas Limmer, Dieter C. Wirtz, and Sascha Gravius. 2014. 'Interleukin-6 in serum and in synovial fluid enhances the differentiation between periprosthetic joint infection and aseptic loosening', *PLOS ONE*, 9: e89045-e45.
Raphel, J., M. Holodniy, S. B. Goodman, and S. C. Heilshorn. 2016. 'Multifunctional coatings to simultaneously promote osseointegration and prevent infection of orthopaedic implants', *Biomaterials*, 84: 301-14.
Ravi, S., M. Zhu, C. Luey, and S. W. Young. 2016. 'Antibiotic resistance in early periprosthetic joint infection', *ANZ J Surg*, 86: 1014-18.
Reish, T. G., H. D. Clarke, G. R. Scuderi, K. R. Math, and W. N. Scott. 2006. 'Use of multi-detector computed tomography for the detection of periprosthetic osteolysis in total knee arthroplasty', *J Knee Surg*, 19: 259-64.
Ren, K., A. Dusad, F. Yuan, H. Yuan, P. E. Purdue, E. V. Fehringer, K. L. Garvin, S. R. Goldring, and D. Wang. 2014. 'Macromolecular prodrug of dexamethasone prevents particle-induced peri-implant osteolysis with reduced systemic side effects', *J Control Release*, 175: 1-9.
Ren, Ke, Anand Dusad, Yijia Zhang, and Dong Wang. 2013. 'Therapeutic intervention for wear debris-induced aseptic implant loosening', *Acta Pharmaceutica Sinica B*, 3: 76-85.
Ribeiro, M., F. J. Monteiro, and M. P. Ferraz. 2012. 'Infection of orthopedic implants with emphasis on bacterial adhesion process and techniques used in studying bacterial-material interactions', *Biomatter*, 2: 176-94.
Riool, M., A. J. Dirks, V. Jaspers, L. de Boer, T. J. Loontjens, C. M. van der Loos, S. Florquin, I. Apachitei, L. N. Rijk, H. A. Keul, and S. A. Zaat. 2017. 'A chlorhexidine-releasing epoxy-based coating on titanium implants prevents

Staphylococcus aureus experimental biomaterial-associated infection', *Eur Cell Mater*, 33: 143-57.
Riool, Martijn, Anna de Breij, Leonie de Boer, Paulus H. S. Kwakman, Robert A. Cordfunke, Or Cohen, Nermina Malanovic, Noam Emanuel, Karl Lohner, Jan W. Drijfhout, Peter H. Nibbering, and Sebastian A. J. Zaat. 2017. 'Controlled Release of LL-37-Derived Synthetic Antimicrobial and Anti-Biofilm Peptides SAAP-145 and SAAP-276 Prevents Experimental Biomaterial-Associated Staphylococcus aureus Infection', *Advanced Functional Materials*, 27: 1606623.
Romanò, Carlo L, Giovanni Manzi, Nicola Logoluso, and Delia Romanò. 2012. 'Value of Debridement and Irrigation for the Treatment of Peri-Prosthetic Infections. A Systematic Review', *HIP International*, 22: 19-24.
Rozkydal, Z., P. Janik, P. Janicek, and R. Kunovsky. 2007. '[Revision knee arthroplasty due to aseptic loosening]', *Acta Chir Orthop Traumatol Cech*, 74: 5-13.
Salton, M.R.J., and K.S. Kim. 1996. 'Structure.' in S. Baron (ed.), *Medical Microbiology* (The University of Texas Medical Branch at Galveston.: Galveston (TX)).
Santavirta, S., Y. T. Konttinen, R. Lappalainen, A. Anttila, S. B. Goodman, M. Lind, L. Smith, M. Takagi, E. Gómez-Barrena, L. Nordsletten, and J. W. Xu. 1998. 'Materials in total joint replacement', *Current Orthopaedics*, 12: 51-57.
Sato, Katsuhiko, Takuto Shiba, and Jun-ichi Anzai. 2013. Ion Permeability of Free-Suspended Layer-by-Layer (LbL) Films Prepared Using an Alginate Scaffold.
Scanzello, C. R., M. P. Figgie, B. J. Nestor, and S. M. Goodman. 2006. 'Perioperative management of medications used in the treatment of rheumatoid arthritis', *Hss j*, 2: 141-7.
Schaer, T. P., S. Stewart, B. B. Hsu, and A. M. Klibanov. 2012. 'Hydrophobic polycationic coatings that inhibit biofilms and support bone healing during infection', *Biomaterials*, 33: 1245-54.
Schlett, Carey D., Eugene V. Millar, Katrina B. Crawford, Tianyuan Cui, Jeffrey B. Lanier, David R. Tribble, and Michael W. Ellis. 2014. 'Prevalence of chlorhexidine-resistant methicillin-resistant Staphylococcus aureus following prolonged exposure', *Antimicrob Agents Chemother*, 58: 4404-10.
Schmalzried, T. P., M. Jasty, and W. H. Harris. 1992. 'Periprosthetic bone loss in total hip arthroplasty. Polyethylene wear debris and the concept of the effective joint space', *J Bone Joint Surg Am*, 74: 849-63.
Schwarz, E. M., R. J. Looney, and R. J. O'Keefe. 2000. 'Anti-TNF-alpha therapy as a clinical intervention for periprosthetic osteolysis', *Arthritis research*, 2: 165-68.
Shah, Nisarg J., Md. Nasim Hyder, Joshua S. Moskowitz, Mohiuddin A. Quadir, Stephen W. Morton, Howard J. Seeherman, Robert F. Padera, Myron Spector, and Paula T. Hammond. 2013. 'Surface-Mediated Bone Tissue Morphogenesis from Tunable Nanolayered Implant Coatings', *Science Translational Medicine*, 5: 191ra83-91ra83.
Shi, Z., K. G. Neoh, E. T. Kang, C. Poh, and W. Wang. 2009. 'Titanium with surface-grafted dextran and immobilized bone morphogenetic protein-2 for inhibition of bacterial adhesion and enhancement of osteoblast functions', *Tissue Eng Part A*, 15: 417-26.
Shinde, U. A., and M. S. Nagarsenker. 2009. 'Characterization of gelatin-sodium alginate complex coacervation system', *Indian J Pharm Sci*, 71: 313-7.
Shockman, G. D., and J. F. Barrett. 1983. 'Structure, function, and assembly of cell walls of gram-positive bacteria', *Annu Rev Microbiol*, 37: 501-27.
Siepmann, J., N. Faisant, J. Akiki, J. Richard, and J. P. Benoit. 2004. 'Effect of the size of biodegradable microparticles on drug release: experiment and theory', *Journal of Controlled Release*, 96: 123-34.
Simonet, W. S., D. L. Lacey, C. R. Dunstan, M. Kelley, M. S. Chang, R. Luthy, H. Q. Nguyen, S. Wooden, L. Bennett, T. Boone, G. Shimamoto, M. DeRose, R. Elliott, A. Colombero, H. L. Tan, G. Trail, J. Sullivan, E. Davy, N. Bucay, L. Renshaw-Gegg, T. M. Hughes, D. Hill, W. Pattison, P. Campbell, S. Sander, G.

Van, J. Tarpley, P. Derby, R. Lee, and W. J. Boyle. 1997. 'Osteoprotegerin: a novel secreted protein involved in the regulation of bone density', *Cell*, 89: 309-19.
Singh, Jasvinder A. 2011. 'Epidemiology of knee and hip arthroplasty: a systematic review', *The open orthopaedics journal*, 5: 80-85.
Singh, Shriti, Santosh Kumar Singh, Indrajit Chowdhury, and Rajesh Singh. 2017. 'Understanding the Mechanism of Bacterial Biofilms Resistance to Antimicrobial Agents', *The open microbiology journal*, 11: 53-62.
Siopack, J. S., and H. E. Jergesen. 1995. 'Total hip arthroplasty', *The Western journal of medicine*, 162: 243-49.
Siu, L. K. 2002. 'Antibiotics: action and resistance in gram-negative bacteria', *J Microbiol Immunol Infect*, 35: 1-11.
Smith, R. C., M. Riollano, A. Leung, and P. T. Hammond. 2009. 'Layer-by-layer platform technology for small-molecule delivery', *Angew Chem Int Ed Engl*, 48: 8974-7.
Stavrakis, Alexandra I., Suwei Zhu, Vishal Hegde, Amanda H. Loftin, Alyssa G. Ashbaugh, Jared A. Niska, Lloyd S. Miller, Tatiana Segura, and Nicholas M. Bernthal. 2016. 'In Vivo Efficacy of a "Smart" Antimicrobial Implant Coating', *J Bone Joint Surg Am*, 98: 1183-89.
Stevenson, C. L., J. T. Santini, Jr., and R. Langer. 2012. 'Reservoir-based drug delivery systems utilizing microtechnology', *Adv Drug Deliv Rev*, 64: 1590-602.
Stinner, D. J., C. A. Krueger, B. D. Masini, and J. C. Wenke. 2011. 'Time-dependent effect of chlorhexidine surgical prep', *J Hosp Infect*, 79: 313-6.
Stoodley, Paul, Sandeep Sidhu, Laura Nistico, Megan Mather, Ashley Boucek, Luanne Hall-Stoodley, and Sandeep Kathju. 2012. 'Kinetics and morphology of polymicrobial biofilm formation on polypropylene mesh', *FEMS Immunology & Medical Microbiology*, 65: 283-90.
Sud, Sudha, Shang-You Yang, Christopher H. Evans, Paul D. Robbins, and Paul H. Wooley. 2001. 'Effects of Cytokine Gene Therapy on Particulate-Induced Inflammation in the Murine Air Pouch', *Inflammation*, 25: 361-72.
Sundfeldt, M., L. V. Carlsson, C. B. Johansson, P. Thomsen, and C. Gretzer. 2006. 'Aseptic loosening, not only a question of wear: a review of different theories', *Acta Orthop*, 77: 177-97.
Sundfeldt, Mikael, Lars V Carlsson, Carina B Johansson, Peter Thomsen, and Christina Gretzer. 2006. 'Aseptic loosening, not only a question of wear: A review of different theories', *Acta Orthopaedica*, 77: 177-97.
Swearingen, M. C., J. F. Granger, A. Sullivan, and P. Stoodley. 2016. 'Elution of antibiotics from poly(methyl methacrylate) bone cement after extended implantation does not necessarily clear the infection despite susceptibility of the clinical isolates', *Pathog Dis*, 74: ftv103.
Syggelos, Spyros A., Alexios J. Aletras, Ioanna Smirlaki, and Spyros S. Skandalis. 2013. 'Extracellular matrix degradation and tissue remodeling in periprosthetic loosening and osteolysis: focus on matrix metalloproteinases, their endogenous tissue inhibitors, and the proteasome', *BioMed research international*, 2013: 230805-05.
Taha, Mariam, Hesham Abdelbary, F. Patrick Ross, and Alberto V. Carli. 2018. 'New Innovations in the Treatment of PJI and Biofilms-Clinical and Preclinical Topics', *Current reviews in musculoskeletal medicine*, 11: 380-88.
Tamanna, T., J. B. Bulitta, and A. Yu. 2015. 'Controlling antibiotic release from mesoporous silica nano drug carriers via self-assembled polyelectrolyte coating', *J Mater Sci Mater Med*, 26: 117.
Tande, Aaron J., and Robin Patel. 2014. 'Prosthetic Joint Infection', *Clin Microbiol Rev*, 27: 302-45.

Tang, Peifu, Wei Zhang, Yan Wang, Boxun Zhang, Hao Wang, Changjian Lin, and Lihai Zhang. 2011. 'Effect of Superhydrophobic Surface of Titanium on Staphylococcus aureus Adhesion', *Journal of Nanomaterials*, 2011: 8.

Thienpont, Emmanuel. 2016. 'Revision knee surgery techniques', *EFORT open reviews*, 1: 233-38.

Thomas, L., A. D. Russell, and J. Y. Maillard. 2005. 'Antimicrobial activity of chlorhexidine diacetate and benzalkonium chloride against Pseudomonas aeruginosa and its response to biocide residues', *J Appl Microbiol*, 98: 533-43.

Tsurufuji, S., A. Kurihara, and F. Ojima. 1984. 'Mechanisms of anti-inflammatory action of dexamethasone: blockade by hydrocortisone mesylate and actinomycin D of the inhibitory effect of dexamethasone on leukocyte infiltration in inflammatory sites', *J Pharmacol Exp Ther*, 229: 237-43.

Tyas, B., M. Marsh, C. Molyneux, R. Refaie, T. Oswald, and M. Reed. 2016. 'Antibiotic Resistance Profiles of Surgical Site Infections in Hip Hemiarthroplasty: Comparing Low-Dose Single Antibiotic Versus High-Dose Dual Antibiotic Impregnated Cement', *Orthopaedic Proceedings*, 98-B: 37-37.

Udagawa, N., N. Takahashi, T. Katagiri, T. Tamura, S. Wada, D. M. Findlay, T. J. Martin, H. Hirota, T. Taga, T. Kishimoto, and T. Suda. 1995. 'Interleukin (IL)-6 induction of osteoclast differentiation depends on IL-6 receptors expressed on osteoblastic cells but not on osteoclast progenitors', *The Journal of experimental medicine*, 182: 1461-68.

Ulrich, Slif D., Thorsten M. Seyler, Derek Bennett, Ronald E. Delanois, Khaled J. Saleh, Issada Thongtrangan, Michael Kuskowski, Edward Y. Cheng, Peter F. Sharkey, Javad Parvizi, James B. Stiehl, and Michael A. Mont. 2008. 'Total hip arthroplasties: what are the reasons for revision?', *International orthopaedics*, 32: 597-604.

Utting, Matthew R., B. J. A. Lankester, L. K. Smith, and R. F. Spencer. 2005. 'Total hip replacement and NICE', *BMJ (Clinical research ed.)*, 330: 318-19.

Vaishya, Raju, Mayank Chauhan, and Abhishek Vaish. 2013. 'Bone cement', *Journal of clinical orthopaedics and trauma*, 4: 157-63.

Variola, Fabio, Sylvia Francis Zalzal, Annie Leduc, Jean Barbeau, and Antonio Nanci. 2014. 'Oxidative nanopatterning of titanium generates mesoporous surfaces with antimicrobial properties', *International Journal of Nanomedicine*, 9: 2319-25.

Vasconcelos, Daniel M., Manuel Ribeiro-da-Silva, António Mateus, Cecília Juliana Alves, Gil Costa Machado, Joana Machado-Santos, Diogo Paramos-de-Carvalho, Inês S. Alencastre, Rui Henrique, Gilberto Costa, Mário A. Barbosa, and Meriem Lamghari. 2016. 'Immune response and innervation signatures in aseptic hip implant loosening', *Journal of translational medicine*, 14: 205-05.

Villarino, Alejandro V., Yuka Kanno, John R. Ferdinand, and John J. O'Shea. 2015. 'Mechanisms of Jak/STAT signaling in immunity and disease', *J Immunol*, 194: 21-27.

Wang, Dong, Scott C. Miller, Xin-Ming Liu, Brian Anderson, Xu Sherry Wang, and Steven R. Goldring. 2007. 'Novel dexamethasone-HPMA copolymer conjugate and its potential application in treatment of rheumatoid arthritis', *Arthritis research & therapy*, 9: R2-R2.

Wang, Long, Pengfei Lei, Jie Xie, Kanghua Li, Zixun Dai, and Yihe Hu. 2013. Medium-term Outcomes of Cemented Prostheses and Cementless Modular Prostheses in Revision Total Hip Arthroplasty.

Wang, Tao, Jun-Ying Sun, Xi-Jiang Zhao, Yong Liu, and Hai-Bo Yin. 2016. 'Ceramic-on-ceramic bearings total hip arthroplasty in young patients', *Arthroplasty Today*, 2: 205-09.

Wang, Yi, Geetha Jayan, Dinesh Patwardhan, and K. Scott Phillips. 2017. 'Antimicrobial and Anti-Biofilm Medical Devices: Public Health and Regulatory Science Challenges.' in.

Willert, H. G., and M. Semlitsch. 1977. 'Reactions of the articular capsule to wear products of artificial joint prostheses', *J Biomed Mater Res*, 11: 157-64.
Williams, D. L., and J. W. Costerton. 2012. 'Using biofilms as initial inocula in animal models of biofilm-related infections', *J Biomed Mater Res B Appl Biomater*, 100: 1163-9.
Williams, Rhodri, Peter Mihok, and James Murray. 2016. Novel Antibiotic delivery and Novel Antimicrobials in Prosthetic Joint infection.
Wong, S. Y., J. S. Moskowitz, J. Veselinovic, R. A. Rosario, K. Timachova, M. R. Blaisse, R. C. Fuller, A. M. Klibanov, and P. T. Hammond. 2010. 'Dual functional polyelectrolyte multilayer coatings for implants: permanent microbicidal base with controlled release of therapeutic agents', *J Am Chem Soc*, 132: 17840-8.
Wright, H. L., H. S. McCarthy, J. Middleton, and M. J. Marshall. 2009. 'RANK, RANKL and osteoprotegerin in bone biology and disease', *Current reviews in musculoskeletal medicine*, 2: 56-64.
Wu, K., Y. C. Chen, Y. M. Hsu, and C. H. Chang. 2016. 'Enhancing Drug Release From Antibiotic-loaded Bone Cement Using Porogens', *J Am Acad Orthop Surg*, 24: 188-95.
Wyatt, Michael, Gary Hooper, Christopher Frampton, and Alastair Rothwell. 2014. 'Survival outcomes of cemented compared to uncemented stems in primary total hip replacement', *World journal of orthopedics*, 5: 591-96.
Xia, W., K. Grandfield, A. Hoess, A. Ballo, Y. Cai, and H. Engqvist. 2012. 'Mesoporous titanium dioxide coating for metallic implants', *J Biomed Mater Res B Appl Biomater*, 100: 82-93.
Xiong, Ailian, Zhengduo Yang, Yicheng Shen, Jia Zhou, and Qiang Shen. 2014. 'Transcription Factor STAT3 as a Novel Molecular Target for Cancer Prevention', *Cancers*, 6: 926-57.
Yamaguchi, Seiji, Shekhar Nath, Yoko Sugawara, Kamini Divakarla, Theerthankar Das, Jim Manos, Wojciech Chrzanowski, Tomiharu Matsushita, and Tadashi Kokubo. 2017. 'Two-in-One Biointerfaces—Antimicrobial and Bioactive Nanoporous Gallium Titanate Layers for Titanium Implants', *Nanomaterials*, 7: 229.
Yoshitake, F., S. Itoh, H. Narita, K. Ishihara, and S. Ebisu. 2008. 'Interleukin-6 directly inhibits osteoclast differentiation by suppressing receptor activator of NF-kappaB signaling pathways', *J Biol Chem*, 283: 11535-40.
Zaborowska, M., K. Welch, R. Branemark, P. Khalilpour, H. Engqvist, P. Thomsen, and M. Trobos. 2015. 'Bacteria-material surface interactions: methodological development for the assessment of implant surface induced antibacterial effects', *J Biomed Mater Res B Appl Biomater*, 103: 179-87.
Zhang, Chaofan, Chun Hoi Yan, and Wenming Zhang. 2017. 'Cemented or cementless fixation for primary hip arthroplasty—evidence from The International Joint Replacement Registries', *Annals of Joint*, 2.
Zhang, F., Z. Zhang, X. Zhu, E. T. Kang, and K. G. Neoh. 2008. 'Silk-functionalized titanium surfaces for enhancing osteoblast functions and reducing bacterial adhesion', *Biomaterials*, 29: 4751-9.
Zhang, Peng, Zhiguo Zhang, and Wei Li. 2013. 'Antibacterial Coating Incorporating Silver Nanoparticles by Microarc Oxidation and Ion Implantation', *Journal of Nanomaterials*, 2013: 8.
Zhang, Yuqing, and Joanne M. Jordan. 2010. 'Epidemiology of osteoarthritis', *Clinics in geriatric medicine*, 26: 355-69.
Zhao, L., H. Wang, K. Huo, L. Cui, W. Zhang, H. Ni, Y. Zhang, Z. Wu, and P. K. Chu. 2011. 'Antibacterial nano-structured titania coating incorporated with silver nanoparticles', *Biomaterials*, 32: 5706-16.
Zhong, Guoxing, Wenlu Guo, Yan Liu, Yuemei Wei, Xiangguo Meng, Zhaoyong Hu, and Fangfang Liu. 2015. 'Preparation of tetrasulfide-functionalized silica

particles by hydrothermal assisted grafting method for removal of lead (II) via dynamic solid phase extraction', *Colloids and Surfaces A: Physicochemical and Engineering Aspects*, 485: 63-72.

Zhou, Guanghong, Liping Ma, Junhai Jing, and Hao Jiang. 2018. 'A meta-analysis of dexamethasone for pain management in patients with total knee arthroplasty', *Medicine*, 97: e11753.